Investigating the Effects of Photodynamic Therapy on Cells of the Nervous System In Vitro

Thesis

UNRESTRICTED

Investigating the Effects of Photodynamic Therapy on Cells of the Nervous System *In Vitro*

Miss Kathleen E. Wright B.Sc. (Hons)

A thesis submission to

The Open University for the degree of Doctor of Philosophy

Department of Life Sciences

The Open University

Walton Hall

Milton Keynes

United Kingdom

Submitted 30th September 2009

DATE OF SUBMISSION: 30 SEPT 2009

DATE OF AWARD: 19 MAY 2010

Declaration

I hereby assert that the content of this submitted thesis, unless specified otherwise, is derived entirely from my own work. I further assert that this thesis does not exceed 100, 000 words, including headers and references.

At the time of submission parts of this work have been published in abstract, poster and oral presentation forms.

List of published journal articles

Wright, K.E., Liniker, E., Loizidou, M., Moore, C., MacRobert, A.J. and Phillips, J.B. (2009) "Peripheral neural cell sensitivity to mTHPC-mediated photodynamic therapy in a 3D *in vitro* model", The British Journal of Cancer **101**: 658-665.

List of published abstracts

Wright, K.E., MacRobert, A.J. and Phillips, J.B. (2009). "Cellular antioxidant pathways protect mammalian sensory neurons in 3D culture from mTHPC-mediated PDT." Joint 13th European Society for Photobiology (ESP) Congress and 2nd European Platform for Photodynamic Medicine (EPPM) 5-10 Sept, Wroclaw, Poland): 61. (**Oral presentation** OC108)

Wright, K.E., MacRobert, A.J. and Phillips, J.B. (2009). "Mammalian sensory neurons in 3D culture retain their regenerative functionality after surviving mTHPC-mediated PDT," Joint 13th European Society for Photobiology (ESP) Congress and

2nd European Platform for Photodynamic Medicine (EPPM) 5-10 Sept, Wroclaw, Poland): 148. (**Poster** 741)

Wright, K.E. and Phillips, J.B. (2009 in press). "Regenerative Capacity of Cultured Neurons Following Photodynamic Therapy in a 3D Collagen Gel Culture System." eCells and Materials: Tissue and Cell Engineering Society 8-10 July, Glasgow, UK). (**Poster** 73)

Wright, K.E., MacRobert, A.J. and Phillips, J.B. (2008). "Differences in sensitivity of mTHPC-mediated photodynamic therapy of neurons, glial cells and MCF7 cells in a 3-dimensional cell culture model." Photodynamic Therapy and Photodiagnosis in Clinical Practice 7-11 Oct, Brixen, Italy). (**Oral presentation**)

Wright, K.E., MacRobert, A.J. and Phillips, J.B. (2008). "Assessing the Effects of Photodynamic Therapy on Peripheral Nerve and Cancer Cells, Using a Thin Tissue Engineered Collagen Culture Model." eCells and Materials: Tissue & Cell Engineering Society 2-4 July, Nottingham, UK), 16 (3):13 (ISSN 1473-2262). (**Oral presentation** T1-3)

Wright, K.E., MacRobert, A.J. and Phillips, J.B. (2007). "Intracellular localisation of mTHPC and effect of photodynamic therapy in cells of the mammalian peripheral nervous system." 12th European Society for Photobiology (ESP) Congress 1-6 Sept, Bath, UK): 156. (**Poster** 732)

Wright, K.E., Liniker, E., MacRobert, A.J., Saffrey, M.J., Brown, R.A and Phillips, J.B. (2006). "Use of a tissue engineered model to investigate the effects of photodynamic therapy on peripheral nerves." Tissue Engineering International and

Regenerative Medicine Society (TERMIS): European Chapter Meeting, Rotterdam, The Netherlands): 193. (**Poster** 60)

Wright, K.E., Liniker, E., MacRobert, A.J., Brown, R.A., Saffrey, M. J. and Phillips, J.B. (2006). "Investigating the effect of photodynamic therapy on nerves using tissue engineered culture models." eCells and Materials: Tissue and Cell Engineering Society 3-4 July, Sheffield, UK), 11(3): 51 (ISSN 1473-2262). (**Poster P22**)

Kathleen Wright

Miss Kathleen E. Wright B.Sc. (Hons)

Acknowledgements

Firstly, I would like to thank my supervisors Dr James B. Phillips and Dr Margaret Jill Saffrey for their invaluable supervision, support and patience. Thanks to our collaborators Dr Alexander MacRobert and Dr Josephine Woodhams at the National Medical Laser Centre, UCL; and Prof Robert A. Brown at the Tissue Repair Unit, UCLMS. Thanks also to The Open University for funding this research project.

I would like to thank my late father Srgt Neville Wright and grandmother Mrs Miranda Robinson-Thompson, my uncle Mr Keith M^{c}Neish and family, my mother Mrs Fay Phillips-Brown, without whom I could not have reached this milestone. Special thanks to Herr Dietmar Moritz; Sr Regina Ho, icm; Mrs Bernice Gibson and family for their love, friendship and support over the years. To my aunt Joan, sister Florence and family, brother Daniel, and cousins for all the entertainment and hominess. To grandaunt Lyn and granduncle Lenard, "Yuh 2 live fi si tings!" To the St. Pius X Church/ Dupont Primary School Community, Kingston Jamaica for their continued friendship and spiritual support.

Thanks to Dr Jon Golding, Dr Carole Midgley, Dr Jamie Harle, Dr Emma East, Dr Paul Gabbott, Dr Robert Saunders and the CMN group 2005-2009. Special thanks to Mrs Jacqueline Brown, Mrs Chris Lancashire, Mrs Chris Elcote, Mrs Julia Barker, Mrs Tina Wardhaugh, Mr John Ireland, Mr Steve Walters, Mrs Karen Evans, Mr Farrah Mohamed, Mrs Heather Davis, Mrs Janet Vroone, and Shirley and Jane.

Thanks to My friends Melessia and family; Miss Margret and family; Barba and Opi; Tsitsi; Isabel; Caroline; Bart; Helen; Isacc; Lambert; Becky, VJ, Waheda, etc; Andrew, Lorraine, Olwseun, Ross and NIBSC; the South Mimes/Ridge bell ringers; the Woughton on the Green bell ringers; and the Milton Keynes Rowing

Club. Thanks to my fellow students Monika; Joachim; Sandeep; Sarat; Dinar; Joan; Hadassah; Stanley; Liz; Ya; Sarah; Ralph; Farrah; Alex; Ting; Anesa; Mohammed and Armstrong.

Thanks to the ESP society for an ESP fellowship and the Open University Department of Life Sciences for a travel grant for conference attendance. Finally thanks to my examination panel: Dr A. J. Loughlin (internal examiner), Prof. S. Bown (external examiner) and Dr I. A. Romero (exam chair).

I dedicate this thesis with much love and good wishes to my nephews Masters Dylan and Liam Wright, and to the highly talented and ambitious youths of Tower Hill and Olympic Gardens, Kingston, Jamaica, West Indies.

"*Believe in better!*"

Abstract

The effect of photodynamic therapy (PDT) on neural cells is important when tumours are adjacent to or within the nervous system. The primary purpose of this study was to investigate PDT treatments using the photosensitiser *meta*-(tetra-hydroxyphenyl) chlorin (*m*-THPC) on cells of the peripheral nervous system. There is evidence that, during clinical PDT-treatment of tumour sites near important nerve structures, peripheral neural cells respond differently to *m*-THPC-mediated PDT than do tumour cells. In this study, the response to PDT-treatment of rat dorsal root ganglia (DRG) neurones co-cultured with satellite cells were compared with separately cultured human breast adenocarcinoma cell line (MCF-7) in innovative *in vitro* culture systems.

Epi-fluorescence microscopy confirmed that *m*-THPC was incorporated into all cell types, excluding photosensitiser uptake as a reason for differences in the response to *m*-THPC-mediated PDT *in vitro*. Sensitivity of cells exposed to *m*-THPC-mediated PDT (0-10 μg/ml *m*-THPC with 1 J/cm^2 white light) was determined in a 1 mm thin bespoke 3-dimensional (3D) collagen hydrogel culture system. Cell death was quantified using propidium iodide (PI) exclusion and DRG neurones were identified in co-culture using immunocytochemistry for βIII-tubulin. MCF-7 cells, DRG satellite cells and astrocytes (of the central nervous system) were significantly more sensitive to *m*-THPC-mediated PDT treatments than were DRG neurones. Importantly, the dose of interest, 4 μg/ml *m*-THPC-mediated PDT, caused no significant DRG neurone death in comparison with untreated controls, but was sufficient to elicit substantial cell death in the other cell types The cell death protocol was validated using a second photosensitiser, hypericin (0-3μg/ml with 1 J/cm^2 white light), which caused substantial DRG neurone death equivalent to other cell types studied.

Following *m*-THPC-mediated PDT treatments, DRG neurones displayed a loss of their neurites. An assessment of the ability of these cells to regenerate neurites after *m*-THPC-mediated PDT treatments was performed and neurite extension was found to be equivalent to that in untreated controls, demonstrating that the treated DRG neurones were viable and retained their neurite projecting function. Inhibiting specific cell antioxidant pathways gave an insight into the mechanism by which neurones survived *m*-THPC-mediated PDT. The results suggested that DRG neurones were protected from the phototoxic effects of *m*-THPC-mediated PDT by superoxide dismutase-1 (SOD-1) and the glutathione synthase antioxidant pathways.

DRG neurones used in this study survived *m*-THPC-mediated PDT under conditions sufficient to kill tumour cells and other nervous system cells. Identifying and understanding this phenomenon could provide the basis for developing PDT treatments that reduce nerve damage during cancer therapy. The question of whether *m*-THPC-mediated PDT has different effects on DRG neurone survival and/or function depending on which part of the cell is illuminated is of particular interest. Preliminary experiments are described in which 2D and 3D tissue engineered nerve cultures were developed and assessed for use in evaluating focally applied *m*-THPC-mediated PDT treatment to different parts of DRG neurones. These peripheral nerve culture systems have controllable cellular environments that make them attractive experimental tools for further investigations into the effect of PDT on peripheral nerves.

Table of Contents

List of Figures

List of Tables

Abbreviations

Ab	Antibodies
AlPcSn	Sulphonated aluminium phthalocyanine
ALA	5- Aminolevulinate
ANS	Autonomic Nervous System
ATP	Adenosine Triphosphate
BBB	Blood-Brain Barrier
BPD-MA	Benzoporphyrin derivative monoacid ring A
Ca^{2+}	Calcium ion
ChOOHs	Cholesterol hydroperoxides
CNS	Central nervous system
CO_2	Carbon dioxide
Cu^{2+}	copper ion
DAB	Diaminobenzidine
DCF	2', 7' –Dichlorofluorescin diacetate
DDC	Diethyldithiocarbamate
DMEM	Dulbecco's Modified Eagle's Medium
DNA	Deoxyribonucleic acid
DNase	Deoxyribonuclease
DR	Death receptors
ECACC	European Collection of Cell Cultures
EDTA	Ethylene-daiminetetra-acetic acid
ENS	Enteric nervous system
ER	Endoplasmic reticulum
FCS	Foetal calf serum
FITC	Fluorescein isothiocyanate

GFAP	Glial fibrillary acidic protein
GFP	Green fluorescent protein
GGT	γ-glutamyl-transferase
GPx	Glutathione peroxidise
GR	Glutathione reductase
GSH	Reduced glutathione
GSSG	Glutathione disulfide
GST	Glutathione-*S*-transferase
GST P1	Glutathione-*S*-transferase pi gene
GGT	γ-glutamyl transpeptidase
γGCS	γ-glutamyl-cysteine synthetase
γGCT	γ-glutamyl-cyclotransferase
H^+	Proton
HDL	High density lipoprotein
$HO^{\bullet}$	Hydroxyl radical
H_2O_2	Hydrogen peroxide
.i.v.	Intravenous
i.p.	Intraperitoneal
L-BSO	DL-buthionine-(S,R)-sulfoximine
LDL	Low density lipoprotein
LOOHs	Lipid hydroperoxides
MCF-7	Human breast adenocarcinoma cell line
mg	milligram
$MgSO_4$	Magnesium sulphate
ml	Millilitre
m-THPC	*meta*-(tetra-hydroxyphenyl) chlorin or Foscan®

MTT	[3-(4, 5-dimethylthiazol-2-yl)-2, 5-diphenyltetrazolium bromide]
mM	Millimolar
Mn^{2+}	Manganese ion
NAC	N-AcetylCysteine
NAD(P)H	Nicotinamide adenine dinucleotide phosphate (reduced form)
$NADPH^{+}$	Nicotinamide adenine dinucleotide phosphate (oxidised form)
NGF	Nerve growth factor
NO	Nitric oxide
PBS	phosphate buffer saline
PDT	Photodynamic therapy
Pen/Strep	Penicillin/ Streptomycin
PI	Propidium iodide
PKC	Protein kinase C
PDL	Poly-D-Lysine
PLL	Poly-L-Lysine
PNS	Peripheral nervous system
PpIX	Protoporphyrin IX
ROS	Reactive oxygen species
-SH	Sulphydryl group
SNS	Somatic nervous system
SOD	Superoxide dismutase
TRITC	Tetramethylrhodamine isothiocyanate
2D	2-dimensional
3D	3-dimensional

2-MeOE_2	2-Methoxy-estradiol
$^1O_2$	Reactive singlet oxygen (toxic)
$^3O_2$	Triplet ground state molecular oxygen (non-toxic)
$O_2^{\bullet-}$	Superoxide anion radical (toxic)
^0S	Ground state of a photosensitiser molecule
^1S	Singlet state of a photosensitiser molecule
^3S	Excited triplet state of a photosensitiser molecule
v/v	Volume per volume
w/v	Weight per volume
µg	Microgram
µl	Microlitre
µM	Micromole
µm	Micrometre
Zn^{2+}	Zinc ion

Chapter 1: Introduction

This introduction begins with a short general introduction to photodynamic therapy (PDT). This is followed by an overview of neural cell biology, and the relationship between neurones and glial cells (the main cell types used in this study); descriptions of the mechanism of PDT action; types of cell death; background on a selection of antioxidant pathways; a review of the literature about the effects of PDT on neural tissue; and the aims of this project.

1.1 Introduction to PDT

PDT or photochemotherapy (Mandys *et al.*, 1998) is a well-established treatment for a variety of malignant and non-malignant diseases (Laveille *et al.*, 2003). Castano *et al.* (2005) and Krasnovsky Jr. (2007) reported that over the past century PDT has developed from the phenomenon 'photodynamic action' reported in 1900 by Raab and Tappeiner, to PDT as it is today; a dynamic physicochemical method for focal treatment, which combines the use of a light sensitive agent (known as a photosensitiser) with laser light to treat cancer. Initially, PDT was used to treat skin and superficial cancers that were associated with the lining of internal organs. This limitation to PDT use was due to restrictions in methods of light delivery. However, following the introduction of optical fibre light guides, PDT is now used in the treatment of small solid *in situ* and micro-invasive tumours, e.g. prostate cancer (Rousset *et al.*, 2000; Marchal *et al.*, 2004; Plant, 2007b), and for treating patients with inoperable tumours in which conventional treatments have proven ineffective (Rousset *et al.*, 2000).

The mechanism by which PDT destroys unwanted tissue is by overproduction of toxic oxygen species (i.e. reactive oxygen species (ROS), molecules with unpaired electrons such as superoxide anions ($O_2^{\bullet-}$) and hydroxyl radical ($HO^{\bullet}$); and singlet oxygen ($^1O_2$). Therefore, PDT utilises targeted or focally applied oxidative stress to cause selective killing of tumours (Figure 1.1). However, detailed mechanistic information is sparse for photosensitisers used in PDT, and also tissue-specific responses have not been completely characterised (Dabrowski *et al.*, 2006).

PDT as a treatment method does have some side effects, which can include some pain and swelling in the treated area (Plant, 2007b). However, PDT is known to cause less damage in comparison to conventional surgery; and it allows future treatment options for diseased sites; it has better functional results; and it may also be delivered away from a hospital setting (Nyst *et al.*, 2009). PDT has also been reported to have no cumulative toxicity (Castano *et al.*, 2005; Plant, 2007b) or known maximum cumulative dose associated with it; this is in contrast with the use of ionising radiation and chemotherapy. It is also thought that much of the resistance that emerges (due to mutations) after treating cancer cells with radiation and chemotherapy, does not lead to cross-resistance to PDT (Oleinick *et al.*, 2002; Heinzelmann-Schwarz *et al.*, 2003; Castano *et al.*, 2005). In addition, *meta*-tetrahydroxyl-phenyl-chlorin (*m*-THPC)-mediated PDT on a human breast adenocarcinoma cell line (MCF-7 cells) does not induce resistance to subsequent cycles of PDT (Hornung *et al.*, 1998). This makes PDT a useful adjunctive treatment after treating patents with these conventional methods.

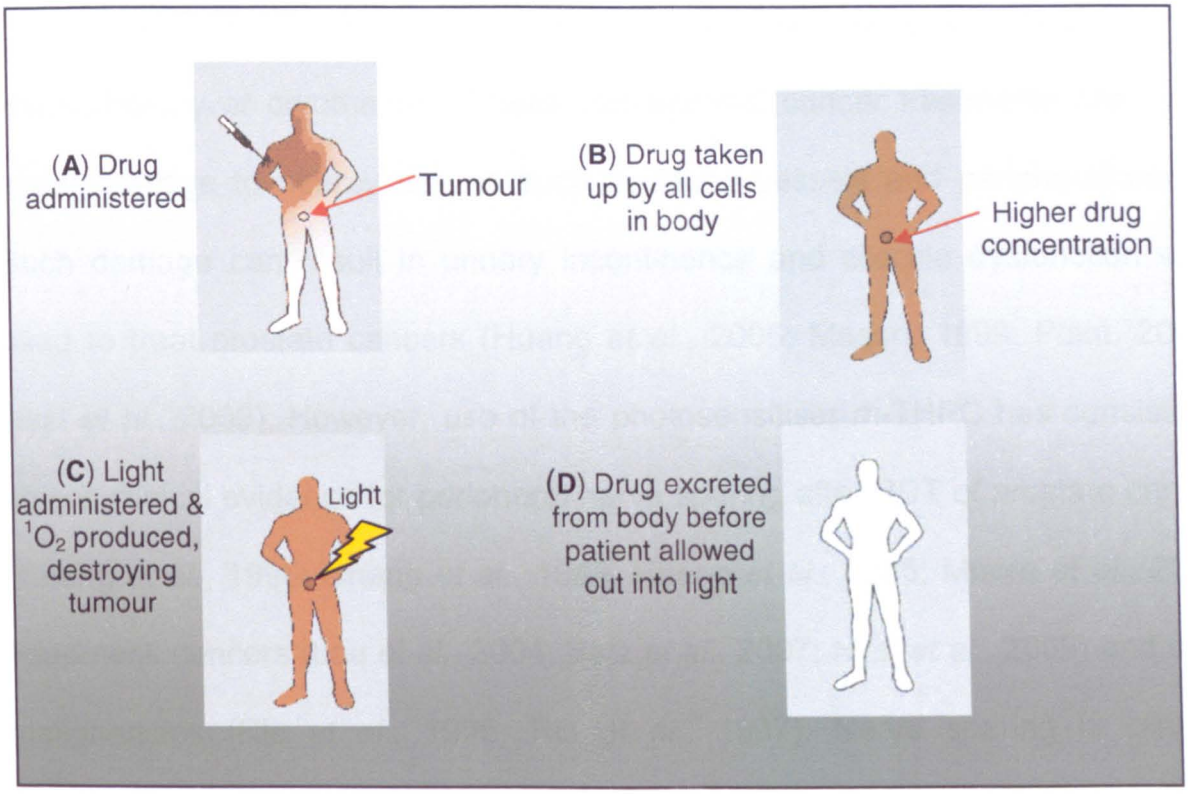

Figure 1.1
An illustration of the treatment of a tumour with PDT.
(**A**) Photosensitiser injected into patient; (**B**) photosensitiser taken up by tumour and non-tumour cells in the body. Over time a greater accumulation of the photosensitiser in tumour cells can occur due to faster metabolic rate of tumour cells and increased vascularisation of the tumour; (**C**) Light is directed only at tumour to cause focal PDT and (**D**) photosensitiser is excreted from the body. (Adapted from http://www.bmb.leeds.ac.uk/pdt/PDToverview.htm)

Despite the availability and many advantages of treatment modalities such as PDT, most cancers are still treated by surgical intervention, radiotherapy, chemotherapy or cryotherapy. These conventional cancer treatments can cause major damage to nearby tissues such as blood vessels and peripheral nerves. Such damage can result in urinary incontinence and erectile dysfunction when used to treat prostate cancers (Huang *et al.*, 2005; Mason, 1999; Plant, 2007a; Nyst *et al.*, 2009). However, use of the photosensitiser *m*-THPC has consistently shown clinical evidence for peripheral nerve sparing after PDT of prostate cancers (Chang *et al.*, 1996; Chang *et al.*, 1999; Huang *et al.*, 2005; Moore *et al.*, 2006), head/neck cancers (Lou *et al.*, 2004; Betz *et al.*, 2007; Nyst *et al.*, 2009) and chest malignancies (Ris *et al.*, 1996; Ris *et al.*, 1997). Nerve sparing is clinically important because it reduces the likelihood of patients losing sensory or motor function at the treatment site and associated areas. The potential for nervous system damage would also have implications in the use of PDT to treat tumours in association with important CNS structures (e.g. the spinal cord or brain).

It is clear that understanding the effect of PDT on the nervous system is important for the future of clinical cancer treatment. This therefore requires study of the cellular and molecular responses of nerves to *m*-THPC-mediated PDT treatment, which is the basis of the work described in this thesis.

1.2 Mammalian nervous system

The mammalian nervous system is subdivided into 2 main parts; the central nervous system (CNS) and the peripheral nervous system (PNS). The CNS consists of the brain and the spinal cord, and the PNS consists of all nervous tissue situated outside the CNS (Figure 1.2a). The PNS includes cranial nerves

and branches; spinal nerves and branches; sensory, autonomic and enteric ganglia and the processes arising from the cells of these ganglia. The PNS can be functionally subdivided into the somatic nervous system (SNS), which controls voluntary actions; the autonomic nervous system (ANS), which controls involuntary actions; and the enteric nervous system (ENS), which specifically controls gut functions.

Various parts of the peripheral nervous system may be exposed to PDT during cancer treatment, although the motor, sensory and autonomic nerves that innervate the urinogenital regions are most likely to be exposed during PDT treatment of prostate cancer. This study focused on the effects of PDT on the sensory ganglia.

1.2.1 Tissues and cells of the somatic nervous system

1.2.1.1 Sensory ganglia

Sensory ganglia are small masses of nervous system tissue that are closely associated with cranial and spinal nerves (Figure 1.3). The sensory ganglia primarily contain neuronal cell bodies and supporting glial cells (satellite cells). Dorsal root ganglia (DRG) (Figure 1.3), used in this study, are small sensory ganglia situated parallel to the spinal cord.

1.2.1.2 Somatic nerves

There are two types of nerves in the voluntary nervous system; afferent (sensory) and efferent (motor) nerves (Figure 1.3). Sensory nerves conduct impulses from

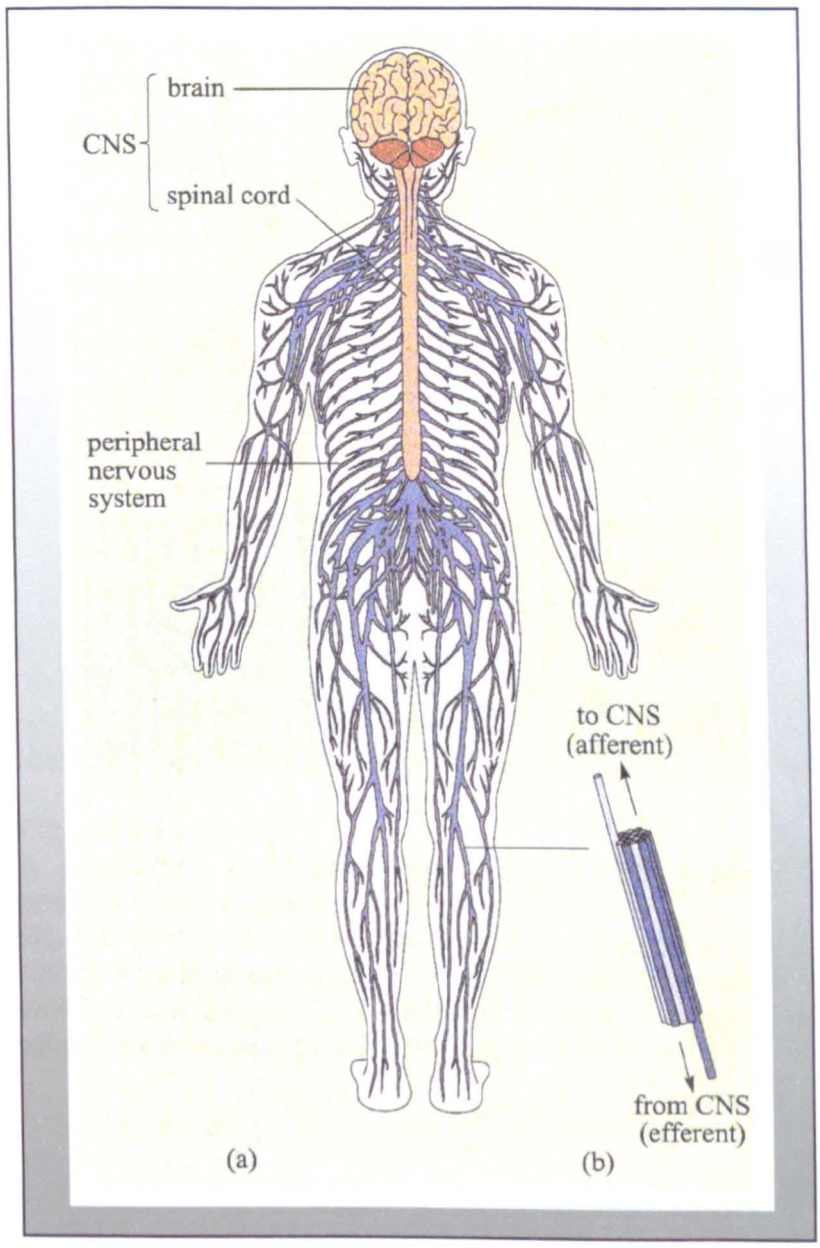

Figure 1.2
A simplified illustration of the human nervous system.
This illustration shows (**a**) the central nervous system (brain and spinal cord) and the somatic part of the peripheral nervous system; and (**b**) a bundle of axons showing the direction of nerve signals. This illustration only shows the somatic part of the nervous system, it does not reflect the autonomic or the enteric parts. (Taken from Toates, 2004)

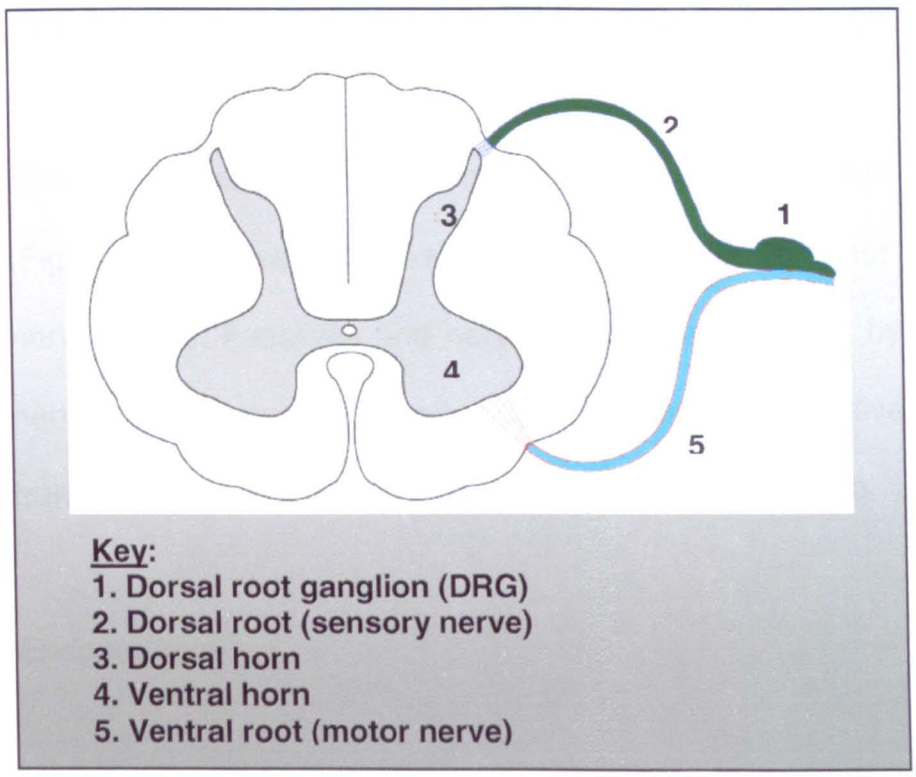

Figure 1.3
A simplified illustration of a transverse section through the spinal cord and associated PNS nerves and ganglion.
Illustration shows a cross section of a spinal cord with dorsal and ventral horns, sensory nerve, motor nerve and a DRG. Each DRG neuronal cell body projects a single axon which branches into 2; one extends towards the dorsal horn into the spinal cord, while the other extends towards the periphery.

sensory receptors in the periphery (e.g. skin, etc.) to the CNS (Figure 1.2b); whereas motor nerve fibres conduct impulses from the CNS to skeletal muscles.

Somatic nerves (sensory and motor) are grouped together into fascicles of axons (Figure 1.4); these fascicles are in turn grouped together into larger bundles, or nerve trunks. Fascicles and nerve trunks are protected by connective tissue and nerve trunks receive a blood supply. The main connective tissue layers of nerve trunks are the endoneurium, perineurium and epineurium.

Endoneurium

Endoneurium contains axons, connective tissue cells (e.g. fibroblasts), immune system cells (e.g. mast cells and macrophages) and hypertonic endoneurial fluid. It also contains parallel type I collagen fibrils, Schwann cells, myelin and ground substance. Ground substance is the extracellular matrix that imbeds fine bundles of fibrous connective tissue, and contains primarily collagen running longitudinally in the nerve. It further contains amorphous viscoelastic gel made of anionic polysaccharides (glycosaminoglycans): hyaluronic acid, dermatan sulphate, and chondroitin-6-sulphate that binds water and is produced and degraded by fibroblasts and mast cells (Winsz-Szczotka *et al.*, 2006). These macromolecules are involved in cell migration, adhesion and proliferation of nerve cells (Winsz-Szczotka *et al.*, 2006). Within the region of the matrix of the ground substance is the Schwann cell basal lamina, which is a continuous tube surrounding axons. It is composed of myelin, the extracellular matrix component laminin-2, heparansulfate proteoglycans (e.g. perlecan, argin, etc), collagen type IV, and fibronectin (Martini,

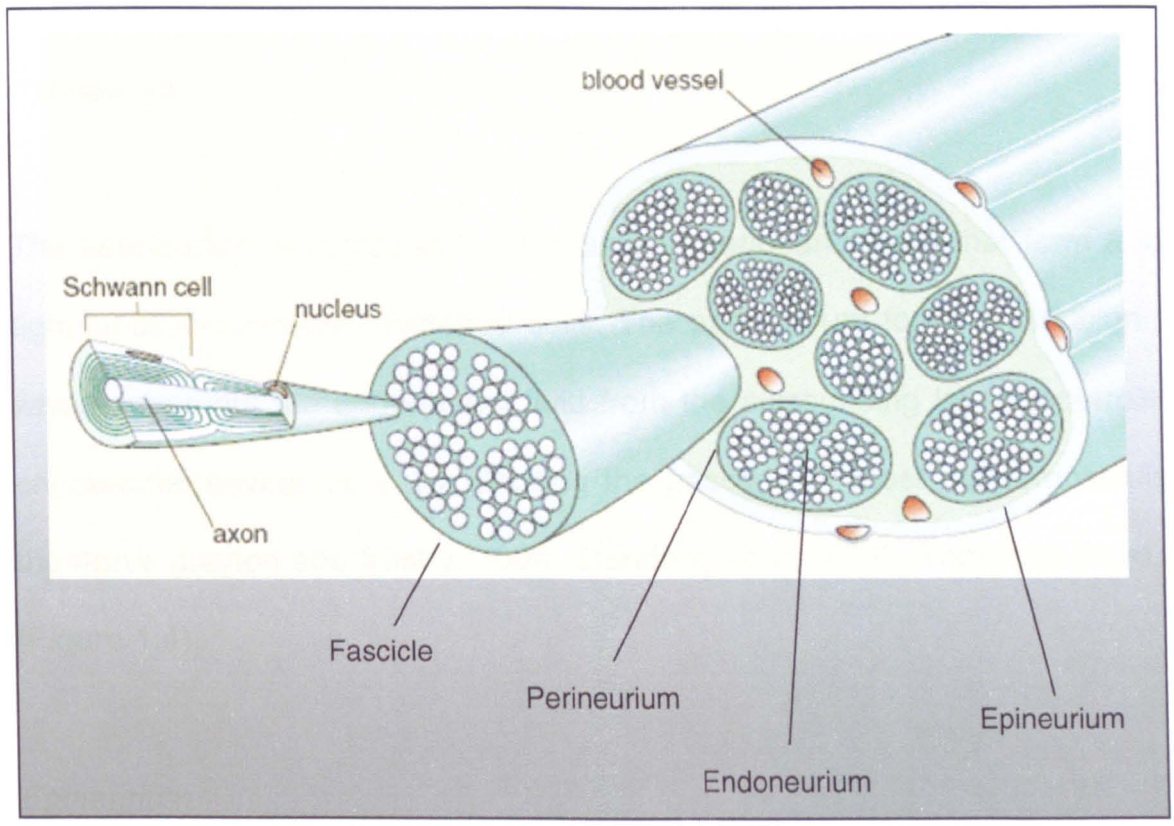

Figure 1.4
A simplified illustration of the integral structures of a human peripheral nerve trunk. Illustration shows that axons are protected by a series of layers epineurium, perineurium, endoneurium and Schwann cells. The illustration also shows the presence of blood vessels in the nerve trunk. (Adapted from Phillips and Harle, 2008)

2005). The endoneurium is surrounded by a further cell layer, termed the perineurium (Figure 1.4).

Perineurium

The perineurium is composed of specialised perineurial cells that form a layer of tight-junction-connected flattened cells. The perineurium forms a diffusion barrier which separates the endoneurial fluid from the surrounding layers controlling the endoneurial environment, by blocking the passage of most macromolecules into the nerve (Layton and Sastry, 2004; Standring *et al.*, 2005, Topp and Boyd, 2006) (Figure 1.4).

Epineurium

The epineurium is a layer of connective tissue, which groups the fascicles together. Human nerves tend to be multi-fasciculated (several fascicles) (Figure 1.4); while in some parts of the rat sciatic nerves used in this study, there is only one fascicle (Layton and Sastry, 2004). The epineurium contains fibroblasts and a large amount of basket-like woven collagen, and is a loosely connected outer layer of the nerve trunk.

Blood supply

Blood vessels supplying nerves form a capillary plexus in the epineurium (Figure 1.5); these pierce the perineurium and run parallel with the nerve fibres in the endoneurium. They have short transverse vessels linking them to form a vascular mesh. Capillaries in the endoneurium are generally larger and further apart compared to those in other tissues. Basal nerve blood flow is high relative to

metabolic requirements, and this coupled with the unusual capillary arrangement ensures nerves are richly supplied with blood. There is a blood-nerve barrier within the endoneurium with tight junctions between the endothelial cells (i.e. this is like the blood-brain barrier (BBB) in the CNS). The efficiency of the blood-nerve barrier is known to vary anatomically, for example ganglia and distal parts of peripheral nerves are situated outside the protection of this blood-nerve barrier (Standring *et al.*, 2005). This leaves neuronal cell bodies and satellite cells more exposed to stressors than axons and Schwann cells contained in nerve trunks.

1.2.2 Neurones

1.2.2.1 Neurone structure

The function of the neurone is to receive, process and to transmit electrical and chemical signals to another neurone or to a secretory cell or to a muscle. In general neurones can be classified into 1 of 3 major types (Figure 1.6).

Motor neurones are multipolar (Figure 1.6A), whereas primary sensory neurones are bipolar (axons extensions in two directions) (Figure 1.6B) or pseudounipolar (a CNS branch and a PNS branch) (Figure 1.6C and 1.7). Primary sensory neurones have large round neuronal cell bodies of between 25 and 50 μm in diameter (McHugh and McHugh, 2004). Pseudounipolar sensory neurones (e.g. in DRGs), are specialised to be sensitive to a particular physical stimulation (e.g. touch, pressure or pain) (Kandel, 1991) (Figure 1.7).

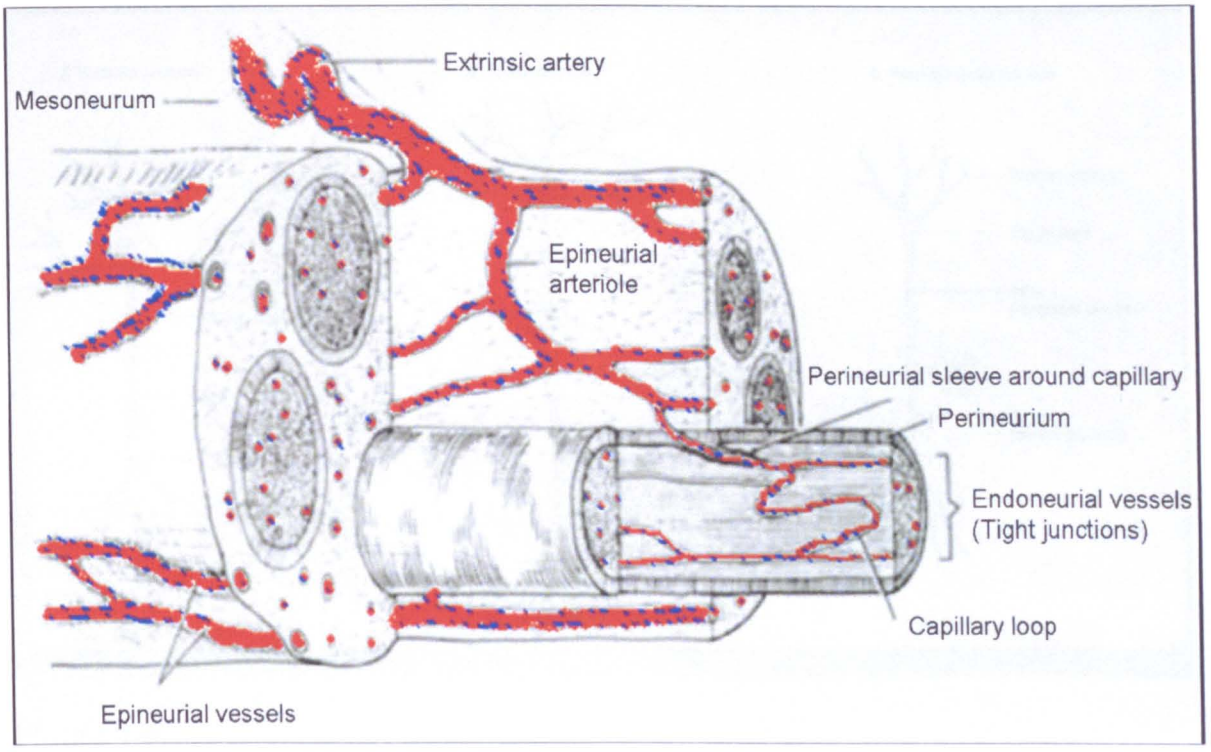

Figure 1.5
A simplified illustration of the peripheral nerve trunk capillary network.
The blood vessels are intimately woven into the structures of the nerve trunk to form a mesh of capillaries in the endoneurium. (Adapted from Robinson and Bryant, 2006)

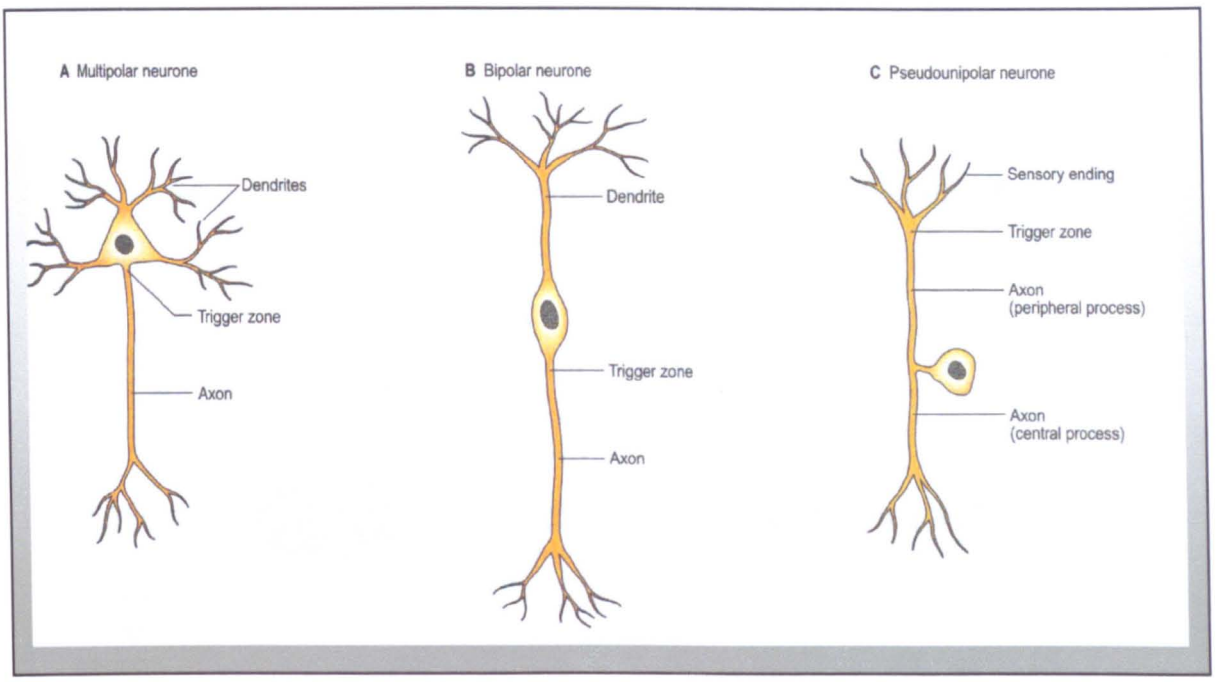

Figure 1.6.
Simplified illustrations of different types of neurones.
(**A**) Multipolar neurone, (**B**) Bipolar neurone and (**C**) Pseudounipolar neurone. (Taken from Michael-Titus *et al.*, 2008)

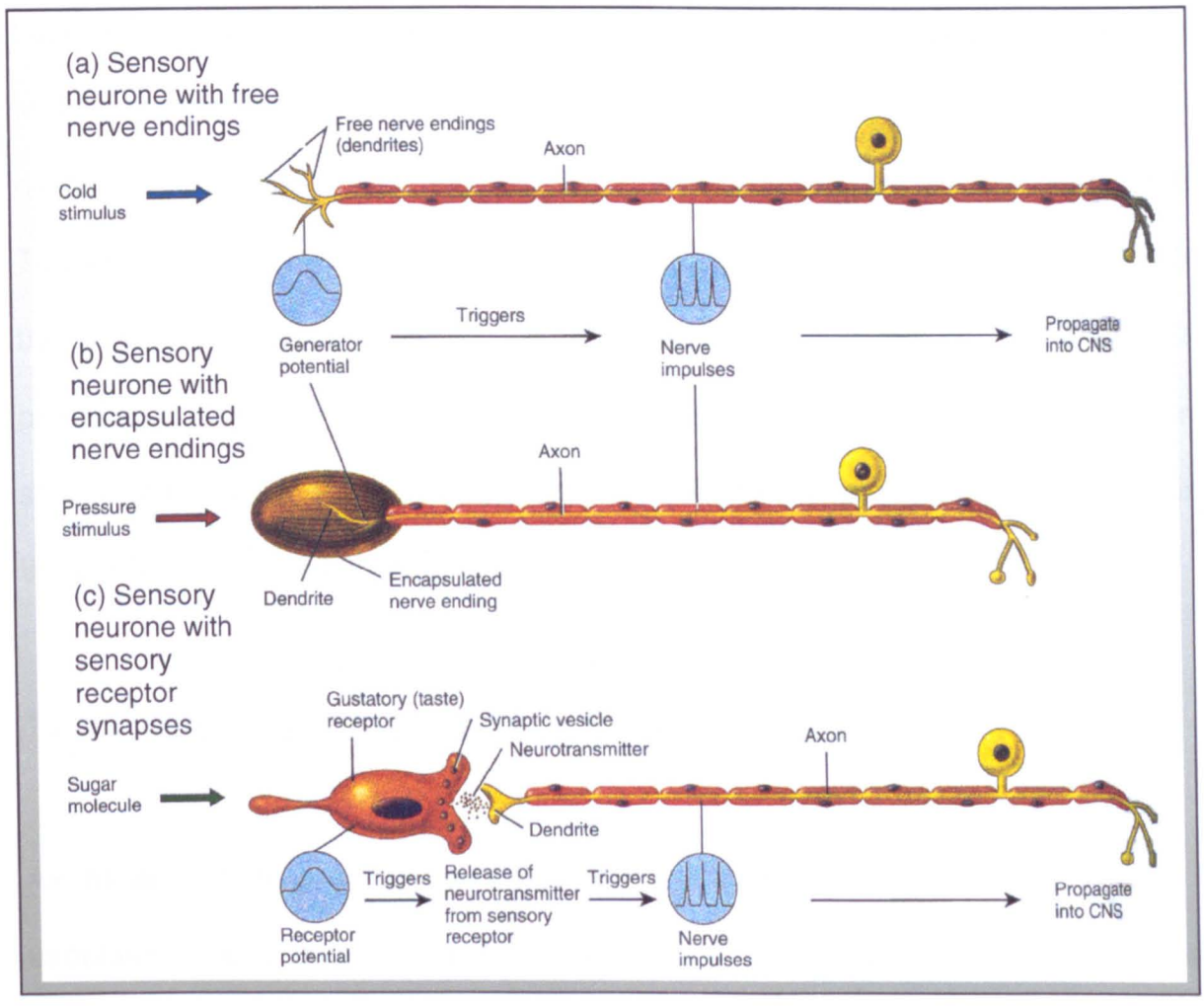

Figure 1.7
Simplified illustrations of types of pseudounipolar sensory neurones and their relationship with sensory receptors.
Primary sensory neurones are pseudounipolar neurones, which have a single dendrite and axon arising from a common site of the neuronal cell body. Axons of sensory neurones enter the spinal cord and a peripheral process that receives the sensory information projects to the periphery, which may be skin, internal organ etc (Taken from Tortora and Derrickson, 2006b).

There are three types of sensory neurones in DRGs, which are classified on the basis of their neurochemistry (expression of peptides and receptors), morphology (diameter size and myelination state), trophic factor requirements and sensory modality (peripheral mechanoreceptors or nociceptive types) (Tonge *et al.*, 1997; Tucker *et al.*, 2005). These three types of sensory neurones were further defined by Nascimento *et al.* (2008) on the basis of cytoplasmic densities. DRG pseudounipolar neurones have an axon branching into the CNS with similar structural features as the PNS portion, with the exception that the CNS portion of the DRG nerve is not ensheathed with an epineurium layer.

1.2.2.2 Ultrastructural characteristics of neurones and axons

Axons arise from projections of the neuronal cell body called axon hillocks. The axoplasm (axon cytoplasm) has been reported to have smooth endoplasmic reticulum (ER) throughout the mammalian axon (Goldberg, 2003), however it has also been stated that the axoplasm does not contain ER by Bancroft and Stevens (1990c) and Tortora and Derrickson (2006a). The axoplasm contains mitochondria, microtubules and neurofibrils; and it is surrounded by the axolemma (plasma membrane of the axon).

1.2.2.3 Neuronal transport

Transport of molecules along axons occurs by transport within vesicles along microtubules. Neuronal transport occurs from neuronal cell bodies to the nerve endings and *vice versa* by both slow and fast transport mechanisms. Slow transport conveys axoplasm in one direction from neuronal cell bodies towards axonal terminals; and fast transport conveys organelles and material in both

directions along the surface of microtubules, by protein motors called dynein and kinesin (reviewed by Goldstein and Yang 2000; Hirokawa and Takemura, 2005) (Figure 1.8). These microtubules contain βIII-tubulin and neurofilaments (NF, composed of neurofilament protein), both of which can be used to identify neurones immunocytochemically in culture and in tissue sections.

1.2.3 PNS glial cells

Peripheral glial cells include enteric glial cells (in enteric ganglia), satellite cells, Schwann cells and teloglia (reviewed by Jessen, 2004). Figure1.9 shows the 2 types of glial cells in the part of the PNS of interest in this study, satellite cells and Schwann cells. Schwann cells completely surround axons in the nerve trunk, while satellite cells surround neuronal cell bodies in the DRG. Specific marker used for satellite cells and Schwann cell identification is the immunocytochemical detection of the S100 protein in culture and in tissue sections.

1.2.3.1 Satellite cells

Satellite cells have extensive cytoplasm and completely ensheath neuronal cell bodies in DRGs. They provide structural support and regulate exchange of material between neuronal cell bodies and the interstitial fluid. Satellite cells and DRG sensory neurones are involved in non-synaptic cell-to-cell cross-excitation within the DRG (Shinder *et al.*, 1994). Nascimento *et al.* (2008) have recently further defined 3 types or states of satellite cells: satellite cells with heterochromatic nuclei and electron-dense cytoplasm; satellite cells with euchromatic nuclei and electron-lucent cytoplasm; and satellite cells that are not in contact with any neurones.

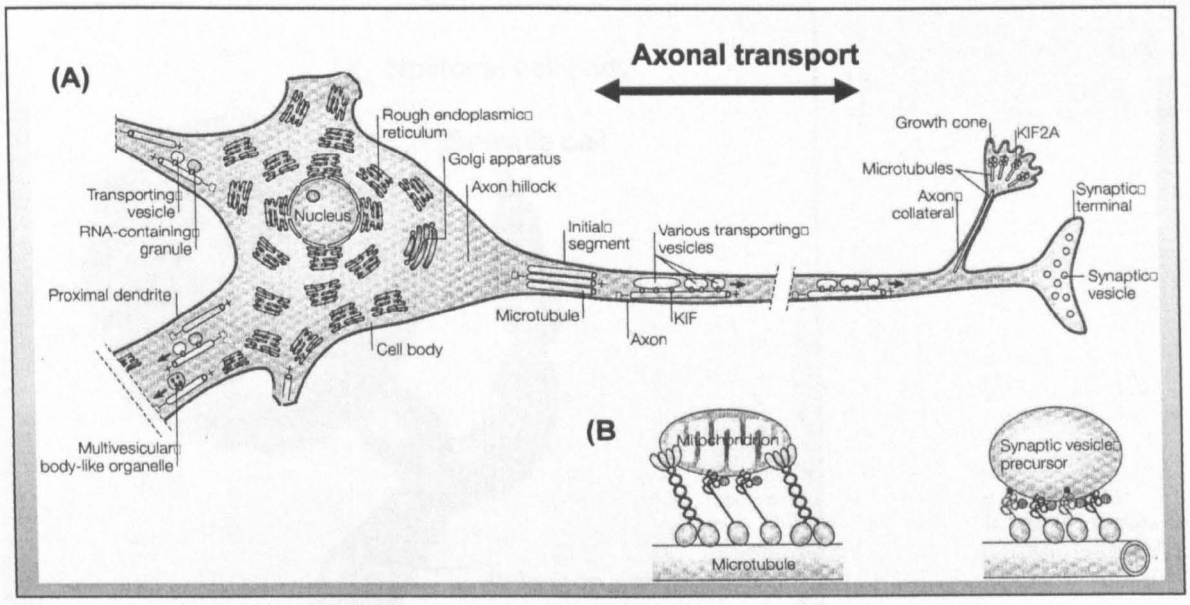

Figure 1.8
A simplified and generalised ultrastructure of a neurone and transport molecules. (**A**) The axon contains highly organised microtubule and microfilament structures, which provide internal support and transfer proteins from the neuronal cell body to the axon terminal; (**B**) Examples of transport complexes. KIF (kinesin superfamily proteins) and KIF2A (controls microtubule dynamics and the extension of axon collaterals). (Adapted from Hirokawa and Takemura, 2005)

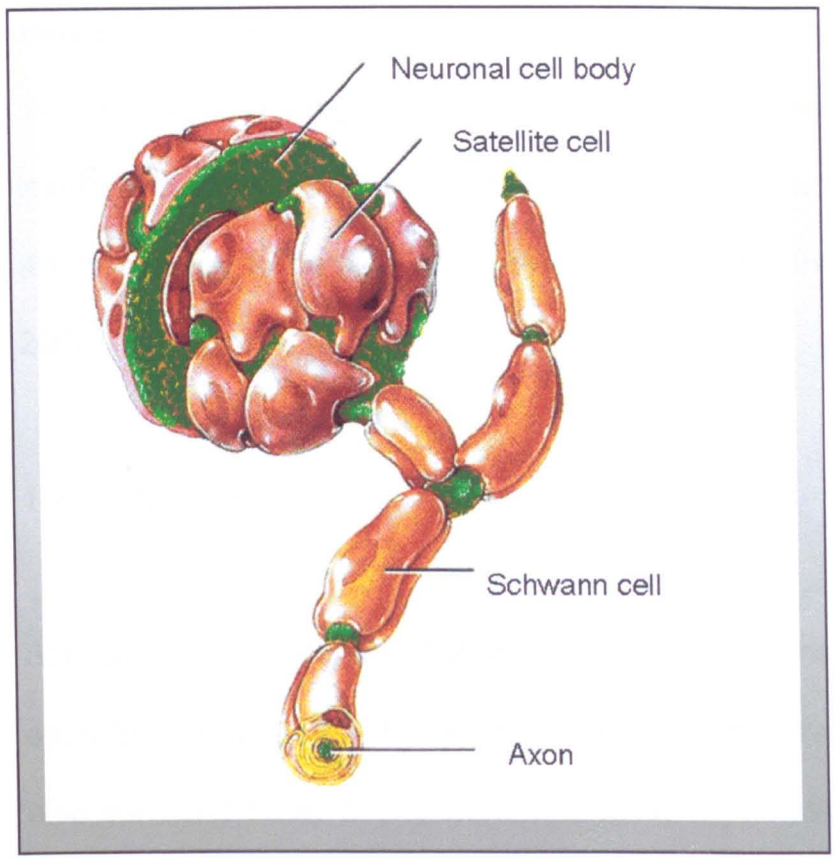

Figure1.9
A simplified isolated unit of satellite cells and Schwann cells interacting with a DRG neurone.
Neurone (green), satellite cells surrounding neuronal cell body (red) and Schwann cell (orange/yellow) wrapped around axon. (Adapted from Tortora and Derrickson, 2006a)

Satellite cells play an important role in controlling the survival of axotomised sensory neurones, although their behaviour and phenotype in conditions of degeneration and regeneration of neurites of sensory neurones has received insufficient study (Raginov *et al.*, 2004). Further studies of isolated satellite cells are necessary to better clarify differences among these cells (Nascimento *et al*, 2008)

1.2.3.2 Schwann cells

Schwann cells encircle peripheral axons several times, and form myelin sheaths; each Schwann cell myelinates only one axon, however a single Schwann cell can also surround many axons without actually myelinating them (Syroid *et al.*, 1996; Mirsky and Jessen, 1996; Topp and Boyd, 2006; Michael-Titus *et al.*, 2008; Standring *et al.*, 2005). These glial cells are situated in the nerve trunk, and act as electrical insulation by wrapping around individual or clusters of nerve fibres (Standring *et al.*, 2005), facilitating saltatory conduction. Schwann cells guide the growth of axons during peripheral nerve development (Standring *et al.*, 2005; Ndubaku and de Bellard, 2008) and are also known to influence axon regeneration (Standring *et al.*, 2005; Tortora and Derrickson, 2006a). They aid the digestion of dying neurones, and leave an empty tube through which a new axon can grow from a severed neurone end (Standring *et al.*, 2005; Syroid *et al.*, 1996). Schwann cells and other nerve cells (i.e. fibroblasts) distal to nerve damage sites are known to change their metabolism as a result of losing contact with axons; thereby producing signals which stimulate nerve regeneration (Standring *et al.*, 2005; Tonge *et al.*, 1997).

1.2.3.3. Teloglia

The third type of glial cells are the terminal glial cells, also called teloglia or perisynaptic glial cell, which help to maintain stability of the neuromuscular junction and regulate synaptic transmission (reviewed by Jessen, 2004; Martini, 2005).

1.2.4 CNS glial cells

During CNS development, glial cells have a dominant role in setting up the basic scaffolding of the brain. There are 3 main types of glial cell in the CNS: astrocytes, oligodentrocytes and microglia (reviewed by Jessen, 2004; Standring *et al.* 2005; Michael-Titus *et al.*, 2008). In regards to the CNS, the focus here is on astrocytes, because they are the cells that have been studied in order to gain an insight into the response of CNS cells to *m*-THPC-mediated PDT.

Astrocytes are the most common glial cells in the CNS (Figure 1.10) and they play a very important function in the differentiation, survival, pharmacological properties and resistance to injury (de Bernardo *et al.*, 2004) of the brain and the spinal cord. Astrocytes are distinguished from neurones in the brain by their expression of glial fibrillary acidic protein (GFAP). One of the most important roles of astrocytes is their involvement in the formation of the BBB. The BBB is formed when astrocyte processes are in association with blood vessels and protects the CNS from

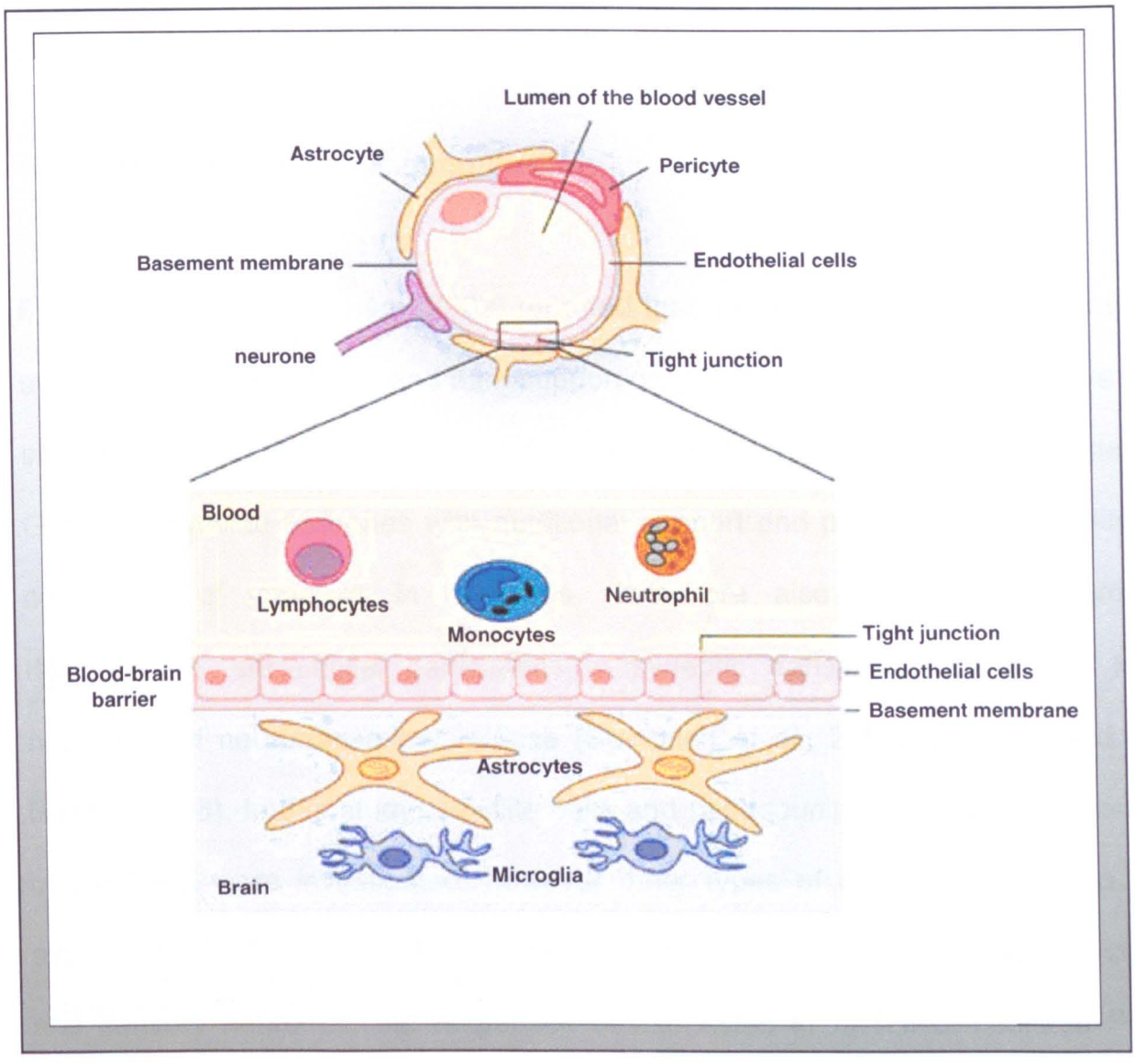

Figure 1.10
A simplified illustration of an astrocyte in association with a CNS neurone and capillary forming the blood-brain barrier.
The BBB is created by the tight apposition of endothelial cells lining blood vessels in the brain, forming a barrier between the circulation and the brain parenchyma. Blood cells such as lymphocytes, monocytes and neutrophils cannot penetrate this barrier. A thin basement membrane, comprising laminin, fibronectin and other proteins, surrounds the endothelial cells and associated pericytes, and provides mechanical support and a barrier function. (Taken from Francis *et al.*, 2003)

unwanted substances in the general blood circulation (reviewed by Francis *et al.*, 2003; Standring *et al.*, 2005)

1.2.5 Neuronal-glial cell communication

Fields and Stevens-Graham (2002) reported that there is a 2-way communication system between neurones and their supporting glial cells. This interaction plays an important role in the development, function and survival of the nervous system. Glial cells provide neurones with nutritional support and protection, and facilitate conduction of impulses in neurones. They are also involved in neurone development, are critical participants in synaptic transmission, and are key regulators of neurotransmitter release (Standring *et al.*, 2005; Ndubaku and de Bellard, 2008). In this study, satellite cells and pseudounipolar sensory neurones of the DRG were investigated; however other types of neurones may also be exposed to PDT, for example during PDT in the brain. In addition to satellite cells and sensory neurones, the responses of astrocytes to *m*-THPC-mediated PDT were investigated because they are the predominant glial cell types in the CNS, and are vital to CNS neuronal function and survival.

1.3 PDT

PDT is a non-invasive, focal cancer therapy, which allows for repetitive clinical administration to treatment sites. It results in damage to cancerous and non-cancerous cells, by apoptotic and/ or necrotic cell death modes (Ball *et al.*, 1998; Becker and Bonni, 2004). Clinical PDT can kill tumour cells by the uptake of more photosensitiser over non-tumour cells, and/or by causing microvascular injury resulting in the tumour being starved of nutrients and oxygen (Marshal *et al.*,

2004). PDT is a promising therapy for a wide variety of tumours, skin conditions, bacterial and viral infections. Clinical PDT utilises the administration of a photosensitiser orally, by intravenous injection (i.v.) (Plant, 2007b) or by topical administration to the skin. In a laboratory setting, the administration of a photosensitiser is by incubation with cells or tissue culture systems, as was performed in this study.

An excited photosensitiser molecule is one that has absorbed a quantum of light. The first law of photochemistry states that 'Only light absorbed by a molecule can produce photochemical changes in that molecule'. PDT involves the use of lasers or other light sources in combination with photosensitisers and molecular oxygen ($^3O_2$) present in tissues and cells to destroy unwanted cells. In most cases lasers have been used as the light source for clinical and experimental PDT, because of their emission of monochromatic light, high power output and easy delivery of light by optical fibres. The development of high power diode lasers with appropriate wavelength have been a major step forward for clinical application of PDT (Berg, 2007). In a laboratory setting, simple light sources are commonly used in order to activate photosensitisers *in vitro*. PDT therefore offers a method by which tumour cells can be specifically targeted in a localised manner. This is an invaluable feature which is not offered with standard systemic chemotherapy treatments (Dabrowski *et al.*, 2006; Nyst *et al.*, 2009).

There are 2 main generations of photosensitiser commonly referred to as first and second generation photosensitisers. The first generation photosensitisers are the first set of photosensitisers used in the establishment of PDT (e.g. Photofrin®). The second generation of photosensitisers are those most commonly used to date, for example *m*-THPC (Vrouenraets *et al.*, 1999; Morlet *et al.*, 1997; Laville *et al.*,

2003; Marchal *et al.*, 2005; Sasnouski *et al.*, 2006) and hypericin. Second generation photosensitisers are more effective and are the clinically preferred photosensitisers over first generation photosensitisers, because they have increased photodynamic efficiency with reduced phototoxic side effects (Ochsner, 1997). Two second generation photosensitisers *m*-THPC and hypericin have been investigated in this study.

1.3.1 Photochemistry of PDT

1.3.1.1 Jablonski energy level diagram

A Jablonski energy level diagram is commonly used to illustrate the process of energy transfer from a light source to ground state photosensitiser (^{0}S) (Figure 1.11) (reviewed by Macdonald and Dougherty; 2001; Wilson, 2003; Lichtman and Conchello, 2005), which takes place during PDT. The short-lived, excited singlet state of the photosensitiser (^{1}S) changes to a lower energy level called an excited triplet state (^{3}S), which occurs by a process called intersystem crossing (the spin of an excited electron reverses) (reviewed by Macdonald and Dougherty, 2001; Lichtman and Conchello, 2005; Wilson, 2003). Auto-fluorescence properties of photosensitisers are generated from the excited ^{1}S changing directly back into ^{0}S (Lichtman and Conchello, 2005; Wilson, 2003).

1.3.1.2 Molecular orbital theory

Molecular orbital theory can be used to explain the electronic structures of $^3O_2$ utilised in PDT (Zhao, 2001). $^3O_2$ in its primary or triplet ground state ($^3\Sigma_g^-$) is the lowest electronic state of oxygen, which involves 2 unpaired electrons in the

highest occupied orbital (reviewed by Macdonald and Dougherty, 2001; Zhao, 2001; Lane, 2002). This is converted into $^1O_2$ or singlet state ($^1\Delta_g$), which consists of a pair of electrons in the highest occupied orbital. Because these electrons are paired, $^1O_2$ is not considered as a free radical (Dugan and Choi, 1999) (Figure 1.12). $^1O_2$ is also not 'spin restricted' and therefore can accept pairs of electrons making $^1O_2$ react quickly (Lane, 2002). This quicker reaction is in contrast to spin restriction of O_2 which makes it prefer to accept electrons one at a time; therefore explaining why O_2 reacts sluggishly with most non-radicals.

^0S are activated clinically by visible, non-thermal, tissue-penetrating light of a specific wavelength. This activation energy is transferred to $^3O_2$ present at treatment sites. This photochemical reaction as shown in Figure 1.12 is generally known to predominantly result in the conversion of non-toxic $^3O_2$ into toxic $^1O_2$, by transfer and pairing of electrons in a lower orbital with the use of energy from ^3S (Huang *et al.*, 2005; Zhao, 2001).

1.3.1.3 Photodynamic action

In the 1960s, Schenck *et al.* formulated the concept that photodynamic action occurs by 2 different types of primary processes, type I or type II (Krasnovsky Jr, 2007).

Type I process

Under hypoxic conditions excited triplet state photosensitisers (^3S) will generate cytotoxic radicals (ROS) including $HO^{\bullet}$ and $O_2^{\bullet-}$ (Dabrowski *et al.*, 2006).

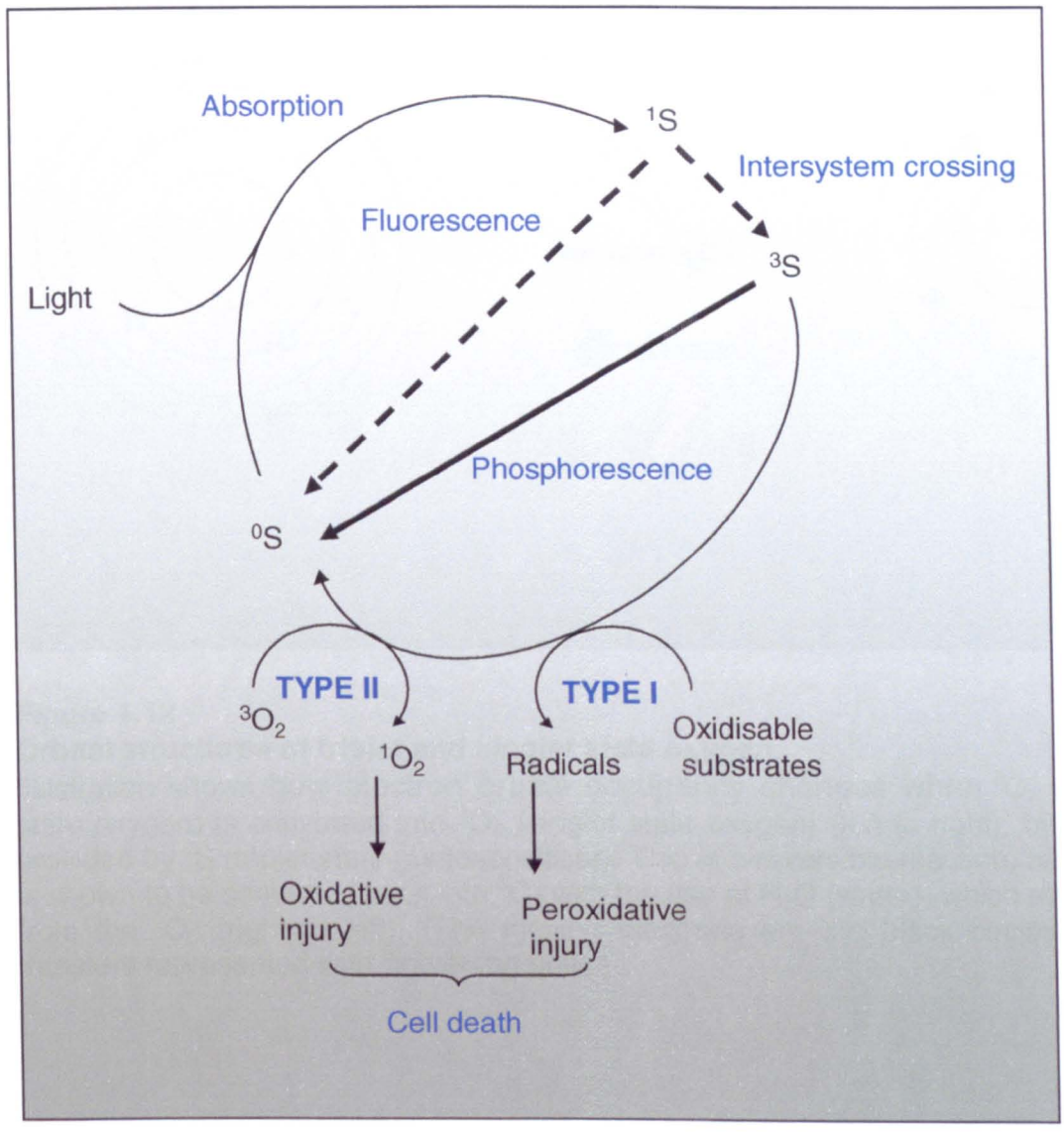

Figure 1.11
Simplified Jablonski energy level diagram of photosensitiser in combination with 2 types of PDT processes which result in cell death.
The Jablonski energy level diagram shows the electronic states following absorption of light by the photosensitiser. This pathway shows ^0S (ground state photosensitiser) being excited to short-lived ^1S. ^1S changes to a lower energy ^3S (triplet state photosensitiser). Electron transfer occurs between the ^3S and $^2O_3$ (molecular oxygen), producing toxic $^1O_2$/ROS and returns photosensitiser to ^0S. $^1O_2$/ROS generated by type I or type II process (see section 1.3.1.3) causes tissue/cell damage or death. Also a transition from ^1S directly to ^0S can also occur, this result in the emission of auto-fluorescence from the photosensitiser, which can be detected by fluorescence microscopy (Adapted from Macdonald and Dougherty, 2001).

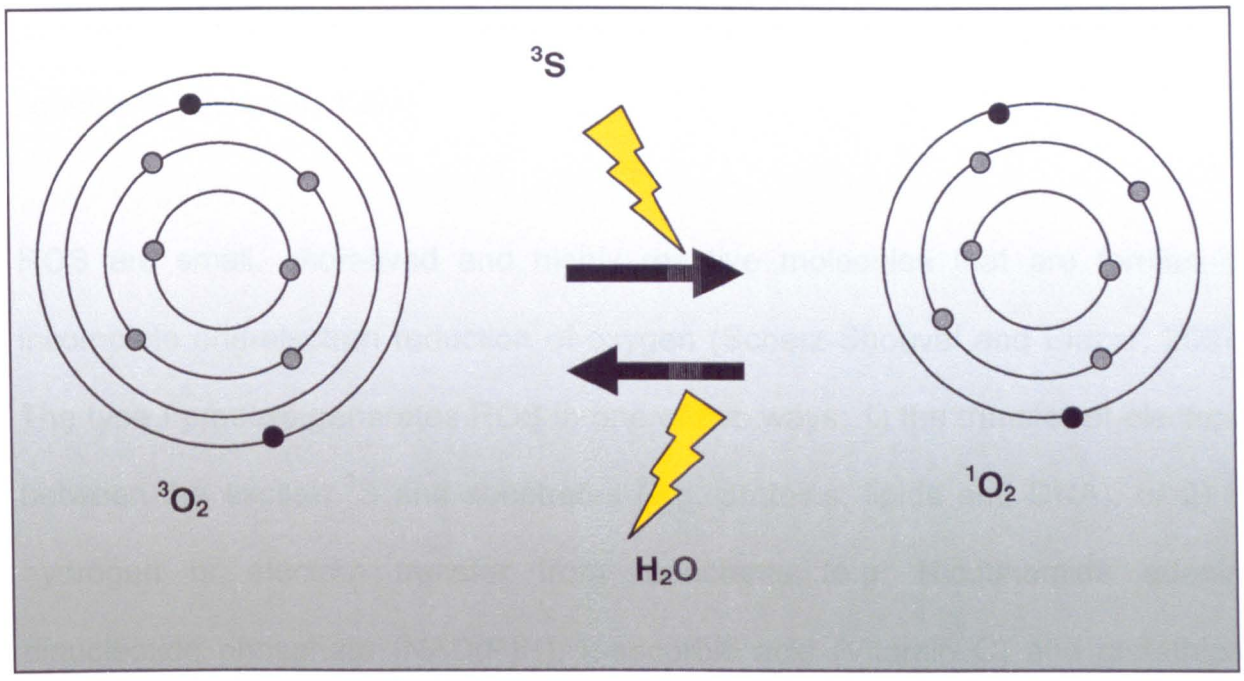

Figure 1.12
Orbital structures of triplet and singlet state oxygen.
Illustration shows how electron orbital occupancy changes when $^3O_2$ (triplet ground state oxygen) is converted into $^1O_2$ (singlet state oxygen) (left to right), by using energy provided by ^3S (triplet state photosensitiser). This is a reversible reaction, and as such $^1O_2$ is shown to be converted back into $^3O_2$ with the use of H_2O (water), which removes energy from the $^1O_2$ (right to left). (The moving electrons are the black circles, with energy transfers represented with 'lightening bolts').

Photosensitiser molecular structures that are readily oxidised (e.g. phenols and amines) or reduced (e.g. quinones) will facilitate the type I process under hypoxic conditions (Ochsner, 1997).

ROS are small, short-lived and highly reactive molecules that are formed by incomplete one-electron reduction of oxygen (Scherz-Shouval and Elazar, 2007). The type I process generates ROS in one of two ways: 1) the transfer of electrons between the excited ^3S and substrates (e.g. proteins, lipids and DNA), or 2) by hydrogen or electron transfer from reductants (e.g. Nicotinamide adenine dinucleotide phosphate (NAD(P)H), L-ascorbic acid (Vitamin C) and glutathione (GSH)) to the excited ^3S (Ochsner, 1997; Melnikova *et al.*, 1999c; Girotti, 2001; Berg, 2007) (Figure 1.13). ROS generated in this hypoxic condition are then auto-oxidised (Melnikova *et al.*, 1999c; Girotti, 2001) by $^1O_2$ already present in the system to generate products of oxidation (Figure 1.13).

In addition the type I process can also dominate the PDT process under conditions of high photosensitiser concentrations associated with the cell (MacDonald and Dougherty, 2001).

Type II process

PDT usually involves the type II process which requires oxygen rich conditions, and in contrast to type I process generates singlet state oxygen (singlet oxygen; $^1O_2$). The mechanism of the type II process is as follows. The excited ^3S transfers energy to a nearby $^3O_2$ and generates $^1O_2$, which rapidly reacts with organic molecules (substrates) (Lane, 2002; Girotti, 2001; Zhao, 2001; Wilson, 2003) (Figure 1.12 and 1.13).

However, in practice a combination of both types I and II processes may occur during treatment (Ochsner, 1997; Zhao, 2001). In addition to type I and/or type II processes occurring, a type II process can be changed to a type I process during PDT. This may be as a result of local hypoxia developing at the treatment area (Ochsner, 1997). Therefore a good oxygen supply is essential for type II PDT processes to persist.

1.3.2 Photosensitisers used in this study

Various different types of photosensitisers are used in PDT, each for their specific properties. Table 1.1 shows a list of commonly used photosensitisers in PDT.

1.3.2.1 General features of *m*-THPC and *m*-THPC-mediated PDT

m-THPC is derived from chlorin and gets its fluorescence properties from aromatic rings (benzene rings and porphyrin structures) (Figure1.15A). *m*-THPC is lipophilic and non-polar (Müller *et al.*, 1998), received regulatory approval in 2002 in the European Union for human patients for advanced palliative treatment of head and neck cancers, and has since been shown to be effective in treating early squamous cell carcinoma (Laville *et al.*, 2003; Sasnouski *et al.*, 2006).

m-THPC has strong absorption in the visible light region of 650- 652 nm with an absorption coefficient of 22400 l/mol/cm (Müller *et al.*, 1998) (Figure 1.14). *m*-THPC also has high photochemical efficiency, which means that lower light doses and/or shorter illumination times are required to display a tumouricidal effect of

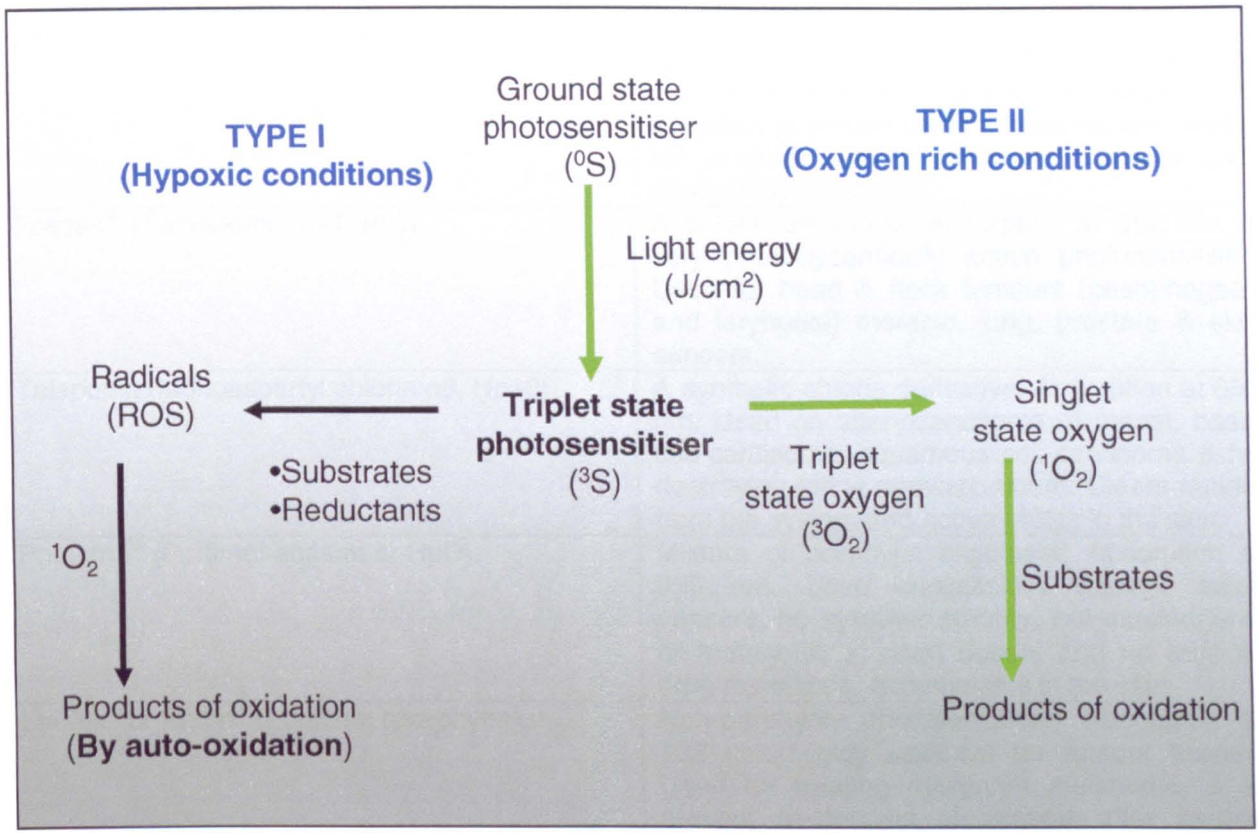

Figure 1.13
Type I and II PDT processes leading to oxidation products.
Light energy absorbed by ground state photosensitiser (^{0}S) results in excited triplet state photosensitiser (^{3}S). ^{3}S fuels either the type I or the type II process; both these processes can result in oxidative tissue damage due to the generation of products of oxidation.

Photosensitisers	Details
Levulan® (5- Aminolevulinate; 5-ALA)	Pro-drug of the photosensitiser protoporphyrin-IX (PpIX): Absorption at 635 nm. Used for superficial tumours, actinic keratosis, the detection of certain bladder tumours, and tested for prostate cancer treatment. Causes pain during PDT treatment.
Foscan® (Temoporfin; *m*-THPC)	A chlorin derivative: Absorption at 652 nm. A very photodynamically active photosensitiser. Used for head & neck tumours (oesophageal, and laryngeal) thoracic, lung, prostate & skin cancers.
Talaporfin (Monoaspartyl chlorin e6, Npe6)	A synthetic chlorin derivative: Absorption at 664 nm. Used on adenocarcinoma of breast, basal cell carcinoma, squamous cell carcinoma & for destroying retina neovasculature. Clears rapidly from the system and accumulates in the skin.
Photofrin® (Porfimer sodium or HpD)	Mixture of porphyrin oligomers: Absorption at 630 nm. Used successfully against many cancers, no systemic toxicity, not carcinogenic or mutagenic at used doses, and no multiple drug resistance. Accumulates in the skin.
Lu-Tex® or Antrin® (Lutetium texaphyrin)	Non-porphyrin photosensitiser: Absorption at 732 nm. Highly selective for tumour tissues. Used for treating malignant melanoma, & to prevent re-stenosis of vessels after cardiac angioplasty.
Visudyne® (Verteporfin)	Benzoporphyrin derivative monoacid ring A (BPD-MA): Absorption at 690 nm. Low tumour selectivity, unfavourable for PDT of some cancers (clears too quickly from system), and tested for vertebral metastases. Used for treating wet form of age-related macular degeneration by destroying neovasculature.
Hypericin	Natural compound extracted from *St John's Wort*: Absorption at 599 nm. Promising photosensitiser agent for pituitary and prostate tumours
Photosens (AlPcSn)	Sulphonated aluminium phthalocyanine: Absorption at 675 nm. Tested for brain and liver tumours, and age-related macular degeneration.

Table 1.1
Some frequently administered photosensitisers.
(Chang *et al.* 1997;Colasanti *et al.* 2000; reviewed by Macdonald and Dougherty, 2001; Algermissen *et al.* 2003; Burch *et al.* 2003; Moore *et al.* 2006; Betz *et al.* 2007; Cole *et al.* 2008; Nyst *et al.* 2009)

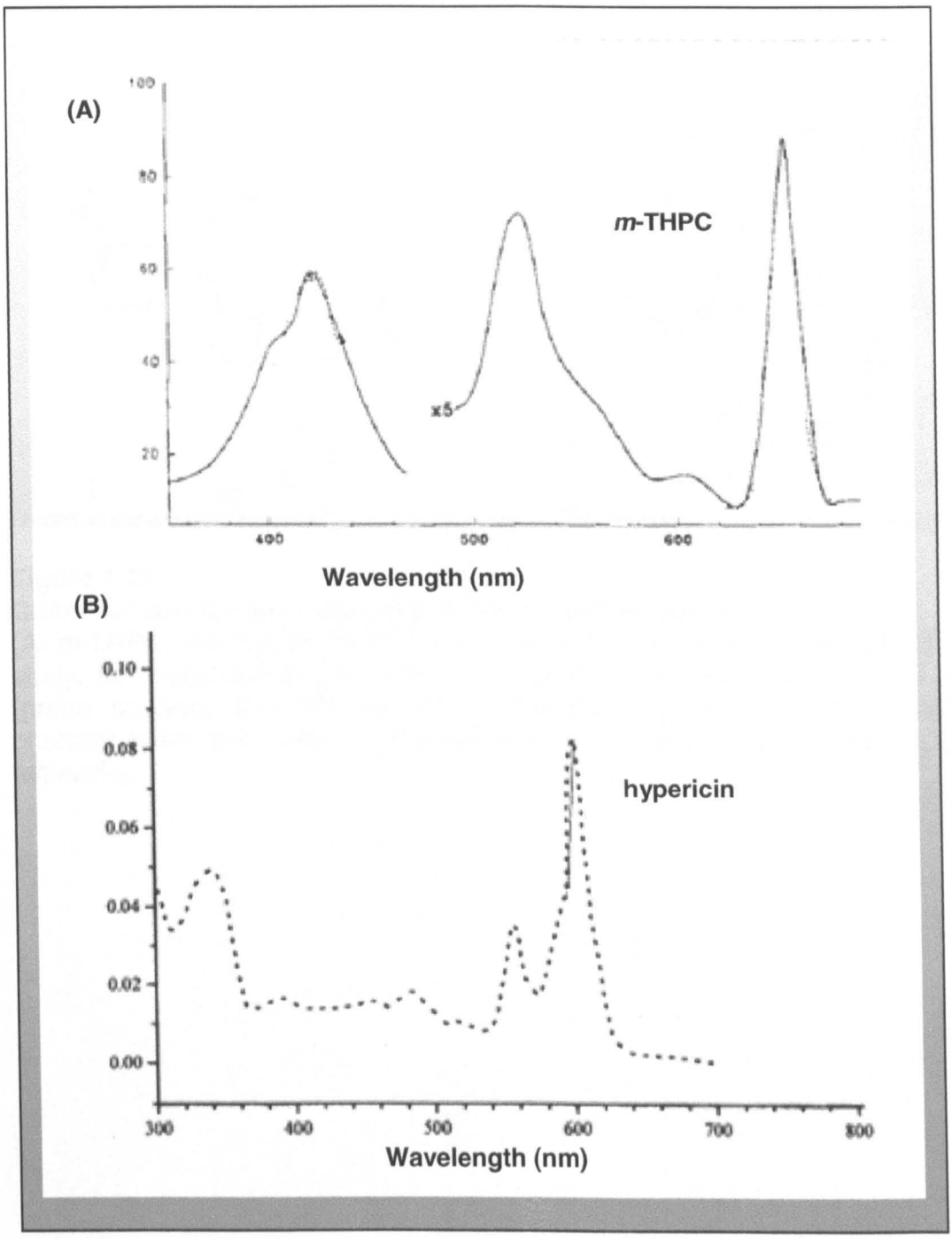

Figure 1.14
Spectra of *m*-THPC and hypericin.
(**A**) 0.5 µg/ml *m*-THPC incubated for 24 h in MEM with 10 % serum, peak absorption at 652 nm wavelength (Adapted from Ma *et al.*, 1994) and (**B**) 1 µg/ml hypericin dissolved in DMSO and then culture medium, peak absorption at 592 nm wavelengths. (Taken from Colasanti *et al.*, 2000)

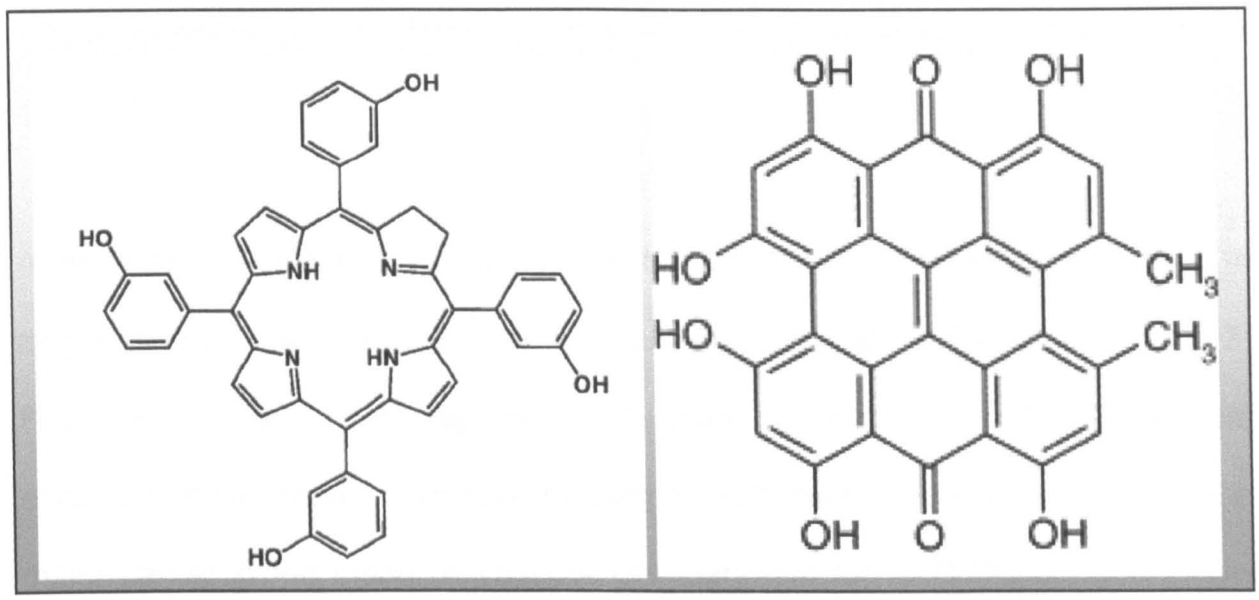

Figure 1.15
Chemical structures of photosensitisers used in this study.
(**A**) *m*-THPC (Adapted from Klein *et al.*, 1997). This is the photosensitiser of interest in this study, its structure shows 4 benzene rings (Blue circles) attached to a porphyrin ring (green square), and (**B**) hypericin (Adapted from Saw *et al.*, 2005). This is a photosensitiser also used in this study; it has benzene ring structures (a polyphenol molecule).

m-THPC-mediated PDT in comparison to other photosensitisers (Morlet *et al.*, 1997; Vrouenraets *et al.*, 1999; Moan *et al.*,1999; Marchal *et al.*, 2005; Moore *et al.*, 2006).

A side-effect of *m*-THPC use is its induction of skin photosensitisation due to its long-lasting localisation in skin tissues (Moore *et al.*, 2006; Morlet *et al.*, 1997). Sasnouski *et al.* (2006) reported that upon i.v. injection, *m*-THPC will first encounter blood plasma proteins; binding to high density lipoprotein (HDL) as its major carrier in the blood. A vascular compartment for *m*-THPC storage *in vivo* influences the rate of *m*-THPC redistribution in the body and gives *m*-THPC a lower rate of redistribution in comparison to other photosensitisers. *m*-THPC is redistributed in the blood by binding to different plasma proteins, this is while it remains tightly bound to lipoproteins and HDL. HDLs are large complexes which prevent a rapid diffusion of *m*-THPC through the blood vessel walls and into the surrounding tissue, and so also results in the long retention of *m*-THPC in the vasculature (Sasnouski *et al.*, 2006). This long retention in the vasculature can be additionally used in PDT as a means of destroying blood supply to tumours.

m-THPC-mediated PDT has been shown to cause photodamage, at least in part, by a type II process *in vitro* (Figure 1.11 and 1.13); as determined with the aid of molecular scavengers (Ma *et al.*, 1994; Melnikova *et al.*, 1999b). This dependence on oxygen to display tumourcidal effects; therefore makes *m*-THPC-mediated PDT very sensitive to oxygen concentration at treatment sites (Sasnouski *et al.*, 2006). However, Ochsner (1997) has also reported that *m*-THPC-mediated PDT may act not only by a type II process, but by both type I and type II processes *in vitro*.

1.3.2.2 General features of hypericin and hypericin-mediated PDT

Another photosensitiser used in PDT is hypericin (Figure 1.15B). Hypericin is a naturally-occurring polycyclic quinone photosensitiser compound, which can be extracted from the herb *Hypericum perforatum* (St. John's Wort) (reviewed by Kubin *et al.* 2005; Mikeš *et al.*, 2007). Hypericin has aromatic benzene ring structures (a polyphenol molecule) which gives this compound its fluorescent properties (Figure 1.15B), and is sparingly soluble in water (hydrophobic) (Saw *et al.*, 2005; Van De Putte *et al.*, 2006). Like *m*-THPC, hypericin has been investigated for its usefulness in treating prostate cancer (Colasanti *et al.*, 2000; Xie *et al.*, 2001), bladder cancer (Kamuhabwa *et al.*, 2004), breast cancer (Blank *et al.*, 2004) and brain associated tumours: pituitary (Cole C.D. *et al.* 2008) and gliomas (Miccoli *et al.*, 1998; Ritz R. *et al.*, 2005; Ritz R. *et al.*, 2007).

Kubin *et al.* (2005) reported hypericin as a compound with diverse uses. In addition to its use as a photosensitising agent in PDT it is commonly tested and used as an anti-depressive, anti-retroviral, anti-neoplastic, and as a photodiagnostic agent. Hypericin is also reported to have anti-inflammatory properties (Pajonk *et al.*, 2005) and, on light activation, anti-viral and anti-tumour activity (Das K. *et al.*, 1999).

Hypericin-mediated PDT has been reported as occurring by a type II process (Kubin *et al.*, 2005). But, Mikeš *et al.* (2007) have reported high efficiency in the production of both $^1O_2$ (type II) and $O_2^{\bullet-}$ (type I) after visible light illumination of ~ 600 nm wavelength (Figure 1.14), and hypericin has low or no dark toxicity. These findings were similar for *m*-THPC-mediated PDT.

1.3.3 Effects of $^1O_2$ /ROS on biological molecules of the cell

Under normal conditions, cytosolic ROS can be generated in eukaryotic cells during normal energy metabolism (e.g. mitochondrial electron transport and oxidative phosphorylation) and by metabolism of redox-cycling xenobiotics (e.g. anthracyclines) (Girotti, 2001; Du *et al.*, 2001; Scherz-Shouval and Elazar, 2007). These ROS are usually kept under control by antioxidant molecules such as glutathione (GSH) and antioxidant enzymes such as superoxide dismutase (SOD), and therefore do not cause toxic effects in cells.

Superoxide ($O_2^{\bullet-}$) is the major type of ROS generated in mitochondria and can interact with nitric oxide ($NO^{\bullet}$) to form reactive non-radicals (i.e. peroxynitrite ($ONOO^-$)), which may also damage cells by promoting membrane lipid peroxidation and nitration of proteins on tyrosine residues (Keller *et al.*, 1998). $O_2^{\bullet-}$ is usually considered as a precursor of more reactive species; it is known to promote the production of secondary derivatives such as hydrogen peroxide (H_2O_2), and $HO^{\bullet}$ in intracellular oxidative chain events (Du *et al.*, 2001). Reductant species also produce these cytotoxic species (Melnikova *et al.*, 1999c; Girotti, 2001) (Table 1.2).

However, the high level of $^1O_2$/ROS generated by PDT is known to affect many biological molecules within the cell. Nucleic acids, proteins and unsaturated lipids are prominent targets of $^1O_2$/ROS attack in cells exposed to PDT (Girotti, 2001).

Free radicals ions		Reactive non-radicals	
Superoxide	$O_2^{\bullet-}$	Hydrogen peroxide	H_2O_2
Hydroxyl	$HO^{\bullet}$	Lipid hydroperoxide	LOOH
Hydroperoxyl	$HOO^{\bullet}$	Cholesterol hydroperoxide	ChOOH
Lipid peroxyl	$LOO^{\bullet}$	Peroxynitrite	$ONOO^-$
Nitric oxide	$NO^{\bullet}$	Singlet oxygen	$^1O_2$
Thiol radicals	$RS^{\bullet}$		

Table 1.2
Simplified table of some reactive radical and non-radical molecules that commonly form in cells.
Increased formation of these cell toxic molecules occurs during the application of PDT.

1.3.4 Subcellular localisation of PDT-induced oxidative stress

In biological systems, PDT generated $^1O_2$ diffuses short distances from the point of generation, and hence principally causes damage close to the site of production. $^1O_2$ has a half-life of < 0.04 μs, and a radius of action of approximately 0.01-0.02 μm (Agostinis *et al.*, 2004; Buytaert *et al.*, 2007; Berg, 2007).

PDT-induced oxidative stress can cause damage to specific organelles including plasma membranes, mitochondria, lysosomes and ER (Ball *et al.*, 1998; Castano *et al.*, 2005). If the photosensitiser used in PDT is amphiphilic (having both hydrophilic and hydrophobic properties) (reviewed by Macdonald and Dougherty, 2001) and localises in the lipid bilayer, membrane lipids such as phospholipids and cholesterol, which are known targets for oxidative modification, may be affected. Lipid hydroperoxides (LOOHs) are formed, resulting in membrane damage and cell death (Girotti, 2001; Wang *et al.*, 2001). LOOHs including cholesterol hydroperoxide (ChOOH) are key reactive non-radical intermediates in the mechanism of PDT (Girotti 2001; Wang *et al.*, 2001) (Table 1.2). LOOHs are also involved in the mediation of signalling cascades, which either fortify antioxidant defences of cells or evoke apoptotic cell death if the oxidative pressure is too great. In addition, cholesterol hydroperoxide (ChOOH) is generated by both type I and type II processes (Girotti, 2001).

1.4 Mechanisms of PDT-induced cell death

Cell death primarily occurs through 2 pathways: apoptosis and/or necrosis. There is also a third mode of cell death, which is known as autophagic cell death. Ionising radiation and chemotherapy can induce apoptosis in cancer cells by

damaging DNA. In contrast, PDT produces an acute stress response that can lead to apoptosis, necrosis and/or autophagy. In this section, the main characteristics of these different cell death mechanisms are summarised, followed by a description of how PDT activates these processes.

1.4.1 Apoptosis

Apoptosis is a regulated complex process, which involves the activation of a cascade of proteases, known as caspases (Banasiak *et al.*, 2000). Apoptotic caspases act in 2 main pathways: the intrinsic pathway in which mitochondria play a central role; and the extrinsic pathway which is triggered by binding of death ligands to cell plasma membrane death receptors (DR) (Gupta, 2002; Agostinis *et al.*, 2002; Simstein *et al.* 2003; Agostinis *et al.*, 2004; Artal-Sanz and Tavernarakis, 2005; Castano *et al.*, 2005; Buytaert *et al.*, 2007) (Figure 1.16).

Apoptotic cell death involves a characteristic sequence of morphological, biochemical and energetic changes. Initial stages of this active cell death show little damage to the organelles, and plasma membranes remain intact (Becker and Bonni, 2004; Plaetzer *et al.*, 2003; Buytaert *et al.*, 2007). Cells dying by apoptosis are known not to adversely affect neighbouring cells, because cell contents are digested and not released. *In vivo*, apoptotic cells are characterised by cell rounding and loosening from their surroundings. Morphological features of apoptotic cell death also include cell shrinkage, shrunken nuclei with condensed chromatin, DNA fragmentation at inter-nucleosomal sites, formation of autophagic vacuoles in the dying cell cytoplasm, cell surface membrane blebbing, and plasma membrane breakdown in later phases (Collins *et al.*, 1997; Willingham, 1999; Noodt *et al.*, 1999; Banasiak *et al.*, 2000; Leung *et al.*, 2002; Inbal *et al.*, 2002;

Zong and Thompson, 2006; Buytaert *et al.*, 2007). Also in the later phase of apoptosis, condensed apoptotic bodies develop, which contain cytoplasm, whole organelles and nucleic fragments (Noodt *et al.*, 1999; Inbal *et al.*, 2002; Zong and Thompson, 2006).

In relation to PDT, ROS generated from a type I process is more likely to result in the activation of an intrinsic apoptosis pathway in cells, rather than $^1O_2$ generated from a type II process (Buytaert *et al.*, 2007).

1.4.2 Autophagic cell death

In mammalian cells, autophagy is generally known to promote cell survival by removing damaged organelles, toxic metabolites and intracellular pathogens by delivering them to lysosomes for recycling (Buytaert *et al.*, 2007; Scherz-Shouval and Elazar, 2007; Chen *et al.*, 2008) (Figure 1.17). However, unregulated autophagy can result in cell death rather than cell survival. During autophagic cell death, structures called autophagosomes (double membrane structures) are formed from membranes enclosing cytoplasm; these fuse with lysosomes to be degraded by the cell (Mizushima *et al.*, 2002).

The main features of autophagy are appearances of abundant autophagic vacuoles in the cytoplasm, which are accompanied by mitochondrial dilation, enlargement of ER and Golgi apparatus, nuclear pyknosis, membrane blebbing, and heterophagic elimination (Inbal *et al.*, 2002).

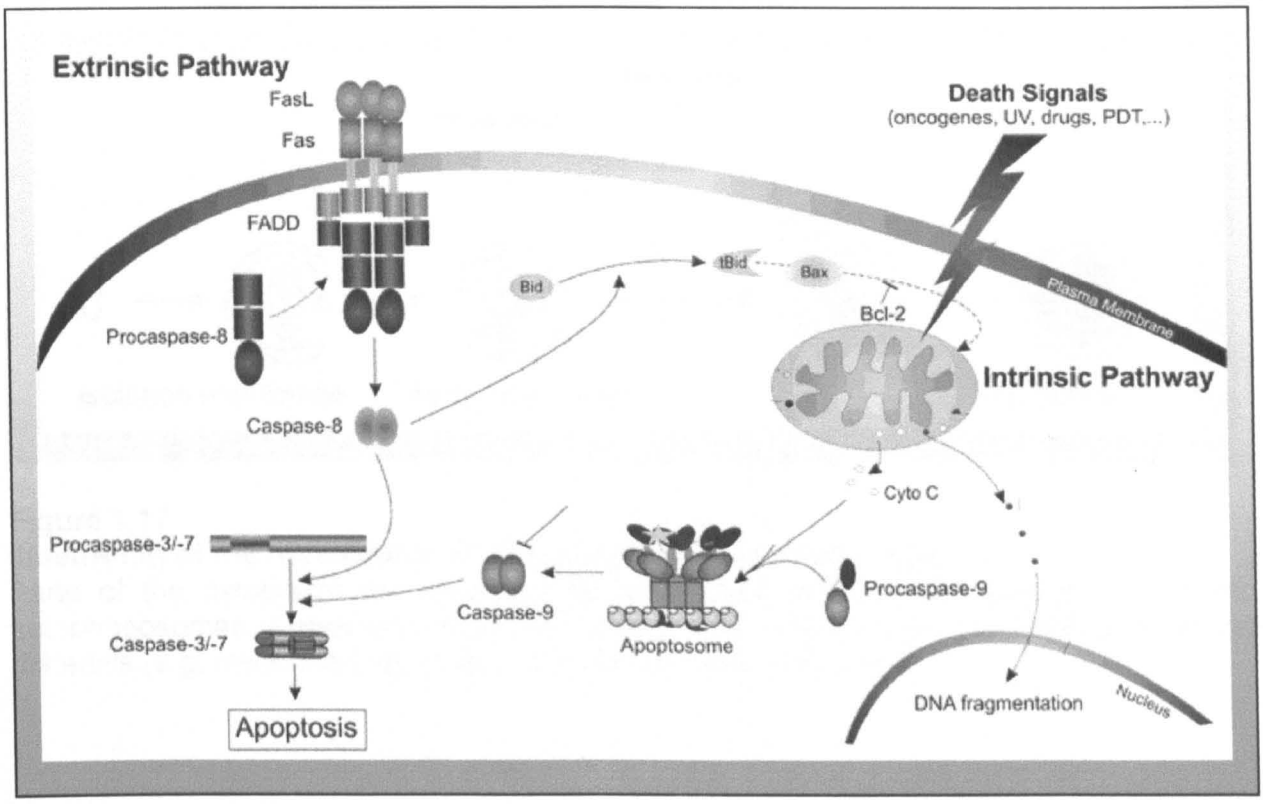

Figure 1.16
Illustration shows a simplified diagram of the intrinsic and extrinsic apoptotic pathways.
Apoptotic cell death involves many molecular 'players', some of which are shown in this diagram. Bcl-2 (a family of proteins that regulate apoptosis), which includes Bid (BH3 interacting domain death agonist) and Bax (Bcl-2–associated X protein), are involved in this mechanism of cell death. Fas (death receptor, DR), FasL (DR ligand), FADD (Fas-associated protein with death domain), Cyto *C* (Cytochrome *C*) (Adapted from Agostinis *et al.*, 2004)

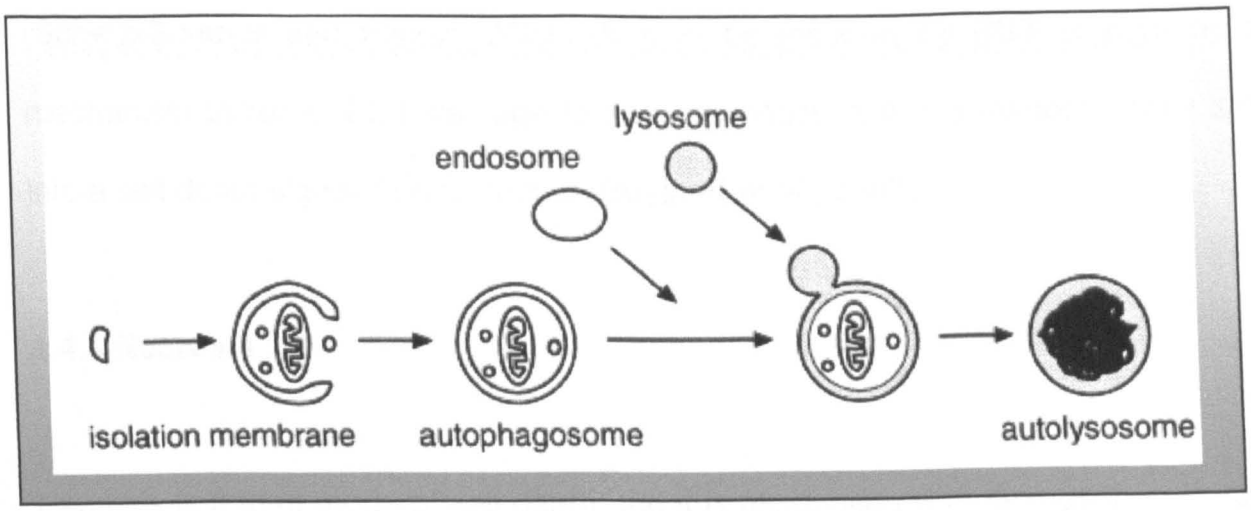

Figure 1.17
Illustration of the mechanism of autophagy in mammalian cells.
Parts of the cytoplasm are enclosed by autophagic isolation membrane. This forms autophagosomes. These then fuse with endosomes or lysosomes to degrade enclosed materials (e.g. mitochondria). (Taken from Mizushima *et al.*, 2002)

Autophagy has an important role in the cellular responses to oxidative stress (Scherz-Shouval and Elazar, 2007). It may be induced by PDT in cells as a mechanism to repair PDT damage to key organelles, but this response may turn into a cell death signal if uncontrolled (Buytaert *et al.*, 2007).

1.4.3 Necrosis

Necrosis is a third mode of cell death and it is associated with disruption or break-down of the plasma membrane. Unlike apoptosis it results in damage to neighbouring cells, and *in vivo* it results in the development of inflammation due to uncontrolled leakage of intracellular material into the extracellular space (Ball *et al.*, 1998; Plaetzer *et al.*, 2003). Necrosis is often thought of as a rapidly occurring event, the primary cause of which is the consequence of loss of membrane integrity and alterations or loss in metabolic homeostasis control, due to peroxidation of membrane lipids and proteins (Banasiak *et al.*, 2000; Plaetzer *et al.*, 2003). Therefore necrotic cell death occurs due to deregulation of normal cellular activities, for example after exposure to extreme stress conditions (Artal-Sanz and Tavernarakis, 2005), resulting in intracellular adenosine triphosphate (ATP) depletion to a level that is incompatible with cell survival or with apoptosis (Plaetzer *et al.*, 2003; Buytaert *et al.*, 2007). Necrosis is therefore generally thought to be a passive form of cell death (Plaetzer *et al.*, 2003; Ball *et al.*, 1998). However, recent studies have indicated that necrotic cell death may be actively propagated as part of a signal transduction pathway (Buytaert *et al.*, 2007). Necrosis can also occur late in apoptosis (Heinzelmann-Schwarz *et al.*, 2003); this type of necrosis is referred to as apoptotic necrosis or secondary necrosis (Zong and Thompson, 2006).

Morphological characteristics of necrosis includes vacuolisation of the cytoplasm, cell swelling and breakdown of the plasma membrane, ill-defined cytoplasm, coarse chromatin pattern, karyolysis and dilation of the ER (Leung *et al.*, 2002; Plaetzer *et al.*, 2003; Artal-Sanz and Tavernarakis, 2005; Buytaert *et al.*, 2007). In addition, electron microscopy can identify necrotic cell death as defined by electron-lucent cytoplasm, swelling of cellular organelles, and loss of plasma membrane integrity (Zong and Thompson, 2006).

Buytaert *et al.* (2007) reported that $^1O_2$ produced during PDT at the membranes of ER and Golgi apparatus is able to mediate necrosis in PDT treated cells. While no definitive biochemical pathway mediating necrosis following PDT has been identified as yet, certain factors such as Ca^{2+} overload and the origin and type of generated ROS may be decisive in promoting a necrotic cell death pathway. Further to this, with the use of membrane-associated photosensitisers, a shift from apoptotic to necrotic cell death is usually provoked by an increase in oxidative stress generated during PDT (e.g. by increasing either applied light, and to some extent photosensitiser concentration or incubation time) (Plaetzer *et al.*, 2003; Agostinis *et al.*, 2004; Buytaert *et al.*, 2007).

1.5 A review of nerve response to PDT

Since 1996, most research published on the effect of PDT on peripheral nerves *in vitro* has been performed by Uzdensky *et al.* Their research mainly focused on the use of an isolated crayfish abdominal stretch receptor (mechanoreceptor) nerve culture system that consists of 2 sensory neurones enwrapped by satellite cells (Uzdensky *et al.*, 2005; Uzdensky *et al.*, 2007; Fedorenko and Uzdensky, 2008; Fedorenko and Uzdensky, 2009) (Figure 1.18).

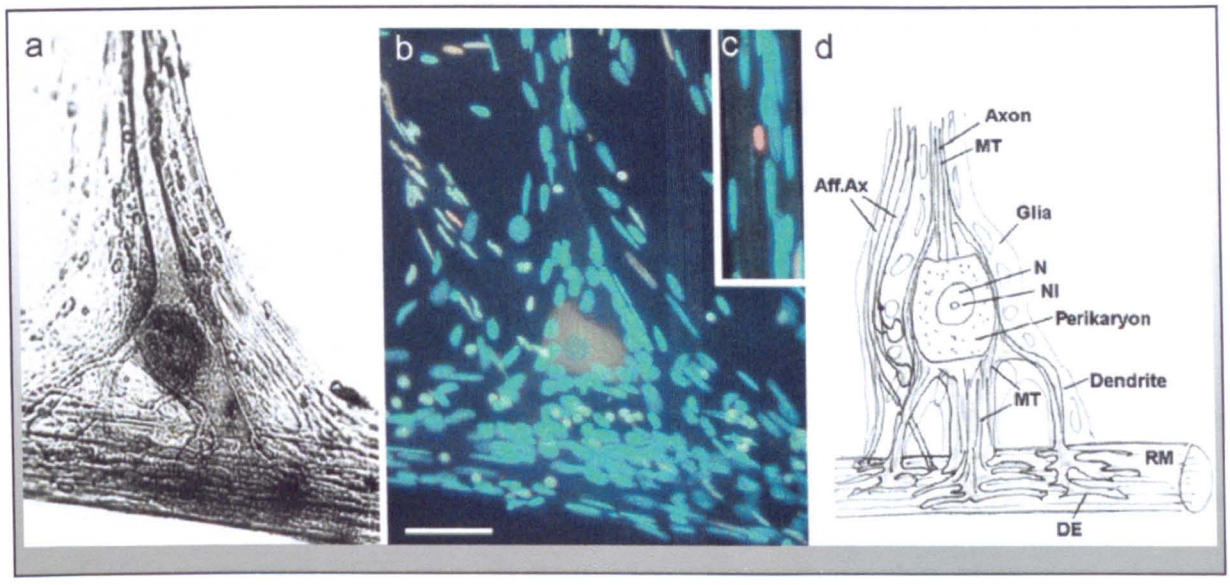

Figure 1.18
An isolated crayfish mechanoreceptor.
(**a**) Brightfield micrograph; (**b**) Fluorescence micrograph; (**c**) Fluorescence micrograph of the stretch receptor; and (**d**) Diagram of the nerve culture system preparation. Hoechst DNA nuclei stain (blue-green), propidium iodide (PI) dead cell nuclei stain (red). RM (receptor muscle), MT (microtubules), DE (dentritic ending), N (nucleus), Nl (nucleolus) and Aff.Ax (afferent axons) and scale bar is 50 μm. (Taken from Fedorenko and Uzdensky, 2009)

Work of this research group touched briefly on the effects of *m*-THPC-mediated PDT on isolated crayfish nerves. They have shown high PDT efficiency at 0.001-1 μM (0.007-7 μgml) *m*-THPC, in relation to loss of nerve firing potential. In general the life time of neuronal survival in these crayfish nerves was found to depend on the concentration of the photosensitiser used for PDT treatment. The use of some concentrations of photosensitisers tested by this group showed reversible cessation of neural activity; however, it was found that with *m*-THPC-mediated PDT, the concentration of *m*-THPC did not correlate with neuronal death. Instead, *m*-THPC-mediated PDT was observed to cause irreversible cessation of neurone activity at nanomolar or nanogram concentrations (Uzdensky *et. al.* 2004).

In addition to *m*-THPC, hypericin was studied in the crayfish nerve culture system (Bragin *et al.* 2003). Hypericin was also initially studied as a protein kinase C (PKC) inhibitor, and then later as a photosensitiser in its own right (Bragin *et al.*, 2003; Uzdensky *et al.*, 2003). Hypericin was found to be toxic to crayfish nerves at concentrations higher than 20 μM (11 μg/ml), and was predominantly located in glial cells surrounding the neurone. Only a small amount of hypericin was detected in the neurone perinuclear region, which is known to be rich in organelles, and on illumination hypericin was found to be redistributed from the plasma membrane to intracellular organelles (Uzdensky *et al.*, 2003).

The photosensitiser Photosens ($AlPcS_n$) was the most extensively studied photosensitiser by this group, and like hypericin, also showed predominant localisation in glial cells. This finding suggested that glial cells would be more vulnerable to photodamage than neurones during PDT with this photosensitiser. This observation opened up the possibility of selective PDT killing of malignant glial cells in the nervous system (e.g. in the brain); therefore possibly allowing

neurones to remain undamaged after Photosens-mediated PDT (Uzdensky *et al.*, 2005). Further to these studies, Kolosov and Uzdensky (2006) have shown that neurones in this crayfish nerve culture system were possible protecting glial cells from Photosens-mediated PDT-induced apoptotic cell death. There were also indications that this possible protection was mediated by the release of signalling molecules from neurones.

Photosens-mediated PDT on intact isolated crayfish nerve showed irreversible functional inactivation (nerve firing) and necrosis in neurones (Uzdensky *et al.*, 2007). Using dissociated neural cells from these crayfish nerves revealed a combination of necrosis, apoptosis and proliferation of satellite cells *in vitro* (Lobanov and Uzdensky, 2005). Crayfish satellite cells were found to be more sensitive to photosens-mediated PDT treatments than neurones (Lobanov and Uzdensky, 2005). Uzdensky *et al.* (2002) also demonstrated with photosens-mediated PDT, that different death modes were achievable with the administration of different concentrations of a photosensitiser. Intense photosensitisation resulted in necrosis, and weaker photosensitisation resulted in apoptosis. Recent studies by this group reported slight changes in neuronal ultrastructure in neurones 5 min post-PDT treatment for example alterations in some mitochondria and vascularisation of cytoplasm, and compensatory changes such as formation of lysosomes and autophagosomes. However, after 30 min post-PDT they detected more marked changes such as abolition of neurone firing, and destruction of mitochondria and Golgi apparatus (Fedorenko and Uzdensky, 2008).

Other research in relation to the effect of PDT on peripheral nerves includes the work of Kübler *et al.* (2003), who reported that 24 h after the administration of 0.3 mg/kg *m*-THPC to rabbits *in vivo*, followed by the illumination of nerves in the neck

and groin area, damage to connective tissue was observed, and there was 75 % demyelination to the nerve that did not result in any clinical symptoms. Also, Ris *et al.* (1997) has reported that virtually all intrathoracic tissue were severely damaged, but not the nerves, 12 h to 6 days after the administration of 0.1 mg/kg *m*-THPC-mediated PDT in minipigs.

1.6 Cellular antioxidant protective pathways

Low levels of ROS are normally reduced by non-enzymatic and enzymatic antioxidising agents (i.e. GSH, thioredoxin, SOD, catalase and peroxidises), in order to keep cells alive (Table 1.3) (Scherz-Shouval and Elazar, 2007). The interplay of SOD, catalase and GSH with the aid of glutathione peroxidise (GPx) controls the intracellular accumulation of H_2O_2 (Figure 1.19) and therefore protects the cells against oxidative damage induced by H_2O_2 itself or by $HO^{\bullet}$.

1.6.1 Glutathione synthase intracellular antioxidant pathway

1.6.1.1 Glutathione synthase pathway

The γ-glutamyl cycle (Meister, 1994; Marks *et al.*, 1996a), also known as the glutathione synthase pathway, generates the antioxidant molecule GSH (Mytilineou *et al.*, 1999). This pathway regulates the cytoplasmic and mitochondrial localised GSH antioxidant pools, which represent the mammalian cells main redox buffer against oxidative stress (Nicole *et al.*, 1998; Nicholls and Budd, 2000); therefore modest changes in GSH concentration can strongly alter the redox state of cells (Nicole *et al.*, 1998). GSH is the most abundant intracellular small molecule thiol present in mammalian cells (Mytilineou *et al.*, 1999; Scherz-Shouval

Antioxidants	Functions
GSH	Reacts with a number of oxidising agents
SOD	Catalyses the formation of H_2O_2 from ROS
GPx	Catalyses the breakdown of H_2O_2 by reacting with GSH
Catalase	Catalyses the breakdown of H_2O_2
Vitamin E	Important in limiting damage to membrane during lipid peroxidation
Vitamin C	Deactivating ROS and aiding Vitamin E
Thioredoxin	Facilitates reduction using cysteine thiol-disulphide exchange

Table 1.3
Primary antioxidant defences.
Table shows a list of antioxidant defence molecules which act in unison to protect the body against cell damage. GSH (*N*-(*N*-L-γ-glutamyl-L-cysteinyl)glycine) or glutathione), SOD (superoxide dismutase), GPx (glutathione peroxidise), H_2O_2 (hydrogen peroxide), ROS (reactive oxygen species), Vitamin C (L-ascorbic acid) and Vitamin E (α-tocopherol).

and Elazar, 2007; Lewis-Wambi *et al.*, 2008), it is present in cells at a millimolar concentration, and is the main alternative target for ROS apart from protein-sulfhydryl (-SH) groups in cells (Witold and Grzegorz, 2000). In the brain GSH concentration has been reported at a level of 1 to 2 mM (Mytilineou *et al.*, 1999). GSH functions to detoxify peroxides and ROS from cells, providing cells with a reducing ability (Nicole *et al.*, 1998; Mytilineou *et al.*, 1999; Lewis-Wambi *et al.*, 2008).

In this study the inhibition of the rate-limiting step enzyme γ-glutamyl-cysteine synthetase (γ-GCS) (Figure 1.19 and1.20) was investigated for its effect on PDT induced cell death of neural cells.

1.6.1.2 Glutathione oxidation-reduction pathway

The glutathione oxidation-reduction pathway links the glutathione synthase pathway to the SOD pathway (Figure 1.19). The main half of the glutathione oxidation-reduction pathway involves the formation of glutathione disulfide (GSSG) from the oxidation of the protein–SH group (an electron donor) of GSH, when H_2O_2 is reduced to H_2O with GPx (GSH peroxidase) (Meister, 1994; Marks *et al.*,1996b; Nicole *et al.*, 1998; Alberts *et al.*, 2008), a direct reaction of GSH scavenging for free radicals.

The second half of the glutathione oxidation-reduction pathway involves the re-formation of the antioxidant molecule GSH using nicotinamide adenine dinucleotide phosphate ($NADPH^+$) and a proton (H^+) from the pentose phosphate pathway (Meister, 1994; Marks *et al.*, 1996b), in combination with GR (GSH)

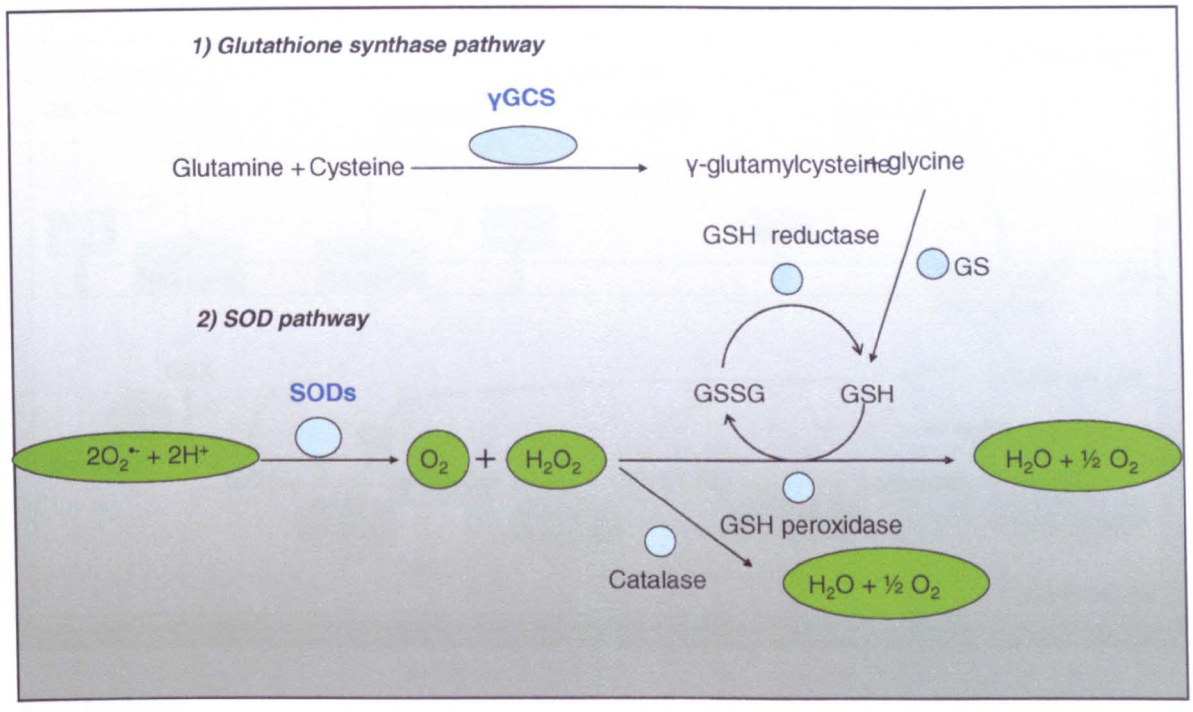

Figure 1.19
A simplified illustration of the interactions of the glutathione synthase, SOD and catalase intracellular antioxidant pathways.
GSH (reduced glutathione), GSSG (oxidised form of GSH-glutathione disulfide glutathione), GS (Glutathione synthase), γ-GCS (γ-Glutamyl-Cysteine synthetase) and (SOD) superoxide dismutase.

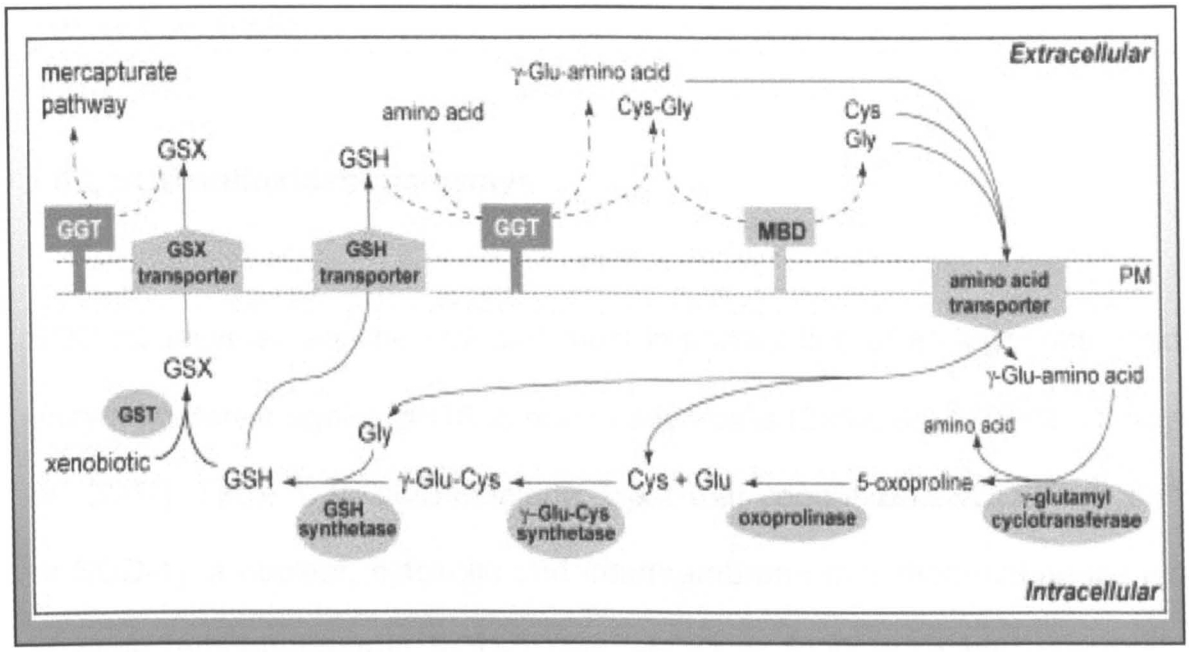

Figure 1.20
Illustration of the glutathione synthase pathway.
Illustration shows that GSH is exported through the cell membrane and is metabolised by the membrane-bound GGT (γ-glutamyltransferase) and MBD (membrane bound Cys-Gly dipeptidase). This cleaves GSH into its component amino acids (cysteine, glycine and glutamine), which are ultimately recycled to form new GSH molecules. In the extracellular space γ-glutamyl covalently bonded to amino acids is transported into the cell through amino acid transporters. Amino acids are then removed from the γ-glutamyl-amino acid molecule by γ-GCT (γ-glutamyl-cyclotransferase) forming 5-Oxoproline. 5-Oxoproline is cleaved releasing glutamyl. This glutamyl molecule is linked to cysteine by γ-GCS (γ-glutamyl-cysteine synthetase) to form γ-glutamylcysteine. This ATP-dependent reaction is the overall rate-limiting step in the pathway. GSH synthetase is used to link Gly to γ-glutamylcysteine forming GSH. GSH is either exported out of the cell directly by GSH transporters or combines with xenobiotics using GST to form GSX for cell export (Taken from Martin *et al.*, 2007).

reductase) (Meister, 1994; Marks *et al.*, 1996b; Nicole *et al.*, 1998) (Figure 1.19), directly from GSSH.

1.6.2 SOD antioxidant pathways

SOD isoenzymes are the first and most important line of endogenous antioxidant enzyme defence against ROS in mammalian cells (Zelko *et al.*, 2002; Dimayuga *et al.*, 2007) (Table 1.3). SODs include: the dimer copper-zinc SOD (Cu^{2+},Zn^{2+}-SOD or SOD-1), a nuclear, cytosolic and intermembrane mitochondrial space localised enzyme; homotetrameric SOD-2 (Mn^{2+}-SOD or SOD-2); a mitochondrial matrix localised enzyme (Keller *et al.*, 1998; Zelko *et al.*, 2002; Antonyuk *et al.*, 2009; Perry *et al.*, 2009); and copper (Cu^{2+})- and zinc (Zn^{2+})-containing glycoprotein dimer (extracellular-SOD or SOD-3), a soluble extracellular enzyme (Zelko *et al.*, 2002; Antonyuk *et al.*, 2009; Perry *et al.*, 2009). These enzymes are critical in controlling levels of ROS within cells (Perry *et al.*, 2009). SOD scavenges $O_2^{\bullet-}$ (Tanioka *et al.*, 2005; Ochsner, 1997), preventing its accumulation by converting it to H_2O_2 (Keller *et al.*, 1998), by catalyzing the reaction shown in Figure 1.19. Toxic H_2O_2 generated from the SOD pathway is further metabolised to H_2O by either the glutathione oxidation-reduction pathway or the catalase pathway (Alberts *et al.*, 2008) Figure 1.19.

In this study, the inhibition of SOD enzymes (Figure 1.19) was investigated for their effects on PDT-induced cell death of neural cells.

1.7 Research aims and objectives

The overall aims of this research project were to provide scientific insight into the biological basis of peripheral nerve sparing during PDT; to increase the understanding of the interactions of *m*-THPC-mediated PDT with the adult mammalian peripheral nervous system at a cellular level; and to develop suitable nerve models for use in this study and future nerve PDT investigations. No previous cell culture research on the effects of *m*-THPC-mediated PDT on mammalian peripheral nerves has been performed, so this work represents the first reported study.

The objectives of the work were first, to determine the cell-specific effects of PDT on neural cells in comparison to tumour cells. This led to a second objective; to determine why DRG neurones were less susceptible to *m*-THPC-mediated PDT in comparison to other cell types (satellite cells, astrocytes and the human breast cancer cell line MCF-7). A third objective was to develop 2-dimensional (2D or monolayer) or 3D tissue engineered nerve culture systems, suitable for use in evaluating the effects of focally applied PDT. The culture system would enable different parts of the neurone to be exposed to PDT (i.e. neuronal cell bodies, neurites or growth cones).

Results from this project will be of interest to both researchers and clinicians who are involved in the study and treatment of tumours in close association with nerve structures.

Chapter 2: Materials and Methods

2.1 Suppliers and materials

Generally all reagents were of tissue culture and/ or analytical grade:

2.1.1 Photosensitisers

bioLITEC PHARMA Ltd AG, Jena (Germany) **Gift of Dr Alexander MacRobert (National Medical Laser Centre, (UCL))**	**Foscan® containing 4 mg/ml temoporfin, Meta-(tetra-hydroxyphenyl) chlorin (*m*-THPC)**
TOCRIS bioscience, Tocris Cookson Ltd (UK)	1,3,4,6,8,13-Hexahydroxy-10,11-dimethylphenanthro[1,10,9,8-opqra]perylene-7,14-dione (hypericin) (Cat. no.1520)

2.1.2 Primary antibodies (Ab)

COVANCE, California (USA)	**Mouse Monoclonal Antibody Anti-Neurofilaments Hypophosphorylated (SMI 35) (Cat. no. SMI-35R)**
DakoCytomation (Denmark)	Rabbit Polyclonal Antibody Anti-S-100 (Cat. no. Z0311)
Sigma Aldrich (UK)	Mouse Monoclonal Antibody Anti-β-tubulin Isotype III, Clone SDL-3D10 (Cat. no. T-8660)

	Rabbit Polyclonal IgG Anti-Laminin 1 (Cat. no. L-9393)
Upstate Cell Signalling Solutions (USA)	Mouse Monoclonal IgG_1 Anti-phospho-Ser/Thr-Pro, P-MPM-2 (Cat. no. 05-368)

2.1.3 Fluorescently conjugated secondary antibodies

Sigma Aldrich (UK)	**Goat Antibody Anti- rabbit IgG FITC conjugated (Cat. no. F-6005)**
	Goat Antibody Anti-rabbit IgG TRITC conjugated (Cat. no. T-5268)
	Sheep Antibody Anti-mouse IgG FITC conjugated (Cat. no. F-6257)
	Goat Antibody Anti-mouse IgG TRITC conjugated (Cat. no. T-5393)

2.1.4 Fluorescent cell probes

Molecular Probes™ Invitrogen Ltd (UK)	**LysoTracker® Green DND-26 (Cat. no. L-7526)**
	MitoTracker® Green FM (Cat. no. M-7514)
Sigma Aldrich (UK)	Bisbenzimide H33258 (Cat no. 14530)
	Propidium Iodide (Cat. no. 81845)
	Acridine Orange (Cat. no.01662)

2.1.5 Inhibitors

Sigma Aldrich (UK)	**Colchicine (A gift from (Mr Ya Gao) (Cat. no. 27650)**

	Diethyldithiocarbamic Acid sodium Trihydrate
	crystalline (Cat. no. D-3506)
	DL-Buthionine-(S,R)-Sulfoximine (Cat. no. B-2640)
	2-Methoxyestradiol (Cat. no. M-6383)

2.1.6 Other reagents

BDH Laboratory Supplies (UK)	**Chromium (III) Potassium Sulphate 12-Hydrate (Prod. 277584S)**
	Iso-Pentane (Cat. no. 294526 G)
Bright Instrument Company Ltd (UK)	Cryo-M-Bed
CALBIOCHEM® (USA)	TdT-FragEL™ DNA Fragmentation Detection Kit, Colorimetric-TdT Enzyme (Cat. no. QIA33)
Citifluor Ltd (UK)	Citifluor AF2
DakoCytomation (Denmark)	Swine Serum (Normal) (Cat. no. X0901F)
First link (UK) Ltd.	Type I Rat Tail Collagen
Fisher Scientific (UK) Ltd	Sucrose (Code S/8600/60)
	$MgSO_4$ (Code M/1050/53)
Hayman Ltd (UK)	Absolute alcohol 100, ethanol
Mikrobiologie, MERK (Germany)	Gelatine (Cat. no. 4070)
Sigma Aldrich (UK)	Bovine serum albumin (Cat. no. A-7906)
	Collagenase, Crude (Cat. no. C-9407)
	Deoxyribonuclease 1 Type II (Cat. no. D4527-40KU)

	2', 7'-Dichlorofluorescin Diacetate (Cat. No. D-6883)
	Dimethyl Sulfoxide (DMSO) (Cat. no. D2650)
	D-(+)-Glucose (Cat. no. G5400)
	Laminin (Cat no.)
	Menadione (Vitamin K3) (Cat. no. M57405)
	Phosphate Buffer Saline Tablets (Cat. No. P4417-100TAB)
	Poly-D-Lysine Hydrobromide (Cat. no. P7280)
	Poly-L-Lysine Hydrobromide (Cat. no. P-1274)
	Triton® X-100 (Cat. no.T8787)
	Trypan Blue (T-8154)
	Trypsin/EDTA solution (x1) (Cat. no.T3924)
	Soybean trypsin inhibitor (x1) (Cat. no.T6414)
TAAB (UK)	Paraformaldehyde EM (Code P001)

2.1.7 Culture media reagents

All reagents in this section were supplied by Sigma Aldrich, UK. Foetal calf sera (FCS) were supplied by Sigma Aldrich, UK and GIBCO, UK.

Dulbecco's Modified Eagles Medium *with L-glutamine and phenol red* (Cat. no. D-6429)

Dulbecco's Modified Eagles Medium *without L-glutamate and phenol red* (Cat. no. D-5921)

Pen/Strep solution containing 10,000 U/ml penicillin and 10 mg/ml streptomycin) (Cat. no. P0781)

Foetal calf serum (Cat. no. F7524)

200 mM L-glutamine (Cat. no. G-7513)

Minimum Essential Medium (x10) (Cat. no. M0275)

Ca^{2+}- and Mg^{2+}- free Earle's Balanced Salt Solution (Cat. no. E6267)

2.1.8 Tissue and cell culture materials

Nerve tissue of adult Sprague Dawley rats (250-350 g), on average 6 months old, was obtained from the Open University in-house animal breeding unit.

2.1.8.1 Dissected tissue materials

- Sciatic Nerves
- Dorsal Root Ganglia

In addition, sciatic nerves were dissected and collected from 200 g female Wistar rats pre-injected for 24 h with 0.3 mg/kg Foscan®, (A Gift from Dr Josephine Woodhams, National Medical Laser Centre, UCL)

2.1.8.2 Cells

A Gift of Drs James B. Phillips & Emma East. (The Open University)	**Primary astrocyte cultures**
ECACC A Gift of Dr Marliena Loizidou (Dept of Surgery, UCL)	Oestrogen-dependent human breast adenocarcinoma cell line (caspase 3 -/-) (MCF-7)

2.1.9 Imaging equipment:

Leica (Germany)	**Leica DMIL light microscope.** Leica TCS NT fluorescence scanning confocal microscope, with Leica confocal software
Olympus (UK)	Olympus BX61 fluorescence microscope, with a CCD camera and analySIS imaging software Olympus SZ40 (Dissection microscopes) with Volpi, Intralux® 6000 (Optical fibre light source)

2.1.10 Other equipment

Beckman Coulter Ltd (UK)	**Centrifuge (BECKMAN TJ-6)**
BDH Laboratory Supplies (UK)	Rectangular Cover Glass, 22 x 50 mm

	(Cat. no. 406/0188/42)
BioQuell (UK)	BiOQuell, HERAsafe Class II cabinet
	Fumehood with TEL AFA 1000
FALCON (UK)	Disposable 24 multiwell plates, clear and flat bottomed
GRI Lab Care Services	Alphalmager & High Performance Transilluminator UVP, model TFM-26, 25W Transilluminator: For digital imaging
Imaging Research Inc	NorthernLight Illuminator, adjustable day light white light of 1000-6500 Calvin, evenly illuminated, no flicker, stable light output within ± 0.1 %, stable temperature.
JENCONS Plc (UK)	Spectrafuge 24D
Laser Line (UK) Ltd (Borrowed from The National Medical Laser Centre, UCL)	**LICONIX model 55PM Light Meter (portable)**
Leica (Germany)	Leica Cryostat CM 1900
NUNC (UK)	Disposable 12 multiwell plates, clear and flat bottomed (Ref. no. 150628)
	Tissue Culture Flasks (T25 & T75) filtered and non-filtered
Scanbur BK (Denmark)	Scantainer filter cabinets
Sigma Aldrich (UK)	Slides, Microscope, Frosted one end, size:

	25 mm x 75 mm (Cat. no. S8400-1PAK)
The Open University (UK)	633 nm (red) Laser Light source
VWR International	Circular Cover Glass, 19 mm circular, thickness no.1.5, Borosilicate glass. Cat# 631-0156
	Super Premium Microscope Slides, 1,0-1,2 mm Thick/Twin-Frost (Cat. no. 631-0112)

2.2 Methods

2.2.1 Primary cell cultures

2.2.1.1 Dorsal root ganglia cultures

All animal tissue was obtained according to UK Home Office regulations following approval by the Open University Animal Ethics Advisory Group. Dorsal root ganglia (DRGs) were dissected from 250-350 g adult Sprague Dawley rats culled using carbon dioxide (CO_2) asphyxiation. Thoracic sections of rat spinal columns were removed within 5 min post-mortem and stored in 0.01M phosphate buffered saline (PBS) at pH 7.4 to preserve tissue viability (All PBS used in this study was of this concentration and pH value). Tissue explants were placed in Petri dishes for micro-dissection using an Olympus SZ40 microscope with a Volpi, Intralux® 6000 optical fibre light source. Spinal columns were divided longitudinally into two sagittal hemi-sections. Spinal cords were discarded, and approximately 26 DRGs were dissected from each intervertebral foramen per spinal column with fine-forceps. Curved micro-surgical scissors were used to trim DRGs of all nerve processes.

Trimmed DRG explants were pooled together in Dulbecco's Modified Eagle's Medium *with L-glutamine* (DMEM) supplemented with 100 U/ml penicillin and 100 µg/ml streptomycin (pen/strep) solution and 10 % (v/v) foetal calf serum (FCS) (DMEM-complete culture medium). Trimmed DRGs were dissociated in approximately 2 ml 0.125 % (w/v) collagenase solution (prepared in serum-free DMEM medium supplemented with 100 U/ml /100 µg/ml pen/strep solution) for 90

min under standard cell culture conditions (37° C in a 5 % CO_2 humidified incubator). Collagenase-treated explants were mechanically dissociated (triturated) into single cell suspensions with a 1 ml Gilson pipette. Collagenese was removed from cells by rinsing twice with approximately 20 ml DMEM-complete culture medium. Cell pellets were collected by centrifugation with a BECKMAN TJ-6 centrifuge at 100 x g for 5 min at room temperature. Collagenase was decanted and cell pellets re-suspended in appropriate volumes of DMEM-complete culture medium for use in the various culture systems where neurones were required. This methodology was adapted from Delree *et al.* (1989) and Phillips *et al.* (2005).

2.2.1.2 Satellite cell-enriched cultures

DRG cell suspensions as described above were used in the preparation of satellite cell-enriched (Satellite cell) cultures. DRG cultures in DMEM-complete culture medium (section 2.2.1.1) were seeded into 75 cm^3 culture flasks which had been pre-coated for 60 min at room temperature with 20 µg/ml poly-L-lysine (PLL). After 2 days under standard cell culture conditions, culture medium was replaced with a 1:3 DRG-conditioned culture medium (3 parts fresh DMEM-complete culture medium mixed with 1 part DMEM-complete culture medium from a previous DRG culture). DRG-conditioned medium supplied satellite cells with naturally secreted growth factors, which helped maintain satellite cell populations. Cells were cultured under standard cell culture conditions until approximately 80 % confluent, as observed under phase-contrast microscopy. Satellite cells were vigorously shaken by hand to dislodge neurones, and rinsed with autoclaved PBS to remove neurones. Cells were further expanded to dilute residual neurone content by exposing cultures to several cycles of trypsinisation. Neurones are post-mitotic

and therefore will not proliferate in culture (Becker and Bonni, 2004). Each time, 1 flask was shaken by hand to dislodge neurones, washed briefly with PBS, then satellite cells trypsinised (0.25 % Trypsin-EDTA, 5-10 min at 37° C), collected by centrifugation at 100 x g for 5 min at room temperature, re-suspended in fresh culture medium and plated into 2 new flasks pre-coated with PLL. Satellite cells were maintained in culture with 1:3 DRG-conditioned medium. After immunocytochemistry for βIII-tubulin/FITC positive cells, satellite cell cultures had no detectable neurones. Cells were used at passage number 2 and above.

2.2.1.3 Schwann cell/fibroblast cultures

Sciatic nerves in 250-350 g adult Sprague Dawley rats culled by CO_2 asphyxiation were exposed at mid-thigh, excised with fine-forceps and micro-dissection scissors within 5 min post-mortem and stored in PBS. Dissected nerves were de-sheathed (stripped of their epineurium and outer layers of their perineurium) under a dissecting microscope. Nerve explants were twice rinsed in warmed DMEM-complete culture medium (section 2.2.1.1), before being chopped transversely into 1 mm pieces with a curved scalpel blade. Nerve pieces were then incubated for 4 days in DMEM-complete culture medium under standard cell culture condition, to encourage denervated Schwann cells to adapt a proliferative state (Li *et al.*, 1998; Funk *et al.*, 2007). Following 4 days incubation, explants were incubated in 0.125 % (w/v) collagenase solution for 18 h under standard cell culture conditions. Explants were mechanically triturated with a 1 ml Gilson pipette and collagenase was removed by centrifugation with a BECKMAN TJ-6 centrifuge at 100 x g for 5 min at room temperature. Pellets (each from 1 pair of sciatic nerves) were re-suspended in approximately 20 ml DMEM-complete culture medium and seeded into a 75 cm^3 culture flask pre-coated with PLL. Every 2 days half the culture

medium was replaced with fresh DMEM-complete culture medium. Cells were cultured under standard cell culture conditions until they were approximately 80 % confluent, as observed under phase-contrast microscopy, then passaged by trypsinisation with 0.25 % trypsin-EDTA solution for 5 min at 37° C. These cells were re-suspended in required volumes of DMEM-complete culture medium for use in the various culture systems in this study. This methodology was adapted from Li *et al.* (1998) and Phillips *et al.* (2005). Schwann cell/fibroblast (Schwann cells) cultures were characterised using immunocytochemistry with anti-S-100 (S-100 is a protein found in Schwann cells but not fibroblasts), for the percentage of Schwann cells present.

2.2.1.4 Sciatic nerve fibroblast-enriched culture

Schwann cell cultures above were used as the starting culture for nerve fibroblast-enriched cultures. Fibroblast-enriched (fibroblast) culture preparation was adapted from Bampton and Taylor *et al.* (2005). Schwann cell cultures were repeatedly allowed to proliferate to 100 % confluency for 2 weeks before passaging as described above. Fibroblast cultures were used at passage number 3 and above.

2.2.1.5 Astrocyte-enriched cultures

Mixed glial cell cultures were prepared from cerebral cortices of 2 day old Sprague-Dawley rats culled by decapitation according to the methods of Dutton *et al.* (1981) and Fallon (1985). The cerebral cortices were removed, cleaned of meninges and vasculature with fine-forceps under a dissection microscope, and then placed in a few drops of sterile disaggregation medium (14 mM glucose, 3

mg/ml bovine serum albumin (BSA) and 1.5 mM $MgSO_4$) prepared in Ca^{2+}- and Mg^{2+}- free Earle's Balanced Salt Solution.

Cortices were chopped using a sterile scalpel blade before being transferred to a centrifuge tube containing 250 µg/ml trypsin-EDTA prepared in 10 ml disaggregation medium for 15 min under standard cell culture conditions. 10 ml of a solution containing 21 µg/ml soybean trypsin inhibitor, 6 µg/ml deoxyribonuclease 1 (DNase) and 240 µM $MgSO_4$ in disaggregation medium was then added in order to neutralise trypsin. Tissue suspensions were sedimented using a BECKMAN TJ-6 centrifuge at 100 x g for 2 min at room temperature. Supernatants were removed and pellets collected and re-suspended in a further 500 µl of solution containing 133 µg/ml soybean trypsin inhibitor, 40 µg/ml DNase and 1.5 mM $MgSO_4$ in disaggregation medium. Tissue suspensions were mechanically dissociated by gentle trituration with a 1 ml pipette and then debris allowed to settle and the supernatant cell suspension was collected. This dissociation step was repeated twice. The final cell suspension was under laid with 2 ml 4 % (w/v) BSA in disaggregation medium. Intact cells were pelleted through the BSA underlay by centrifugation at 100 x g for 5 min at room temperature. Cell pellets were collected and re-suspended in DMEM-complete medium to give a plating density of 1-2 cortices in 20 ml per 75 cm^2 culture flasks pre-coated with 20 µg/ml poly-D-lysine (PDL). Cultures were maintained under standard cell culture conditions for 14 days until confluent. (Cultures were prepared in this manner by Drs E. East and J.B. Phillips, The Open University, UK.)

Under standard cell culture conditions, microglia were detached from astrocyte/microglia monolayer cultures by shaking culture flasks on a rotary shaker (ELMI Sky Line Shaker S-3.16L) at 150 rpm for 4 h at 37° C. The culture medium

containing microglia was disposed of and remaining astrocyte-enriched culture (astrocytes) were collected by trypsinising cells with 5 ml 0.25 % trypsin-EDTA solution for 10 min at 37° C. These astrocyte cultures were re-suspended in required volumes of DMEM-complete culture medium (section 2.2.1.1). This process yielded approximately 95 % astrocytes as determined by immunocytochemistry for GFAP positive cells in monolayer cultures pre-coated with 20 µg/ml PDL (East *et al.*, 1999).

2.2.2 Human breast cancer cells

MCF-7 cells are tumour cells which are known to be oestrogen-dependent (Müller *et al.*, 1998). They express the oncogene *Wnt7B* (Huguet *et al.*, 1994) and have inactivated *GSTP1* which encodes pi-class glutathione-*S*-transferase (GST) (Figure 1.21) similar to prostate and liver cancers (Lin and Nelson, 2003). MCF-7 cells were used in this study as a control for tumour cell death after treatment with *m*-THPC or hypericin-mediated PDT.

MCF-7 cells obtained as a gift from Dr Marliena Loizidou, Department of Surgery, UCL, UK, were propagated *in vitro* in DMEM-complete culture medium. Master and working cell banks of this cell line were prepared at passage 303 and 1 x 10^6 cells/ml stored at -80° C in freezing medium (DMEM; 10 % (v/v) Dimethyl Sulfoxide (DMSO); 20 % (v/v) FCS and 2 mM L-glutamine). MCF-7 cells were reconstituted by defrosting quickly at 37° C in a water bath then DMSO concentration was reduced by the drop wise addition of 10 ml DMEM-complete medium. MCF-7 cells were cultured in 25 cm^3 culture flasks overnight, and then culture medium was completely replaced with 10 ml fresh DMEM-complete medium. Confluent 25 cm^3 culture flasks were trypsinised with 0.25 % trypsin-EDTA solution for 5-10 min at

37° C then plated into three 75 cm^3 culture flasks. In this study MCF-7 cells were used at passages 305 to 321.

2.2.3 Standard monolayer and collagen gel cultures

2.2.3.1 Determination of cell numbers

After trypsinisation of cell cultures to be used in culture systems, total viable cell numbers were determined with the use of Trypan blue exclusion. A 50:50 mixture of 0.4 % (w/v) Trypan blue solution with cell suspension was made and incubated for 2 min at room temperature. Culture samples were then viewed under phase contrast microscopy and quantified using a haemocytometer. Dead cells were blue-brown with this assay which distinguished them from viable cells.

2.2.3.2 Standard monolayer cultures

Monolayer culture preparations are quick and easy to prepare and are commonly used as experimental tools. These cultures were used in some cases to characterise cell culture preparations, and to assess photosensitiser uptake and localisation.

100 µl cell suspensions (typically between 100,000 and 200,000 cells per ml) were plated onto cover-glasses (19 mm in diameter) which had been pre-coated for 60 min at room temperature with 20 µg/ml PLL or laminin, in 12-well culture plates. Under standard cell culture conditions, cells were allowed to settle and adhere for 30 min, before incubation with 1 ml culture medium per well.

2.2.3.3 Standard cell-seeded collagen cultures

A key aim of this work was to establish accurate sensitivity profiles for the effects of different doses of PDT on different cell populations. A common problem with using traditional monolayer cultures for cell death assays such as these is that dead cells tend to be lost from the culture surface. This prevents the inclusion of accurate dead cell counts, and restricts analysis to monitoring numbers of remaining attached cells, which can be misleading. Furthermore, subsequent characterisation of dead cells (e.g. to identify cell type in a mixed culture) is hard to achieve. Here, a 3D collagen hydrogel culture system was developed which effectively trapped all cells (live and dead) throughout treatment, subsequent cell death analysis and identification of cell types.

Type I rat-tail collagen (2 mg/ml in 0.6 % acetic acid) and 10x Minimum Essential Medium (MEM) were combined and allowed to equilibrate for 30 min at 4° C, before neutralisation with drop-wise addition of 1 M sodium hydroxide (NaOH). During neutralisation, indicated by a colour change in medium phenol red pH indicator (from yellow to orange/red), collagen/MEM solution was swirled constantly to maintain an even distribution of collagen/MEM solution. Cell suspensions were mixed into neutralised collagen/MEM in a final mixture ratio of: 80 % (v/v) collagen; 10 % (v/v) 10x MEM and 10 % (v/v) cell suspension (primary neural and MCF-7 cells) prepared in DMEM-complete culture medium (Eastwood *et al.*, 1998; Porter *et al.*, 1998; Phillips *et al.*, 2005).

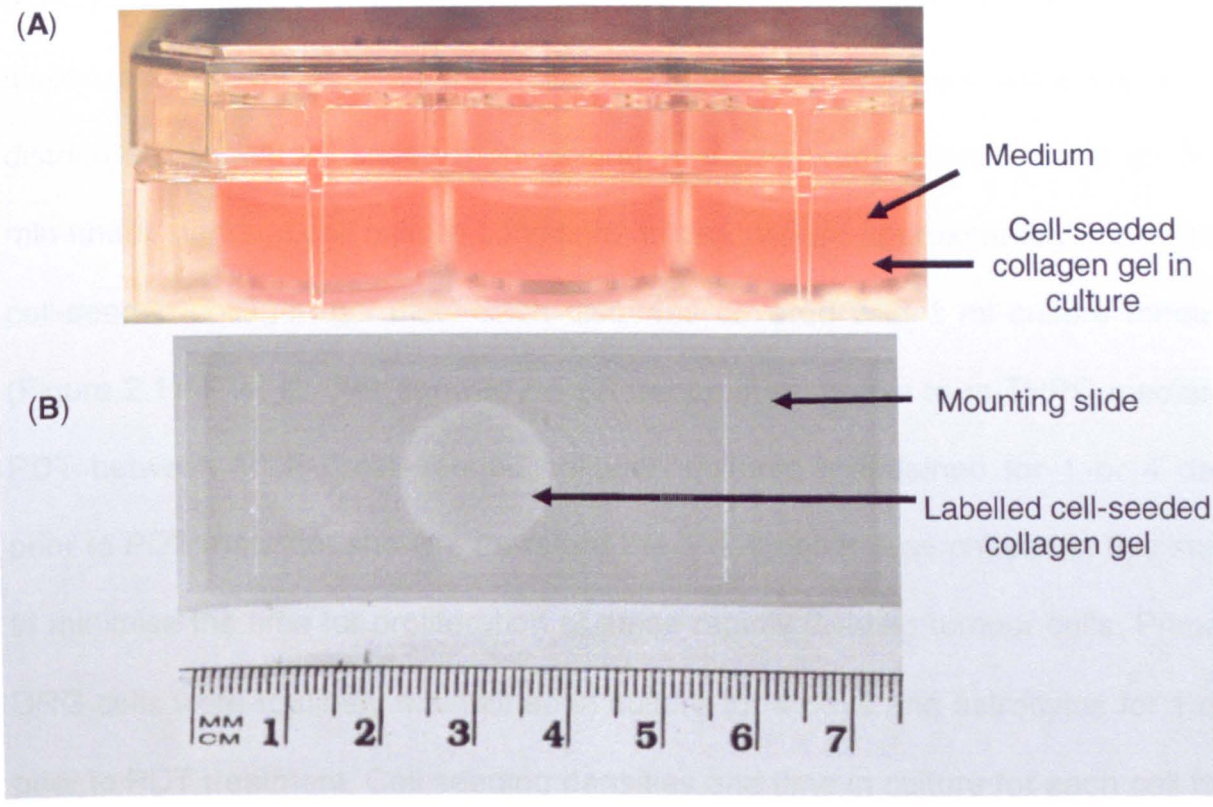

Figure 2.1
Cell-seeded collagen cultures.
(**A**) Gels in base of 24-well culture plates and (**B**) Gel mounted between a glass slide and a cover-glass ready for microscopic analysis.

Collagen/cell suspensions were gently mixed to ensure even cell distribution then pipetted into moulds for setting. Aliquots of 200 µl collagen/cell suspensions were dispensed into wells of 24-well culture plates. Culture plates were swirled to distribute collagen/cell suspensions evenly and gels were allowed to set for 5-10 min under standard cell culture conditions to produce an approximately 1 mm thick cell-seeded collagen gel disc. Each disc was covered with 1 ml culture medium (Figure 2.1). Pilot studies showed no difference in response to *m*-THPC-mediated PDT between MCF-7 cell-seeded collagen cultures maintained for 1 or 4 days prior to PDT (data not shown); therefore the 1 day option was chosen in this study to minimise the time for proliferation of these rapidly dividing tumour cells. Primary DRG cells were routinely maintained in culture for 4 days and astrocytes for 1 day prior to PDT treatment. Cell seeding densities and time in culture for each cell type are listed in Table 2.1.

2.2.4 Photodynamic therapy (PDT) treatment parameters

2.2.4.1 Photosensitiser preparations

The test photosensitiser ethanol-soluble (*m*-THPC, $C_{44}H_{30}N_4O_4$), was supplied as a 4 mg/ml temoporfin (MW 680.24, the active ingredient) in solution with ethanol and anhydrous propylene glycol (BioLITEC PHARMA Ltd, Ireland). A second photosensitiser used as a comparator, hypericin, (a polycyclic aromatic quinine) was supplied as powdered 1,3,4,6,8,13-Hexahydroxy-10,11-dimethylphenanthro[1,10,9,8-opqra]perylene-7,14-dione (MW 544.98, active ingredient) (TOCRIS Cookson Ltd, UK) and was made into a stock concentration of 10 mM in ethanol. Hypericin, like *m*-THPC, is a lipophilic photosensitiser and,

Cell types	Approximate seeding densities	Culture period (days)
DRGs (neurones and satellite cells)	2.0 x10^4 cells/ 200 µl gel (equivalent of 1 DRG/ 200 µl)	4
Astrocytes	4.0 x10^5 cells/ 200 µl gel	1
MCF-7 cells	2.0 x 10^4 cells/200 µl gel	1

Table 2.1
Cell seeding densities in collagen cultures.
Culture period refers to the number of days cells were maintained in collagen gels prior to PDT treatment.

when used in PDT, generates a large quantum yield of singlet oxygen/ROS (Paba *et al.*, 2001; Ritz *et al.*, 2005; Theodossiou *et al.*, 2004; Mikeš *et al.*, 2007).

Photosensitiser stocks were stored at -20° C protected from light. Working dilutions were prepared in serum- and phenol red- free DMEM culture medium supplemented with 100 U/ml/100 µg/ml pen/strep and 2 mM L-glutamine. Serum-free culture medium at pH 7.4 was used to prepare working dilutions of photosensitisers because 10 % serum is thought to reduce *m*-THPC uptake by 80-90 % due to the formation of photosensitiser aggregates (Friberg *et al.*, 2003). Phenol red-free medium was used to prevent any interference by phenol red in the PDT process or fluorescence investigations.

Photodynamic therapy (PDT) doses are defined as the product of photosensitiser concentration and applied light-fluence. In these experiments the photosensitiser concentration was altered and light-fluence was maintained at a constant level. Incubation time for 4 µg/ml *m*-THPC use was assessed using monolayer cultures. *m*-THPC was incubated on DRG cells for 4, 7 and 24 h before being fixing with 4 % (w/v) PFA for 10 min. 5 neuronal cell bodies were assessed in 2 cover glasses per time point. *m*-THPC fluorescence intensity was assessed form fluorescence micrographs using Analysis® software-pixel value tool, in 3 random points per neuronal cell body (but not including the nuclear region).

2.2.4.2 Light source (white light)

The light-fluence (a measure of applied light energy) for *m*-THPC recommended by the supplier for clinical use is 20 J/cm^{2}of 652 nm. The light-fluence used *in vitro* is much lower as cells are directly exposed to light without the protection of

surrounding tissue layers. In this study a light-fluence of 1 J/cm^2 (Figure 2.2) was applied unless otherwise indicated.

A transilluminator with adjustable white light of 1000-6500 Calvin, evenly illuminated, with no flicker, a stable light output within ± 0.1 % and stable temperature was used for all experiments unless otherwise indicated. This light source was set at its maximum setting and the energy emission assessed to be 3.6 mW with an optical power meter. Samples were exposed to this light source for a period of 10 min by placing multiwell plates containing monolayer or cell-seeded collagen cultures onto the surface of the illuminator.

The PDT light dose in this study was calculated using a model for light-fluence calculation adapted from Li *et al.* (2008). This calculation was used with the assumption of uniform photosensitiser concentration in samples (Figure 2.2). Samples for light exposure were placed within a rectangular region of 14 cm x 20 cm, marked out at the centre of the illuminator. Multiple readings using an optical power meter with readout in Watts (W) indicated no variability in the light levels at different positions within this area.

2.2.4.3 PDT treatment

Concentrations and times used in this study were chosen on the basis of previous work with these photosensitisers performed by other groups: 0-10 µg/ml *m*-THPC (Rousset *et al.*, 2000; Kunz and MacRobert, 2002; Bourré *et al.*, 2002) for 4 h (Bourré *et al.*, 2002; Kiesslich *et al.*, 2007) and 0-2.7 µg/ml hypericin for 7 h (Theodossiou *et al.*, 2004; Kiesslich *et al.*, 2007). Culture medium was replaced with 1 ml incubation solution containing the photosensitiser under test and

samples were protected from light during photosensitiser incubations at 37° C. Photosensitiser solutions were subsequently replaced with 1 ml phenol red-free culture medium (phenol red-free DMEM supplemented with 100 U/ml/100 µg/ml pen/strep and 10 % FCS). Test samples were exposed to 1 J/cm^2 white light and control samples (no light controls) were treated in the same manner but wrapped in aluminium foil to exclude light from the transilluminator (Vandenbogaerde *et al.*, 1997). Samples were then incubated under standard cell culture conditions for a further 24 h post PDT in the dark and assayed for cell death using a propidium iodide (PI) exclusion assay and specific cell types were identified with immunocytochemistry. In some cases, cells were maintained in culture for longer or shorter times than 24 h post-PDT (i.e. 1, 8, 16, and 36 h in a time course assay).

2.2.5 Cell survival evaluation

2.2.5.1 Cell death detection using PI exclusion

PI is a membrane-excluded nuclear DNA dye, which is non toxic to cells and commonly used as a marker of cell death because it only enters cells with damaged plasma membranes (i.e. those undergoing late apoptotic, and necrotic cell death) (Sattler *et al.*, 1997; Leung *et al.*, 2002; Baskić *et al.*, 2006). PI intercalates with double-stranded DNA and undergoes a fluorescent enhancement upon binding to nucleic acids and is relatively resistant to photobleaching (Sattler *et al.*, 1997). PI fluorescence is detectable at excitation around 493 nm and emission around 630 nm. Bisbenzimide H33258 (Hoechst 33258) was used as a

Light-fluence = (fluence rate x exposure time)

Power of white light source was 0.0036 W over a detector area of 2.3 cm^2

Therefore energy emission (Fluence rate)

$$=0.0036/\ 2.3\ W\ cm^{-2}$$

$$=0.002\ W\ cm^{-2}$$

Exposure time = 10 min

Light fluence

$$= 0.002 \times 600\ W\ sec\ cm^{-2}$$

$$= 1.2\ J/cm^2, \text{ rounded down to } \mathbf{1\ J/cm^2}$$

Figure 2.2
Calculation of light-fluence.

counterstain in order to establish total cell numbers, since it is a plasma membrane permeable fluorescent nuclear DNA probe detectable at approximate excitation 345 nm and emission 455 nm. Apoptotic cell death results in cells with condensed, bright red and/or fragmented PI-stained nuclei, and necrotic cell death results in non-condensed, bright red PI-stained nuclei. Live cells are only stained with Hoechst 33258 (blue) because PI (red) is excluded by live cell plasma membranes (Leung *et al.*, 2002; Rancan *et al.*, 2005; Mikeš J. *et al.*, 2007).

200 µl of a 200 µg/ml PI solution (in PBS) were incubated on monolayer and collagen gel cultures for 10 min (20 min on thicker collagen gels such as tethered glia-seeded collagen cultures) at room temperature under subdued light. Cultures were rinsed 3 times with PBS to remove excess unbound PI, and then fixed overnight with 4 % (w/v) PFA at 4° C. Cultures of astrocytes and MCF-7 cells were counterstained for 45 min with 10 µM Hoechst 33258 in PBS at room temperature. DRG cultures were immunostained for βIII-tubulin/FITC positive cells and counterstained with Hoechst 33258. Samples were stored in 1 ml PBS and analysed using fluorescence microscopy. Representative images were captured with a charged–coupled device (CCD) camera (ColorView Soft Imaging System).

Collagen gels were coded and randomised prior to cell death analysis to ensure the operator was blinded with respect to treatment conditions. The numbers of live and dead satellite cells, MCF-7 cells and astrocytes were determined by manually counting and scoring all cells in 3 fields of each gel or cover glass (typically a total of ~160 cells per gel). Fields were chosen at random using a x40 objective. For collagen gels, the operator focussed through all planes of the gel during the counting process, so that each field was a cylindrical sample through the gel from top to bottom. Pilot experiments confirmed that sampling 3 fields in this way was

sufficient to provide an accurate representation of the whole gel. There were considerably fewer neurones than satellite cells in each gel, hence all of the βIII-tubulin/FITC immunoreactive cells in each gel (typically up to 50 neurones) were identified and classified as being live or dead. For statistical analyses, live/dead cell counts from the 3 pooled 3D fields (MCF-7 cells, satellite cells and astrocytes) or all the neurones in each of the 9 independent gels (*m*-THPC) or 6 independent gels (hypericin) were analysed using one-way analysis of variance (ANOVA) with Tukey's post-hoc test to compare groups.

Microsoft® Office Excel 2003 and GraphPad Prism® 4.03 software were used to analyse data sets. Differences were defined as significant when $p<0.05$ (*), and highly significant when $p< 0.01$ (**) or $p< 0.001$ (***).

To validate these approaches, the ability to detect 100 % dead cells, and specifically to detect dead neurones, was tested on cell-seeded collagen gels equivalent to those used in these experiments. Culture medium was replaced with 200 µl 5 % (v/v) Triton® X-100 detergent for 10 min at room temperature to permeabilise plasma membranes of cells, before incubation at room temperature with PI. All cultures were rinsed between incubations with PBS. The effect of the permeabilisation would be to allow entry of PI into all cells; therefore resulting in 100 % cell death.

The effect of fixing cells with 4 % (w/v) PFA on the results of the PI exclusion assay was assessed. Culture medium was removed from cell-seeded collagen cultures and 400 µl 4 % (w/v) PFA was incubated for 10 min at 4°C. Cultures were treated with PI before or after fixing cells with PI, to determine whether fixation

resulted in permeabilisation of plasma membranes and entry of PI. Cultures were rinsed between incubations with PBS.

Other live/dead detection methods including Acridine orange in combination with Hoechst 33258 counterstaining and trypan blue in combination with Hoechst 33258 counterstaining were tested and rejected as they were deemed unsuitable for this experiment.

2.2.5.2 Apoptotic cell death detection using a TdT-FragEL™ assay kit

The presence of early apoptosis in DRG cultures after *m*-THPC-mediated PDT was detected using a terminal deoxynucleotidyl transferase-Fragment End Labelling (TdT-FragEL™) assay kit to label free 3'-OH groups at the end of DNA fragments which were generated by apoptosis. This allowed for the detection of apoptotic cells on the catalytic addition of biotin-labelled deoxynucleotides. These biotinylated nucleotides were detected using streptavidin-horseradish peroxidase conjugates. An insoluble coloured substrate was generated at the site of DNA fragmentation by the addition of diaminobenzidine (DAB) which reacted with the labelled sample. Here, fixed DRG seeded-collagen gels at 8 h post *m*-THPC-mediated PDT were tested with this TdT-FragEL™ kit; for the presence or absence of apoptotic cells (e.g. neurones) (see Appendix I).

2.2.6 Immunocytochemisty

2.2.6.1 Cell staining

After fixation of PI-stained samples with 4 % (w/v) PFA at 4° C, these samples were permeabilised by being incubated with Triton® X-100 followed by non-specific binding blocking by incubating with normal swine serum, before primary antibodies were applied. These samples were incubated at room temperature, and all reagents used were prepared in PBS. Samples were rinsed 3 times with PBS between all reagent incubations (as described in Table 2.2).

Primary antibodies used were: mouse anti-β-tubulin isotype III Clone SDL-3D10 (anti-βIII-tubulin) to identify neurones and/ or polyclonal rabbit anti-S-100 (anti-S-100) to identify glia (satellite and Schwann cells), which were incubated for 60 min at room temperature on monolayer and cell-seeded collagen cultures. 1:100 TRITC or FITC conjugated anti-mouse IgG, or anti-rabbit IgG secondary antibodies were incubated for 45 min along with 10 μM Hoechst 33258.

Incubation times were doubled for immunostaining the thicker tethered glia-seeded collagen gels, and for *ex-vivo* nerve models in collagen gels, and primary antibody was incubated at 4°C overnight. Following immunostaining, collagen gels were stored in PBS, while monolayer cultures were mounted with aqueous Citifluor AF2 mountant and sealed with nail varnish, refrigerated at 4° C and protected from light.

Representative fluorescence images of Hoechst 33258 labelled nuclei were captured using excitation filter 350 nm and emission filter 455 nm (blue). Images of the same field were captured of PI-labelled nuclei, using excitation filter 595 nm and emission filter 615 nm (red). Neurones were identified by examining samples for βIII-tubulin/FITC immunoreactivity in DRG cultures using approximate excitation of 494 nm and emission of 518 nm (green).

Reagents	Concentration or dilution	Incubation time (min)
Triton X-100	0.5 % (v/v)	10
Swine Serum	5 % (v/v)	10
Primary antibody mouse anti-βIII-tubulin or rabbit anti-S-100	1:400 or 1:200	60
Fluorescently conjugated secondary Ab	1:100	45
Hoechst 33258	1:1000	45

Table 2.2
Summary of conditions for immunocytochemistry.

Confocal microscopy was performed in some cases using a Leica TCS-NT laser scanning microscope with an oil immersion objective to capture images of PI fluorescence and βIII-tubulin/FITC immunostaining

2.2.6.2 Mitotic cell staining

In order to determine the cause of an observed change in the morphology of satellite cell and MCF-7 cell nuclei in experiments with hypericin, mitotic cell markers were used to determine whether cells were entering a mitotic state or whether nuclear morphology changes were due to apoptotic DNA fragmentation.

Colchicine was used to arrest cells in mitosis for use as a positive control of cells in the mitotic phase of the cell cycle. Anti-phospho-Ser/Thr-Pro (P-MPM-2) recognises epitopes of phosphoproteins (MAP2, HSP70, cdc25, and DNA topoisomerase IIα) phosphorylated during the onset of mitosis. This mouse primary antibody was then detected with a secondary antibody conjugated with FITC fluorescent fluorochromes. Hoechst 33258 was used in order to identify and quantify total cell numbers. All reagents were prepared in PBS, and there were three PBS washes between each step. DRG-seeded collagen gels were treated with either 1.6 μg/ml hypericin-mediated PDT (as described in Section 2.2.4.3) or incubated with 50 ng/ml colchicine in DMEM-complete culture medium for 17 h under standard cell culture conditions. Samples were then immunostained as described in Section 2.2.6.1 using the mouse primary antibody P-MPM-2 (1:200) for 45 min.

2.2.7 Photosensitiser uptake and compartmental distribution

m-THPC and hypericin have innate fluorescent properties which means that their uptake and distribution could be studied in specific cells types using fluorescence microscopy. The association of these photosensitisers with specific organelles was investigated using MitoTracker® Green FM (MitoTrk-green) and LysoTracker® Green DND-26 (LysoTrk-green) which was first assessed for their ability to label mitochondria and lysosomes respectively.

MitoTrk-green is concentrated by active mitochondria, becoming fluorescent only once it has accumulated in the lipid environment of the mitochondria and become oxidised (Peng *et al.*, 2005; Rancan *et al.*, 2005; Stasio *et al.*, 2005; Ji *et al.*, 2006; Marchal *et al.*, 2007; Kiesslich *et al.*, 2007; Ke *et al.*, 2008). LysoTrk-green selectively labels and tracks spherical acidic organelles (i.e. lysosomes) in live cells, by becoming fluorescent on contact with lysosomes. This probe consists of fluorophores linked to a weak base that is only partially protonated at neural pH. In addition, the lipophilic fluorochrome CM-DiI (CellTrk-red) (Brandt *et al.*, 1995 and Andrade *et al.*, 1996) was used in cell labelling to test its usefulness in live neurite staining and tracking.

Monolayer neural and MCF-7 cultures (as prepared in Section 2.2.3.2) were incubated with 4 µg/ml *m*-THPC for 4 h; or 1.6 µg/ml hypericin for 7 h or their respective no drug controls. MitoTrk-green and LysoTrk-green probes were prepared in phenol red- and serum- free DMEM culture medium. Pilot studies were performed with a range of doses of MitoTrk-green (25-300 nM) or LysoTrk-green (25-500 nM) with incubation times of 10-60 min. Cultures were fixed for 10 min

with 4 % (w/v) PFA at 4°C before being fluorescently labelled with 10 μM Hoechst 33258 for 45 min at room temperature.

To show the extent of co-localisation between the fluorescent probes and photosensitisers, fluorescence images were displayed as green and red, false coloured micrographs and electronically overlaid to visualise dual localisation using AnalySIS® software. When probes and photosensitisers localised in the same regions the fluorescence appeared yellow-orange. Co-localisation of photosensitisers with MitoTrk-green in cells was estimated using the polygon line tool, producing independent fluorescence spectra of red (photosensitiser) and green (MitoTrk-green) fluorescence intensities (Teiten *et al.*, 2003b; Gallagher *et al.*, 2005; Stasio *et al.*, 2005; Marchal *et al.*, 2007).

2.2.8 $^1O_2$/ROS detection

The cell permeable, non-fluorescent probe 2', 7'-Dichlorofluorescin diacetate or 2', 7'-Dichlorodihydrofluorescin diacetate (H_2DCF-DA) was used here as a detector of intracellular oxidising reactions, for example the detection of $^1O_2$/ROS production in cells exposed to *m*-THPC-mediated PDT or an oxidative stress inducer such as mendione, a redox cycling agent that results in ROS production in cells (Hempel *et al.*, 1999; Kunz and MacRoberts, 2002; Kiesslich *et al.*, 2005; Watts *et al.*, 2005; Oberdanner *et al.*, 2005; Miller *et al.*, 2007). When H_2DCF-DA comes into contact with products of oxidising reactions it is converted by hydrolysis to highly fluorescent Dichlorofluorescin (DCF).

Prior to using H_2DCF-DA in conjunction with PDT, oxidative stress was generated within cells using menadione. Monolayer cultures of MCF-7 cells were incubated

with 100 μM menadione for 60 min then H_2DCF-DA for 60 min, both in phenol red and serum-free DMEM culture. All incubations were performed under standard cell culture conditions and samples were rinsed in PBS between incubations. Cultures were then fixed with 4 % (w/v) PFA at 4° C, before being incubated with 10 μM Hoechst 33258 for 45 min at room temperature then mounted with Citifluor AF2 on glass slides and sealed with nail varnish.

For experiments which used H_2DCF-DA to probe oxidative stress following PDT, monolayer neural and MCF-7 cultures were first exposed to *m*-THPC or appropriate control incubations (as described in Section 2.2.4.3) followed by incubations with or without H_2DCF-DA at parameters of either 25 μM for 30 min or 100 μM for 60 min under standard cell culture conditions. Samples were rinsed in PBS between incubations, test samples were exposed to 1 J/cm^2 light and then fixed with 4 % (w/v) PFA at 4° C. Cell samples were then labelled with 10 μM Hoechst 33258 and neurites were identified using βIII-tubulin/TRITC immunostaining. Samples were mounted with aqueous Citifluor AF2 on glass slides then sealed with nail varnish. After immunostaining the presence of $^1O_2$/ROS in cell types was determined from fluorescence images. Images of photosensitiser were captured using excitation 595 nm and emission 615 nm. Green DCF fluorescence was captured using excitation of 494 nm and emission of 518 nm.

2.2.9 Confirmation of neuronal survival after *m*-THPC-mediated PDT

To assess the ability of neurones which had been subjected to 3, 4 and 10 μg/ml *m*-THPC-mediated PDT to regenerate their neurites, cells were extracted from the collagen lattice 24 h post PDT treatment by digestion with 0.125 % (w/v)

collagenase for 30 min under standard cell culture conditions. DMEM-complete culture medium was added and cell pellets collected with 5 min centrifugation at 100 x g, re-suspended in appropriate volumes of DMEM-complete culture medium, then cells from 2 gels were combined with 1 x 10^4 satellite cells (as described in Section 2.2.1.2) in a total of 100 µl DMEM-complete culture medium. Co-cultures were seeded onto PLL coated cover-glasses, and maintained in culture for 2 days under standard cell culture conditions then fixed in 4 % PFA at 4° C and immunostained for βIII-tubulin/FITC positive neurites (as described in Section 2.2.6.1).

All the neuronal cell bodies detected on each of two cover-glasses per treatment condition were assessed for the presence or absence of neurite growth. In addition, the mean detectable neurite length per cover-glass was assessed by tracing all neurites visible with βIII-tubulin immunostaining (green) on digital micrographs (Figure 2.3). The mean total length (in mm) of all detectable neurites per cover glass (n=2) were calculated per treatment. The data was collected in this way because not all neurones expressed neurites. 1-way ANOVA with Dunnett's post test were used to compare treatment conditions to controls.

2.2.10 Inhibition of neuronal survival pathways

In order to investigate the mechanism by which neurones were being protected during *m*-THPC-mediated PDT, specific cellular antioxidant pathways involving GSH and SOD were inhibited prior to *m*-THPC-mediated PDT treatment (administered as described in Section 2.2.4.3).

The glutathione synthase pathway was inhibited with 500 µM DL-Buthionine-(S, R)-Sulfoximine (L-BSO) incubated for 24 h (Roychowdhury *et al.*, 2002). L-BSO inhibits glutathione synthesis by irreversible inhibition of the enzyme *γ-glutamyl cystein synthetase* (Brezis *et al.*, 1983, Meister, 1995; Vandenbogaerde *et al.*, 1997; McNaught and Jenner, 1999; Roychowdhury *et al.*, 2002; Gegg *et al.*, 2005; Kiesslich *et al.*, 2005; Wang *et al.*, 2006). The 2 SOD antioxidant pathways involving constitutive SOD-1 and inducible SOD-2 were inhibited using 50 µM

Diethyldithiocarbic acid sodium trihydrate (DDC) for 1.5 h (Rothstein *et al.*, 1994; Du *et al.*, 2001; Miller *et al.*, 2007) or 1 µM 2-Methoxyestradiol (2-MeOE$_2$) for 24 h respectively (Gołąb *et al.*, 2003). Inhibitors were prepared in 1:3 DRG-conditioned medium for DRG cultures or DMEM-complete culture medium for MCF-7 cultures and incubated with cells in the thin collagen gels under standard cell culture conditions prior to PDT. Cell death was assessed 24 h post-PDT as described previously. In some instances the inhibitor treatments were combined to assess the effect of blocking multiple antioxidant pathways simultaneously.

2.2.11 Development of advanced nerve culture systems for investigating focal PDT treatment

In order to investigate the effect of directing PDT towards a particular part of a neurone in culture (i.e. either the cell body or somewhere along the neurite), more advanced culture systems were required. Unlike the simple 3D and monolayer neuronal cultures described previously, these would guide neurite growth away from the neuronal cell body in a linear manner, providing a distinct 'neurite' or 'neuronal cell body' zone towards which light treatment could be directed. 2

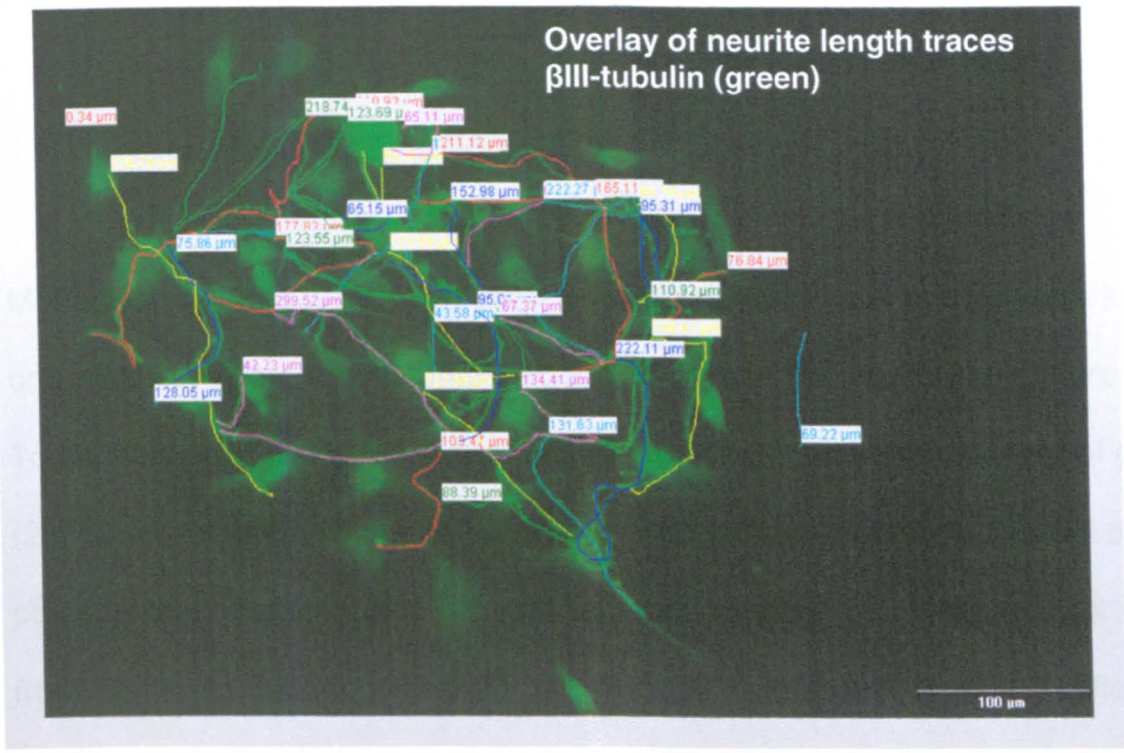

Figure 2.3
Example of neurite length determination using analySIS® software.

approaches were explored, using either 2D or 3D cell culture technology to align neurite growth.

2.2.11.1 2D glial substrate culture system

Monolayer cultures were developed in which neuronal cell bodies were located in one distinct region, with neurites extending across the rest of the culture surface. To support neuronal survival and neurite projection, a supporting layer of glial cells (2×10^5 cells/ ml Schwann cell or satellite cell cultures) was first seeded onto PLL-coated glass surfaces and allowed to reach confluence. Medium was removed from confluent cultures, then 20 µl DRG cell suspension (1×10^4 cells/ml) was applied to a small region at one end of the culture surface (Figure 2.4A). DRG cells were allowed to adhere for 30-60 min in a humidified incubator before medium was replaced and neurites were allowed to grow for 8 days.

In this study the use of satellite cell cultures was chosen to be a more effective substrate layer than Schwann cell cultures. After 8 days neurite growth, glial substrate culture systems were incubated with photosensitisers (as described in Section 2.2.4.3), then specific regions were illuminated using a transilluminator, allowing white light (light-fluence 1 J/cm^2) to pass through slits made by masking surrounding areas with black electrical tape (Figure 2.4B). In this way, neurites could be illuminated while their cell bodies remained shielded from the light. Cultures were incubated for 24 h post PDT and cell death was assessed as before with the use of PI exclusion and immunostaining for βIII-tubulin/FITC.

2.2.11.2 Aligned three dimensional neuronal growth models

The monolayer system in which neurones extended neurites over the surface of a confluent monolayer of glial cells (Figure 2.4) enabled focal PDT wounding, but it was not optimal for these studies due to detachment of dead cells as previously described. Therefore, a 3D culture system in which neurites extended away from the neuronal cell bodies was developed (Figures 2.5 and 2.6).

Collagen gels seeded with satellite cell cultures or a combination of these cultures with nerve fibroblasts were prepared (as described in Sections 2.2.1.2; 2.2.1.4 and 2.2.3.3). These cultures were set within rectangular moulds, with the collagen gel integrated within fixed mesh bars at each end of the moulds effectively tethering the gel in place (Eastwood *et al.*, 1994; Eastwood *et al.*, 1998; Phillips *et al.*, 2005). Rectangular culture moulds were constructed from nylon or stainless steel, and tethering bars were cut from sheets of nylon cross-stitch mesh. Nylon tethering bars were inserted into culture moulds before gelation. This allowed the culture mixture to enter spaces of the nylon mesh where the collagen sets, moulded to the nylon mesh, forming two tethered ends. Nylon moulds (Figure 2.5 A) were larger, and were seeded with 2.5 ml gel, whereas the smaller stainless steel moulds (Figure 2.5B) were seeded with 750 µl gel. Previous work using this arrangement of tethered cell-seeded rectangular collagen gels has shown that contraction of cells results in their alignment along the axis of principal strain and the formation of unaligned regions at each end, due to stress shielding (Figure 2.6) (Eastwood *et al.*, 1998; Porter *et al.*, 1998; Phillips *et al.*, 2005). In effect, the tethered collagen gel narrows along the un-tethered edges, while being prevented from narrowing at the tethered ends.

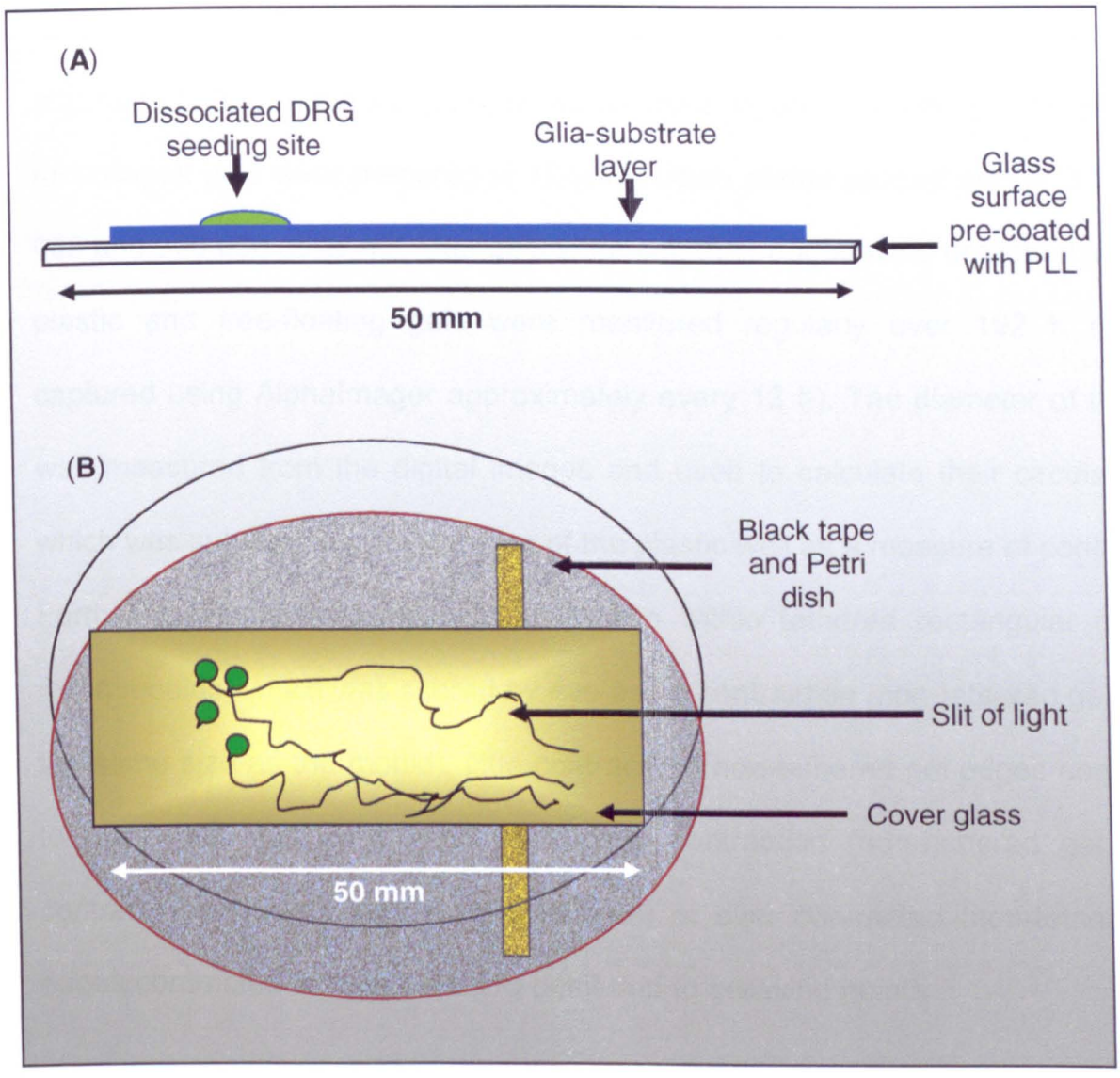

Figure 2.4
Focal PDT application to glial substrate culture system.
(**A**) Glial cells were allowed to form a confluent monolayer (blue), and then dissociated DRGs were seeded at one end (green). Neuronal cell bodies remained at the seeding site and neurites extended all over the surface of the glia. (**B**) Masking the underside of the culture plate enabled focal light administration via a narrow slit.

Initial experiments were conducted to establish the optimal seeding density and ratio of Schwann cells to fibroblasts which gave sufficient contraction and alignment to form a stable environment for the support of neurite growth. Round 1 ml collagen gels were prepared in 12-well culture plates seeded with 0, 3 000, 30 000 and 300 000 cells/ ml. After gels were set, their edges were detached from the plastic and free-floating gels were monitored regularly over 192 h (images captured using AlphaImager approximately every 12 h). The diameter of the gels was measured from the digital images and used to calculate their circular area, which was subtracted from the area of the plastic well as a measure of contraction. Further experiments compared contraction within tethered rectangular gels (in nylon moulds) which was scored by eye as no contraction (non-tethered gel edges the same size as the mould), little contraction (non-tethered gel edges contracted to more than half original size), optimal contraction (non-tethered gel edges contracted to half or less of original size) or over contracted (non-tethered gel edges contracted to near breaking point and to breaking point).

In each case the ratio of Schwann cells to fibroblasts was assessed by seeding 100 µl of cell suspension on to cover glasses, and counting the proportion of S-100 immunopositive cells in three random fields.

As a result of these optimisation experiments, gels were routinely cast using 400 000 cells/ ml of gel, allowed to set for 5 to 10 min under standard cell culture conditions, then DRG explants were pushed into the gels or dissociated DRGs were injected (2×10^4 cells in 10 µl volume) as shown in Figure 2.6A (at the position marked XX). Gels were covered with 7 ml (nylon moulds) or 10 ml (stainless steel moulds) culture media and maintained in culture for a week. The

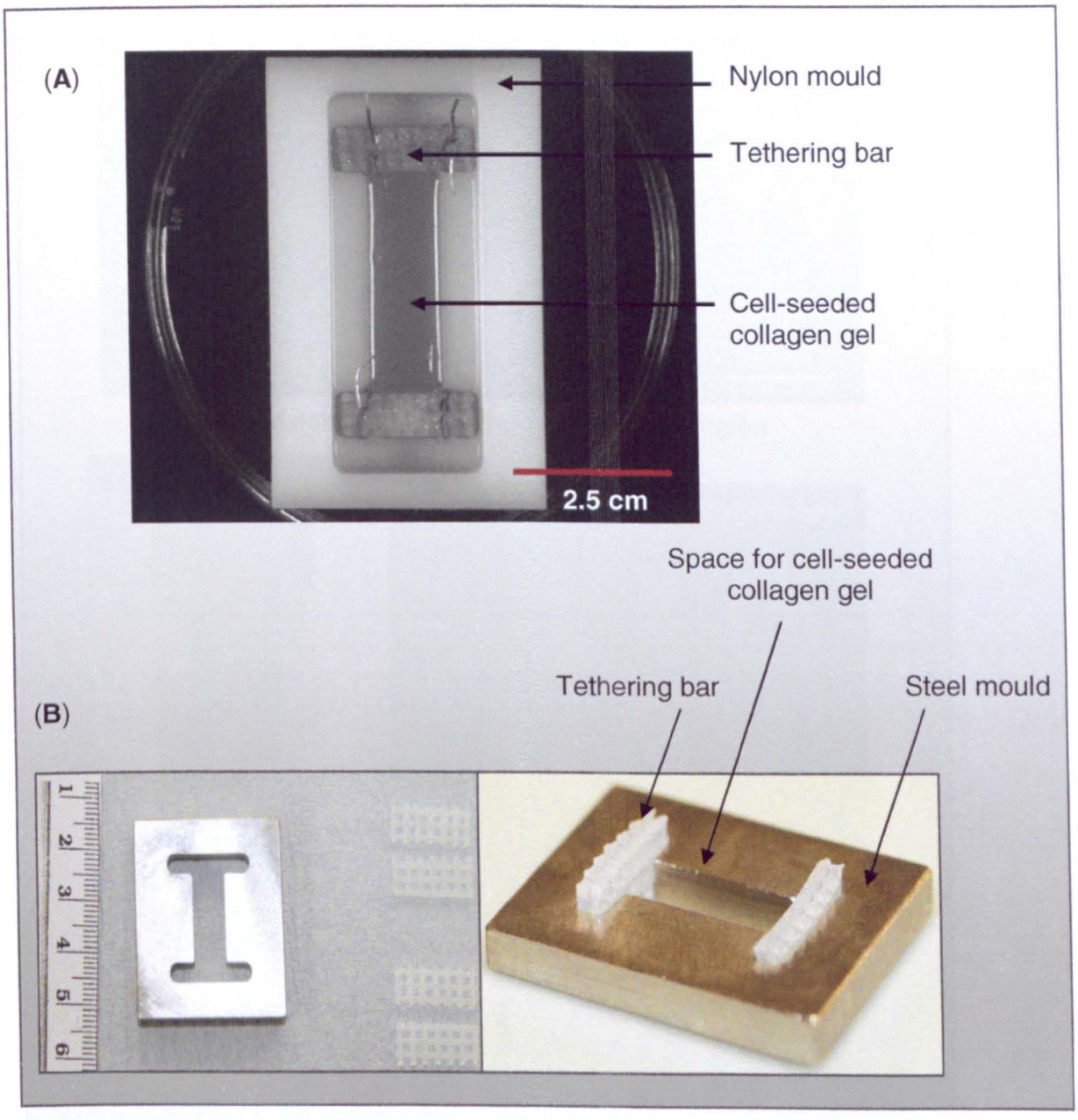

Figure 2.5
Aligned 3D neuronal growth models.
(**A**) Nylon and (**B**) stainless steel moulds with tethering bars made from nylon mesh.

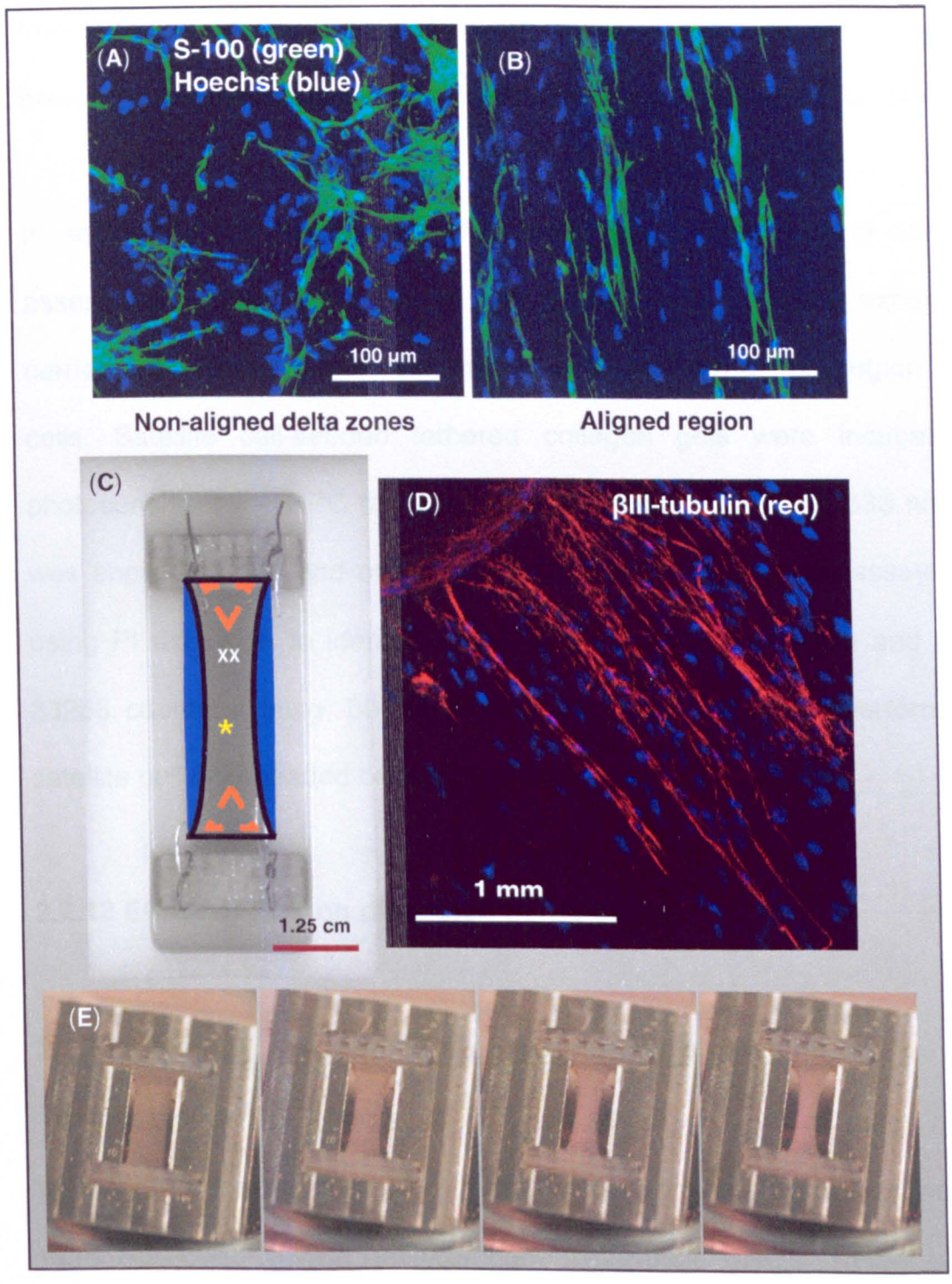

Figure 2.6
Aligned 3D neuronal growth.
Micrographs are of fixed cells, immunostained for glial cells with S-100 (green), neurones with βIII-tubulin (red) and nuclei with Hoechst (blue) (**A**) unaligned glial cells in delta zones (orange triangles in (C)), (**B**) aligned glial cells in contracted areas (* in (C)), (**C**) representation of a contracted gel in a nylon gel mould, and (**D**) DRG with aligned neurites (red) after ~3 days in this culture system (XX marks DRG implantation site in (C)). (**E**) Shows stainless steel mould with contraction of gel over time (images were captured at 2, 4, 8 and 12 h after setting. Gels adopt a characteristic shape as cells contract and align.

culture medium was then removed and gels fixed overnight with 4 % PFA at 4° C. Immunocytochemistry and cell death analysis was performed as described previously and neurite projection detected using βIII-tubulin/FITC immunostaining.

In addition to the assessment of collagen gel contraction and neurone growth assessment performed in these cell-seeded collagen gels, experiments were carried out in order to ascertain the ability to produce a focal region of PDT killed cells. Satellite cell-seeded tethered collagen gels were incubated with the photosensitiser *m*-THPC (as described in Section 2.2.4.3). A 633 nm laser beam was applied to one end of the gel. Collagen gels were then assayed after 24 h using PI exclusion to identify a localised region of cell death and with Hoechst 33258 counterstaining. βIII-tubulin immunostaining was not performed on these satellite cell only-seeded collagen gels.

2.2.12 Effect of PDT on dissected nerve tissue

2.2.12.1 *m*-THPC-mediated PDT on dissected sciatic nerves

To investigate the effects of PDT on nerve cells in a more natural tissue environment than that created in culture systems, sciatic nerves were harvested from Sprague Dawley rats complete with their DRGs. Nerve explants were maintained in culture for up to 2 days. Pilot studies were conducted to detect the ability of neurones to survive in explant culture. The presence of neurones within the nerve was assessed by staining cross-sections for NF immunopositive structures and the proportion of S-100 positive Schwann cell tubes, which contained NF positive axons, were determined.

The suitability of this approach for modelling focal PDT treatment was assessed by incubating the dissected nerves for 24 h in 4 µg/ml *m*-THPC and assessing photosensitiser fluorescence in sections. An alternative approach avoided this incubation stage by obtaining sciatic nerve explants from freshly culled Wistar rats that had been intravenously (i.v.) injected with 0.3 mg/kg *m*-THPC 24 h previously as part of another study (gift from Dr Josephine Woodhams at the NMLC, London).

Dissected nerves were either protected from light or exposed to a beam of light from a red laser diode. Nerves from the experiment in which *m*-THPC was applied in culture were exposed to a 1 mm diameter 633 nm light beam supplied by a diode laser in conjunction with an optical fibre for 20 s (1 J/cm^2 light fluence) at the OU, and nerves from rats injected with *m*-THPC were exposed to a 5 mm diameter 652 nm light beam supplied from a Diomed 652 PDT (clinical laser diode) in conjunction with an optical fibre and diffuser lens for 60s (10 J/cm^3 light fluence) at the National Medical Laser Centre (NMLC), UCL. These light sources were used to produce a site of focal PDT treatment 1.5 cm from the end of the nerve explant, distal to the DRG.

After treatment, dissected nerves were maintained in DMEM-complete culture medium for 24 h under standard cell culture conditions and protected from any further light exposure. Nerves were then fixed with 4 % (w/v) PFA at 4° C on a piece of card, to prevent tissue shrinkage. Regions of interests (midway along the nerve trunk or the focal damage site) were dissected out (Figure 2.7).

2.2.12.2 Cryo- block preparation

Tissue dissected from fixed nerve explants was incubated in 5 ml embedding reagent (20 % (w/v) sucrose in dH_2O) for up to 4 days at 4° C then embedded in warm supporting medium (7 % (w/v) gelatine and 20 % (w/v) sucrose in dH_2O) which was allowed to set at 4° C, removed from moulds and marked for orientation with a permanent marker. Blocks were then snap-frozen in cold iso-pentane on dry ice and samples loosely wrapped in aluminium foil and stored at -20° C for sectioning.

2.2.12.3 Sectioning

Cryo-blocks containing nerve tissue (Figure 2.8) were mounted onto cold chucks using Bright Cryo-M-Bed solution in a pre-cooled Leica Cryostat CM 1900 with chamber at -10° C and chuck head at -20° C. Samples were cut with sharp low-profile cryostat blades, at an angle of 0° and thickness of 10 to 30 µm. Nerve tissue sections were collected and mounted onto warmed glass slides, pre-coated with 0.5 % (w/v) gelatine and 0.05 % (w/v) Chromium III potassium sulphate 12-hydrate. Slides were stored at -20° C protected from light and dehydration.

2.2.13 Immunohistochemistry of nerve tissue sections

4 % (w/v) PFA nerve tissue sections were immunostained for NF, S-100 and laminin immunopositive structures as a means of assessing tissue architecture with and without focal PDT damage. Longitudinal and transverse frozen tissue sections mounted on glass slides were incubated with Triton® X-100, followed by swine serum incubation. Tissue sections were incubated with mouse anti-NF and,

rabbit anti-S-100 and/or anti-laminin primary antibody. All reagents were prepared in PBS, and there were PBS washes between each incubation step. Tissue sections were further incubated at room temperature with FITC or TRITC conjugated secondary antibodies in combination with 10 µM Hoechst 33258 (as described in Table 2.3).

Stained tissue sections were mounted with aqueous Citifluor AF2 mountant under cover-glasses and edges were sealed with nail varnish. Sections were stored at 4° C and protected from light. Samples were viewed and images collected as described previously.

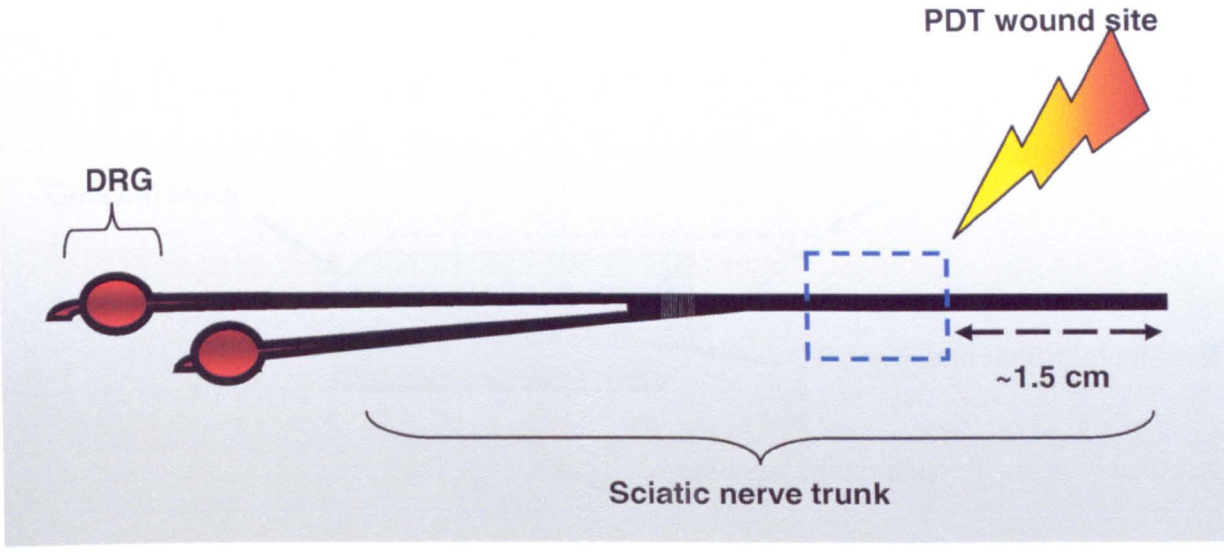

Figure 2.7
Diagram of dissected sciatic nerve showing site of focal PDT application.
DRGs contain neuronal cell bodies and the nerve trunk contains bundles of axonal fibres. Nerve explant was ~ 4 cm in length. Rectangle indicates region of nerve tissue dissected out 24 h post PDT.

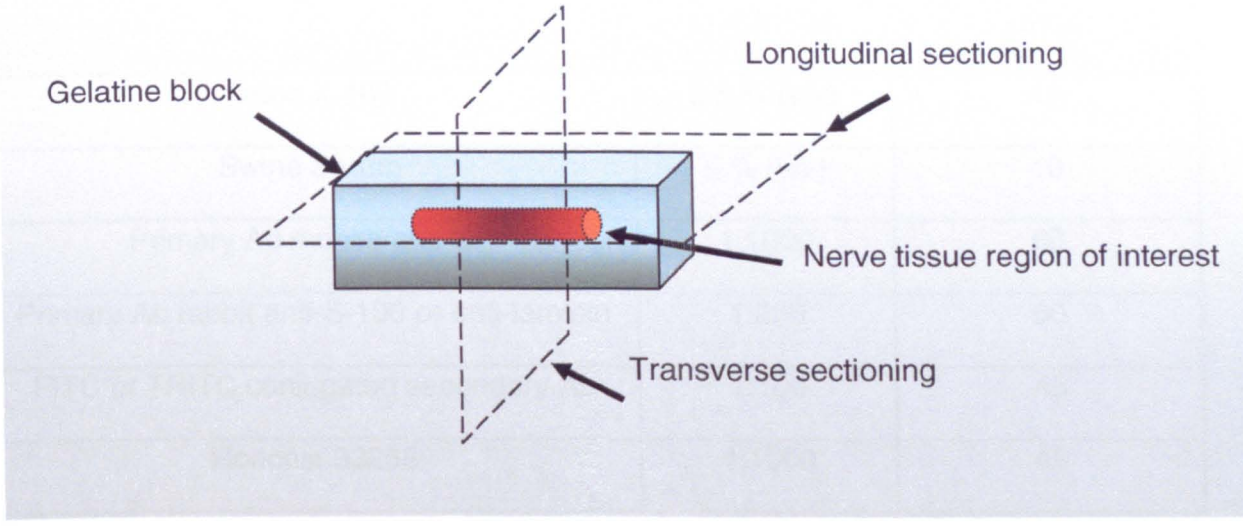

Figure 2.8
Nerve tissue within cryo-block showing planes of sectioning.
Illustration shows an example of an excised piece of nerve trunk embedded in snap-frozen gelatine block. Broken lines represent planes of sectioning.

Chemical	Concentration or dilution	Incubation time (min)
Triton X-100	0.5 % (v/v)	10
Swine Serum	5 % (v/v)	10
Primary Ab mouse anti-NF	1:1000	60
Primary Ab rabbit anti-S-100 or anti-laminin	1:200	60
FITC or TRITC conjugated secondary Ab	1:100	45
Hoechst 33258	1:1000	45

Table 2.3
Summary of conditions for immunohistochemistry of frozen sections of dissected nerves

Chapter 3: Effect of *m*-THPC-Mediated PDT on Neural and Tumour Cells in 2D and 3D Culture Models

3.1 Introduction

To date, a number of photosensitisers have been used clinically to treat areas of the body rich in nerve structures, e.g. the prostate (Chang *et al.*, 1996; Chang *et al.*, 1999; Huang *et al.*, 2005; Moore *et al.*, 2006) and regions of the head/neck (Lou *et al.*, 2004; Betz *et al.*, 2007; Nyst *et al.*, 2009). Research on the effects of *m*-THPC-mediated PDT in experimental models (Kubler *et al.*, 2003), and in clinical trials and practice (Betz *et al.*, 2007; Moore *et al.*, 2006, Lou *et al.*, 2004 and Ris *et al.*, 1996), have reported that no major peripheral nerve damage is associated with the use of this treatment. This nerve sparing was observed alongside effective destruction of tumour cells, suggesting that this treatment may be a useful tool for destroying cancers situated within close proximity to important nerve structures where alternative surgical treatments would carry a greater risk of nerve damage.

Despite the potential usefulness of a treatment that could selectively spare nerve tissue, little has been published about the effects of *m*-THPC-mediated PDT on the non-cancerous cells of the nervous system, although there have been reports on the use of this treatment for destroying cancers of the nervous system, (e.g. glioma, schwannoma, ependymoma, etc (Obwegeser *et al.*, 1998; Lilge *et al.*, 2000; Rousset *et al.*, 2000; Molinari *et al.*, 2007; Mannino *et al.*, 2008)). In this chapter, the sensitivity of primary neural cells and MCF-7 breast cancer cells to *m*-THPC-mediated PDT was established using conventional 2D cultures and also an

innovative 3D collagen hydrogel cell culture system. These were also used to characterise the sensitivity of neural cells and MCF-7 cells to an alternative photosensitiser, hypericin, for which there have not been any reports of nerve sparing.

3.1.1 Cell uptake of photosensitisers

It is generally accepted that non-ionised species can cross the plasma membrane more easily than charged compounds. Hence it is expected that neutral or lipophilic (hydrophobic) photosensitisers would be more readily taken up into membranes than charged or water-soluble (hydrophilic) photosensitisers (Ball *et al.*, 1999). There are three mechanisms by which photosensitiser uptake into cells has been proposed to occur: 1) Simple diffusion of lipophilic photosensitisers, 2) Fluid phase endocytosis (pinocytosis) of water-soluble photosensitisers, and 3) Receptor-mediated endocytosis of low density lipoprotein (LDL)-associated dyes (Ball *et al.*, 1999). It was suggested that the lipophilic photosensitiser *m*-THPC was taken up into cells by multiple mechanisms and was shown to have greater ability than Photofrin® to be sequestered into lipid bilayers where it remains tightly bound (Ball *et al.*, 1999). An HDL-mediated endocytosis mechanism was also proposed as a central mode of *m*-THPC transport into cells (Sasnouski *et al.*, 2006), while Laville *et al.* (2003) reported a mainly passive *m*-THPC uptake with less active transport via LDL.

3.1.2 Cell death after exposure to PDT

PDT can trigger the main modes of cell death in target cells both *in vitro* and *in vivo* (Banasiak *et al.*, 2000; Fabris *et al.*, 2001; Plaetzer *et al.*, 2003). PDT can

cause death via either necrotic, apoptotic or autophagic mechanisms. The cell death mode is dependent on the photosensitiser used, its concentration and subcellular localisation, the cell type and the light dose administered (Bourré *et al.*, 2002; Leung *et al.*, 2002; Almeida *et al.* 2004; Valencia and Morán *et al.*, 2004; Kiesslich *et al.*, 2007). For certain photosensitiser-cell combinations, the mode of cell death can shift from apoptosis to necrosis (Leung *et al.*, 2002; Plaetzer *et al.*, 2003). In the literature apoptosis has been found to be the predominant form of cell death in response to PDT for many cell types in culture, this has been based on observed DNA fragmentation and chromatin condensation (Oleinick *et al.*, 2002). However, necrosis rather than apoptosis seems to be the major cause of short-term cytotoxicity by *m*-THPC-mediated PDT (Heinzelmann-Schwarz *et al.*, 2003). A key event in PDT is the cut off of cellular energy supply by inhibition of mitochondrial enzymes; this is severe enough to cause necrotic cell death (Plaetzer *et al.*, 2003).

In this study the PI exclusion assay was used to determine cell death after PDT. This method was chosen because not only is it able to detect total cell death regardless of the mechanism, but it is also compatible with the immunofluorescence techniques used here for microscopic analysis of specific cell types. In addition, dying cells often do not display characteristics of only 1 of the 2 main modes of cell death; they instead show morphologies that include traits of both necrosis and apoptosis (Banasiak *et al.*, 2000). Permeability of apoptotic cells to PI increases 24 h after PDT; this is due to eventual loss of membrane integrity in the later phases of the apoptotic process (secondary necrosis) (Noodt *et al.*, 1999) (Figure 3.1).

3.1.3 Mammalian nerve culture system for assessing PDT

Relatively few studies have examined the effects of PDT on isolated peripheral nerve cells. The majority of this research has been done using non-mammalian nerve culture systems such as crayfish stretch receptors (Uzdensky *et al.*, 2004; see Introduction, Section 1.5). These nerve culture systems have been useful in comparing photosensitisers and in monitoring their effects on neuronal function, but they are limited in terms of their relevance to the mammalian nervous system.

This study therefore developed and used cell culture models to specifically evaluate the response of primary mammalian neural cells and tumour cells to PDT challenges. Various cell culture systems have been used to study nerve cell responses to different treatments, and to study the intricate interactions between neurones and glial cells (reviewed by East and Phillips, 2008). Recent neuronal culture systems include monolayer cell cultures (Turcu *et al.*, 2003; Tucker *et al.*, 2005; Thompson and Buettner, 2006); and dissected tissue from the nervous system such as nerve trunks and ganglia (Svensson *et al.*, 1995; Tonge *et al.*, 1997; Shi *et al.*, 1998; Gölz *et al.*, 2006) and slices of the spinal cord (Rothstein *et al.*, 1994; Funk *et al.*, 2007). In the present study, both conventional 2D cultures, as well as an innovative thin 3D nerve cell-seeded collagen (Type-I) hydrogel culture system, were used. The advantages of the 3D thin collagen gel culture system over conventional culture systems for this purpose included: allowing cells to grow in a 3D environment, which would mimic some spatial aspects of the

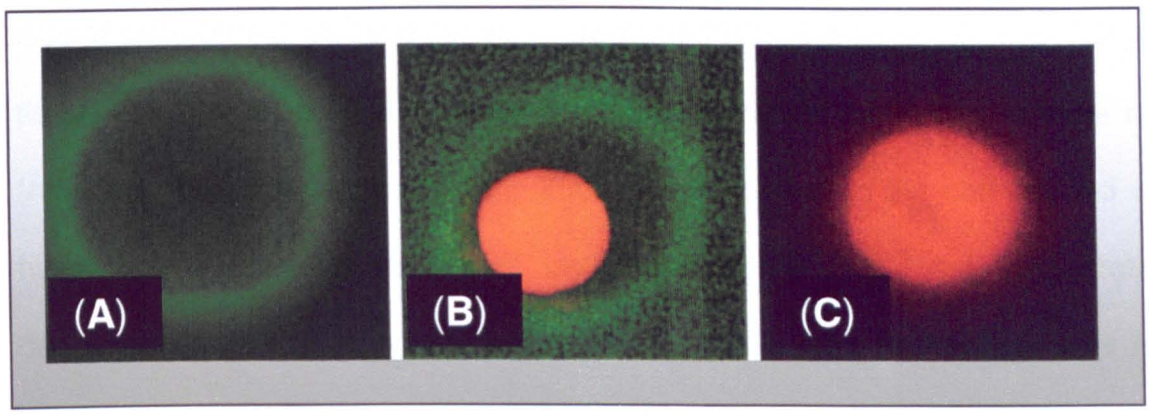

Figure 3.1
PI exclusion assay for staining dead cells.
Micrographs show Annexin-V (green)/PI (red) staining of apoptotic and necrotic cells. These images of peripheral blood mononuclear cells (PBMC) show: (**A**) Early (Annexin-V positive/PI negative) and (**B**) Late (Annexin-V positive/PI positive) apoptotic and (**C**) necrotic (Annexin-V negative/PI positive) cells. These images were taken from (Baskić *et al.*, 2006).

endogenous nerve architecture; and trapping cells in a collagen lattice, to prevent loss of cells during multiple cycles of treatment and washing. For over 30 years 3D tissue engineered culture systems have been used in the field of cancer research (reviewed by Brown and Phillips, 2007). More recently, 3D cell-seeded collagen hydrogels were used to model peripheral nerves, and for implantation into damaged peripheral nerves (Phillips *et al.*, 2005). This technology was modified here to suit the specific requirements of an investigation into PDT, adopting a relatively thin gel profile to facilitate PDT treatment and subsequent cell death analysis.

The uptake mechanism of hypericin, a comparator lipophilic photosensitiser used in this study, has been hypothesised to be similar in nature to *m*-THPC (Saw *et al.*, 2005; van de Putte *et al.*, 2006). Hypericin is known to have a high affinity for cell membrane and cytoplasm, and in culture hypericin was found in small amounts in the nucleus of human cancer cells (T47D, mammary tumour cells) (Miskovsky *et al.*, 1995) and in rat hippocampus neurones (English *et al.*, 1999).

To our knowledge the cellular responses of primary mammalian peripheral neural cells *in vitro* to PDT had not been investigated prior to this study. Therefore, in this study the effects of *m*-THPC- and hypericin-mediated PDT on specific neural cell types and MCF-7 breast cancer cells were investigated.

3.2 Aims and objectives

The aim of this chapter was to assess the sensitivity of key neural cells to *m*-THPC-mediated PDT. As such, the primary objectives were:

i) To assess whether or not *m*-THPC is taken up by the different cell types studied (DRG neurones, satellite cells, astrocytes and MCF-7 tumour cells).

ii) To characterise the level of cell death in specific cell types treated with various doses of *m*-THPC-mediated PDT to reveal any differences in sensitivity to this treatment in neural cells compared to cancer cells.

iii) To validate the culture system by also investigating the response of the various cell types to an alternative photosensitiser, hypericin.

3.3 Results

3.3.1 Cellular uptake and intracellular distribution of photosensitisers

The responsiveness of specific cell types to PDT challenges is dependent on the rate and/ or level of photosensitiser uptake and the subsequent intracellular distribution of photosensitiser. These parameters were therefore investigated in this study.

3.3.1.1 *m*-THPC uptake

Using fluorescence microscopy of monolayer cultures, intense red *m*-THPC fluorescence was detected in the cytoplasm of all cell types, but not in their nuclei in monolayer cultures of dissociated DRGs (set up as described in Chapter 2, section 2.2.3.2), treated for 4 h with 4 µg/m *m*-THPC at 3-4 days *in vitro*, *m*-THPC fluorescence was present in both neurones (Figure 3.2) and satellite cells (Figure 3.3). Satellite cells showed lower fluorescence intensity than neurones, with a more punctuate distribution pattern. The overlay micrograph in Figure 3.2C shows *m*-THPC fluorescence (red) and βIII-tubulin immunostaining (green) co-localised (yellow), confirming the uptake of *m*-THPC into neuronal cell bodies.

The presence of *m*-THPC did not interfere with the ability to detect neurones using βIII-tubulin immunostaining in conjunction with a FITC secondary antibody. FITC fluorescence was restricted to the green channel and was not detected using the red channel used for detecting photosensitiser. Also, *m*-THPC fluorescence was restricted to the red channel and was not detected using the green channel (shown in Chapter 4). In contrast to the presence of *m*-THPC fluorescence in neuronal cell bodies, the overlay micrograph in Figure 3.3C shows neurites labelled with βIII-tubulin/FITC, but without *m*-THPC fluorescence. This suggested that *m*-THPC did not localise within neurites, or alternatively that *m*-THPC fluorescence in neurites could not be detected with the fluorescence microscopy used in this study. Control samples incubated without photosensitiser (no drug) showed no fluorescence attributed to *m*-THPC (Figure 3.2 D, E and F; and 3.3 D, E and F).

Further to this fluorescence study, confocal microscopy was also performed in order to try to detect any low level *m*-THPC fluorescence signal which might be present in DRG neurites but below the limit of detection of the fluorescence microscope or to confirm the results of the fluorescence microscopy. Figure 3.4 shows a single neurone with a neurite bridging two areas of satellite cells. Although *m*-THPC fluorescence was detected in the cell bodies of the neurone and supporting satellite cells (Figure 3.4A), none was detectable along neurites (Figure 3.4A, B and C). These confocal micrographs therefore support the fluorescence results shown in Figure 3.3 that there was no detectable *m*-THPC fluorescence in neurites.

A time course study was performed in order to determine whether an *m*-THPC incubation time of 4 h, as indicated in the literature (Bourré *et al.*, 2002; Kiesslich *et al.*, 2007), enabled a similar amount of *m*-THPC to accumulate in neurones as longer incubations. Figure 3.5 shows a graphical representation of *m*-THPC fluorescence intensity over time as an approximate measure of the levels of *m*-THPC taken up into neurones. A slight increase in *m*-THPC levels in neuronal cell bodies was detected on increasing incubation time from 4 to 7 h. No further increase in *m*-THPC levels was observed up to 24 h incubation. Therefore 4 h was considered to be an adequate incubation time in monolayer cultures to achieve uptake of *m*-THPC into neurones.

In addition to detection of *m*-THPC fluorescence in DRG neurones and satellite cells, *m*-THPC fluorescence was also detected in the cytoplasmic regions of MCF-7 cells (Figure 3.6A) and astrocytes (Figure 3.6B). Uptake into DRG satellite cells is shown for comparison (Figure 3.6C).

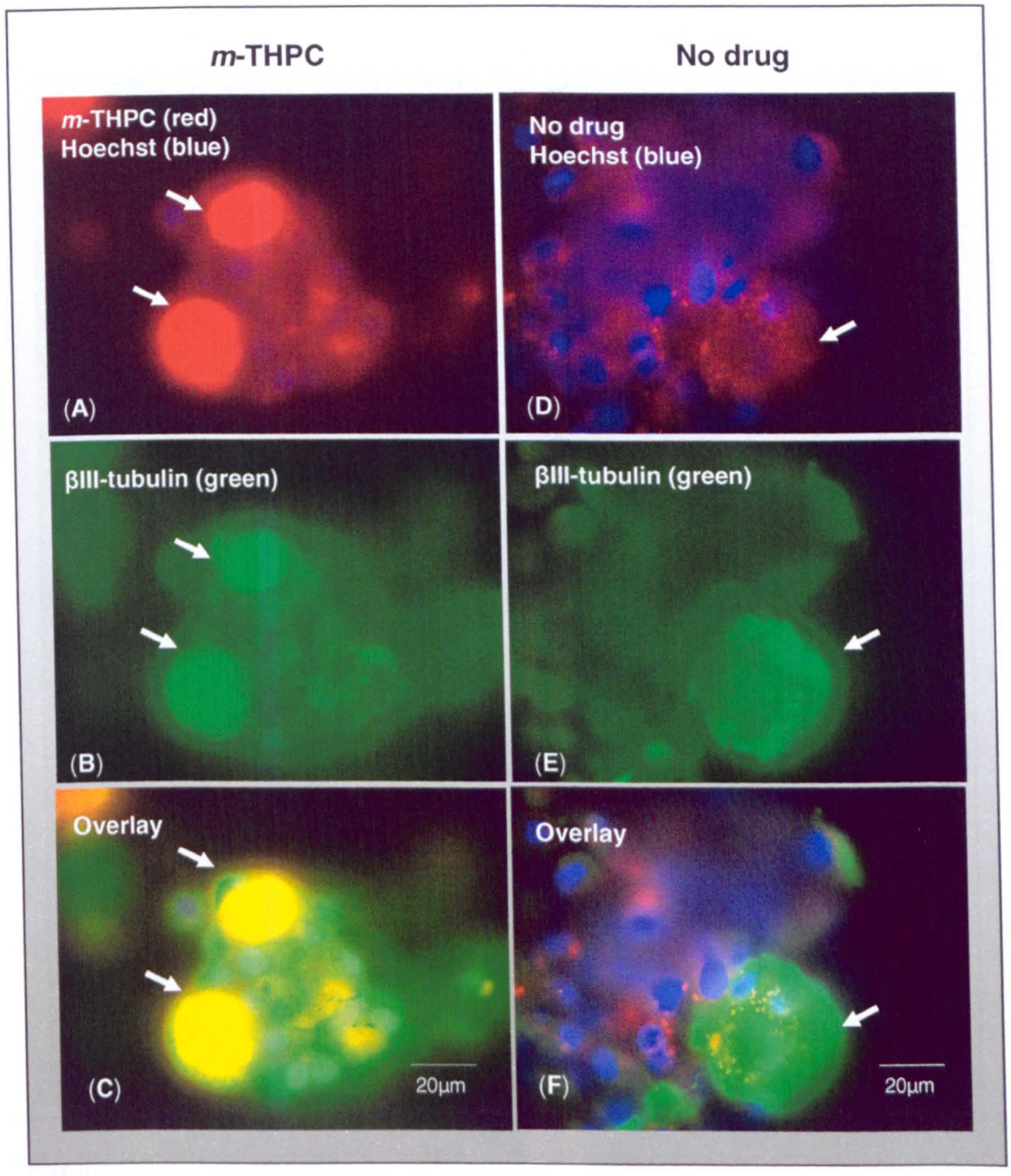

Figure 3.2.
Micrographs of *m*-THPC fluorescence detected in DRG neuronal cell bodies in monolayer cultures.
Micrographs show Hoechst stained nuclei (blue), *m*-THPC fluorescence in neuronal cell body cytoplasm (red), and βIII-tubulin immunolabelled neuronal cell body cytoplasm (green). These cells were fixed and immunostained in monolayer cultures. (**A**, **B** and **C**) incubated 4 μg/ml *m*-THPC for 4 h, this shows intense diffuse *m*-THPC fluorescence in the cytoplasm (red) of neuronal cell bodies (This fluorescence was not localised in neuronal nuclei, which were not visible in these neurones due to a layer of *m*-THPC on top of nuclei) and (**D**, **E** and **F**) incubated no drug control for 4 h, this shows no *m*-THPC fluorescence in neuronal cell body cytoplasm (red). (Arrows indicate position of neuronal cell bodies)

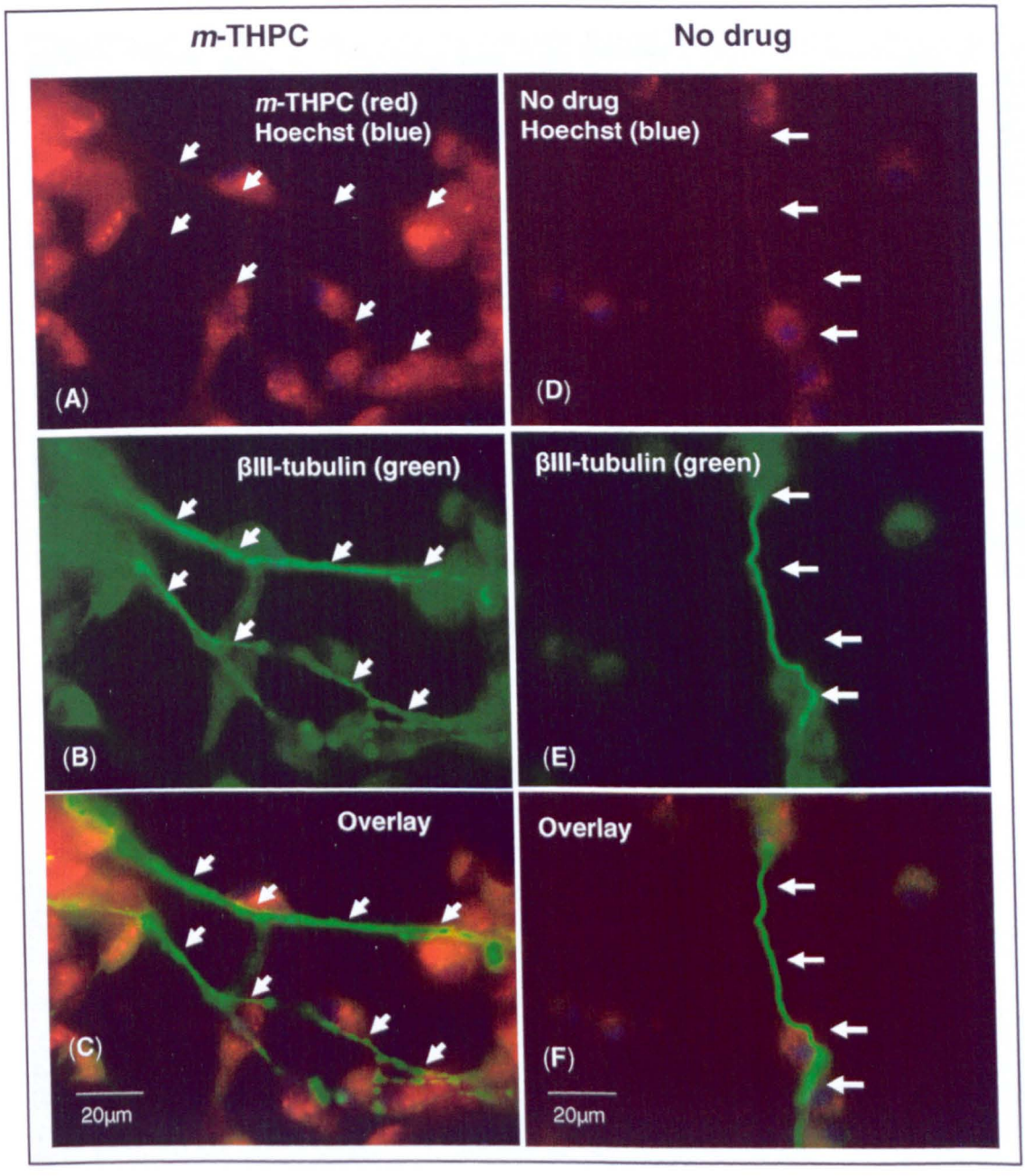

Figure 3.3
Micrographs of *m*-THPC fluorescence detected in DRG satellite cells but not in neurites in monolayer cultures.
Micrographs show Hoechst stained nuclei (blue), *m*-THPC fluorescence in satellite cell cytoplasm (red), and βIII-tubulin immunolabelled neurite cytoplasm (green). These cells were fixed and immunostained in monolayer cultures. (**A**, **B** and **C**) incubated 4 μg/ml *m*-THPC for 4 h, this shows punctuate *m*-THPC fluorescence in cytoplasm of satellite cells (red), no detectable *m*-THPC fluorescence in βIII-tubulin immunolabelled neuite (green) and no *m*-THPC fluorescence shown in cell nuclei. (**D**, **E** and **F**) incubated no drug control for 4 h; this shows no *m*-THPC fluorescence in satellite cell cytoplasm (red) or in βIII-tubulin immunolabelled neuite (green). (Arrows indicate positions of neurites)

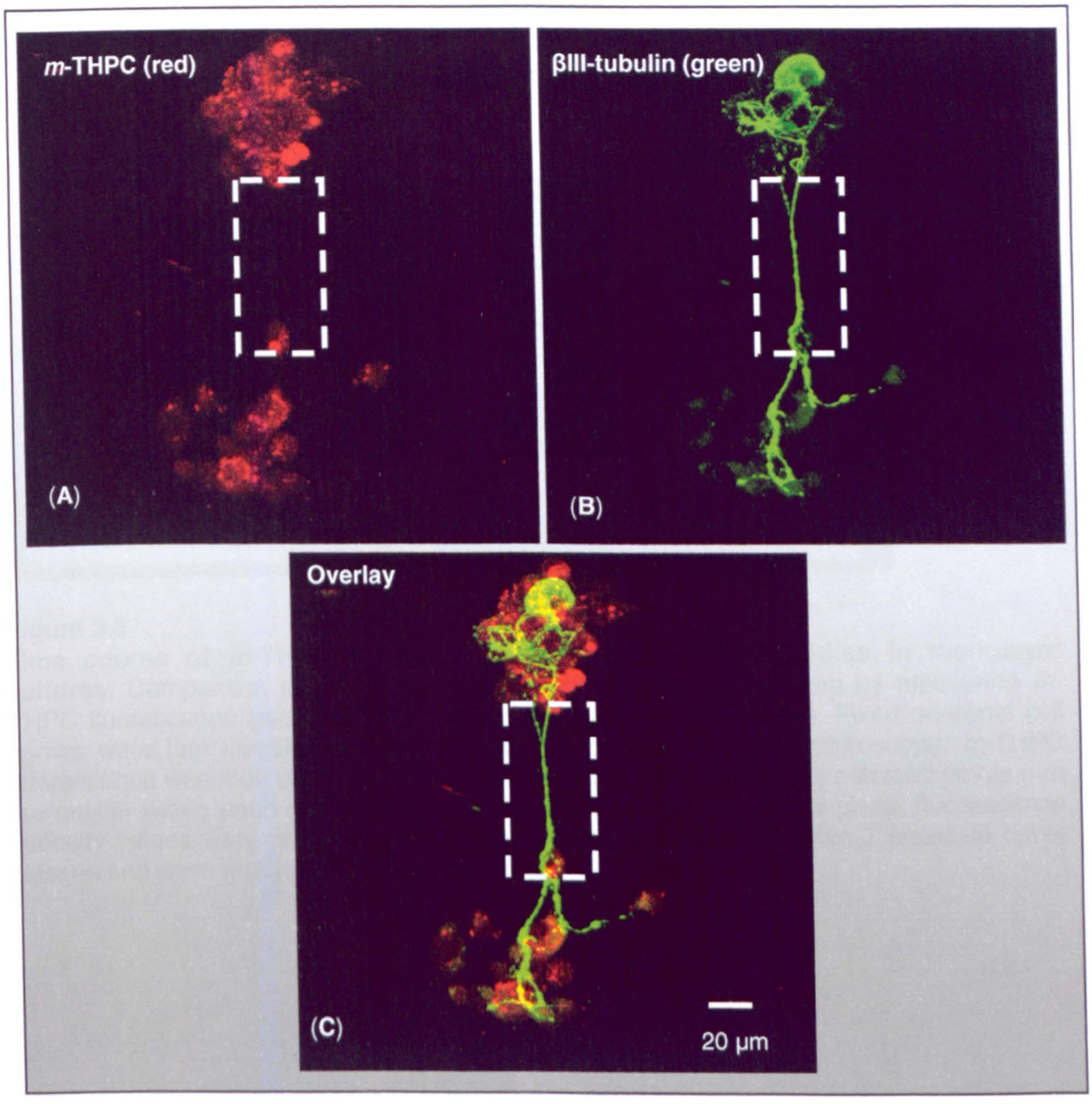

Figure 3.4
Confocal micrographs showing no detectable *m*-THPC fluorescence in neurites of DRG neurones in monolayer cultures.
Micrographs show *m*-THPC fluorescence in satellite cell and neuronal cell body cytoplasms (red) and βIII-tubulin immunolabelled neurone cytoplasm (green). These cells were fixed and immunostained in monolayer cultures. (**A**, **B** and **C**) incubated 4 μg/ml *m*-THPC for 4 h, this shows (**A**) punctate *m*-THPC fluorescence in satellite cell cytoplasm (red), (**B**) no detectable *m*-THPC fluorescence (red) in βIII-tubulin immunolabelling neurite cytoplasm (green), and (**C**) composite micrograph shows no colcalisation of *m*-THPC fluorescence (red) with βIII-tubulin immunolabelled neurite cytoplasm (green). Confocal images are maximum intensity projections from 40 optical sections in a 14 μm z-series. (Rectangular box indicates segment of neurite bridging between areas of satellite cells).

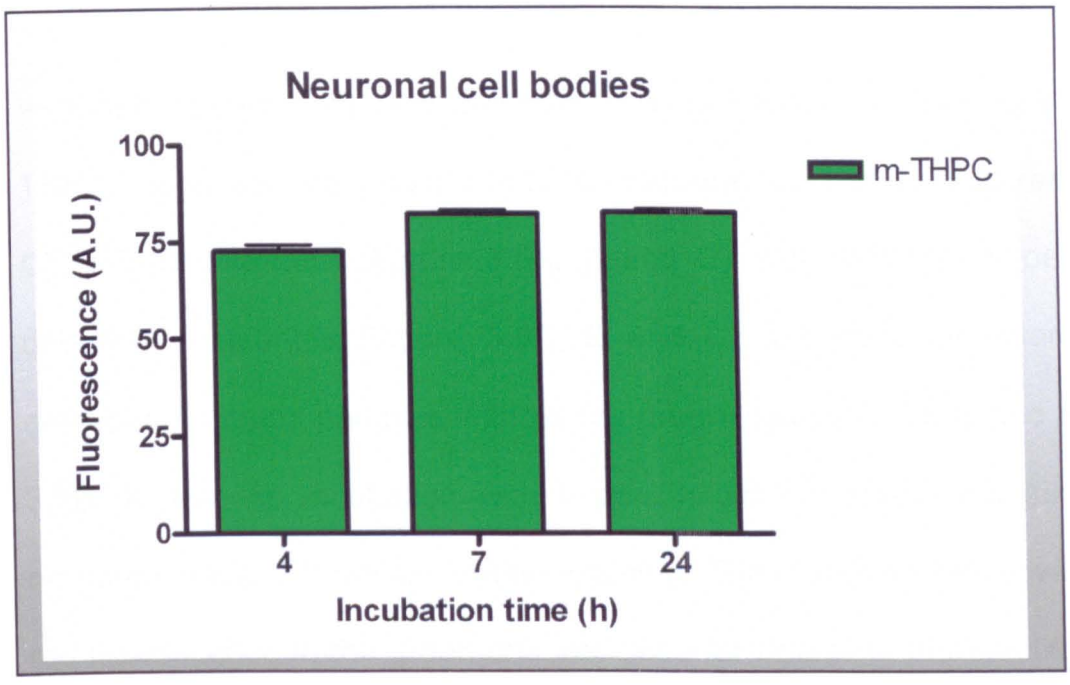

Figure 3.5
Time course of *m*-THPC uptake into DRG neuronal cell bodies in monolayer cultures. Comparison of *m*-THPC uptake over time was determined by measuring *m*-THPC fluorescence (red) intensity, localised in neuronal cell bodies. Fixed neuronal cell bodies were first identified morphologically using phase contrast microscopy. *m*-THPC fluorescence was then captured. Data were obtained from 3 randomly selected points (not the nuclei) within each of a total of 5 neuronal cell bodies per cover glass, fluorescence intensity values were presented as means ± SEM of 5 neurones from 2 separate cover glasses and were analysed at each time point.

3.3.1.2 Hypericin

Hypericin fluorescence was detected in all cell types, but not as strongly as *m*-THPC. Hypericin was present in DRG neuronal cell bodies (Figures 3.7A, B and C) and satellite cells (Figure 3.8A, B and C), like *m*-THPC, hypericin was not detected in neurites (Figure 3.8A, B and C). No hypericin fluorescence was detected in control samples without the drug (Figures 3.7D, E and F, and Figure 3.8D, E and F). Incubation with hypericin did not inhibit the ability to detect neurones using βIII-tubulin immunostaining. There was no crossover of hypericin red fluorescence in the green channel used for detecting βIII-tubulin/FITC (green) fluorescence (shown in Chapter 4).

It was found that after immunostaining, cells did not retain the same level of hypericin fluorescence in comparison to before immunostaining and the distribution of hypericin in cells was different before (Figure 3.9C, D, E and F) and after (Figure 3.9A and B) the immunostaining incubation and wash steps. The level of hypericin present in cells at the time of illumination therefore was likely to be greater than that displayed after immunostaining. No such effect was observed with *m*-THPC (data not shown).

Hypericin fluorescence was also detected in the cytoplasmic regions of MCF-7 cells (Figure 3.10).

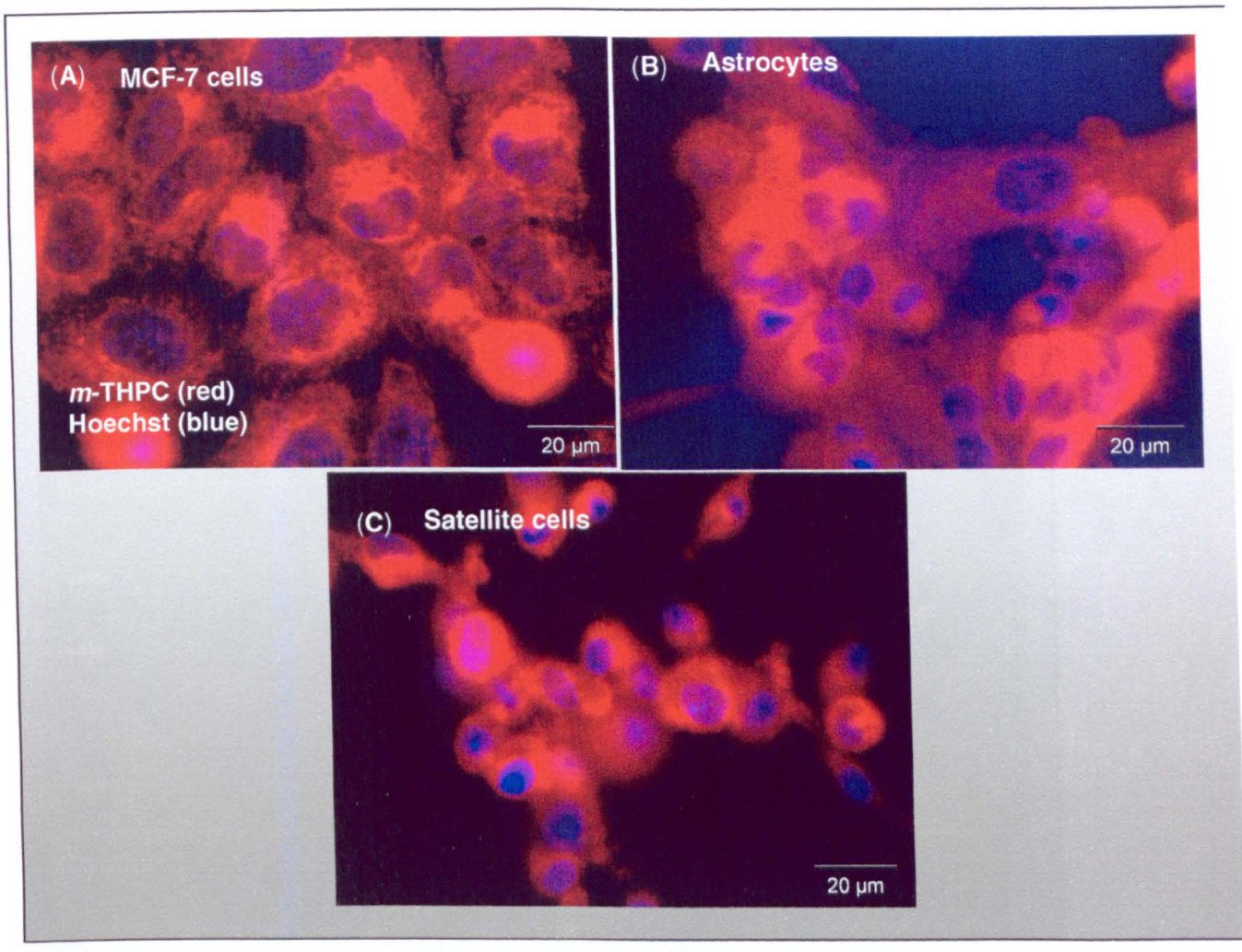

Figure 3.6
***m*-THPC uptake in MCF-7 cells, astrocytes and satellite cells.**
Micrographs show Hoechst stained nuclei (blue) and *m*-THPC fluorescence.in cytoplasm of cell types (red). These cells were fixed, and incubated with 4 µg/ml *m*-THPC for 4 h in monolayer cultures and were not immunostained. (**A**) MCF-7 cells, (**B**) Astrocytes and (**C**) Satellite cells, these micrographs show diffuse and punctate *m*-THPC fluorescence in different cell type cytoplasm (red). No *m*-THPC fluorescence shown in cell nuclei.

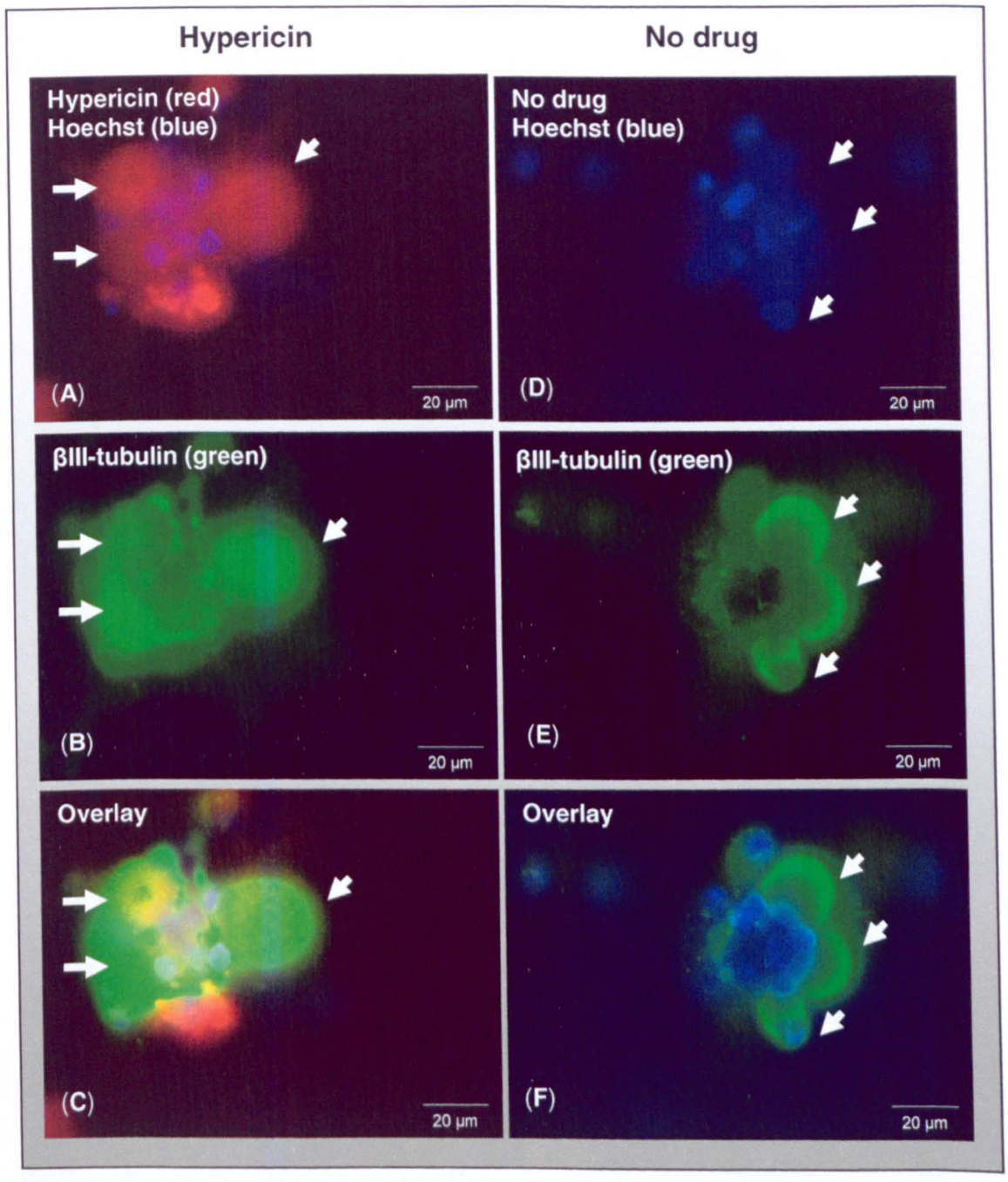

Figure 3.7
Hypericin fluorescence detected in DRG neuronal cell bodies in monolayer cultures. Micrographs show Hoechst stained nuclei (blue), hypericin fluorescence in neuronal cell body cytoplasm (red), and βIII-tubulin immunolabelled neuronal cell body cytoplasm (green). These cells were fixed and immunostained in monolayer cultures. (**A**, **B** and **C**) incubated 1.6 µg/ml hypericin for 7 h, this shows diffuse hypericin fluorescence in neuronal cell body cytoplasm (red) (This fluorescence was not localised in neuronal nuclei, which were not visible in these neurones) and (**D**, **E** and **F**) incubated no drug control for 7 h, this shows no hypericin fluorescence in neuronal cell bodies cytoplasm (red). (Arrows indicate position of neuronal cell bodies)

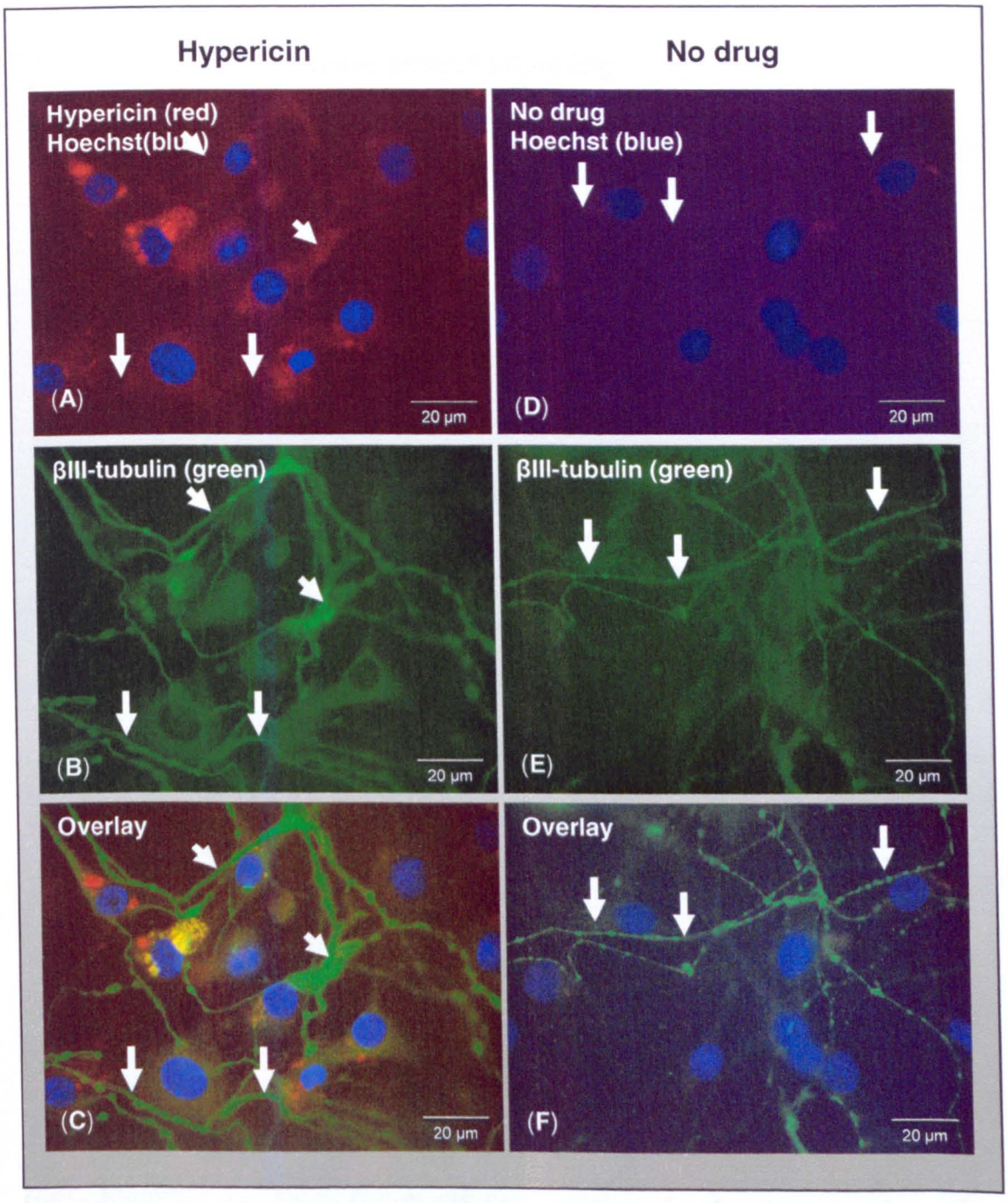

Figure 3.8
Hypericin fluorescence detected in DRG satellite cells but not in neurites in monolayer cultures.
Micrographs show Hoechst stained nuclei (blue), hyperisin fluorescence in satellite cell cytoplasm (red), and βIII-tubulin immunolabelled neurite cytoplasm (green). These cells were fixed and immunostained in monolayer cultures. (**A**, **B** and **C**) incubated 1.6 µg/ml hyperisin for 7 h, this shows some punctuate hypericin fluorescence in cytoplasm of satellite cells (red), no detectable hypericin fluorescence in βIII-tubulin immunolabelled neuite (green) and no hypericin fluorescence shown in cell nuclei. (**D**, **E** and **F**) incubated no drug control for 7 h, this shows no hypericin fluorescence in satellite cell cytoplasm (red) or in βIII-tubulin immunolabelled neuite (green). (Arrows indicate positions of neurites)

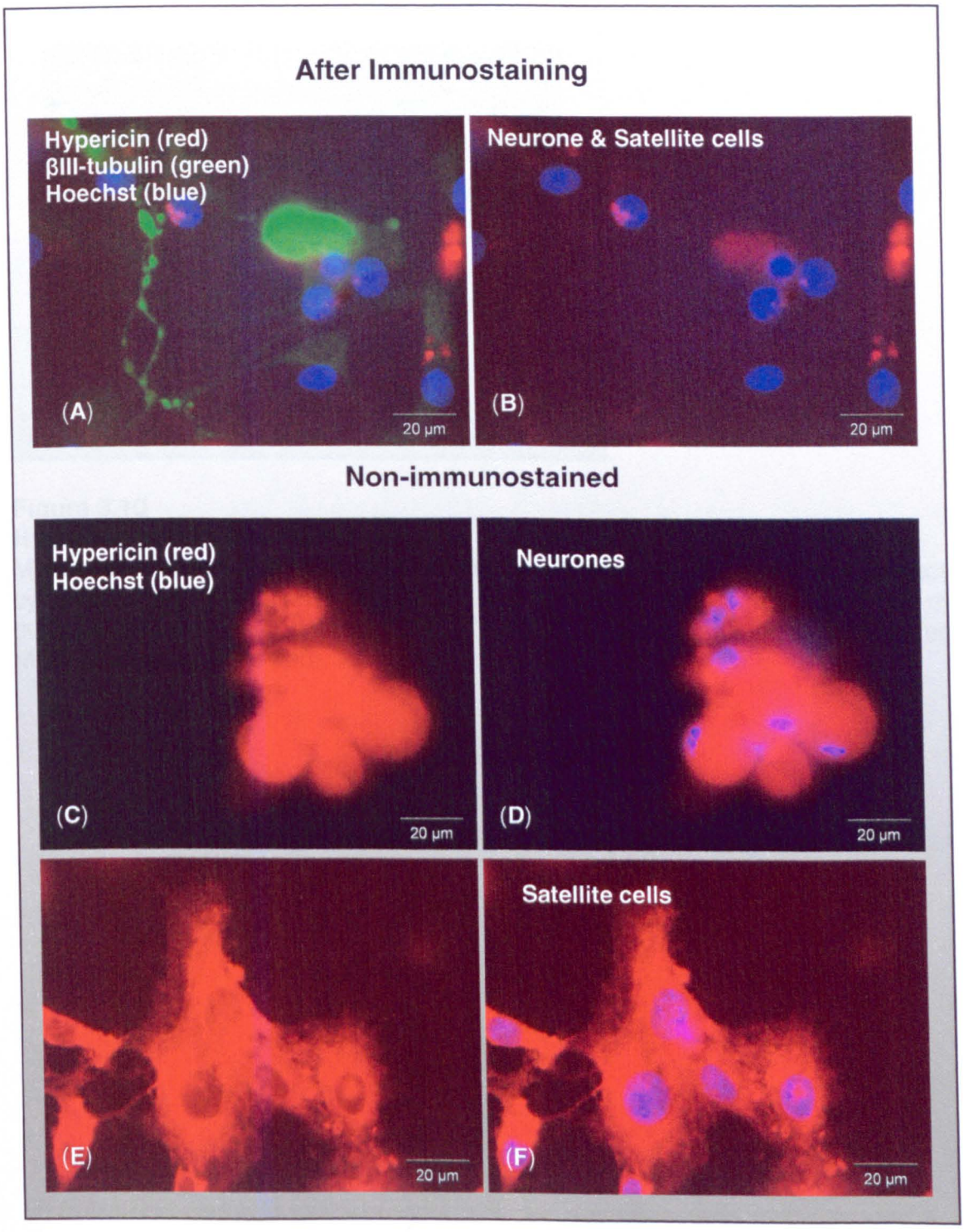

Figure 3.9
Hypericin uptake in DRG culture.
Micrograph shows Hoechst stained nuclei (blue), hypericin florescence in cell cytoplasm (red) and βIII-tubulin immunolabelled neurone cytoplasm (green).These cells were fixed and incubated with 1.6 µg/ml for 7 h in monolayer cultures. (**A** and **B**, **after Immunostaing**) shows greatly reduced hypericin fluorescence in cell cytoplasm (red) in comparison to (**C**, **D**, **E** and **F**, **non-immunostained**). Hypericin is shown to localise in neuronal cell body and satellite cell cytoplasm, but not in nuclei.

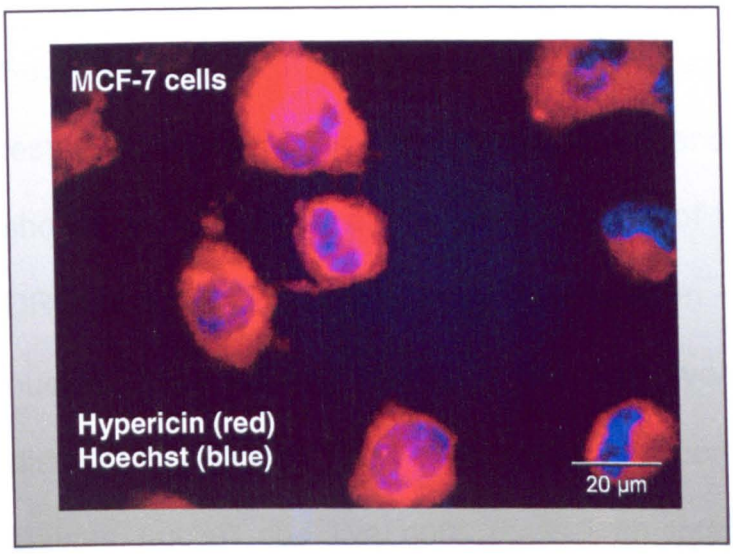

Figure 3.10
Hypericin uptake into MCF-7 cells.
Micrograph shows Hoechst stained nuclei (blue) and hypericin florescence in cell cytoplasm (red). These cells were fixed, and incubated with 1.6 µg/ml for 7 h in monolayer cultures, and were not immunostained. These cells show diffuse hypericin fluorescence in MCF-7 cell cytoplasm (red).

3.3.2 Evaluation of PI exclusion assay for detecting cell death

Several methods of microscopically assessing cell death and cell viability were tested including acridine orange inclusion and trypan blue exclusion (data not shown) as well as PI exclusion. However, of these assays tested in monolayer DRG cultures, PI exclusion by live cells in combination with Hoechst 33258 nuclear DNA staining produced the best live/dead visual distinction system to distinguish between dead cells (cells with compromised membranes: bright red stained nuclei) and live cells (cells with intact membranes: only blue stained nuclei). Furthermore, this PI exclusion method could be combined with neuronal identification with βIII-tubulin immunostaining, providing an approach that enabled the cell death response of distinct cell types to be analysed separately within a co-culture system.

Figure 3.11 shows no drug control versus *m*-THPC-mediated PDT treated DRG satellite cells in collagen gels. These micrographs show clearly the ability to detect and distinguish between live and dead satellite cells in this 3D collagen culture system.

Representative micrographs are shown in Figure 3.12 to illustrate how, in each of the cell populations under investigation, dead cells (PI-stained red nuclei) could be distinguished from live cells (no red staining, Hoechst 33258 blue nuclei). These cultures were within collagen gels and Figure 3.12B also illustrates how PI live/dead analysis could be used in conjunction with βIII-tubulin immunostaining to identify live and dead neurones.

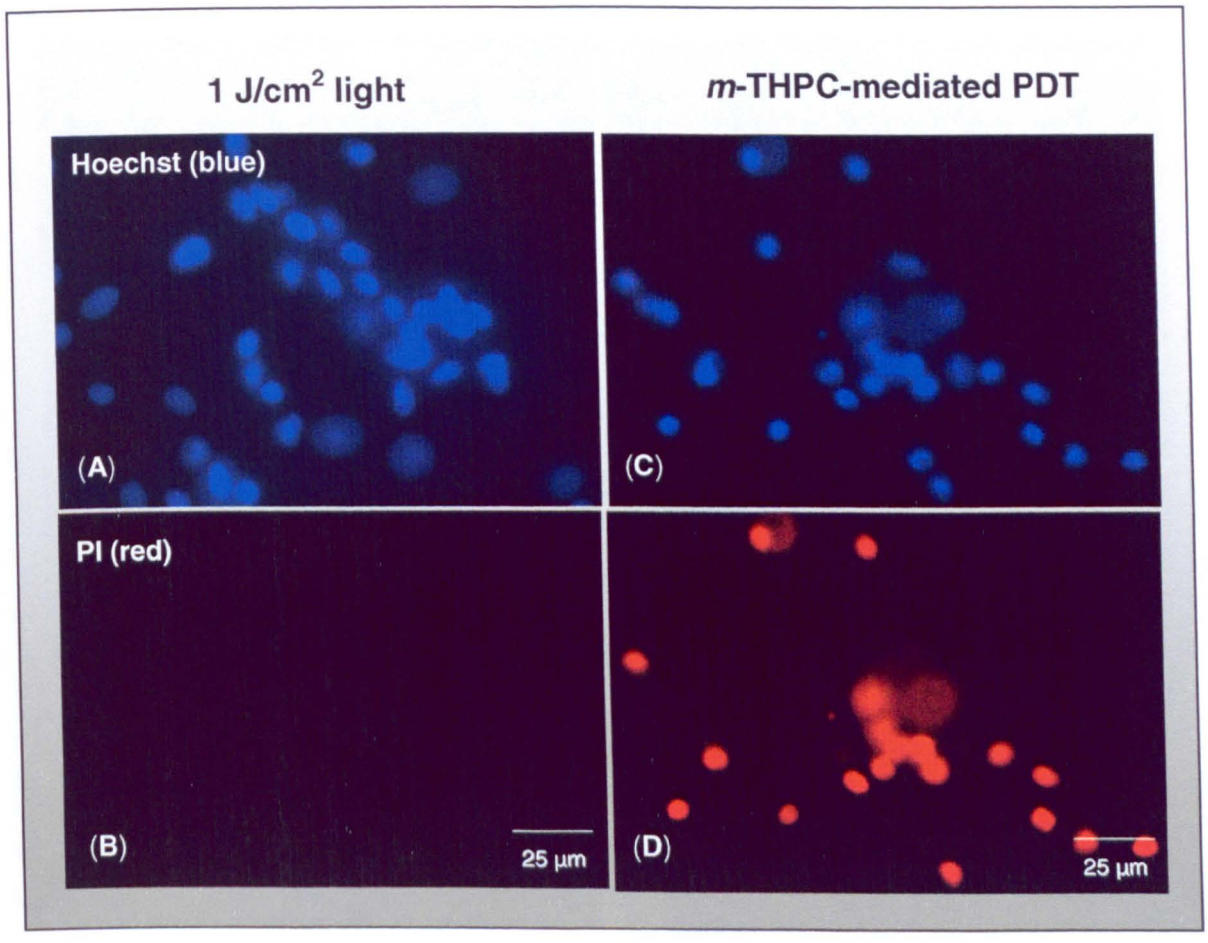

Figure 3.11
PI-stained DRG satellite cell cultures within thin collagen gels after 4 µg/ml *m*-THPC-mediated PDT and 1 J/cm^2 light only (no drug) control.
No dead cells were detected with no drug control (**A** and **B**), but a number of PI-stained dead cells were detected after *m*-THPC-mediated PDT (**C** and **D**).

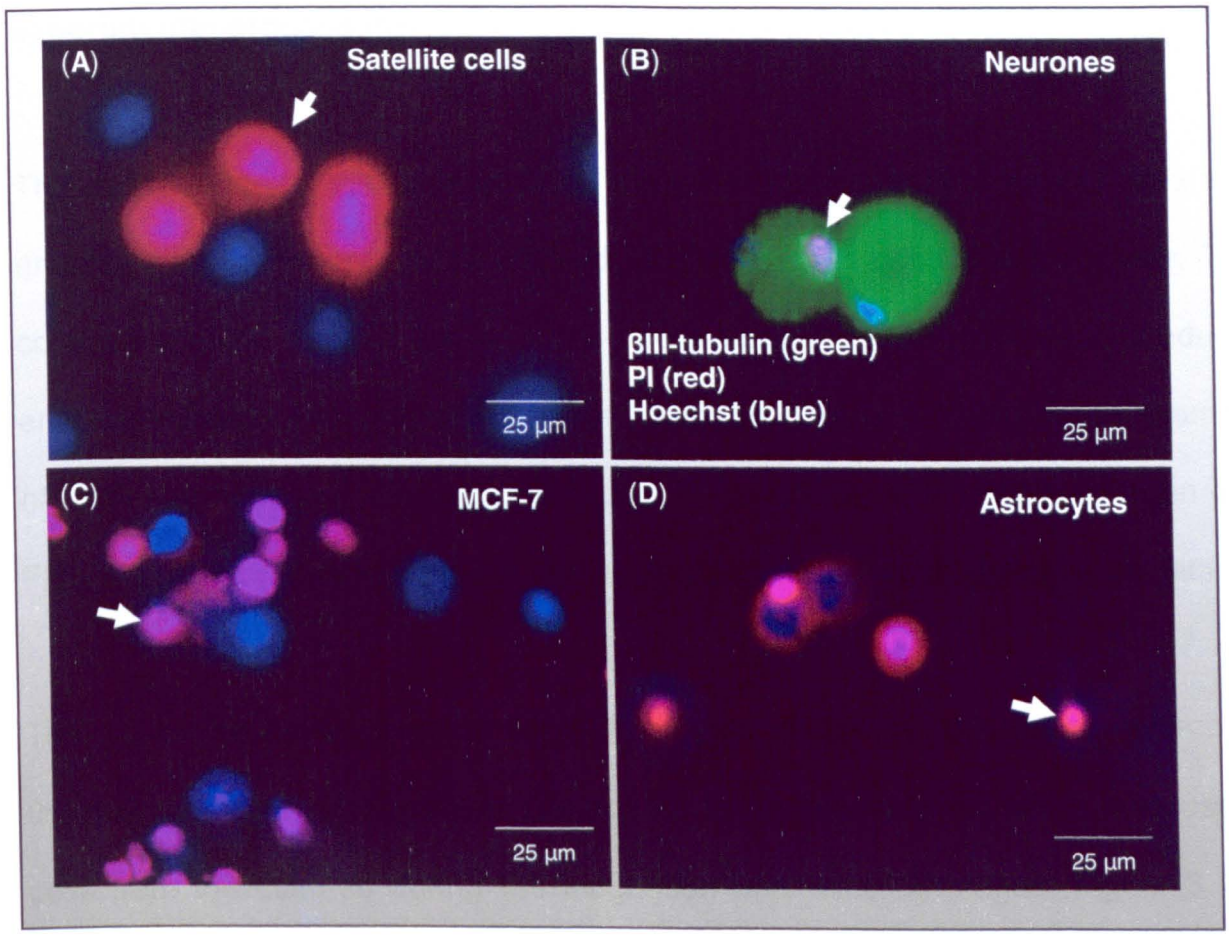

Figure 3.12
PI-stained cell cultures within thin collagen gels after 4 µg/ml *m*-THPC-mediated PDT.
Various cell types (**A**) DRG satellite cells; (**B**) DRG neurones; (**C**) MCF-7 cells; and (**D**) astrocytes were analysed for death after *m*-THPC-mediated PDT using PI staining. Examples of dead cell nuclei are indicated by arrows, βIII-tubulin labelled neurones and Hoechst 33258 labelled all nuclei.

3.3.3 Assessment of monolayer versus cell-seeded collagen cultures post-experimental processing

This collagen model system supported the growth of neural and tumour cells and enabled PDT treatments to be applied in a consistent controllable manner. The collagen scaffold trapped live and dead cells throughout the staining procedures enabling microscopic analyses of treated samples. Figure 3.13 shows an example of DRG neurones and satellite cells grown in co-culture within a thin collagen gel. Figure 3.14 shows neurite growth was supported within the 3D collagen gel lattice.

The reason for developing this thin 3D collagen culture system was to overcome the main limitation of monolayer cultures for these experiments, which was loss of cells from the cultures during the incubation and washing stages. Figure 3.15A shows DRG cells seeded within collagen cultures (3D) exhibited an increase in percentage of dead cells following PDT with increasing *m*-THPC concentrations. The equivalent use of monolayer (2D) cultures is also shown, which indicated a larger increase in percentage dead cells 24 h post-PDT incubation.

However, the apparent increase in percentage cell death in monolayer cultures (white bars) was accompanied by a decrease in overall cell numbers as cells were lost from the monolayer culture system. This resulted in the reduction of mean cell numbers calculated per cover glass in comparison to stable mean cell numbers per gel in the 3D cultures (Figure 3.15B). Treating satellite cell cultures with light only (no drug) did not induce cell loss or death from either monolayer or 3D cultures (Figure 3.15A and B). However, results in Figure 3.15B indicated that the use of monolayer cultures (white bars) was inadequate for the study of accurate

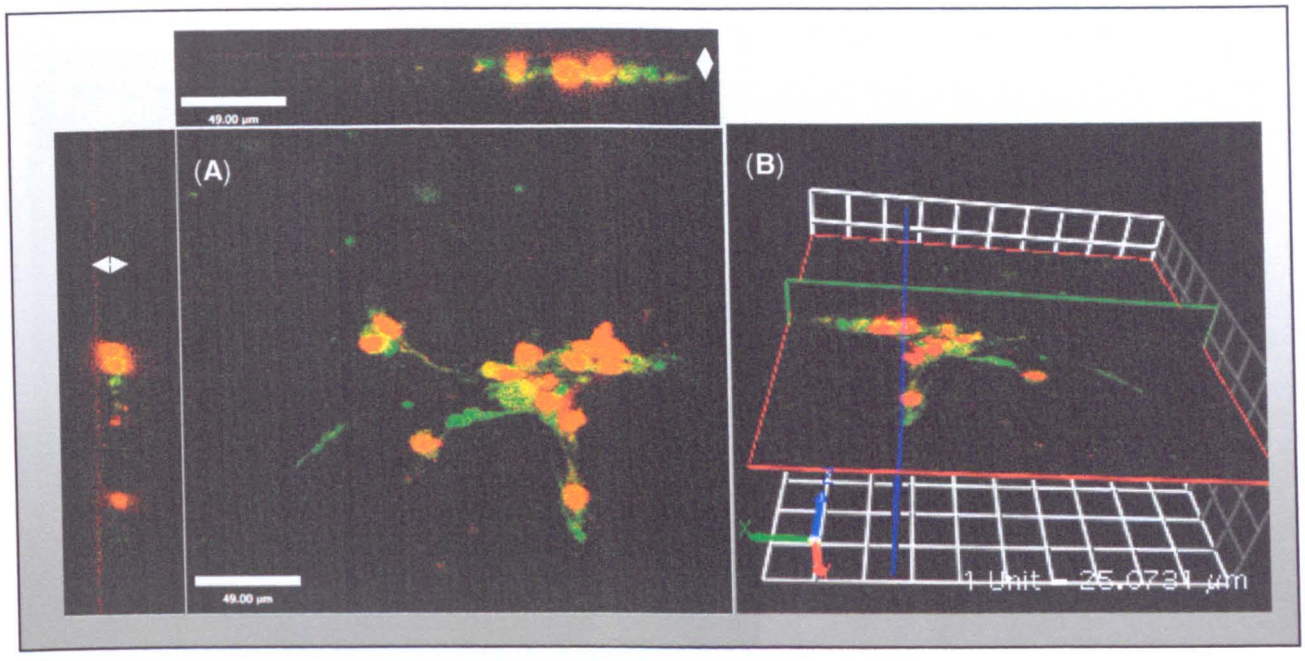

Figure 3.13
Confocal micrograph showing neurones and satellite cells in thin collagen cultures after 4 µg/ml *m*-THPC-mediated PDT.
Micrograph shows PI (dead cells; red nuclei) and βIII-tubulin immunofluorescence (neurone; green). Fixed gels were prepared for microscopy by compressing under cover glasses. Side views of z-stack show cells are within the collagen lattice limits (double headed arrows). (**A**) Confocal image is a maximum intensity projection for 400 optical sections through the flattened gel. Scale bar is 49 µm. (**B**) 3D projection using Volocity imaging software.

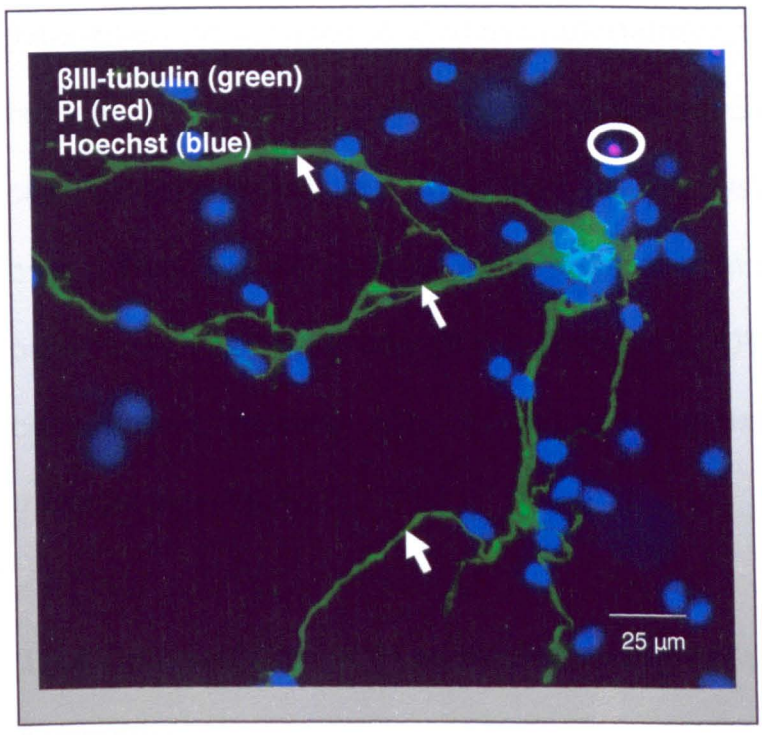

Figure 3.14
Micrograph of neurites grown from DRG neurones within collagen matrix.
Micrograph of fixed and immunostained 3D collagen culture shows Hoechst staining (total cell nuclei, blue), PI (dead cell nuclei, pink) indicated by a circle and βIII-tubulin (DRG neurone with neurites; green) indicated with arrows).

cell death responses following PDT; and supported the use of a 3D culture system (blue bars). The increase in dead cell detection accompanied with reduced cell numbers in monolayer cultures are possible indicators of more live cells than dead cells being lost from the monolayer culture system (Figure 3.15A and B white bars). Thus the 3D culture system gave a more accurate depiction of mean percentage dead cells, was able to withstand PDT and processing by retaining cell content and integrity after immunocytochemistry, and permitted the use of microscopic analysis.

3.3.4 Compatibility of PI exclusion assay with immunocytochemistry fixation procedure

In addition to reducing any cell losses during processing, if neurones were to be successfully identified within co-cultures it was necessary to ensure that the fixation required would not interfere with the PI exclusion assay (live/dead) results. It was important to assess whether PFA fixation might result in additional uptake of residual PI from the collagen gel surroundings into cells which had previously excluded it. Pilot experiments in which cells were fixed with 4 % (w/v) PFA before or after PI staining showed that fixation did not alter the plasma membrane in such a way as to result in an increase in the number of cells stained with PI (Figure 3.15).

This collagen gel culture system in combination with the PI exclusion assay use was also tested for the ability to display 100 % cell death. There were increases in the mean % of PI staining after 10 min incubation with 0.5 % (v/v) tritonX-100, which permeabilised cell plasma membranes allowing entry of PI into cells. Here near maximum cell death was detected for all cell types including neurones

following TritonX-100 treatment (Figure 3.16), confirming that detection of maximal cell death was achievable in this system.

These initial experiments confirmed that the combined use of the thin cell-seeded collagen gels with the PI exclusion assay, followed by fixation with PFA and immunostaining was feasible; therefore these collagen gel culture systems were suited for further use in this investigation.

3.3.5. Comparison of the relative sensitivity of specific cell types to PDT

Having established the effectiveness of the thin 3D culture system for assessing cell death following PDT, studies were undertaken to characterise the sensitivity of a range of cell types to *m*-THPC-mediated PDT. This approach allowed the differential responses of neurones and satellite cells growing in co-culture to be studied and compared to MCF-7 cells and to astrocytes. Studies were also undertaken using hypericin as an alternative photosensitiser, partly to gain an insight into this drug, but mainly to use it as a comparator to *m*-THPC to help validate the culture system. As for *m*-THPC, hypericin fluorescence was detected throughout the cytoplasm in each cell type as previously shown, but was not present in the nuclei or in the neurites.

Comparisons of the sensitivity of neurones, satellite cells and MCF-7 cells to *m*-THPC- and hypericin-mediated PDT are shown in Figure 3.17 and Figure 3.19 in addition to astrocytes in Figure 3.17. It is possible that increasing incubation time,

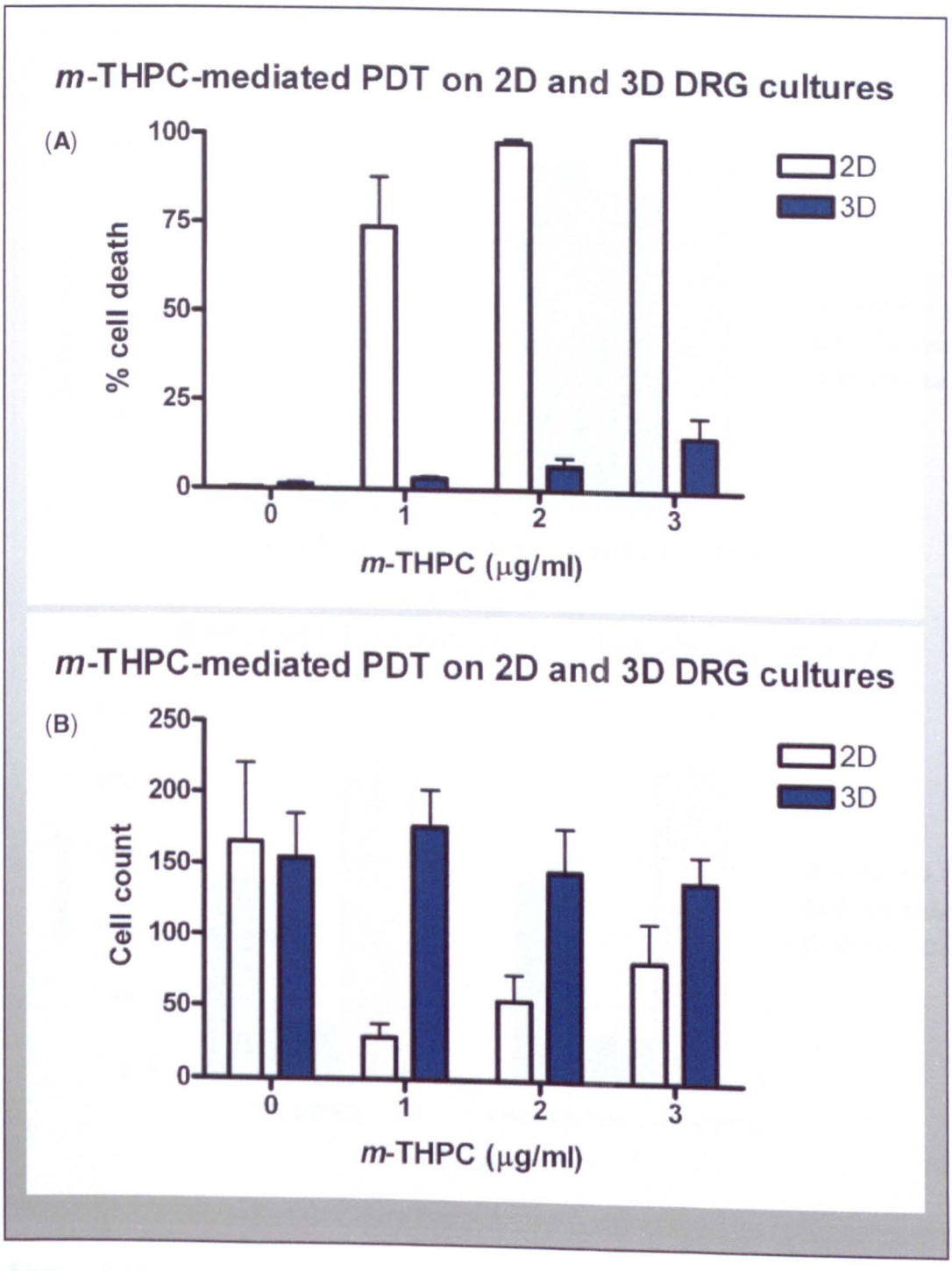

Figure 3.15
The analysis of cell death in monolayer and 3D DRG cultures following PDT.
Graphs show data from fixed and immunostained culture systems (**A**) A comparison of the % of DRG cell death in 2D and 3D culture systems post-PDT and immunostaining and (**B**) A comparison of the mean DRG cell numbers detected per cover glass or gel, in the same experiment. Data were collected from 3 random fields and presented as mean ± SEM of 9 separate cover glasses (2D cultures) and 6 separate gels (3D cultures).

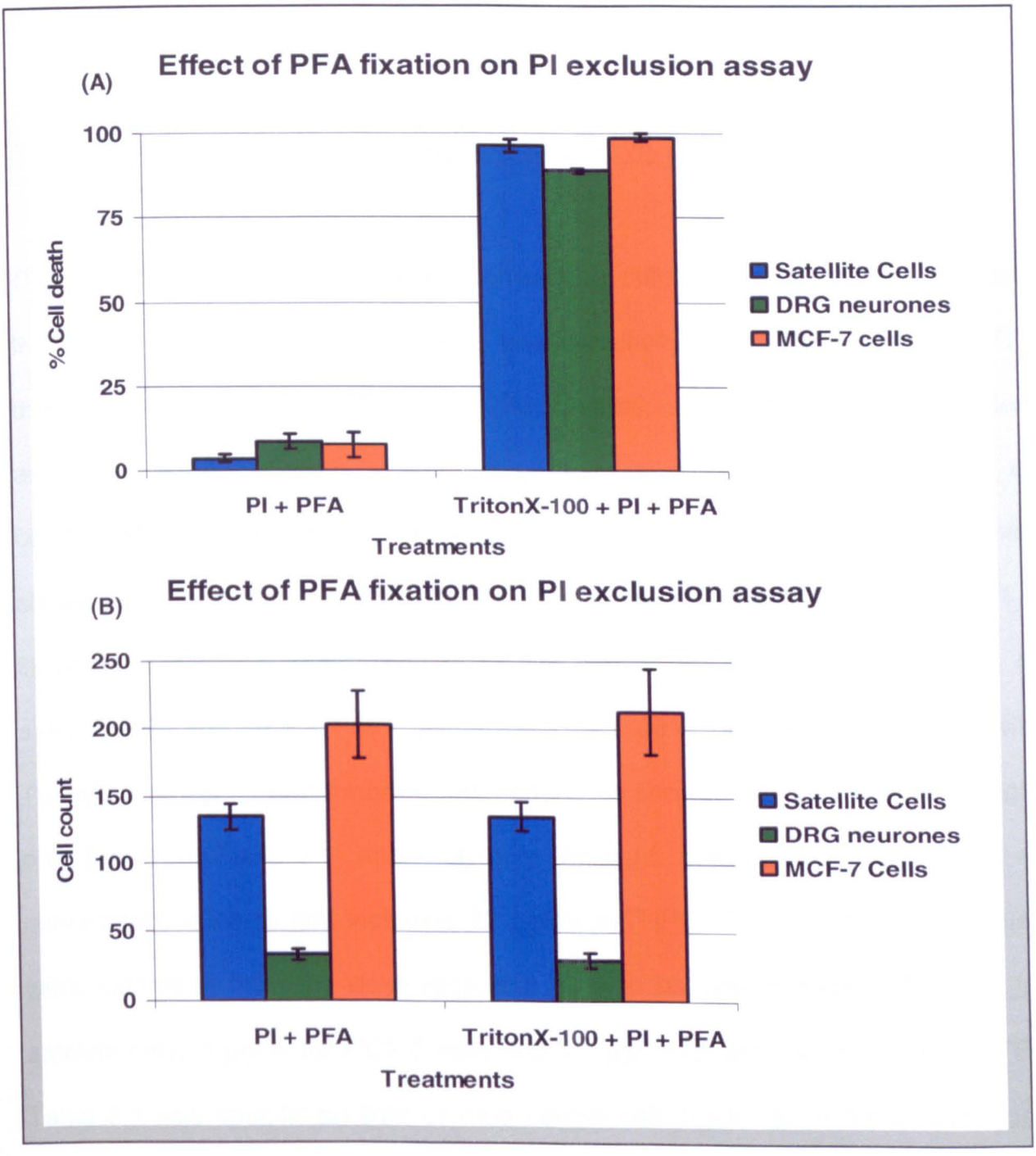

Figure 3.16
Assessment of 100 % cell death detection.
(**A**) PFA fixation did not affect PI exclusion assay results (addition of PI and then PFA); and 100 % cell death detection was possible in this culture system using PI exclusion assay (addition of TritonX-100, then PI and PFA). (**B**) Cell numbers remained constant. Data were collected from 3 representative fields (satellite cells and MCF-7 cells) and all detectable neurones in each gel. Data are presented as mean ± SEM of at least 3 separate gels. (DRG neurones and satellite cells were co-cultured in 3D collagen culture systems)

photosensitiser concentration or light dose may result in an increase in the killing efficiency of PDT on cell types used in this study, including neurones.

3.3.5.1 Relative sensitivity of different cell types to *m*-THPC-mediated PDT

The dose-response profiles obtained showed a difference in sensitivity between the cell types, with neurones showing less sensitivity to *m*-THPC-mediated PDT than the other cell types (Figure 3.17A). Overall, sensitivity was in the order: astrocytes > MCF-7 cells > satellite cells > neurones across the range of concentrations. Interestingly, at 4 μg/ml *m*-THPC-mediated PDT, neurones showed significantly lower sensitivity than the other cell types, with only 11.9 ± 1.4 % neurone death in comparison to 48 ± 5.4 % in MCF-7 cells, 39 ± 4.0 % in satellite cells and 89 ± 3.1 % in astrocytes ($p < 0.001$ using one-way ANOVA with Tukey's post test). Furthermore treated neurones showed no more death than light only (no drug, Table 3.1) and drug only (no light, Figure 3.17B) controls at all concentrations up to and including 10 μg/ml *m*-THPC. PDT-induced EC_{50} values were estimated from the dose response data to be approximately 10 μg/ml for satellite cells, 4 μg/ml for MCF-7 cells and 1.5 μg/ml for astrocytes (Figure 3.17B). Table 3.1 lists specific no light or drug control cell death values for all cell types used, which were similar in value to their respective light only (no drug) controls. Figure 3.18 shows a series of representative micrographs of cell death after *m*-THPC-mediated PDT in each cell type.

3.3.5.2 Relative sensitivity of different cell types to hypericin-mediated PDT

To investigate the sensitivity of these cells to another PDT agent and confirm that neuronal death by PDT could be detected using this culture system, the

experiment was repeated using hypericin. Unlike *m*-THPC-mediated PDT, Figure 3.19A shows neurones, MCF-7 cells and satellite cells were all sensitive to hypericin-mediated PDT in a similar dose-dependent response pattern. At concentrations of 2.2 µg/ml and above, there was a significant difference in cell death between hypericin-PDT-treated neurones and untreated controls (Figure 3.19) ($P<0.001$ using one-way ANOVA with Tukey's post test). Table 3.2 lists the no light or drug control values of cell death for all cell types used, which were similar in value to their respective light only (no drug) controls and Figure 3.20 shows a series of representative micrographs of cell death after hypericin-mediated PDT.

3.3.6 Morphological effect of PDT on neurites

The effect of PDT on neurites of DRG neurones was also of importance in this study. This was because it is the neurites (or axonal projections, *in vivo*), which are commonly at risk of exposure to PDT while treating tumours in areas of the body rich in peripheral nerves. Both *m*-THPC and hypericin fluorescence were shown not to be detected in neurites of these neurones.

Figure 3.21 shows *m*-THPC mediated PDT reduced the neurite length of DRG neurones in monolayer after a 24 latency period. There was no statistically significant effect on the neurite length when drug or light were applied separately, or when PDT was performed using 0.1 µg/ml *m*-THPC, whereas PDT using higher

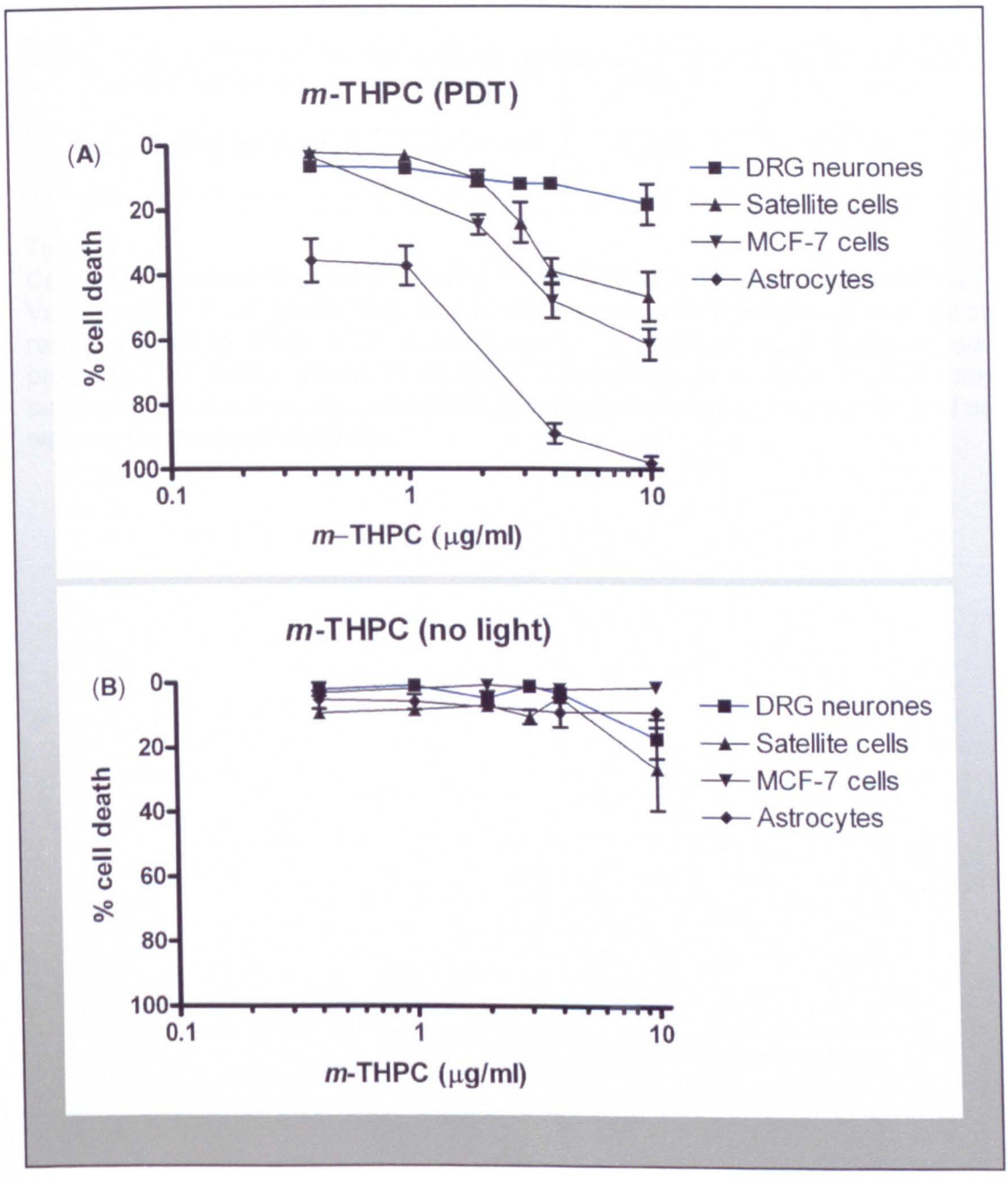

Figure 3.17
Comparison of specific cell type sensitivity to *m*-THPC-mediated PDT treatments. Graphs show comparisons of various cell types (co-cultured DRG neurones and satellite cells, astrocytes and MCF-7 cells). Cells were cultured in 3D collagen culture systems and were fixed and immunostained after PI-exclusion assay was applied (**A**) 24 h after *m*-THPC-mediated PDT and (**B**) their respective no light controls. Data were collected from 3 representative fields of each gel, and presented as mean ±SEM of at least 3 separate gels (no light controls) and 9 separate gels (*m*-THPC-mediated PDT). MCF-7 cells were assessed separately from astrocytes, and DRG cultures (co-cultures of neurones and satellite cells) were also assessed separately.

Further assay controls	Neurones	Satellite cells	Astrocytes	MCF-7 cells
1 J/cm^2 light only	3.52±0.7	4.78±1.1	3.17±0.5	7.6±1.0
No *m*-THPC or light	3.1±1.0	4.22±1.2	8.81±3.1	1.89±0.7

Table 3.1
Comparison of no drug or light and 1 J/cm^2 light only (no drug) controls.
Values are of mean percentage dead cells for each cell type after 4 h incubation of phenol red free DMEM. Data were collected from 3 representative fields of each gel, and presented as mean ±SEM of at least 3 separate gels. MCF-7 cells were assessed separately from astrocytes, and DRG cultures (co-cultures of neurones and satellite cells) were also assessed separately.

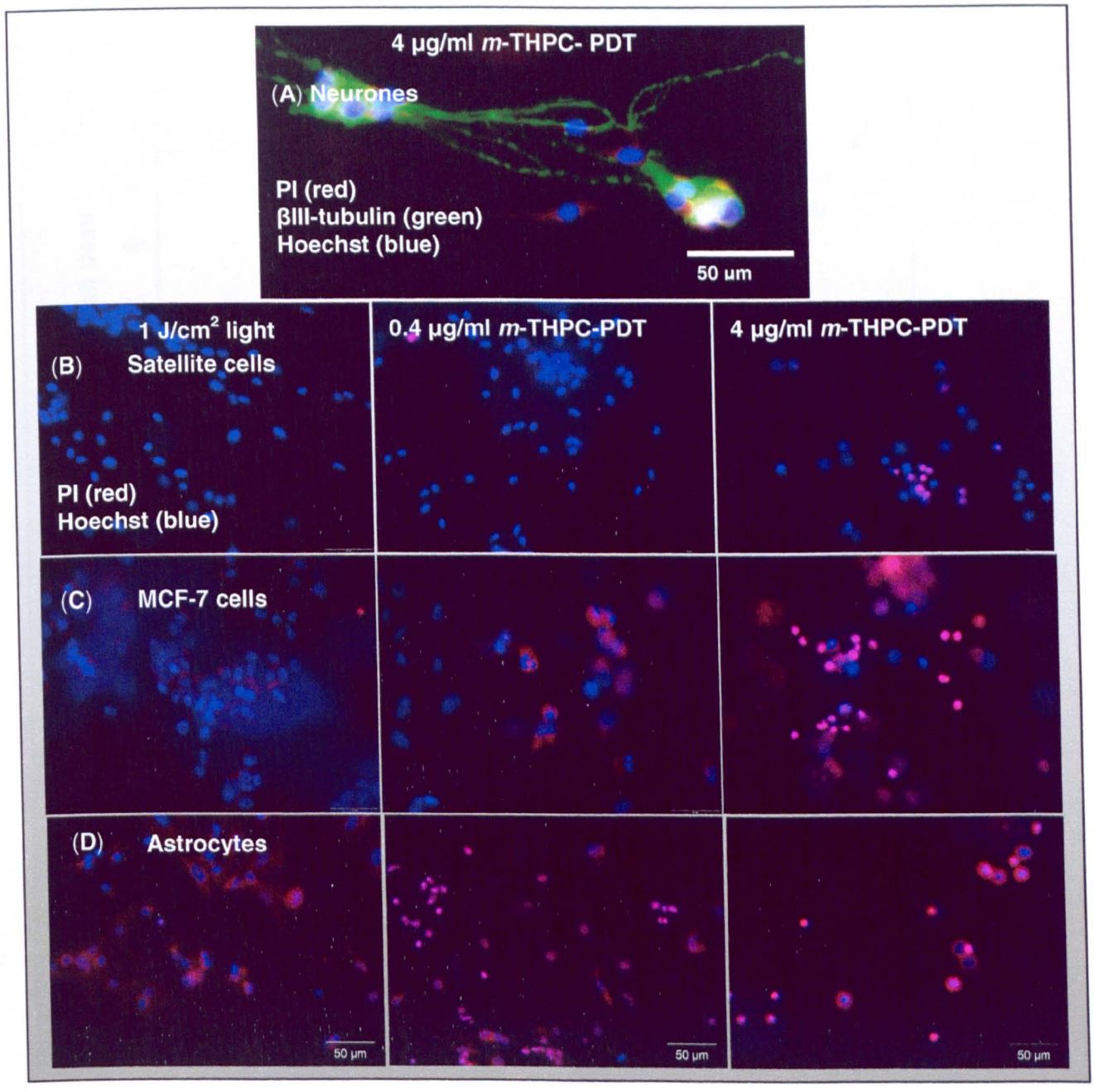

Figure 3.18
Representative micrographs of cell death after *m*-THPC-mediated PDT.
Micrographs are representative images of fields of the fixed 3D collagen culture system after treatment with *m*-THPC-mediated PDT and fluorescence staining. (**A**) Neurones, (**B**) Satellite cells, (**C**) MCF-7 cells and (**D**) Astrocytes. Cells were PI stained 24 h after exposure to light. (Note these images were not used to collect data, and that there is some red cytoplasmic staining which is the *m*-THPC localised in these cells).

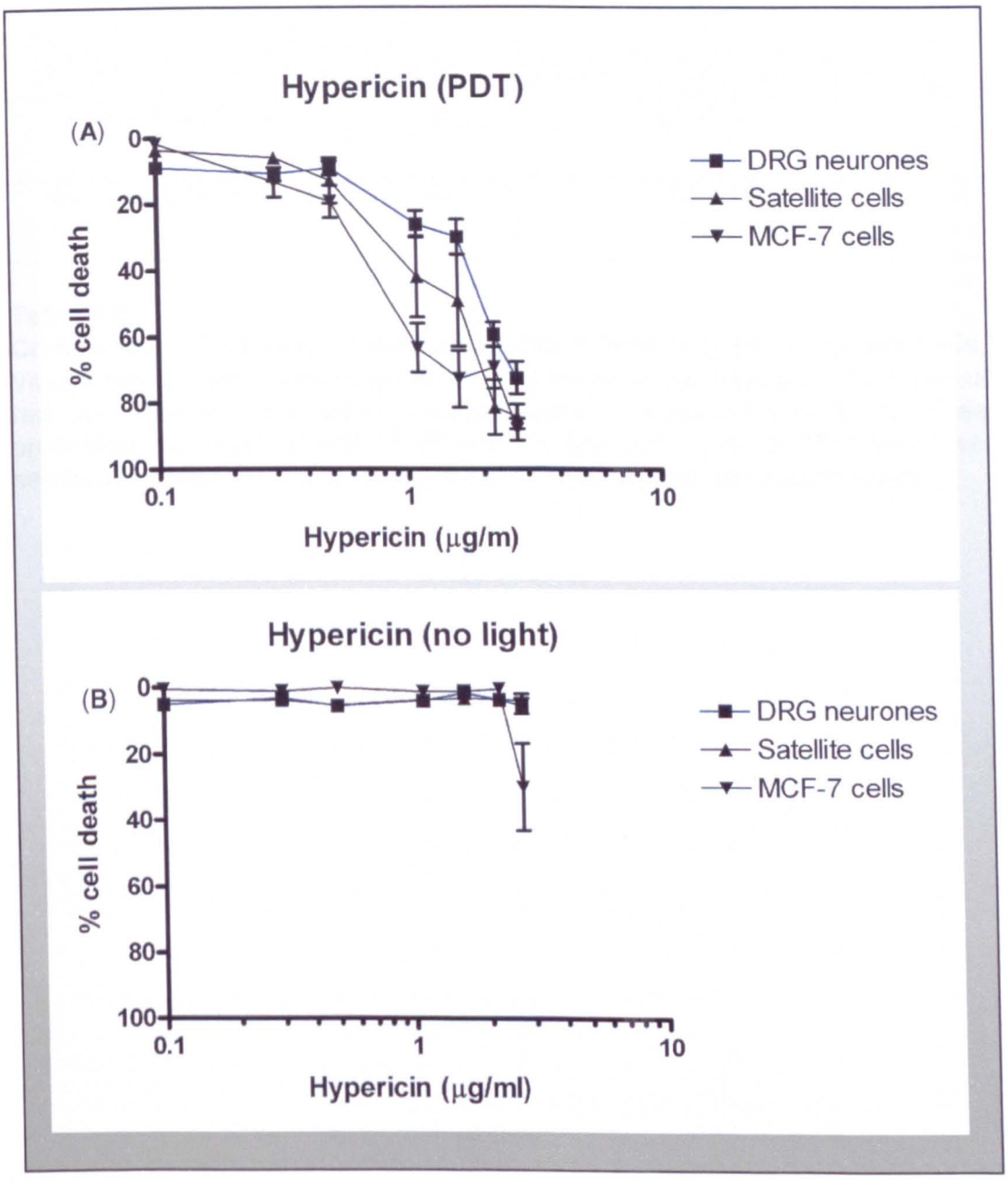

Figure 3.19
Comparison of specific cell type sensitivity to hypericin-mediated PDT.
Graphs show (co-cultured DRG neurones and satellite cells, astrocytes and MCF-7 cells). Cells were cultured in 3D collagen culture systems and were fixed and immunostained after PI-exclusion assay was applied (**A**) 24 h after hypericin-mediated PDT and (**B**) no light controls. Data were collected from 3 representative fields of each gel, and presented as mean ± SEM of at least 5 (no light controls) or 6 (hypericin-mediated PDT) independent gels. MCF-7 cells were assessed separately from DRG cultures (co-cultures of neurones and satellite cells)

Further assay controls	Neurones	Satellite cells	MCF-7 cells
1 J/cm^2 light only	7.9±1.1	4.0±0.9	1.0±0.2
No hypericin or light	5.4±1.27	8.0±2.78	1.61±0.65

Table 3.2
Comparison of no drug or light and 1 J/cm^2 light only (no drug) controls.
Values are of mean percentage dead cells for each cell type after 7 h incubation of phenol red free DMEM. Data were collected from 3 representative fields of each gel, and presented as mean ±SEM of at least 5 separate gels. MCF-7 cells were assessed separately from DRG cultures (co-cultures of neurones and satellite cells)

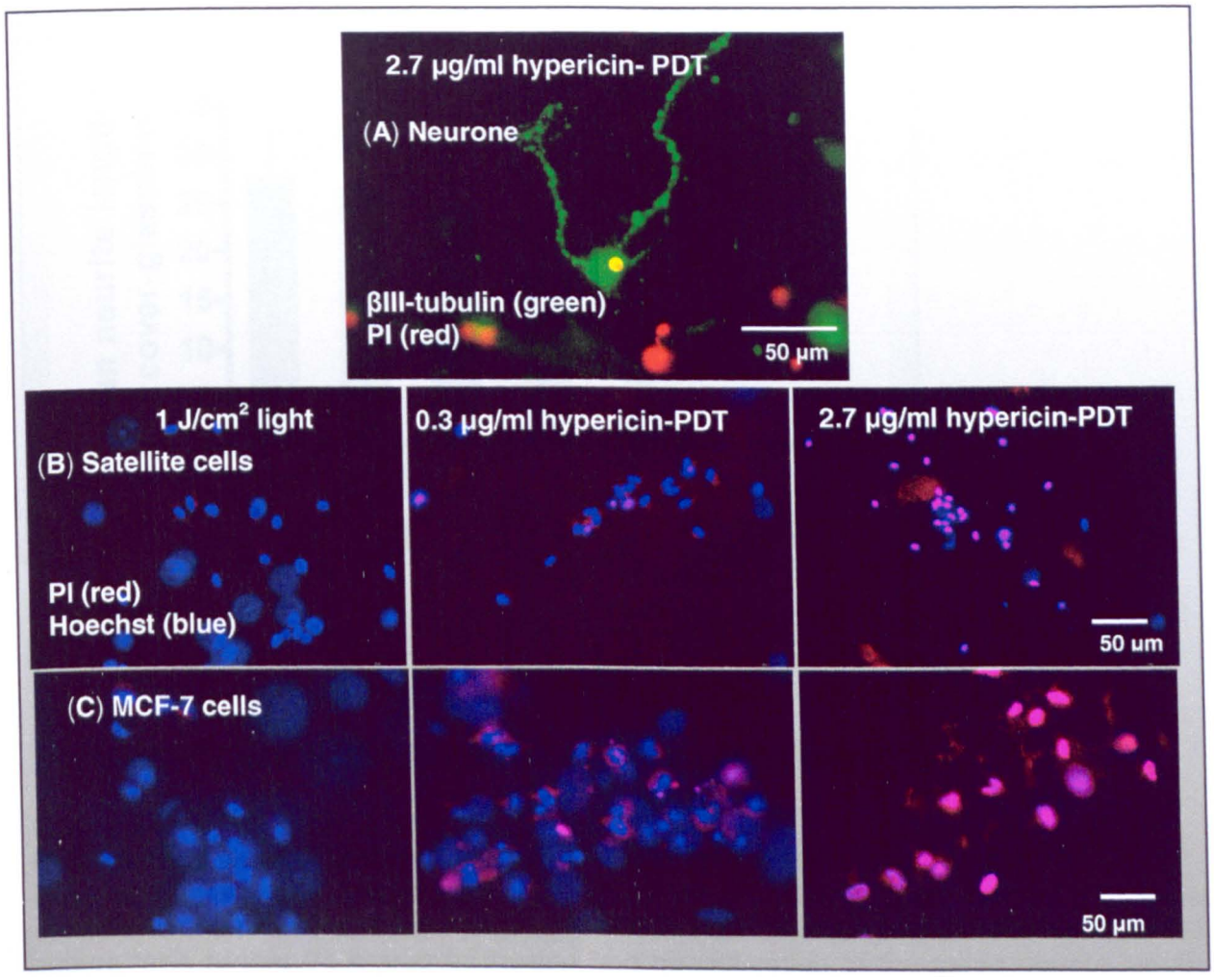

Figure 3.20
Cell death after hypericin-mediated PDT.
Micrographs are representative images of fields of the fixed 3D collagen culture system after treatment with hypericin-mediated PDT and fluorescence staining. (**A**) Neurone, (**B**) Satellite cells and (**C**) MCF-7 cells. Cells were PI stained 24 h after exposure to treatment conditions. (Note these images were not used to collect data, and that there is some red cytoplasmic staining which is the hypericin localised in these cells.)

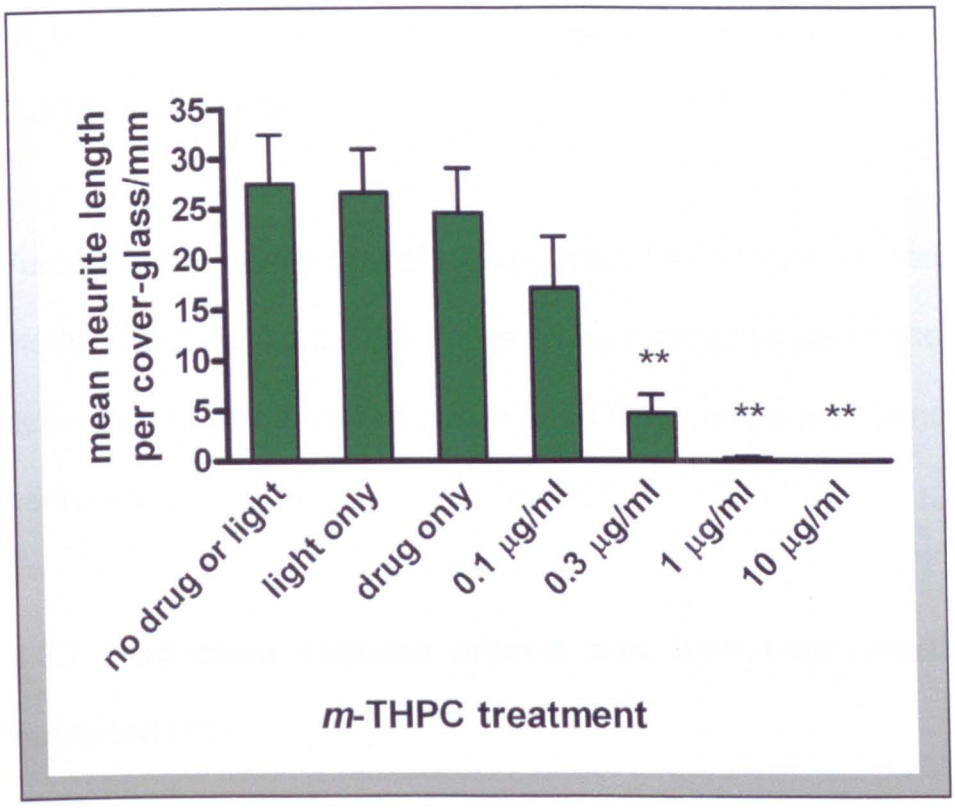

Figure 3.21
Reduction in neurite length due to *m*-THPC-mediated PDT treatments.
DRG neurones were cultured on cover-glass for three days then treated with various concentrations of *m*-THPC and blue light of 4.2 J/cm^2. Samples were then maintained in culture for a further 24 h prior to fixation and quantification of the mean neurite length in millimetres, of all βIII-tubulin immunostained neurites. Data were presented as means ± SEM of 4 separate cover glasses. One-way ANOVA with Dunnett's multiple comparison post test were used to assess neurite lengths. Significant decreases in lengths are marked as (**) $P<0.001$ for treatments compared to no drug or light control. **Figure prepared by** Elizabeth Liniker, in Wright *et al.* (2009).

concentrations of *m*-THPC (0.3 µg/ml and above) caused a significant reduction in neurite length compared with untreated controls ($P<0.001$, one-way ANOVA with Dunnett's post test).

Further to this, in the present study, most DRG neurones assessed for viability in the thin 3D collagen culture system were microscopically observed to be lacking in detectable neurites after exposure to PDT in comparison to non-PDT treated DRG neurones.

3.3.7 Distinction between mitosis and DNA fragmentation post-hypericin-mediated PDT

After treatment with hypericin-mediated PDT, satellite cells and MCF-7 cells displayed some fragmented nuclei, a feature which was not detected in *m*-THPC-mediated PDT and which may have indicated a difference in the type of cell death mediated by the 2 photosensitisers. Nucleus fragmentation can be an indication of apoptosis, but could also be a feature of cells undergoing mitosis at the time of cell death. Hypericin is known to cause cells to arrest in mitosis, so it was useful to investigate this further using a marker of mitosis. Figure 3.22A, B and C shows DNA fragmentation in satellite cells stained with Hoechst 33258 and PI. Mitotic satellite cells were detected using P-MPM2 (green). As a positive control for P-MPM2 staining, cells were poisoned during mitosis using colchicine and Figure 3.22D shows a number of mitotic satellite cells. When the presence of mitosis was investigated in cells after hypericin-mediated PDT (Figure 3.22E) it was clear that the fragmented DNA was not necessarily associated with P-MPM2 positive cells and was therefore likely to indicate apoptosis.

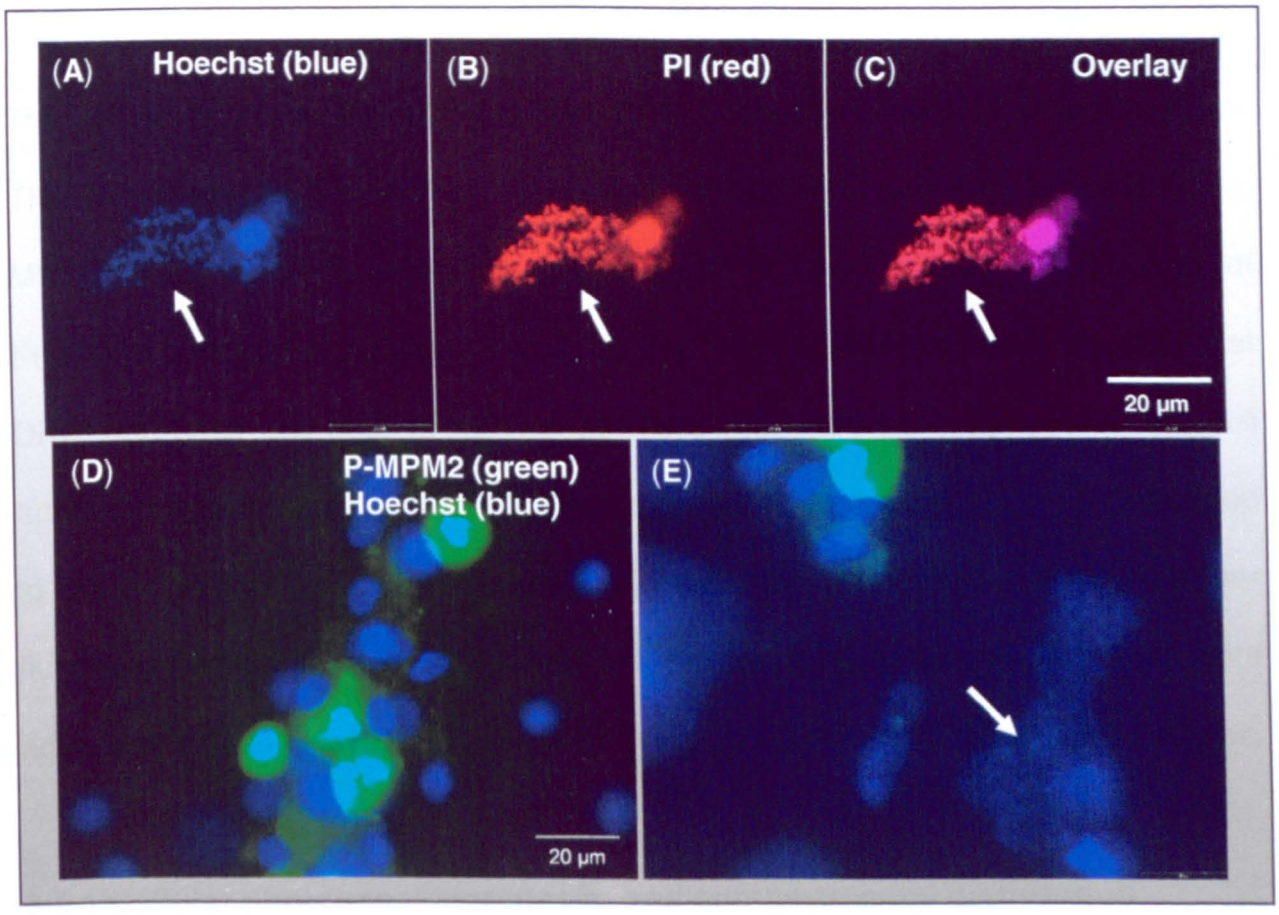

Figure 3.22
Nuclear morphology change and mitosis detection after hypericin-mediated PDT in DRG satellite cells.
Micrographs show fixed and immunostained satellite cells co-cultured with neurones in 3D collagen culture systems (**A**) Hoechst stain (blue) indicating nuclear material , (**B**) PI stain (red) indicating nuclear material of cells with compromised membrane and (**C**) Overlay of Hoechst and PI images to demonstrate the fragmentation observed 24 h after 1.6 µg/ml hypericin-mediated PDT in satellite cells. 50 ng/ml colchicine treatment arrested DRG satellite cells during mitosis showing that they were detectable using (**D**) P-MPM2/FITC immunostaining (green) and (**E**) After 1.6 µg/ml hypericin-mediated PDT, some satellite cells were positive for P-MPM2/FITC staining, but other cells which were not undergoing mitosis exhibited the nuclear fragmentation. (Arrows indicate fragmented nuclei)

3.4 Discussion

The key finding from this study is that DRG neurones were less sensitive to *m*-THPC-mediated PDT than their associated satellite cells and the tumour cell line, MCF-7, both of which exhibited dose-dependent cell death over the range of treatment concentrations used. This is an important observation as it indicates that DRG neurones are able to survive *m*-THPC-mediated PDT treatments that kill tumour cells, offering the possibility that therapeutic regimens could be developed to treat tumours in close proximity to neurones. In addition photosensitiser fluorescence was not detected in neurites, but these neuronal compartments were adversely affected by PDT treatment both in monolayer and in 3D culture systems.

3.4.1 Cellular photosensitiser uptake and compartmental distribution

In this study all cells showed uptake of *m*-THPC and hypericin photosensitisers into the cytoplasm. DRG neurones appeared to accumulate more *m*-THPC in 4 h incubation periods than co-cultured satellite cells on the basis of detected fluorescence intensity; however this may have been to do with their size and shape rather than an actual difference in uptake. *m*-THPC uptake rate has been reported to vary between different cell types, for example Triesscheijn *et al.* (2004) showed that in hMVEC (human dermal microvascular endothelial) cells *m*-THPC content increased linearly for at least 48 h, in comparison to HMESO-1 (mesothelioma-derived cell line) cells, HNXOE (head and neck squamous cell carcinoma cell line) cells and BCT-27 (human fibroblast of normal breast skin) cells which reached maximum fluorescence at 24 h. In this study DRG neurones displayed maximum *m*-THPC fluorescence in neuronal cell bodies by 7 h after

incubation of 4 μg/ml *m*-THPC with no further increase at 24 h. However, since uptake was only slightly greater at 7 h than that at 4 h, the shorter time point was used for convenience. Furthermore, Sasnouski *et al.* (2007) showed that a moderate incubation of 3 h for 7.5 μM (5.1 μg/ml) *m*-THPC resulted in a 1.8 times higher absorbed photons than 24 h incubation in MCF-7 cells, providing further support for the 4 h incubation time chosen here. This may be the result of *m*-THPC self-quenching after aggregation within cells due to high intracellular concentration.

Subcellular localisation of photosensitisers within cells is an important parameter to consider in photodynamic activity, due to the short lifetime displayed by $^1O_2$ generated at photodamaged sites. Phototoxicity may be more accurately deduced from subcellular localisation studies rather than from the amount of photosensitiser taken up by specific cell types (Laville *et al.*, 2003). This is because oxidative damage of cellular components is known to occur within 10 nm of the activated photosensitiser molecule (Sadauskaite *et al.*, 2004).

In previous studies, Sasnouski *et al.* (2007) observed a change in *m*-THPC uptake pattern over time from a more diffuse to a more punctate pattern; this was shown to be accompanied by a reduction in photosensitisation efficiency at high *m*-THPC concentrations within MCF-7 cells, which may be due to photosensitiser aggregation and self-quenching. *m*-THPC uptake in HT29 cells was also reported to display a diffuse *m*-THPC fluorescence with some bright spots in the cytoplasm, but not in the nucleus (Laville *et al.*, 2003). This study showed satellite cells, astrocytes and MCF-7 cells as having a punctiform subcellular distribution pattern, after 4 μg/ml *m*-THPC incubation for 4 h, whereupon illumination of these cells resulted in cell death. Neurones displayed more diffuse *m*-THPC fluorescence in

their cell bodies with no neurone death after illumination. The comparator photosensitiser, hypericin, used at a concentration of 1.6 μg/ml, displayed a diffuse localisation pattern in satellite cells and MCF-7 cells and neurones after 7 h incubation, and resulted in cell death after illumination.

Detailed investigation of the cellular localisation of *m*-THPC within neurones would be a useful future direction as differences in drug distribution between neurones and other cells might account for the differences in sensitivity reported here. This possibility is further investigated in the next chapter.

Intense *m*-THPC and hypericin fluorescence was observed in DRG neuronal cell bodies, with the absence of photosensitiser fluorescence in neurite compartments. This absence of photosensitiser fluorescence detection may be due to a lack of photosensitiser uptake into neurites, or subsequent movement of photosensitiser out of neurites. However, it is also possible that photosensitisers were present within the neurites, but perhaps due to the very narrow dimensions of this cellular compartment the fluorescence was below the level of detection of the microscopy used here.

3.4.2 Thin 3D cell-seeded collagen culture systems

Collagen gels have been used as culture substrates for many years because they provide a 3D environment in which cells can grow in a more natural spatial and physical environment than they would on a stiff monolayer substrate (Kim *et al.*, 2004; Brown and Phillips, 2007). The rate of diffusion of oxygen and other nutrients through collagen gels is relatively rapid, facilitating cell survival under normal conditions and ensuring that oxygen availability does not become a limiting

factor during PDT treatment. However, the main advantage of using a collagen gel system in this study was that cells remained trapped within the gels throughout treatment and in subsequent analysis stages. This meant that cell death could be determined more accurately than in many studies in which conventional cell monolayers were used. In those studies a proportion of cells were washed away during processing stages, and so the resulting analyses of cell death or cell viability do not account for all of the cells. Furthermore, trapping the cells in this manner enabled the multiple washes and incubations required for a PI exclusion assay to be used in conjunction with an immunostaining technique so that numbers of live or dead neurones and satellite cells could be analysed separately within a co-culture.

As the interaction between neurones and their associated satellite cells is important for neuronal function and survival, co-culture systems such as this are often favoured over isolated neuronal cultures. This is the first study in which the differential effects of *m*-THPC- and hypericin-mediated PDT have been shown on mammalian DRG neurones and satellite cells in co-culture. A previous study using isolated crayfish stretch receptors (neurones and glial cells) and the photosensitiser Photosens (a mixture of sulphonated alumophthalocyanines) mentioned that glial cells seemed more sensitive than neurones to proteolytic and PDT treatments in that system (Lobanov and Uzdensky, 2005). It would be interesting to explore whether mammalian neurones and glial cells have different sensitivities to Photosens in our system.

3.4.3 Relative sensitivity of cells to PDT

Primary mammalian DRG neurones in co-culture with satellite cells were shown to be less sensitive to *m*-THPC-mediated PDT than satellite cells, astrocytes and MCF-7 tumour cells. Satellite cells, astrocytes and MCF-7 cells all exhibited dose-dependent cell death over the range of PDT treatments applied. DRG neurones were able to survive *m*-THPC-mediated PDT treatment at doses that killed the other cell types. This neurone sparing, however, was not seen when the comparator, hypericin-mediated PDT treatment was administered.

3.4.3.1 *m*-THPC-mediated PDT

It is important to note that the EC_{50} value for MCF-7 cells (4 µg/ml *m*-THPC-mediated PDT) caused no dark toxic effect on cell types used in this study. Yet, when this concentration of *m*-THPC was activated using 1 J/ cm^2 light, it resulted in substantial glial cell and MCF-7 cell death as previously reported for MCF-7 cells in other culture systems (Koechli *et al.*, 1995). This was with no neurone death (after exposure to 0-10 µg/ml *m*-THPC-mediated PDT) above that seen in untreated controls.

3.4.3.2 Hypericin-mediated PDT

Hypericin was used as an alternative to *m*-THPC primarily to validate the thin 3D collagen culture system. The sensitivity of MCF-7 cells to hypericin-mediated PDT in this system was similar to that previously reported (Vandenbogaerde *et al.*, 1997). The presence of DNA fragmentation after hypericin-mediated PDT suggests that the mechanism of cell death caused by hypericin included apoptosis

to a greater extent than observed with *m*-THPC in MCF-7 and satellite cells (a feature not seen after *m*-THPC-mediated PDT). Similar apoptotic DNA fragmentation was observed 24 h after hypericin-mediated PDT on HeLa cells (Assefa *et al.*, 1999).

In contrast to *m*-THPC-mediated PDT, approximately 90 % neuronal death was detected after hypericin-mediated PDT. This confirmed that the lack of neuronal cell death detection after *m*-THPC-mediated PDT was not due to an inability to detect neuronal death in this culture system.

Together, the *m*-THPC and the hypericin data showed that this thin 3D collagen culture system can be used to compare mixtures of cells, exposing them to PDT and then combining cell death analysis with immunofluorescence identification to dissect out any differences in sensitivity between cell populations. This is a valuable culture system which could facilitate research in which the response of two or more cell types to PDT needs to be evaluated and may be particularly useful for studies comparing responses in tumour cells and non-tumour cells during screening for selective photosensitisers.

3.4.4 DRG neuronal cell body survival with neurite degeneration

The light dose (fluence rate) of 1 J/cm^2, showed no toxic effect to cells used in this study (without photosensitiser incubation). It has been suggested that in general an increase in light dose was less toxic than an increase in *m*-THPC concentration (Rousset *et al.*, 2000). This is because, with increasing light dose, photobleaching would occur which would destroy photosensitiser molecules and therefore reduce the toxic effect of PDT. Increasing the concentration of the photosensitiser would

increase the toxic effect of PDT; however it is possible that quenching of photosensitiser molecules would occur at high concentrations. Therefore this study concentrated on varying the photosensitiser concentration, while maintaining other variables, such as light source and fluence rate.

Previous studies showed that PDT using *m*-THPC was sufficient to inhibit conduction in crayfish stretch receptor neurones at concentrations much lower than those used in this study 10 nM or (0.0068 µg/ml) (Uzdensky *et al.*, 2004). These previous data, together with our neurite loss results, indicated that, in cell culture, neuronal function is compromised by *m*-THPC-mediated PDT, but that unlike other cell types they have the capacity to survive *m*-THPC-mediated PDT treatment, giving them the potential for regeneration and subsequent restoration of function.

Neurones are thought to use a range of intracellular signalling pathways to maintain their survival, and their neurite integrity. Goldberg (2003) suggested that the response of trophic factors may diverge inside neurones (i.e. one response to maintain neurone survival and another to maintain neurite integrity). This may explain the observation of neuronal cell body survival accompanied by neurite loss in this study. However, a review by Conforti *et al.* (2007) reports that neuronal sub-compartments (neuronal cell bodies and neurites) are known to depend on each other for survival. Therefore, impairment of one of these neuronal compartments could in theory result in the degeneration of the other. Survival of the neuronal cell body may therefore be dependent on neurites, while neurites are known to be protected by the slow Wallerian degeneration protein (Wld^s) (reviewed by Conforti *et al.*, 2007) produced by the neuronal cell body.

Previous work from this group showed significant DRG neurite loss after *m*-THPC-mediated PDT in monolayer cultures (Wright et al., 2009) and similar loss of DRG neurites after ALA-mediated PDT. Loss of DRG neurites was also observed but not quantified in this study after using both *m*-THPC- and hypericin-mediated PDT in collagen gels. Interestingly, this phenomenon of neurite loss accompanied by neuronal cell body survival after *m*-THPC-mediated PDT is similar to that reported by Hahn *et al.* (2008) in primary human DRG neurones exposed to HIV. In that culture study, neuronal cell bodies survived oxidative stress imposed by HIV infected macrophage supernatant, while their neurites retracted. These human DRG neurones were also found to have suffered mitochondrial dysfunction in their neuronal cell bodies, but not in the retracted neurites. The damage to neurites was suggested by Hahn *et al.* (2008) to have occurred independently of the induced oxidative stress. It was shown previously by Sayan *et al.* (2004) in rat sciatic nerves injured by ROS, that antioxidants were able to rescue neuronal cell bodies, but not neurites from oxidative stress. These studies re-highlight the point that neurones may have responded to *m*-THPC-mediated PDT using different mechanisms for these 2 neuronal compartments (neuronal cell bodies and neurites).

It is interesting that the decrease in neurite length in monolayer cultures occurred despite the lack of detection of any photosensitiser along the length of the neurites. If there was no photosensitiser present in the neurites, *m*-THPC-mediated PDT in the neuronal cell body might have activated or inhibited pathways which resulted in neurite loss, but not DRG neurone death.

The complex relationship between neurones and glial cells makes it difficult to speculate any further about a mechanism by which *m*-THPC-mediated PDT

reduced neurite length without killing neurones, as neurite outgrowth can be influenced by factors such as the level of activation of the supporting glial cells (Armstrong *et al.*, 2008), membrane proteins expressed on the surface of the glial cells (Castro and Kuffler, 2006) and diffusible factors released from them (Armstrong *et al.*, 2007). This means that the changes in neurite length measured in these co-cultures could be a result of the effect of the PDT on the accompanying satellite cells rather than a direct effect on the neurones. Further studies could address this point by investigating the effects of *m*-THPC on neuronal cultures in the absence of supporting glia; however for this study it was important to use co-cultures since they are more reminiscent of the neuronal environment *in vivo*.

3.5 Conclusions

In summary, the results in this Chapter demonstrated the uptake of photosensitisers (*m*-THPC and hypericin) by neural and MCF-7 tumour cells *in vitro*. Cellular distributions appeared to be cytosolic, with no detectable photosensitiser along the neurites or in nuclei. A useful thin collagen-based culture system was developed in which to investigate the sensitivity of specific cell types to PDT in mixed-cultures and in isolation. The ability to keep both dead and live cells trapped in the collagen gel allowed the accurate detection of cell death and the identification of neurones in mixed cultures. The key finding from these experiments was to identify that there are particular *m*-THPC-mediated PDT conditions in which DRG neurones survive treatment while tumour cells and glial cells are killed. Although the effects of *m*-THPC-mediated PDT on the PNS (satellite cells) and the CNS (astrocytes) glial cells were substantial, these cells

are able to proliferate and to re-innervate intact collagen structures of PDT treated areas. *m*-THPC-mediated PDT treatment may therefore offer the possibility of a therapeutic procedure, which could be refined to treat tumours in close proximity to DRGs (e.g. vertebral tumours (Burch *et al.*, 2005)).

Chapter 4: Investigation of DRG neurone sparing after *m*-THPC-mediated PDT *in vitro*

4.1 Introduction

In Chapter 3, DRG neurones were shown to survive *m*-THPC-mediated PDT doses that killed satellite cells, MCF-7 cells and astrocytes cultured in 3D collagen gels. This DRG neurone-sparing phenomenon is investigated in this chapter. Firstly, the survival of DRG neurones post-*m*-THPC-mediated PDT was assessed for signs of an early phase of apoptotic cell death, which may have been missed in the previous chapter due to the use of the PI exclusion assay (this does not detect early stages of apoptosis) at a single time point, 24 h post-PDT (latency period). The time course of cell death is known to vary between different cell types (Sundquist *et al.*, 2006); and apoptotic cell death rate in PDT killing can vary considerably according to the cell type, the photosensitiser and concentration used, the photosensitiser/light dose interval, and the photosensitiser subcellular localisation (Noodt *et al.*, 1999; Oleinick *et al.*, 2002; Bourré *et al.*, 2002). There is a therefore a possibility that DRG neurones may require a much longer latency period, than other cell types used in this study, before showing signs of a compromised membrane (cell death).

A series of experiments are presented: 1) Shorter and longer latency periods were tested with the PI exclusion assay for DRG neurone and satellite cell death and 2) Assessment of the ability of DRG neurones to function post 4 μg/ml *m*-THPC-mediated PDT in terms of the regeneration of neurites following PDT. Having established that DRG neurones are indeed surviving *m*-THPC-mediated PDT, the

work described in this chapter then starts to investigate the mechanism that may be responsible. Selective inhibition of specific intracellular antioxidant pathways identified potential protective mechanisms within neurones, and detailed analyses of intracellular drug and $^1O_2$/ROS localisation were undertaken to compare neurones to other cells in terms of PDT drug distribution and toxic product generation respectively.

4.1.1 Brief overview of how nerves respond to oxidative stress

The accumulation of ROS in rat sciatic nerves has been shown to cause lipid peroxidation, protein oxidation and DNA damage, which can result in nerve fibre degeneration and the breakdown of the PNS blood-nerve barrier (Sayan *et al.*, 2004). In addition, after constriction injury to rat sciatic nerve the resultant oxidative stress has been shown to increase the enzymes SOD and GPx, and to reduce the activity of the antioxidant GSH and the enzyme catalase in the spinal cord, DRGs, dorsal root and ventral root (Varija *et al.*, 2009). Cells have endogenous intracellular antioxidant pathways, which provide a level of protection from oxidative stress. Interestingly, it has been suggested that in neurones, the neuronal cell bodies are protected from effects of oxidative stress, but not their neurites (Sayan *et al.*, 2004), suggesting the presence of different mechanisms regulating the damage response within each neurone compartment. SOD and GSH are important ways in which neurones deal with oxidative stress, so investigations were made into whether they were involved in DRG neural cell survival after *m*-THPC-mediated PDT.

In this study the intracellular antioxidant pathways investigated in terms of their contribution to protecting neurones during PDT were the SOD-1 and SOD-2

pathways, and the glutathione synthase pathway. These intracellular antioxidant pathways were chosen in preference to others such as catalase (Valencia and Morán, 2004), cytochrome *C* oxidase (Taylor and Moncada, 2009) or heme oxygenase (Gomer *et al.*, 1991; Almeida *et al.*, 2004; Frank *et al.*, 2007) because they are the main pathways associated with neuronal survival in other systems (e.g. brain (Gonzalez-Zulueta *et al.*, 1998; Gegg *et al.*, 2005; Watts *et al.*, 2005) and the spine (Rothstein *et al.*, 1994; Iwasaki *et al.*, 1997)).

4.1.1.1 SOD pathways

The overexpression of SOD-2 and not SOD-1 or SOD-3 has been shown to protect tumour cells against free radical toxicity (Wong, 1995). However Antonyuk *et al.* (2009) have recently shown that SOD-1 may play important roles in protecting mitochondrial components from oxidative damage. In neural cells SOD-1 is known to act as a scavenger enzyme that works by transforming physiologically generated $O_2^{\bullet}$ to H_2O_2 (as previously described in Chapter 1), which feeds into the glutathione peroxidase and/or the catalase reaction pathways, protecting neural cells from the harmful effects of oxidative stress (Raimondi *et al.*, 2006).

4.1.1.2 Glutathione synthase pathway

Investigations into the effects of Photosens-mediated PDT in a crayfish neural cell culture system showed that signalling between neurones and glial cells involves the export of GSH from glial cells, which is subsequently cleaved to Cys-Gly dipeptide by the membrane-bound enzyme GGT, present on the other side of the glial cell (Uzdenskii *et al.*, 2008). This is used to maintain optimal thiol status of

neurones, protecting them from oxidative stress (Mytilineou *et al.*, 1999). The importance of this type of cell antioxidant protective system was reported by Maffi *et al.* (2007), who showed that rat cell populations with suppressed GSH levels resulted in elevated cell death response to ethanol-mediated oxidative stress.

4.1.1.3 Inhibition of cell antioxidant pathways

Oxidative stress occurs when there is an imbalance between the rate of ROS production and the antioxidant defence system that removes it. This may arise from a reduced level of antioxidant, or from an increased production of ROS. If the antioxidant pathways involving SOD-1, SOD-2 or GSH were involved in protecting neurones from death following PDT, a reasonable hypothesis would be that their inhibition would result in neurone death on exposure to *m*-THPC-mediated PDT. Such a result would therefore reveal a cellular mechanism by which DRG neurones were being protected from the effects of *m*-THPC-mediated PDT as observed in Chapter 3.

The inhibitors used in this study were Diethyldithiocarbamate (DDC) (Figure 4.1A), a copper chelator and an inhibitor of the SOD-1 enzyme (Ginsburg *et al.*, 1997; Tanioka *et al.*, 2005; Han *et al.*, 2009). DDC has been shown to decrease levels of SOD activity, while increasing lipid peroxidation products in pancreatic stellate cells (Tanioka *et al.*, 2005). A reduction in the levels of SOD-1 activity with the use of DDC was also observed in rat ventral spinal cord neurones (Iwasaki *et al.*, 1997).

2-Methoxy-estradiol (2-MeOE$_2$) (Figure 4.1B), is an oestrogen derivative that can not bind the oestrogen receptor (Huang *et al.* 2000). This compound was found to

be a chelating agent and a selective inhibitor of the SOD-2 enzyme (Gołąb *et al.*, 2003). It has been used in PDT to potentiate the cytoplasmic effects of sub-lethal doses of PDT on the human breast cancer cell line T47-D (Gołąb *et al.*, 2003).

Also, the inhibitor DL-buthionine-(S, R)-sulfoximine (L-BSO) (Figure 4.1C), was used in this study to inhibit the glutathione synthase pathway (Griffith 1999; Hamilton *et al.*, 2007; Han *et al.*, 2009), by inhibiting the first rate-limiting enzyme γGCS (Devesa *et al.*, 1993; Nicole *et al.*, 1998; Griffith, 1999; Avshalumov *et al.*, 2004; Gegg *et al.*, 2005; Wang *et al.*, 2006; Hamilton *et al.*, 2007). L-BSO is known to cause a dose- and time- dependent accumulation of ROS in rat mesencephalic neurones, and to activate extracellular signal-regulated kinase (ERK-1/2), 4 and 6 h after treatment (de Bernardo *et al.*, 2004).

Concentrations and incubation times of inhibitors were chosen on the basis of reported use in the literature. 50 μM DDC incubated for 1.5 h was used to inhibit SOD-1 in this study. Du *et al.* (2001) used 50 μM DDC for 30 min on Jurkat cells, which resulted in enhancement of methylglyoxal-mediated ASK1 activation; and 10 μM DDC incubated for 4 h enhanced cytotoxicity of microglia to endogenous ROS (Miller *et al.*, 2007). Gołąb *et al.* (2003) experimented with 1 μM 2-MeOE$_2$ incubated for 24 h (as used in this study), resulting in a reduction of SOD activity in C-26 cells (murine colon-26 cells). This study also used L-BSO at similar parameters as Vásquez *et al.* (2001), who reported the use of 0.5 to 1.0 mM L-BSO after 24 h incubation dramatically reduced GSH levels within glial cells by 80 to 94 %. These 3 inhibitors were used individually to block the 3 specific antioxidant pathways identified as being potentially interesting in this study (Figure 4.2). They were also tried in combination to see whether inhibiting multiple

antioxidant pathways would aid in deciphering the mechanism by which neurones are protected from *m*-THPC-mediated PDT.

4.1.2 Photosensitiser and $^1O_2$/ROS localisation

4.1.2.1 Subcellular localisation of photosensitisers

An objective of this chapter was to test whether the localisation of *m*-THPC in cells might help to explain the lack of sensitivity of DRG neurones to *m*-THPC-mediated PDT. Here the subcellular localisation of *m*-THPC was investigated using its ability to fluoresce red upon illumination. As a comparator, hypericin localisation was also investigated. This was in conjunction with green fluorescent cell organelle probes. Photosensitiser localisation patterns in cells have been shown to be an important determinant of the mode of cell death and a possible predictor of PDT efficiency (Ball *et al.*, 1999). Therefore a thorough study of *m*-THPC and hypericin localisation was undertaken involving a range of cell types and various organelle probes: MitoTrk-green (mitochondria), Lyso-Trk-green (lysosomes) and Hoechst 33258 (nuclei).

Chapter 3 showed a difference in sensitivity in neurones between *m*-THPC- and hypericin-mediated PDT and differences in sensitivity to *m*-THPC-mediated PDT between different cell types studied. Such differences in PDT effectiveness can be caused by the intracellular localisation of the photosensitiser. Some photosensitisers used in PDT, including *m*-THPC and hypericin, have been known to display some association with mitochondria, which may explain their efficiency in inducing apoptotic cell death *in vitro* and *in vivo* (Almeida *et al.*, 2004).

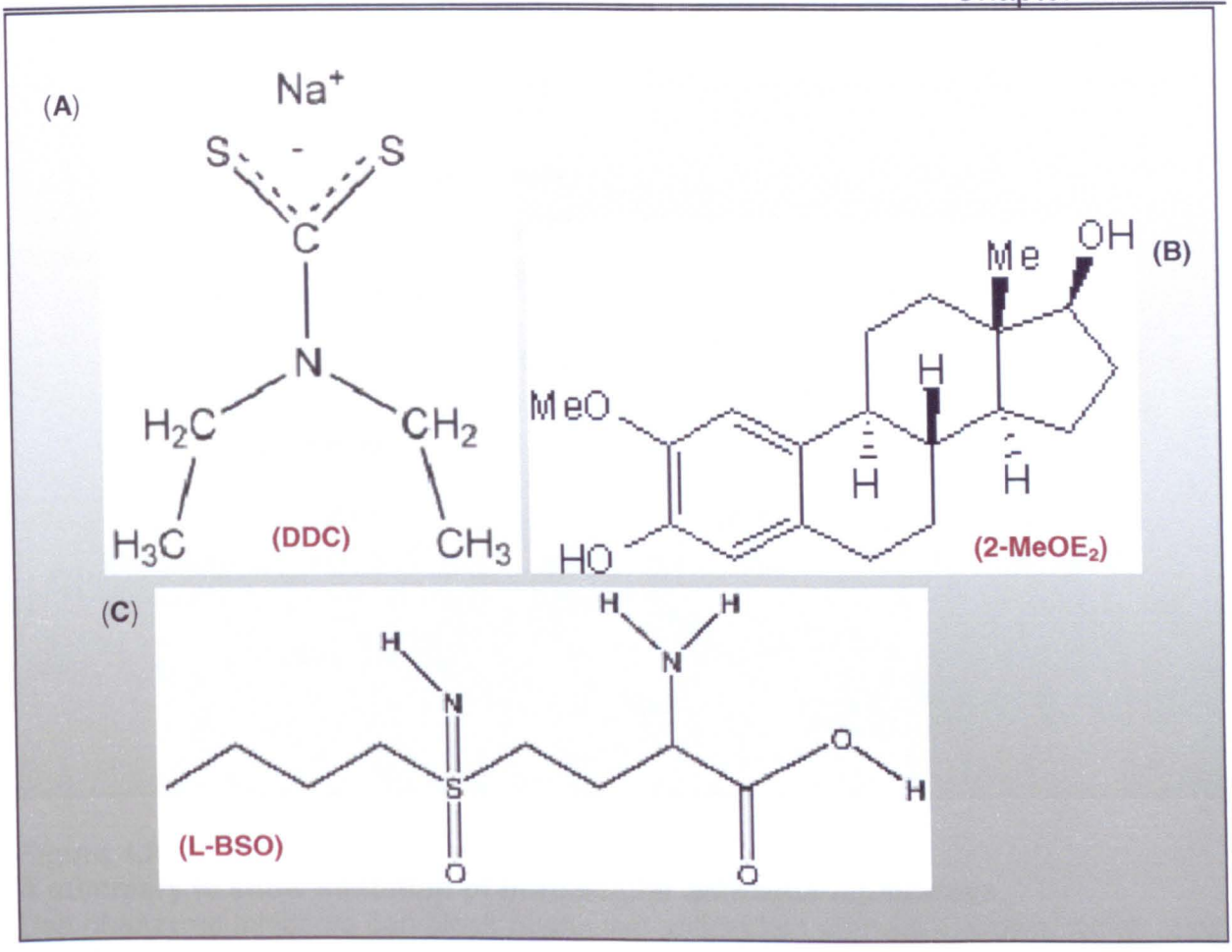

Figure 4.1
Molecular structures of commercially available inhibitors of intracellular antioxidant pathway enzymes.
(**A**) DDC, an inhibitor of the SOD-1 antioxidant enzyme; (**B**) 2-$MeOE_2$ an inhibitor of SOD-2 antioxidant enzyme; and (**C**) L-BSO inhibitor of the γGCS enzyme of the glutathione synthase pathway. (Structures taken from Sigma Aldrich)

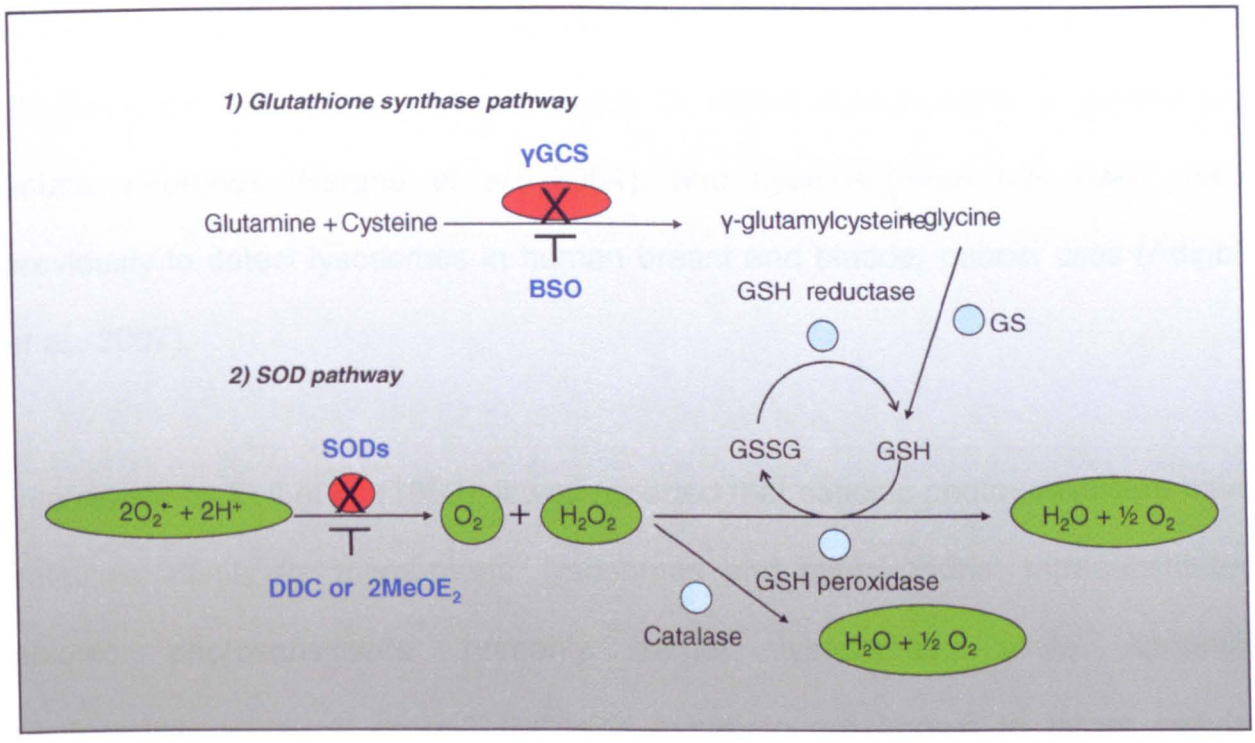

Figure 4.2
A summary to show inhibition of intracellular antioxidant pathways.
Use of enzyme inhibitors can block respective antioxidant pathways shown, which results in reduced endogenous protection of cells and increased oxidative stress sensitivity and may lead to cell death. DDC (SOD-1 enzyme inhibitor), 2-$MeOE_2$ (SOD-2 enzyme inhibitor), L-BSO (γGCS enzyme inhibitor), GSH (reduced glutathione), GSSH (oxidised form of GSH-glutathione disulfide glutathione), GS (glutathione synthase), γGCS (γ-glutamyl-cysteine synthetase or ligase) and SOD (superoxide dismutase).

Therefore; the co-localisation of these photosensitisers with mitochondria, lysosomes and nuclei were assessed in this study. The mitochondrial probe MitoTrk-green has been used previously to detect mitochondria in guinea pig enteric neurones (Berghe *et al.*, 2004), and LysoTrk-green has been used previously to detect lysosomes in human breast and bladder cancer cells (Adigbli *et al.*, 2007).

In a review by Ball *et al.* (1999), it was reported that cationic photosensitisers have selective affinity for membranes, lysosomes and mitochondria; tetrasubstituted anionic photosensitisers primarily target lysosomes; while lipophilic photosensitisers such as *m*-THPC and hypericin are known to target cellular membranes. This implies that the primary mechanism of cell death using *m*-THPC- and hypericin-mediated PDT is to damage membranes. *m*-THPC has been reported to be localised in mitochondria and in lysosomes and this multiple-organelle localisation may occur as a result of different uptake mechanisms (e.g. simple diffusion through lipid bilayer into the cytoplasm and/or endocytosis into intracellular membrane bound transport vesicles). In addition to *m*-THPC, hypericin has also been shown to be localised throughout the cytoplasm of human breast and bladder cancer cells after 24 h incubation, with some degree of co-localisation with lysosomes (Adigbli *et al.*, 2007).

4.1.2.2 $^1O_2$/ROS localisation

$^1O_2$ and ROS are produced at the site of excited ^3S in the presence of $^3O_2$. Cellular structures exposed to high concentrations of photosensitisers and oxygen are therefore potential targets for PDT damage. In the cellular environment $^1O_2$ has a short lifetime and diffuses a distance of less than 0.1 μm, thus limiting oxidative

stress and damage to targets closest to the site of its generation (Peng *et al.*, 1995; Ball *et al.*, 1999).

Malondialdehyde and advanced oxidation protein products have been used to assess oxidative stress under experimental conditions (Varija *et al.*, 2009), and a derivative 2', 7' Dichlorofluorescin diacetate (H_2DCF-DA) (Figure 4.3A) was used by LeBel *et al.* (1990) as an indicator of oxidative stress induced neurotoxic damage in a crude synaptosomal fraction of the brain. This oxidative stress detection agent was used in this study as a means of detecting the *m*-THPC-mediated PDT generated oxidative stress in neural cells and in tumour cells *in vitro*. 2', 7' Dichlorofluorescin (H_2DCF) and similar fluorescent compounds are popularly used in the detection and crude quantification of oxidative stress (Rota *et al.*, 1999; Witold and Grzegorz, 2000). It has been used with superior cervical ganglia cultures to indicate that oxidants were generated intracellularly following cell starvation (Sáez *et al.*, 1987). H_2DCF-DA used in this study, penetrates plasma membranes and is enzymatically converted into non-fluorescent H_2DCF and then oxidised into a highly green fluorescent molecule 2'-7'-dichlorofluorescin (DCF) in the presence of ROS (Hempel *et al.*, 1999; Witold and Grzegorz, 2000; Mauzeroll *et al.*, 2004; Nevřelová *et al.*, 2005; Cao *et al.*, 2007). DCF green fluorescence was used as a marker of $^1O_2$/ROS in monolayer cell cultures.

In conjunction with H_2DCF-DA, the compound 2-Methyl-1, 4-naphthoquinone (Vitamin K3, $C_{11}H_8O_2$ or Menadione) (Figure 4.3B) was used in this study as a positive inducer of DCF fluorescence. Menadione worked by imposing oxidative stress, by generation of ROS (e.g. $O_2^{\bullet-}$, H_2O_2 and $HO^{\bullet}$) by $1e^-$ redox cycling at the mitochondrial outer membrane (Mauzeroll *et al.*, 2004; Nicholls and Budd, 2000).

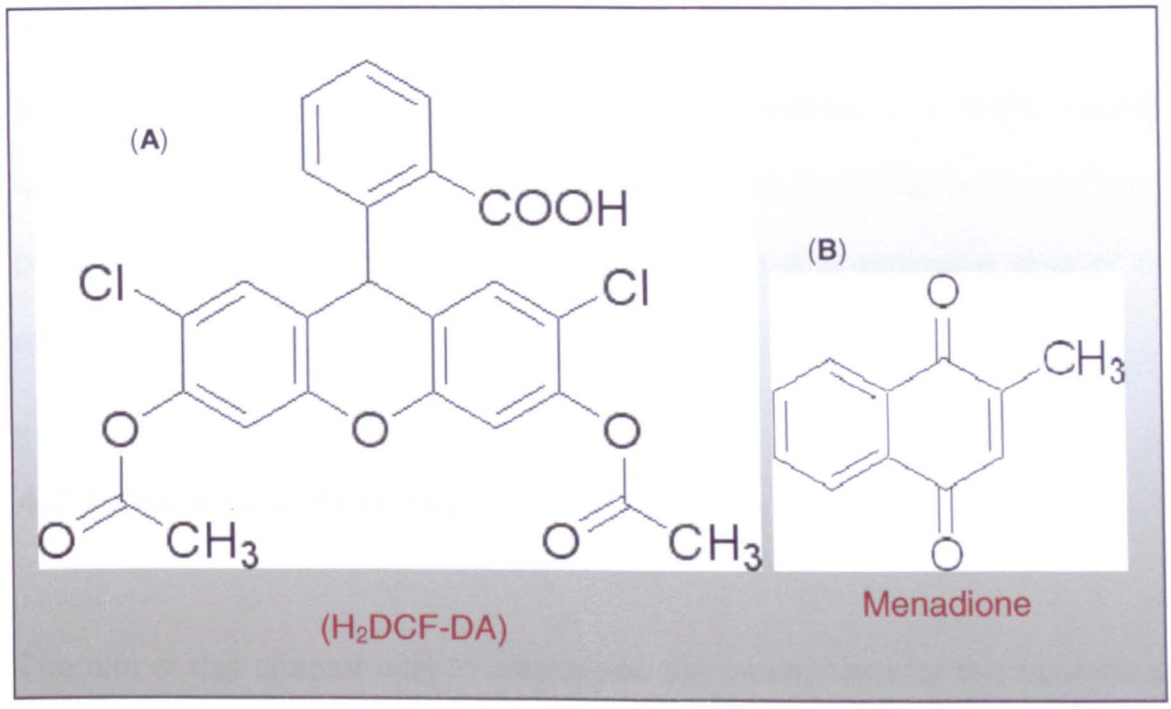

Figure 4.3
Molecular structures of H_2DCF-DA and Menadione.
(**A**) H_2DCF-DA ($C_{24}H_{16}Cl_2O_7$) MW 487.29 (**B**) Menadione. (Structures taken from Sigma Aldrich)

H_2DCF-DA was used in this study to determine the intracellular localisation of $^1O_2$ and ROS in cells, after exposure to 4 and 10 μg/ml *m*-THPC-mediated PDT. In particular, H_2DCF-DA was used for aid in the detection of *m*-THPC fluorescence within neurites of neurones, which were found in Chapter 3 not to exhibit photosensitiser fluorescence despite there being a progressive loss of neurites after PDT.

4.2 Aims and objectives

The aim of this chapter was to investigate the mechanism for the neurone sparing observed with *m*-THPC mediated PDT in the previous Chapter. The primary objectives were:

i) To determine whether or not DRG neurones were truly surviving *m*-THPC-mediated PDT by assessing their PI uptake after a 36 h period post PDT and their ability to regenerate neurites.

ii) To use inhibitors of cellular antioxidant pathways (SOD-1, SOD-2 and γGCS) blockers, to elucidate the involvement of these pathways in neurone survival after *m*-THPC-mediated PDT.

iii) To determine where $^1O_2$/ROS could be detected in cells, in particular in association with neurites of DRG neurones using H_2DCF-DA.

iv) To assess the subcellular localisation of *m*-THPC and hypericin in different cell types (DRG neurones, satellite cells, astrocytes and MCF-7 cells), using organelle markers and photosensitiser fluorescence.

4.3 Results

4.3.1 Neuronal cell death assessment at different times after 4 µg/ml *m*-THPC-mediated PDT

It was important to establish whether the 24 h latency period, post-PDT treatment, was appropriate for this study. This was examined by extending incubation time post-PDT.

Co-cultured neurones and satellite cells in thin collagen gels were treated using 4 µg/ml *m*-THPC-mediated PDT or no light control. Treated and control neurones and satellite cells were maintained in culture up to 36 h and no change in neuronal cell death were observed at different times after PDT. Figure 4.4A and B show the time courses of neurone and satellite cell death detection in thin collagen culture systems after *m*-THPC-mediated PDT using the PI exclusion assay. Data were compared to the 24 h time point for both 4 µg/ml *m*-THPC-mediated PDT and the no light control. There was no apparent difference in the extent of cell death in cultures analysed after these different lengths of time. 36 h post-PDT should have been sufficient time for cell death (i.e. neuronal cell death) in culture to become detectable (Sattler *et al.*, 1997; Leung *et al.*, 2002; Sundquist *et al.*, 2006).

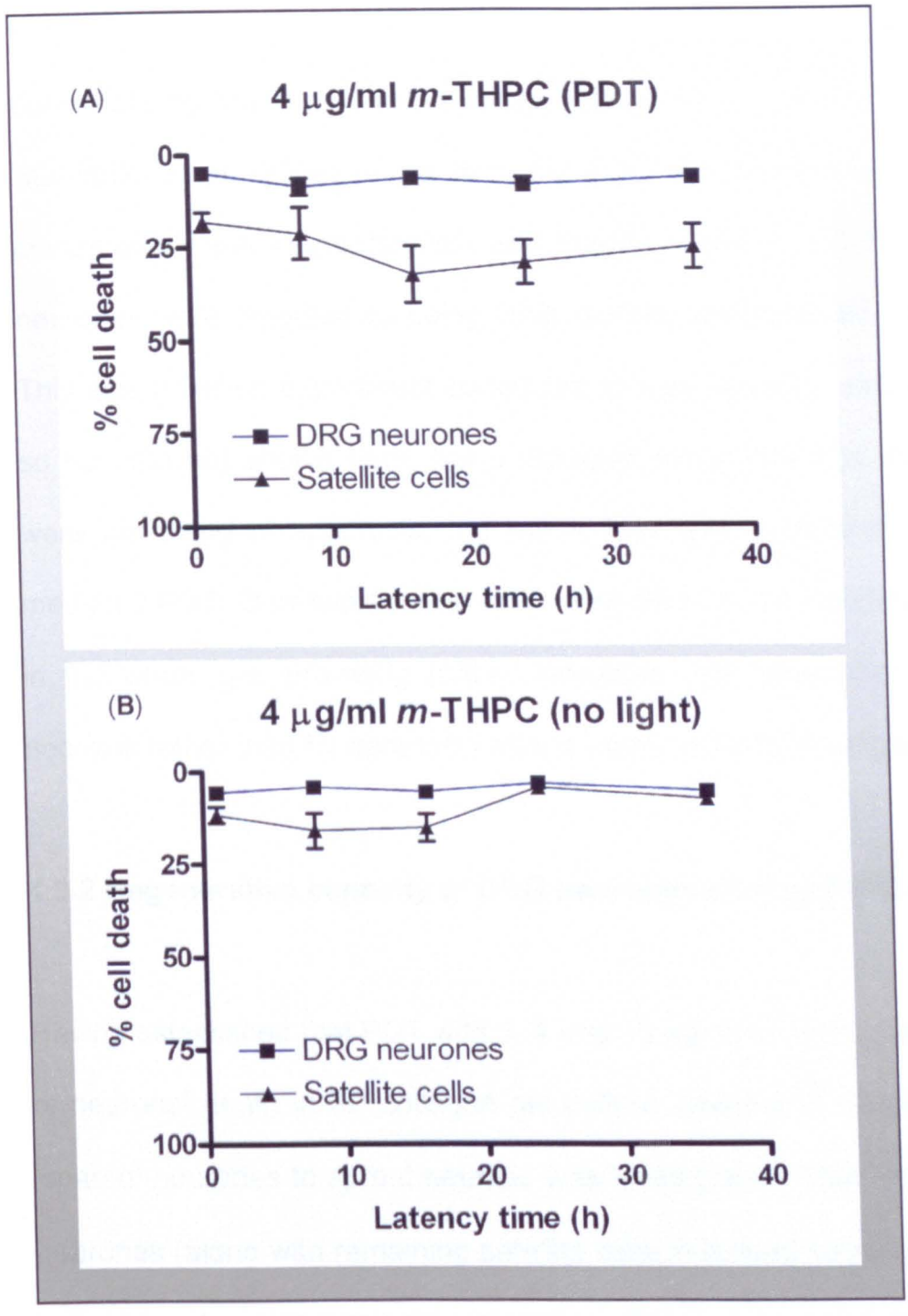

Figure 4.4
Time course of DRG neurone and satellite cell death following 4 μg/ml *m*-THPC-mediated PDT (A) or no light control (B).
Varying latency periods after *m*-THPC-mediated PDT did not affect levels of neurone or satellite cell death. Co-cultured cells in thin collagen gels were exposed to treatment or control conditions then left for increasing latency periods before using PI to detect cell death, fixing and βIII-tubulin immunostaining to detect neurones. Data were collected from all DRG neurones in each gel, typically up to 50 neurones, and satellite cell data were collected from 3 random fields of each of the same gels. Data are presented as means ± SEM of 6 separate gels. A one-way ANOVA was used to compare the different time points, followed by Dunnett's post-test to compare each point to the 24 h time point ($p>0.05$).

In addition to this time course assay, a FragEL™ assay kit (DAB) was used to detect whether any neurones were in an early stage of apoptosis, which is not detectable by the PI exclusion assay (Sattler *et al.*, 1997; Leung *et al.*, 2002; Sundquist *et al.*, 2006). A gel from the 8 h PDT treated sample from the time course assay was counterstained with FragEL™ and no βIII-tubulin labelled DRG neurones were detected as being DAB positive (which would indicate apoptosis). This was a limited experiment conducted in a preliminary manner on a single gel so no data are shown here, but it provided more evidence that DRG neurones were not dying of apoptosis, but rather they were surviving 4 μg/ml *m*-THPC-mediated PDT. Only two satellite cells were detected as positively stained for DAB in the whole gel, providing further indication that satellite cells were dying by necrosis rather than by apoptosis after 4 μg/ml *m*-THPC-mediated PDT.

4.3.2 Regenerative capacity of DRG neurones after *m*-THPC-mediated PDT

Having established that PDT with 3, 4 and 10 μg/ml *m*-THPC resulted in low levels of neuronal death in 3D collagen gel culture systems in Chapter 3, the ability of 'spared' neurones to sprout neurites was investigated. After PDT in collagen gels, neurones (along with remaining satellite cells and dead cells) were harvested from collagen gels using enzymatic digestion. These cells were mixed with untreated satellite cells, and then seeded in monolayer culture systems and maintained in culture for 2 days. Figure 4.5 shows new neurite growth from neurones, in fixed monolayer cultures, assessed after 2 days. Here, the ability of neurones to adhere and regenerate neurites is used as a marker for neurone function. It is clear that DRG neurones which had been treated previously with *m*-THPC-mediated PDT were able to adhere and regenerate neurites in monolayer co-culture with these non-PDT treated satellite cells.

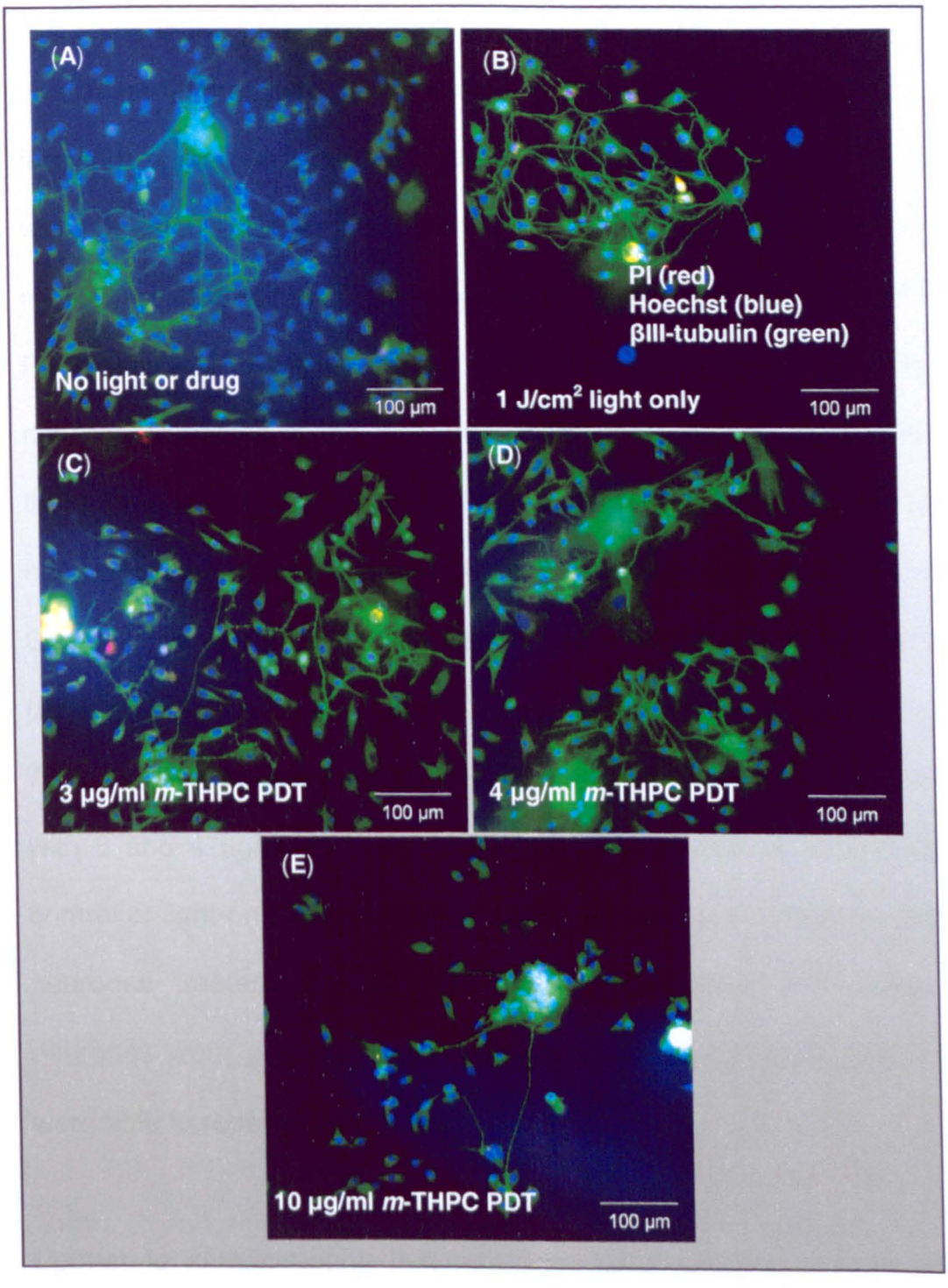

Figure 4.5
Micrographs of PDT-treated DRG neurones following subsequent co-culture with untreated satellite cells.
Representative micrographs show βIII-tubulin neurite growth from neurones (green) and Hoechst 33258 stained nuclei (blue), in fixed monolayer cultures, post exposure to *m*-THPC-mediated PDT. This was following extraction from thin collagen gels and 2 days culture with non-PDT treated satellite cells. Images show (**A**) No light or drug control; (**B**) 1 J/cm^2 light only control; (**C**) 3 µg/ml *m*-THPC-mediated PDT; (**D**) 4 µg/ml *m*-THPC-mediated PDT; and (**E**) 10 µg/ml *m*-THPC-mediated PDT.

Figure 4.6 shows the ability of DRG neurones to regenerate neurites following *m*-THPC-mediated PDT in collagen gels. These graphs show mean numbers of βIII-tubulin immunoreactive neuronal cell bodies in monolayer cultures per cover-glass that showed neurite growth at 2 days after transfer to monolayer co-culture system with untreated satellites cells. Similar mean numbers of neurones were detected in no light or drug control, light only control, and 3 and 4 μg/ml *m*-THPC-mediated PDT samples. However, there was approximately one-third as many mean neurones detected in the 10 μg/ml *m*-THPC-mediated PDT treated samples, as there were in other treatment conditions. There were similar mean percentages of neurones per cover-glass without neurite growth in all groups (Figure 4.6B). Overall, it is apparent that all treated DRG neurones, except for the use of 10 μg/ml *m*-THPC, showed similar % mean neurite re-growth capability, with between 70 to 78 % of detectable neurones having at least one neurite. Neurones treated with 3 and 4 μg/ml *m*-THPC-mediated PDT showed no difference to untreated control or light-only control in their ability to produce neurites. In contrast the DRG neurones treated with 10 μg/ml *m*-THPC-mediated PDT showed far fewer neurones were present in the cultures. Of these detected neurones only 58 % were able to regenerate at least one neurite.

Further to demonstrating that neurones were capable of regenerating neurites following no light or drug control, light only, and 3 and 4 μg/ml *m*-THPC-mediated PDT-treated treatments, Figure 4.7 shows that mean lengths per cover-glass of these neurites, in monolayer cultures, were equivalent to those from untreated neurones, with only the 10 μg/ml *m*-THPC-mediated PDT-treated neurones showing significantly reduced mean neurite outgrowth compared with light only control (one-way ANOVA with Dunnett's post test). Mean neurite lengths were between 20±4.5 to 26 ±6.0 mm. However, 10 μg/ml *m*-THPC-mediated PDT

treated DRG neurones, showed a marked reduction, in detectable neurite length to a mean of 3.1±1.3 mm.

4.3.3 The role of cellular antioxidant pathways in protecting DRG neurones from PDT-induced cell death

In order to determine the mechanism by which co-cultured DRG neurones were protected from *m*-THPC-mediated PDT, inhibitors of γGCS (glutathione synthase pathway), SOD-1 and/or SOD-2 were incubated prior to 4 μg/ml *m*-THPC mediated-PDT.

4.3.3.1 DRG neurones

Figure 4.8A shows that inhibiting the glutathione synthase pathway using L-BSO or the constitutive SOD-1 pathway using DDC, followed by PDT, both caused significant increases in neuronal cell death, in the collagen culture system, ($p<0.01$, one-way ANOVA with Dunnett's multiple comparison post test compared with PDT only). However, inhibition of the inducible SOD-2 pathway using 2-$MeOE_2$ did not show a significant increase in neuronal death at the concentration and incubation time used in this study. Control experiments which received inhibitors with either drug only (Figure 4.8B) or light only (Figure 4.8C) treatments showed no significant increase in neuronal death. The use of no drug or light (Figure 4.8D) treatments showed some significant increases in neuronal death. This was the case treating neurones with L-BSO alone, and on combining L-BSO and DDC in controls with no light or drug, approximately 100 % DRG neurone death was observed Figure 4.8D.

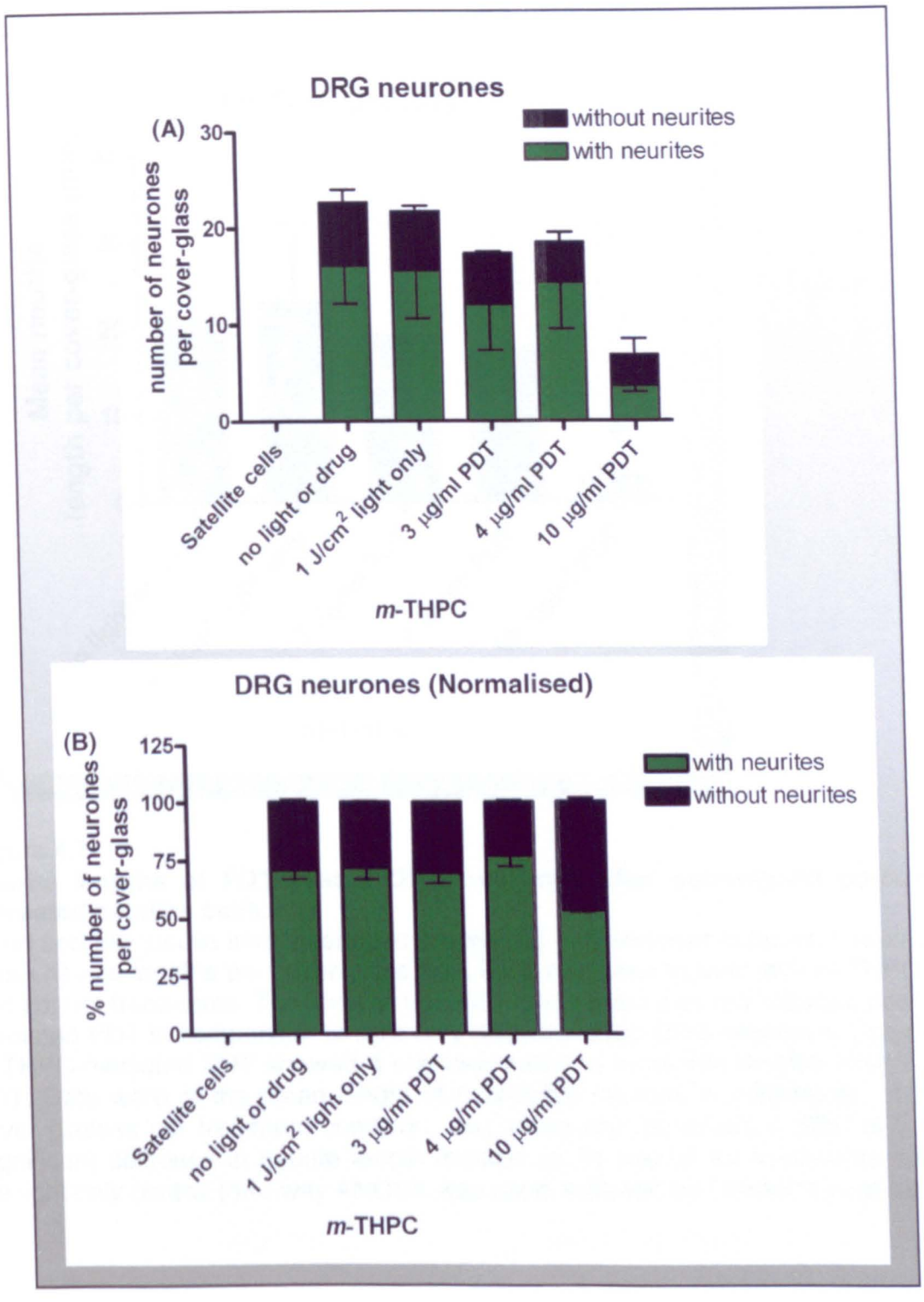

Figure 4.6
PDT-treated DRG neurones regenerated neurites during subsequent co-culture with untreated satellite cells.
Fixed and βIII-tubulin immunostained (neurones) in monolayer cultures (**A**) shows the number of neuronal cell bodies without or with at least one neurite following 2 days in co-culture, after *m*-THPC-mediated PDT and control treatments, and (**B**) shows the same data, normalised to account for variations in the number of neurones analysed, expressed as a percentage. A similar number of neuronal cell bodies had neurites associated with them in the 3-4 µg/ml *m*-THPC-mediated PDT samples as in the controls. The use of a high PDT dose (10 µg/ml *m*-THPC-mediated PDT) shows marked reduction in the mean number of detectable DRG neurones. There was also a slight reduction in the ability of these DRG neurones to re-grow neurites. Data were collected from all detectable DRG neurones on 2 cover-glasses in each case, and presented as means ± SEM of 3 replicates.

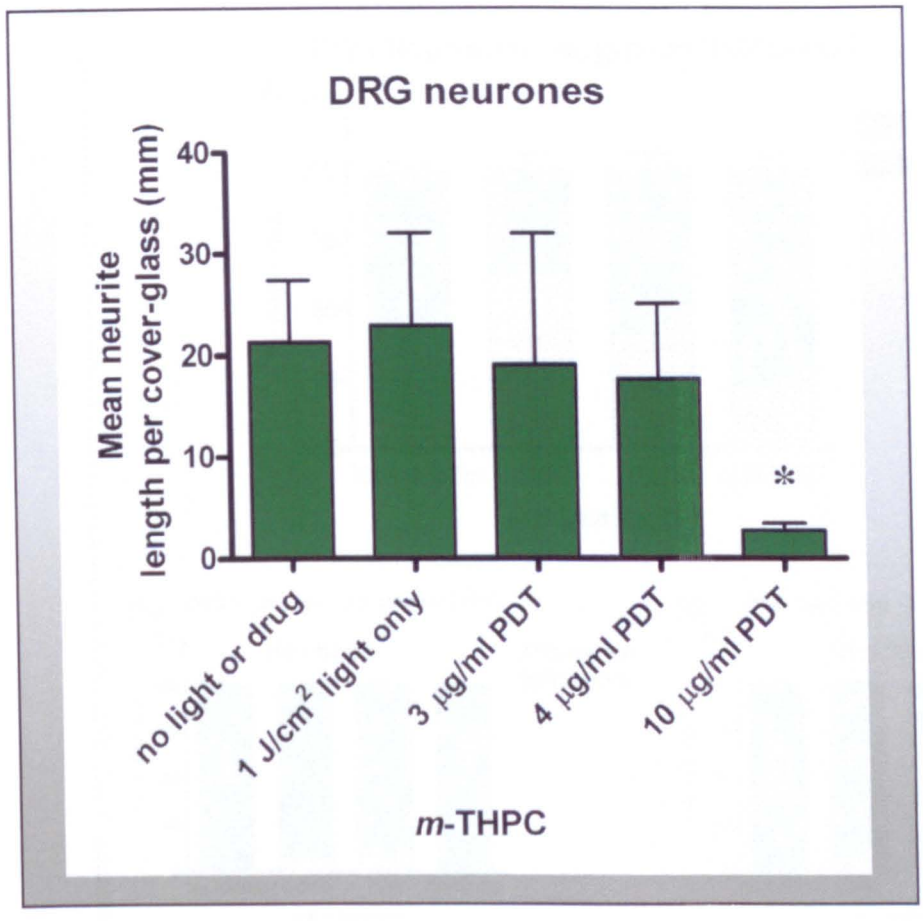

Figure 4.7
Neurite lengths of PDT-treated DRG neurones after subsequent co-culture with untreated satellite cells.
Fixed and βIII-tubulin immunostained (neurones) in monolayer cultures. Graph shows the mean neurite lengths per cover-glass from DRG neurones treated with *m*-THPC-mediated and control treatments. The level of neurite regeneration was not reduced post *m*-THPC-mediated PDT in comparison to light only control treated DRG neurones. Use of 10 μg/ml *m*-THPC-mediated PDT showed a marked reduction in neurite lengths after 2 days post PDT. Data were of the mean length of detectable neurites in millimetres, of 2 separate cover glasses per treatment condition, and presented as means ± SEM of 3 replicates. Significant decrease in neurite length marked as (*) $p<0.05$ for treatments compared to the light only control (one-way ANOVA was used, followed by Dunnett's post-test).

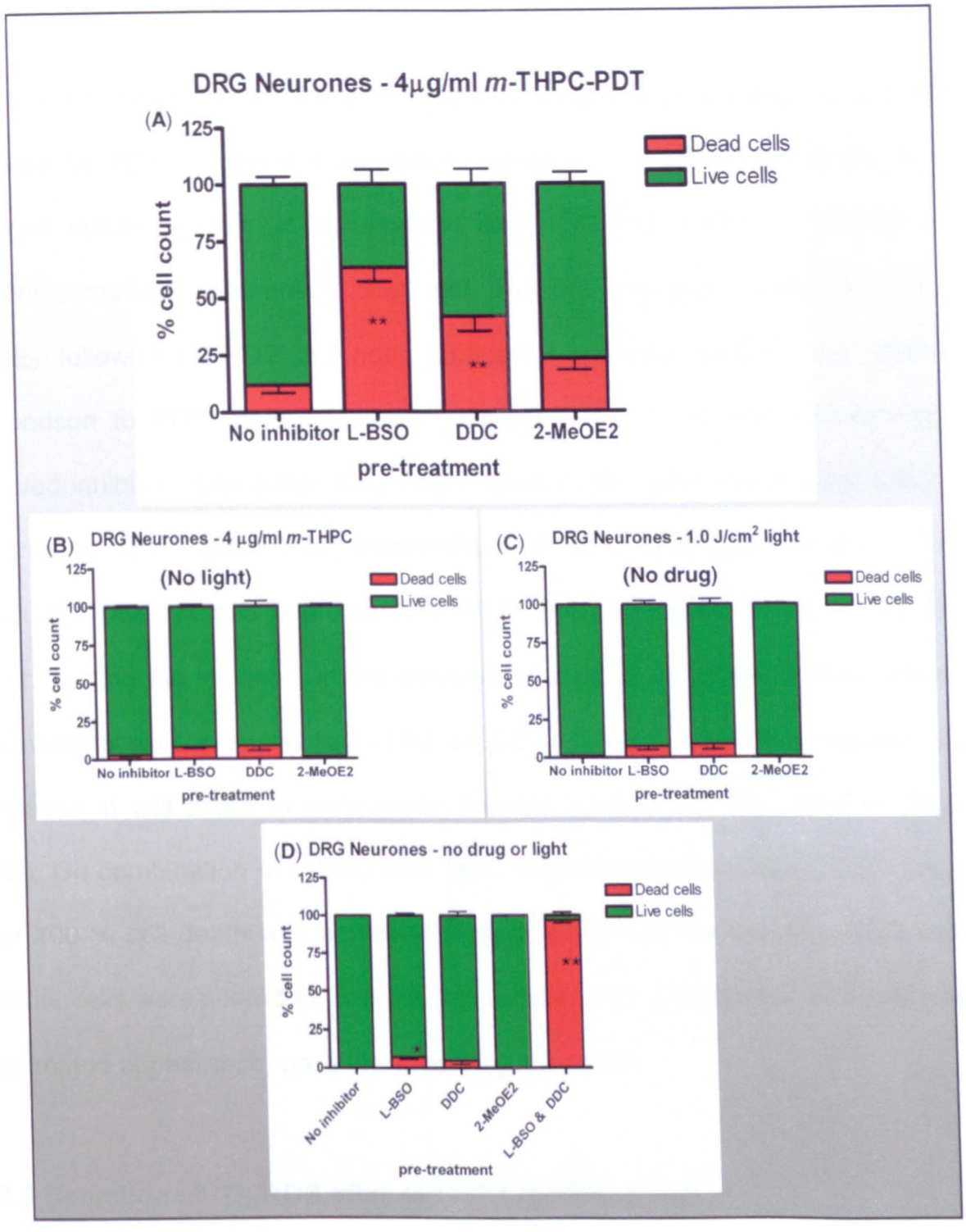

Figure 4.8
DRG neurone death in 3D cultures after 4 µg/ml *m*-THPC mediated-PDT and a 24 h latency period following inhibition of antioxidant pathways.
Fixed and co-cultured with satellite cells in collagen gels (**A**) neurones survived 4 µg/ml *m*-THPC-mediated PDT without inhibitor treatment. After inhibition with the glutathione synthase pathway inhibitor (L-BSO) and the SOD-1 pathway inhibitor (DDC), there were significant increases in neuronal death with no significant increase in neurone death with the SOD-2 inhibitor (2-MeOE$_2$) in comparison to no inhibitor controls. (**B**) 4 µg/ml drug only (no light) control, (**C**) 1 J/cm^2 light only (no drug) control and (**D**) no drug or light control. After inhibition with a combination of L-BSO and DDC but with no *m*-THPC or light, neurones showed near 100 % death. Data were collected from approximately 50 neurones per gel and presented as means ± SEM of 6 separate gels. Significant increases in cell death are marked as (*) $p<0.05$, and (**) $p<0.01$ for treatments compared to respective controls without inhibitor (one-way ANOVA with Dunnett's multiple comparison post test).

4.3.3.2 DRG satellite cells

Figure 4.9A shows that inhibiting the glutathione synthase pathway using L-BSO followed by PDT produced a significant increase in satellite cell death, in the collagen culture system, in comparison with PDT only (one-way ANOVA with Dunnett's multiple comparison post test, $p<0.05$). However, using DDC or 2-$MeOE_2$ followed by PDT did not significantly increase satellite cell death in comparison to PDT without inhibitors (Figure 4.9A). In control cultures which received inhibitors with either drug only (Figure 4.9B), light only (Figure 4.9C), or no drug or light (Figure 4.9D) treatments, L-BSO yielded approximately 100 % death and DDC yielded approximately 50 % death, whereas 2-$MeOE_2$ had little effect. Testing the inhibitors in the absence of drug and light treatments revealed that satellite cells exposed to L-BSO or DDC (but not 2-$MeOE_2$) showed large increases in cell death in comparison to cells treated with no inhibitor, (Figure 4.9D). On combination of L-BSO and DDC a similar result as with L-BSO only of near 100 % cell death was achieved (Figure 4.9D). On the use of L-BSO where satellite cells were scored as dead due to uptake of PI, a proportion of nuclei had a fragmented appearance, possibly indicating apoptosis.

4.3.4 Detection of $^1O_2$/ROS after *m*-THPC-mediated PDT

m-THPC fluorescence was not detected in neurites in Chapter 3, however it may have been present at a level below the detection limit of our microscope. While localisation of drug may be useful in understanding the mechanism of subsequent PDT-induced cell damage, the location of $^1O_2$ or ROS generation during PDT provides an additional level of information. Therefore, the detection of $^1O_2$ and ROS using H_2DCF-DA after *m*-THPC-mediated PDT was tested here.

After loading cells in a monolayer DRG culture system with H_2DCF-DA there was no green fluorescence (Figure 4.10) in untreated DRG cultures, whereas exposure to menadione elicited green fluorescence of DCF which was produced in response to elevated ROS levels.

Exposure of DRG cultures to 4 µg/ml *m*-THPC-mediated PDT elicited an increase in green DCF fluorescence, in monolayer cultures, compared to light only controls (Figure 4.11A and B). Figure 4.11C shows higher levels of green DCF fluorescence in a few neuronal cell bodies after 10 µg/ml *m*-THPC-mediated PDT, with DCF positive neuronal cell bodies displaying less intense *m*-THPC red fluorescence than their non-DCF positive counterparts. At higher magnification DCF green fluorescence was detected within the neuronal cell body and accumulated near the plasma membrane (Figure 4.11D). Figure 4.10E and F show no green fluorescence after light only or 4 µg/ml *m*-THPC-mediated PDT without H_2DCF-DA incubation. In this experiment, neuronal cell bodies were identified morphologically using phase contrast microscopy. In Figure 4.12 the monolayer culture has been immunostained for βIII-tubulin to identify neurites and shows that after 4 µg/ml *m*-THPC-mediated PDT, there was some DCF green fluorescence within neurites. Note that βIII-tubulin immunodetection shares the red fluorescence channel with *m*-THPC in this figure, but the red fluorescence of the neurites is morphologically distinguishable from the diffuse drug fluorescence.

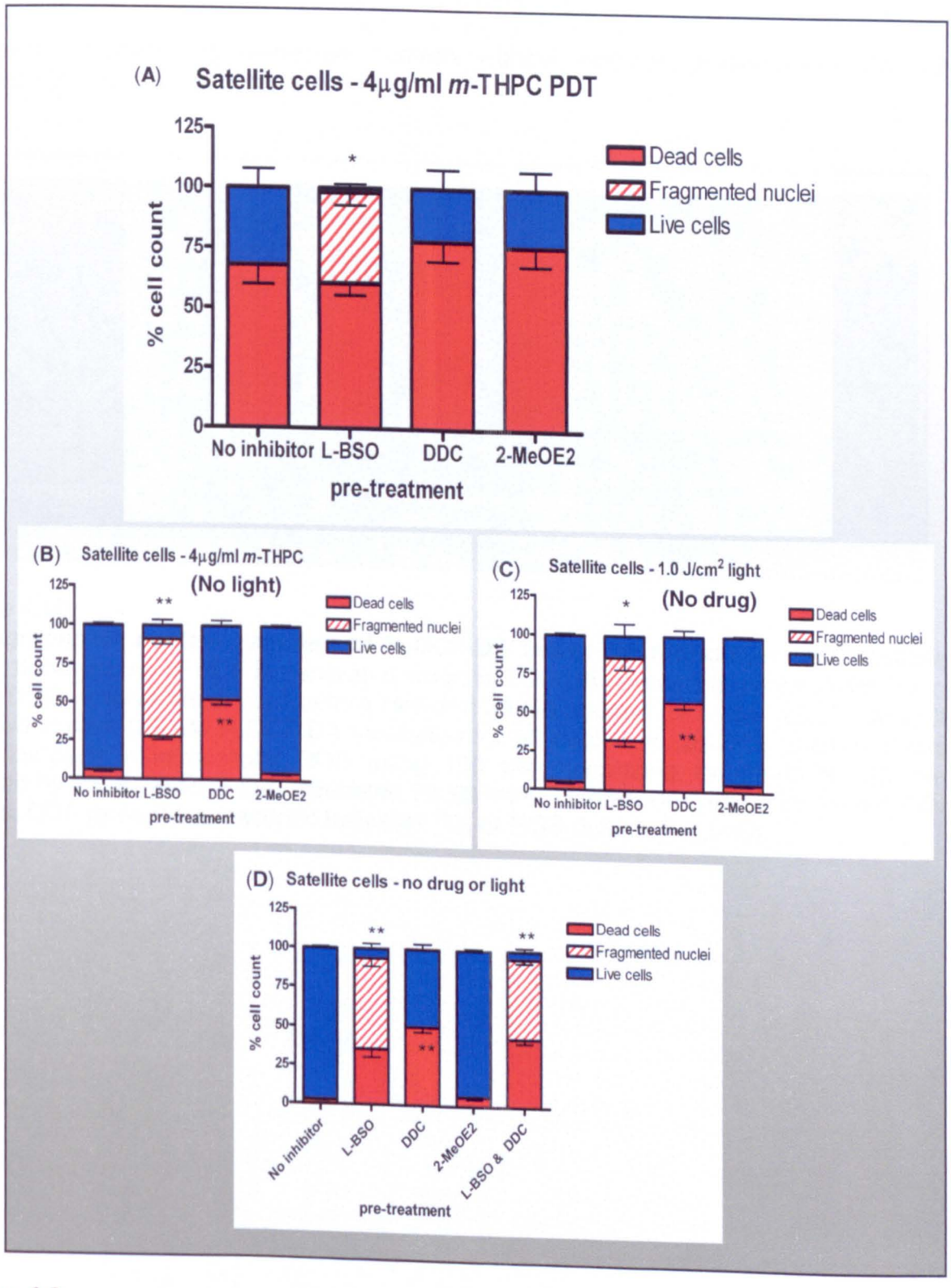

Figure 4.9
DRG satellite cell death in 3D cultures after 4 μg/ml *m*-THPC mediated-PDT and a 24 h latency period following inhibition of antioxidant pathways.
Fixed satellite cells in co-culture with neurones in collagen gels (**A**) Without inhibitor treatment approximately 68 % satellite cells death was observed after 4 μg/ml *m*-THPC-mediated PDT. After inhibition with the glutathione synthase pathway inhibitor (L-BSO) there was a significant increase in death to near 100 %, with no significant increase with the SOD-1 pathway inhibitor (DDC) or SOD-2 inhibitor (2-$MeOE_2$). (**B**) Drug only (no light) control, (**C**) 1 J/cm^2 light only (no drug) control and (**D**) No drug or light control. Inhibition of intracellular antioxidant pathways in controls resulted in near 100 % satellite cell death after L-BSO and 50 % after DDC treatment, but no cell death was observed in controls with $MeOE_2$. Inhibition with a combination of L-BSO and DDC, showed no increase in satellite cell death in comparison to L-BSO only (near 100 % cell death). Data were

collected from 3 random fields per gel, and presented as means ± SEM of 6 separate gels. Significant increases in cell death are marked as (*) $p<0.05$, and (**) $p<0.01$ for treatments compared to respective controls without inhibitor (one-way ANOVA with Dunnett's multiple comparison post test).

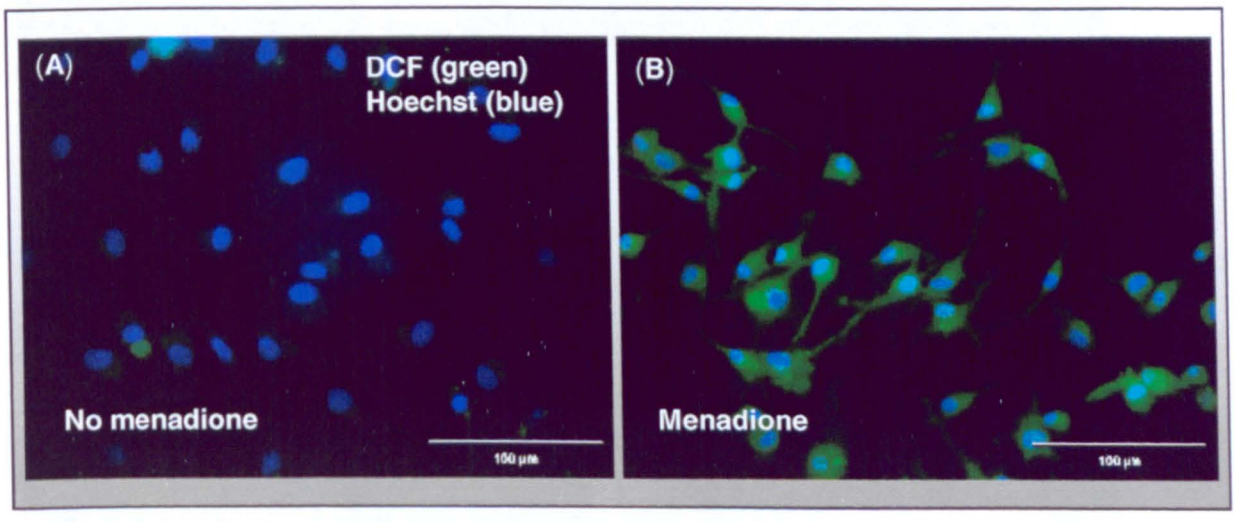

Figure 4.10.
Micrographs of control samples of H_2DCF-DA assay on monolayer DRG culture. Green fluorescence of DCF is generated when H_2DCF-DA comes into contact with $^1O_2$ or ROS. DRG cultures were fixed before Hoechst 33258 stained for nuclei (blue). (**A**) DCF negative control (25 µM H_2DCF-DA incubated for 60 min), and (**B**) DCF positive control (after increase in intracellular ROS using 100 µM menadione incubated for 60 min, followed by 25 µM H_2DCF-DA, incubated for 60 min). Menadione caused increased ROS in cells. DCF (green) fluorescence indicates $^1O_2$ or ROS detection in cells.

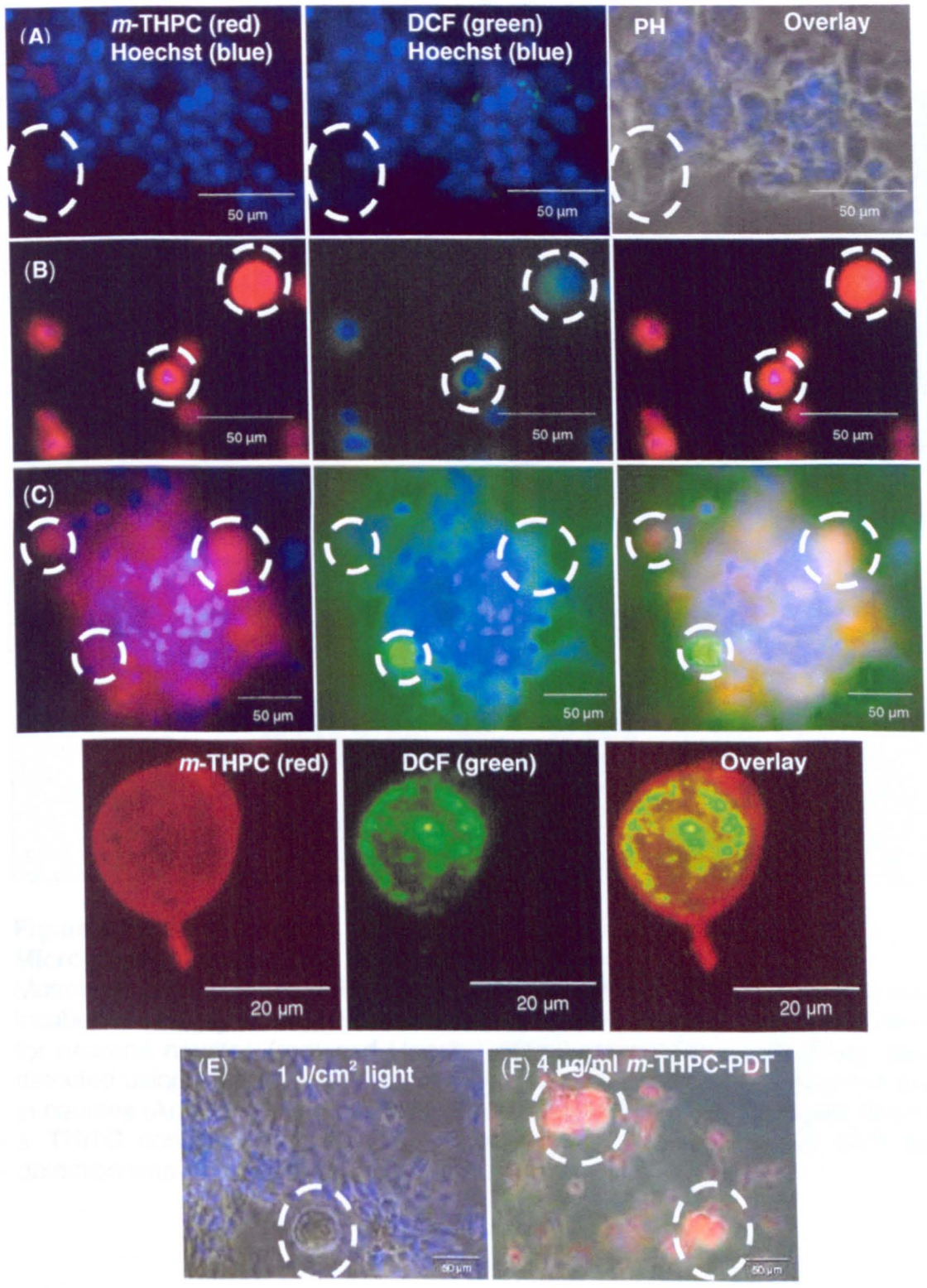

Figure 4.11
Micrographs of DCF detected in neuronal cell bodies of DRG cultures after *m*-THPC-mediated PDT.
Monolayer DRG cultures were treated with and without 100 µM H_2DCF-DA for 60 min followed by test and control PDT treatments. DRG cultures were fixed before Hoechst 33258 stained for nuclei (blue). (**A**) 1 J/cm^2 light only (no drug), (**B**) 4 µg/ml *m*-THPC-mediated PDT, (**C**) 10 µg/ml *m*-THPC-mediated PDT, (**D**) Higher magnification of 10 µg/ml *m*-THPC-mediated PDT and (**E**) 1 J/cm^2 light only (no drug) without H_2DCF-DA and (**F**) 4 µg/ml *m*-THPC-mediated PDT without H_2DCF-DA. In some instances phase contrast (PH) images were shown because PH was used to identify neuronal cell bodies. Circles

indicate neuronal cell bodies). DCF (green) fluorescence indicates $^1O_2$ or ROS detection in cells.

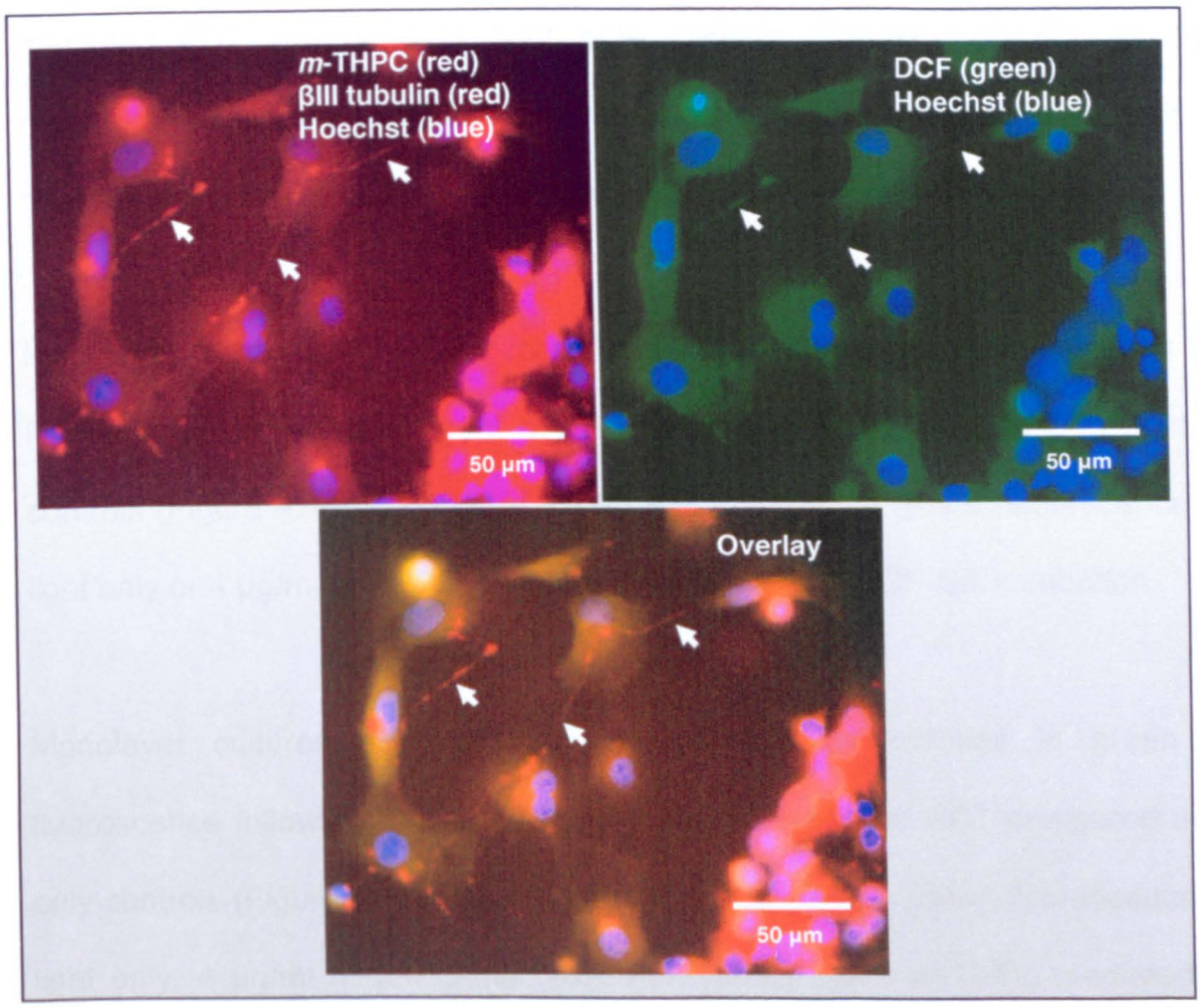

Figure 4.12.
Micrographs showing DCF detected in neurites.
Monolayer DRG cultures were treated with 100 µM H_2DCF-DA for 60 min post *m*-THPC incubation or 4 µg/ml *m*-THPC-mediated PDT. DRG cultures were fixed, immunostained for neurone neurites (red) and Hoechst 33258 stained for nuclei (blue). Neurites were detected using βIII-tubulin/TRITC, and very little DCF (green) fluorescence was detected in neurites (Arrows indicate neurites). (Note neurites are red in this figure due to the use of a TRITC conjugated 2° Ab. This change was because a green DCF fluorescence detection was being tested for in this experiment)

Monolayer cultures of satellite cells (co-cultured with neurones) also showed a clear increase in green DCF fluorescence following 4 and 10 µg/ml *m*-THPC-mediated PDT compared to light only controls (Figure 4.13A-C). At higher magnification, patchy DCF fluorescence was detected within satellite cells and near the cell plasma membrane (Figure 4.13D and E show 2 examples).

Monolayer cultures of MCF-7 cells showed a clear increase in green DCF fluorescence following 4 µg/ml *m*-THPC-mediated PDT compared to light only controls (Figure 4.14A-B). Figure 4.14C and D show no green fluorescence after light only or 4 µg/ml *m*-THPC-mediated PDT without H_2DCF-DA incubation.

Monolayer cultures of astrocytes showed a clear increase in green DCF fluorescence following 4 and 10 µg/ml *m*-THPC-mediated PDT compared to light only controls (Figure 4.15A-C). Figure 4.15D-F shows no green fluorescence after light only, 4 µg/ml *m*-THPC-mediated PDT or 10 µg/ml *m*-THPC-mediated PDT without H_2DCF-DA incubation.

These images have shown that $^1O_2$/ROS generated by *m*-THPC-mediated PDT could be detected within cells using the H_2DCF-DA assay.

4.3.5 Subcellular localisation of LysoTrk or MitoTrk with *m*-THPC or hypericin

LysoTrk-green probe was used as a marker for lysosomes. This probe gave some signal when used on monolayer cultures of MCF-7 cells in combination with 4 µg/ml *m*-THPC incubated for 4 h (Figure 4.16) and with 1.6 µg/ml hypericin

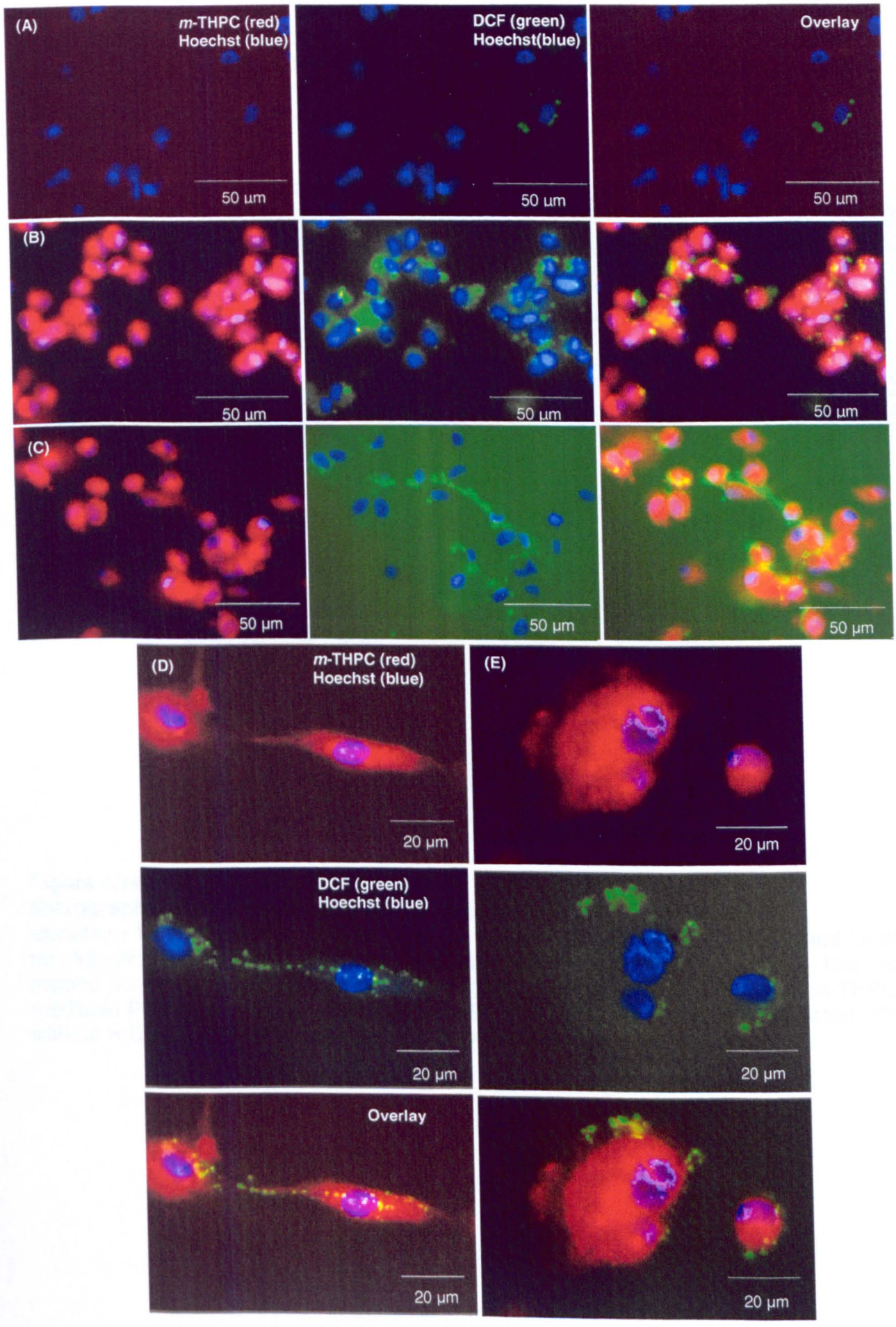
(A)
m-THPC (red)
Hoechst (blue)
50 µm
DCF (green)
Hoechst(blue)
50 µm
Overlay
50 µm
(B)
50 µm
50 µm
50 µm
(C)
50 µm
50 µm
50 µm
(D)
m-THPC (red)
Hoechst (blue)
20 µm
(E)
20 µm
DCF (green)
Hoechst (blue)
20 µm
20 µm
Overlay
20 µm
20 µm

Figure 4.13.

Micrographs of DCF detected in DRG satellite cells after *m*-THPC-mediated PDT. Monolayer DRG cultures were treated with 100 µM H_2DCF-DA for 60 min post 4 h *m*-THPC or no drug incubation. DCF fluorescence was detected in satellite cells after 4 and 10 µg/ml *m*-THPC-mediated PDT. DRG cells were fixed before Hoechst 33258 stained for nuclei (blue). (**A**) 1 J/cm^2 light only, (**B**) 4 µg/ml *m*-THPC-mediated PDT, (**C**) 10 µg/ml *m*-THPC-mediated PDT, (**D** and **E**) Higher magnification of 10 µg/ml *m*-THPC-mediated PDT. DCF (green) fluorescence indicates $^1O_2$ or ROS detection in cells.

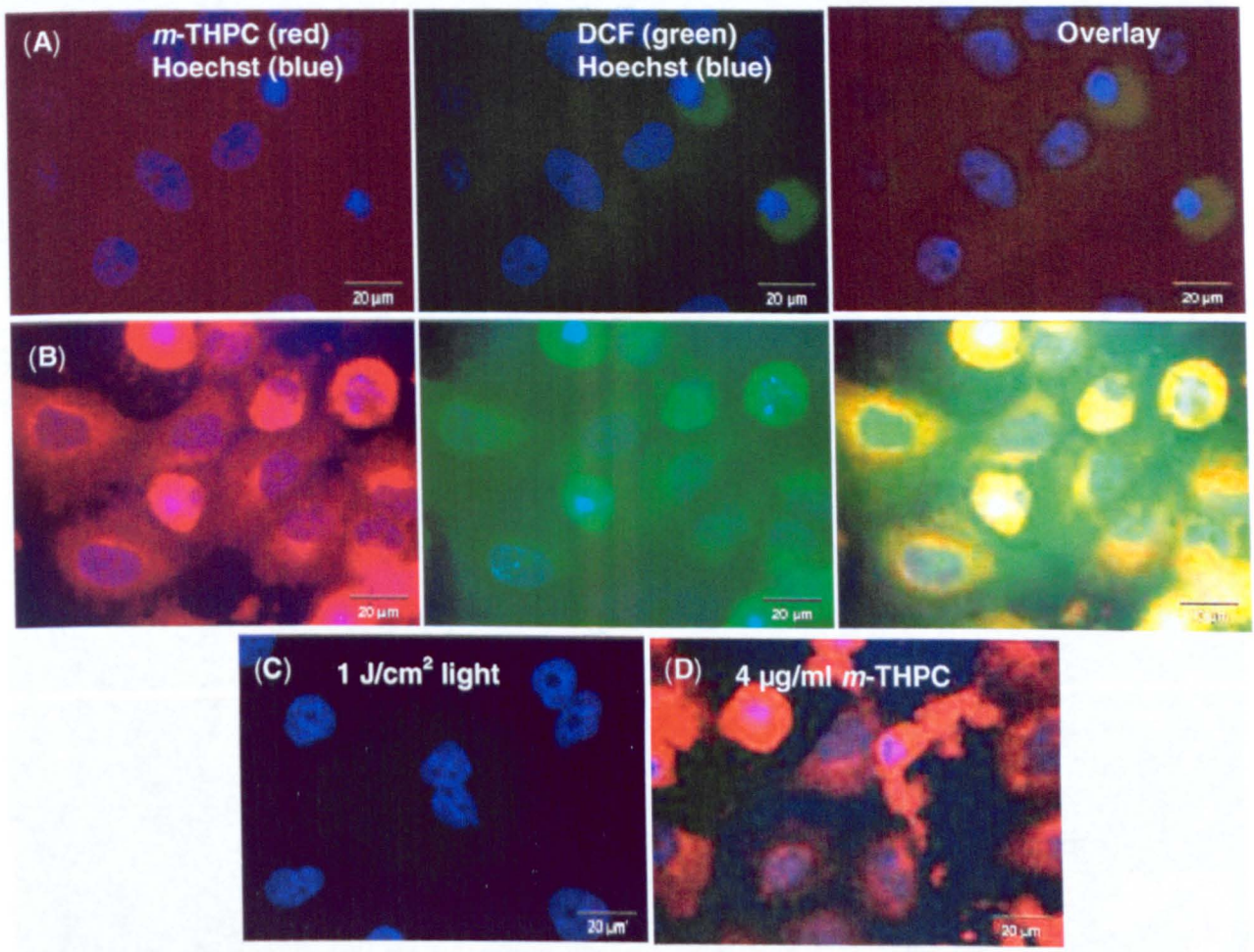

Figure 4.14
Micrographs of DCF detected in MCF-7 cells after *m*-THPC-mediated PDT.
Monolayer MCF-7 cells were treated with and without 100 µM H_2DCF-DA incubated for 60 min following 4 h *m*-THPC or no drug incubation. MCF-7 cells were fixed before Hoechst stained 33258 for nuclei (blue). (**A**) 1 J/cm^2 light only (no drug), (**B**) 4 µg/ml *m*-THPC-mediated PDT, (**C**) light only without H_2DCF-DA and (**D**) 4 µg/ml *m*-THPC-mediated PDT without H_2DCF-DA. DCF (green) fluorescence was detected in MCF-7 cells.

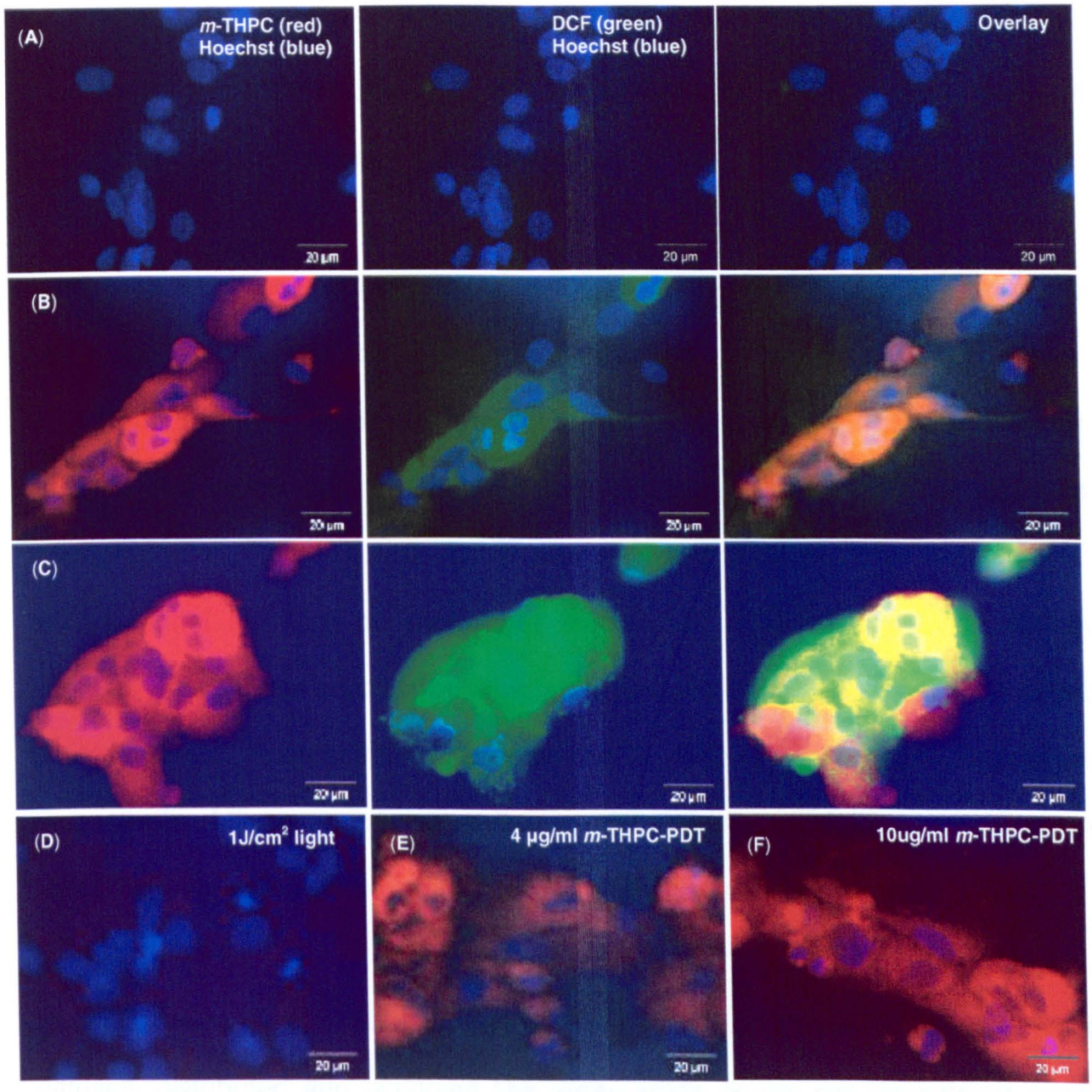

Figure 4.15.
Micrographs of DCF detected in astrocytes after *m*-THPC-mediated PDT.
Monolayer astrocyte cultures were treated with 100 µM H_2DCF-DA incubated for 60 min post 4 h *m*-THPC or no drug incubation. Astrocytes were fixed before Hoechst 33258 stained for nuclei (blue). (**A**) 1 J/cm^2 light only, (**B**) 4 µg/ml *m*-THPC-mediated PDT, (**C**) 10 µg/ml *m*-THPC-mediated PDT, (**D**) 1 J/cm^2 (no drug) without H_2DCF-DA (**E**) 4 µg/ml *m*-THPC-mediated PDT without H_2DCF-DA and (**F**) 10 µg/ml *m*-THPC-mediated PDT without H_2DCF-DA. DCF (green) fluorescence was detected in astrocytes.

incubated for 7 h (Figure 4.17). Both *m*-THPC and hypericin co-localised with LysoTrk-green fluorescence. However, this probe proved to be unreliable in other experiments and inconsistent when this experiment was repeated, so its use was discontinued for the purposes of this study.

Composite fluorescence micrographs in Figure 4.18A and B show there was no green fluorescence emitted by photosensitisers (*m*-THPC or hypericin), which would interfere with organelle tracker green fluorescent signals in monolayer cultures of satellite cells (co-cultured with neurones). Composite fluorescence micrographs in Figure 4.18C, D, E and F show MitoTrk-green fluorescence (mitochondrial staining) on monolayer cultures of DRG neuronal cell bodies (identified with phase contrast by their large rounded morphology and their bright photosensitiser fluorescence), satellite cells, MCF-7 cells and astrocytes respectively. Micrographs also show no red fluorescence was emitted form MitoTrk-green, which would interfere with photosensitiser fluorescence signals.

In DRG neuronal cell bodies (Figure 4.19) *m*-THPC and MitoTrk-green were diffusely distributed and occupied the same areas of the cell suggesting some degree of co-localisation, in monolayer culture, although higher magnification would be required in order to establish the true extent of this. In monolayer cultures of satellite cells (Figure 4.20), MCF-7 cells (Figure 4.21) and astrocytes (Figure 2.22), *m*-THPC was also observed to be generally localised in the cytoplasm in areas around the nucleus and away from the periphery of the cells. While *m*-THPC did co-localise to some extent with MitoTrk-green-labelled mitochondria, these organelles were not the predominant location of *m*-THPC within the cells (Figure 4.19C, 4.20C, 4.21C and 4.22C).

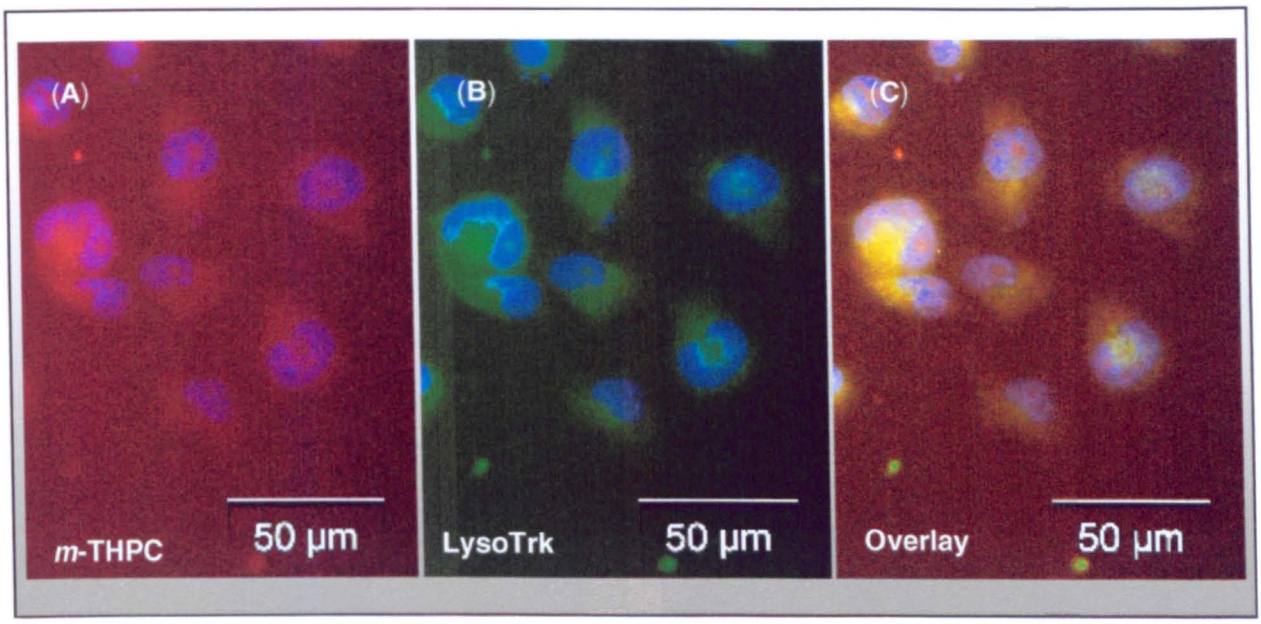

Figure 4.16
Micrographs of MCF-7 cells with *m*-THPC and LysoTrk-green.
Monolayer cultures of MCF-7 cells were treated with 25 nM LysoTrk-green for 60 min following 4 h incubation with 4 µg/ml *m*-THPC. MCF-7 cells were fixed before Hoechst 33258 stained for nuclei (blue). (**A**) *m*-THPC uptake; (**B**) LysoTrk-green fluorescence and (**C**) overlay image showing that both *m*-THPC and LysoTrk occupied the same space within the cell. This assay was discontinued due to inconsistencies with LysoTrk-green probe.

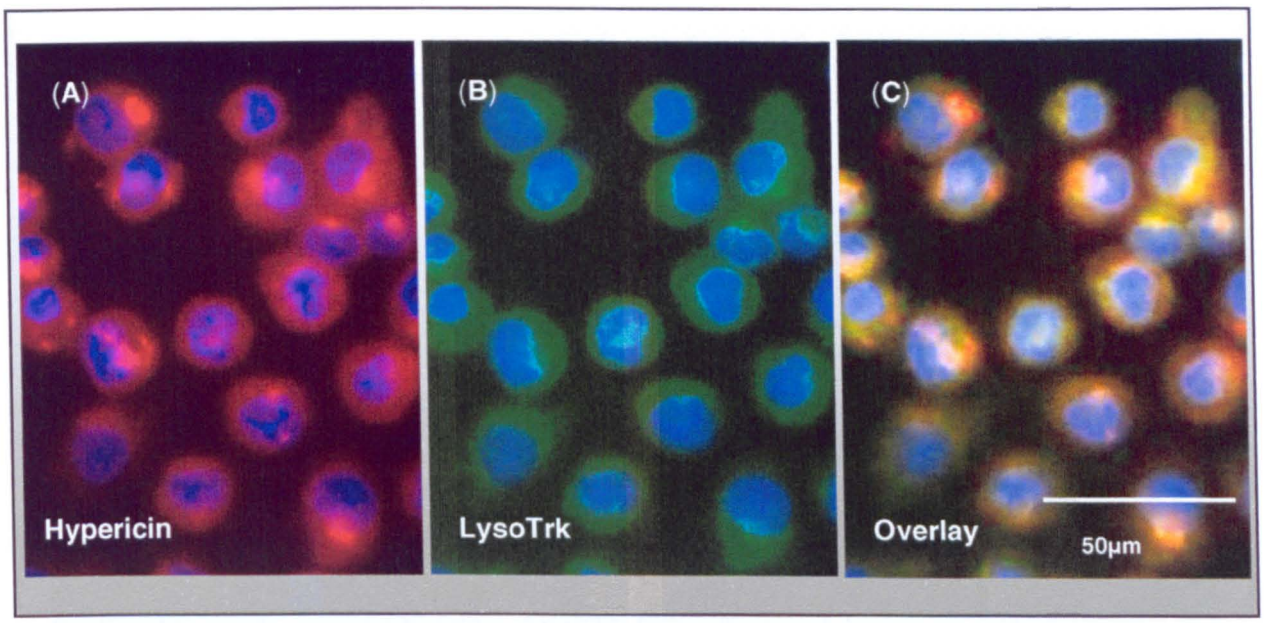

Figure 4.17
Micrographs of MCF-7cells with hypericin and LysoTrk-green.
Monolayer cultures of MCF-7 cells were treated with 25 nM LysoTrk-green for 60 min following 7 h incubation with 1.6 µg/ml hypericin. MCF-7 cells were fixed before Hoechst 33258 stained for nuclei (blue). (**A**) hypericin uptake; (**B**) LysoTrk-green fluorescence and (**C**) Overlay image showing that both hypericin and LysoTrk occupied the same space within the cell. This assay was discontinued due to inconsistencies with LysoTrk-green probe.

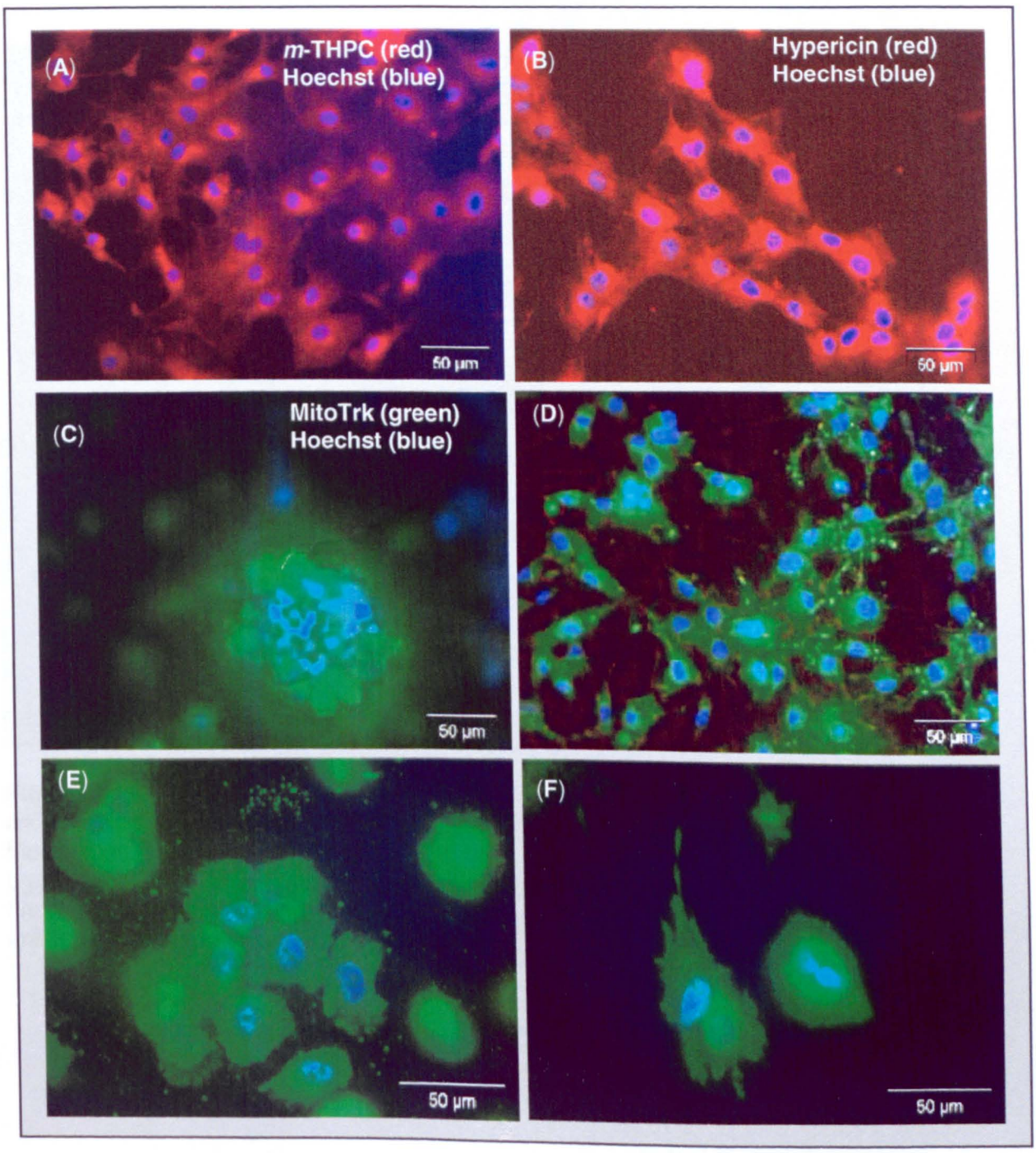

Figure 4.18
Micrographs of photosensitiser and MitoTrk-green controls.
Composite micrographs of monolayer cultures of satellite cells treated with (**A**) 4 µg/ml *m*-THPC (red) for 4 h and (**B**) with 1.6 µg/ml hypericin (red) for 7 h, showed no green fluorescence. Composite micrographs of 300 nM MitoTrk-green (green) incubated for 30 min, and Hoechst 33258 stained for nuclei (blue) after fixing (**C**) DRG neurones, (**D**) satellite cells, (**E**) MCF-7 cells and (**F**) astrocytes, showed no red fluorescence.

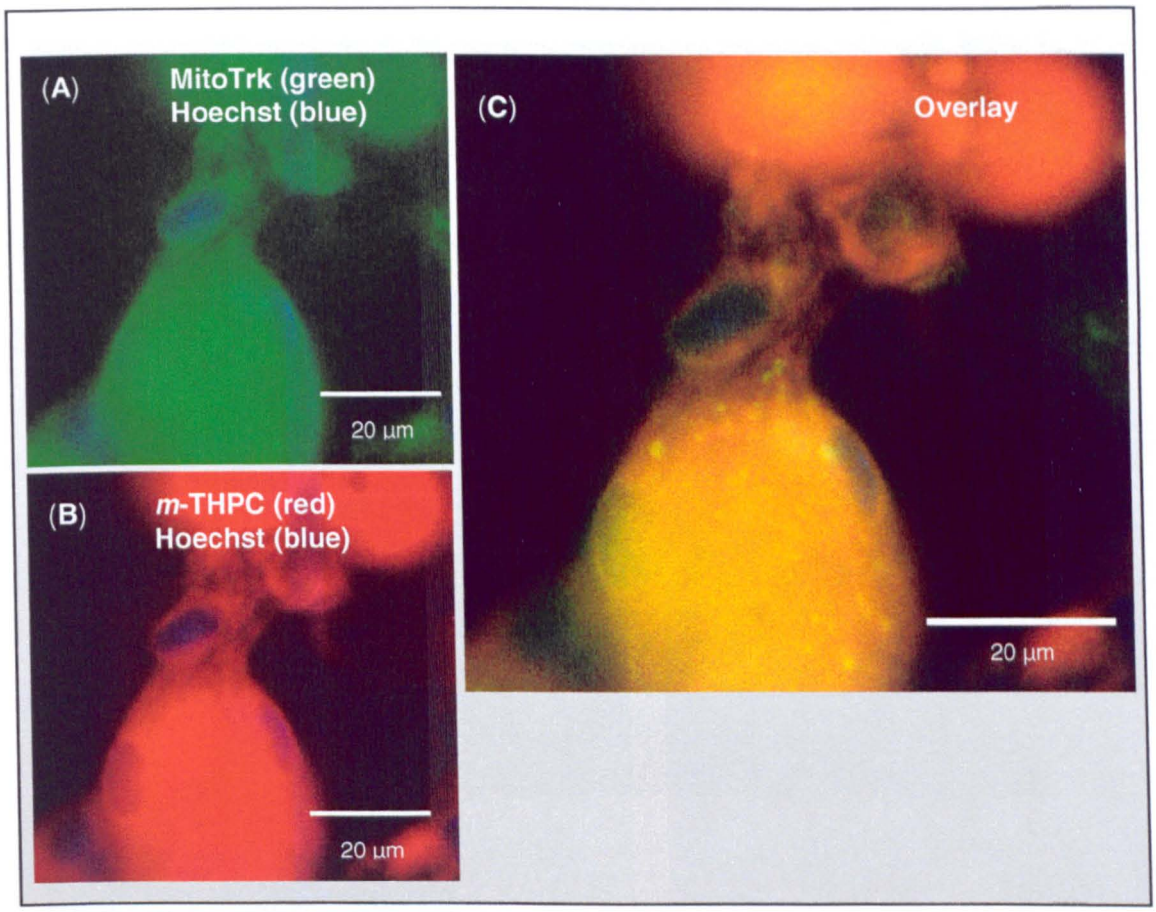

Figure 4.19
***m*-THPC co-localisation with MitoTrk-green in DRG neuronal cell bodies.**
Monolayer DRG cultures were incubated with 100 nM MitoTrk-green for 60 min and 4 µg/ml *m*-THPC for 4 h. Micrographs show (**A**) MitoTrk-green and (**B**) *m*-THPC fluorescence in combination with Hoechst stained nuclei (blue) after fixing. (**C**) Shows an enlarged overlay image of the red, blue and green channels.

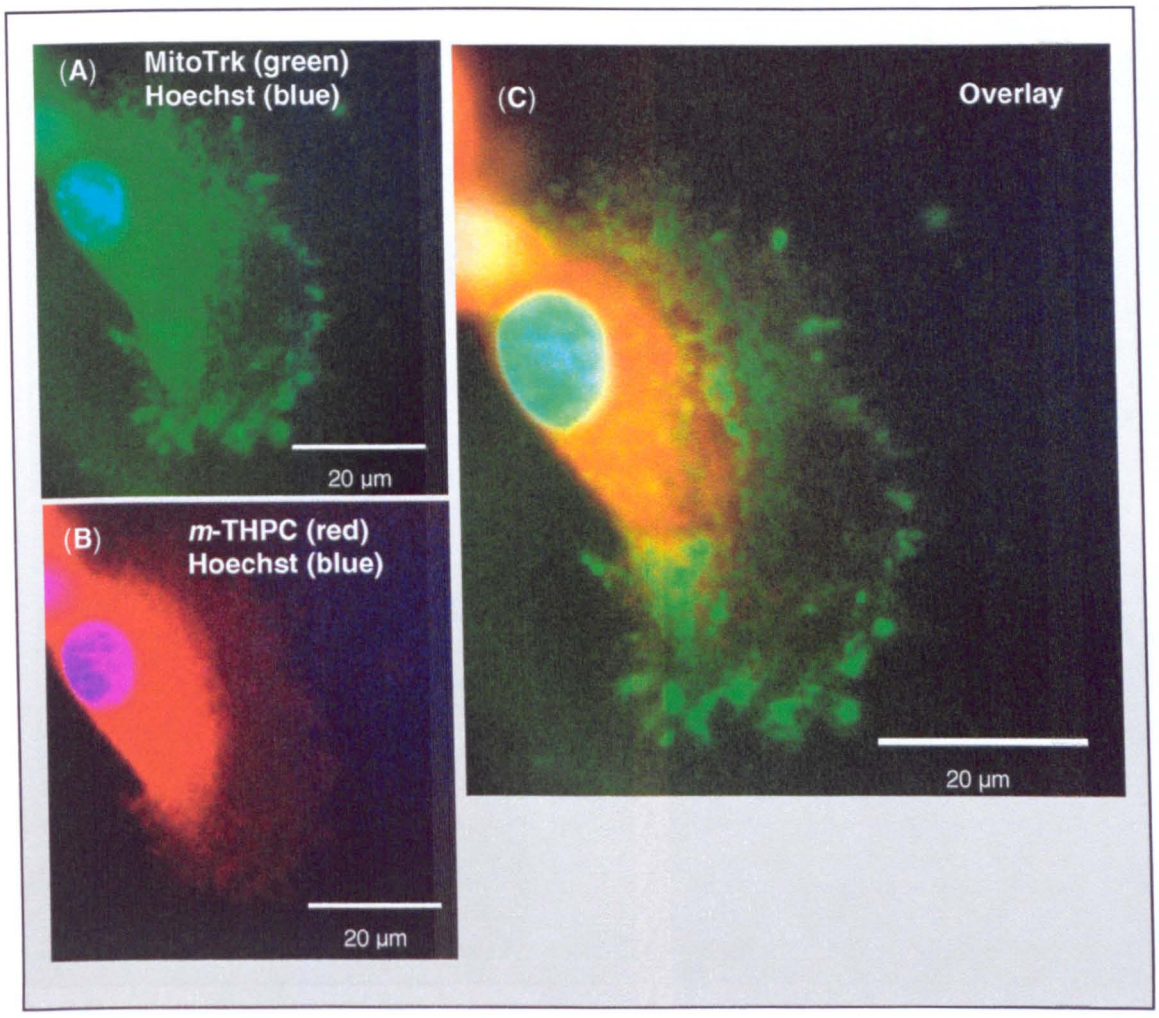

Figure 4.20
***m*-THPC co-localisation with MitoTrk-green in DRG satellite cells.**
Monolayer DRG cultures were incubated with 100 nM MitoTrk-green for 60 min and 4 µg/ml *m*-THPC for 4 h. Micrographs show (**A**) MitoTrk-green and (**B**) *m*-THPC fluorescence in combination with Hoechst 33258 stained nuclei (blue) after fixing. (**C**) Shows an enlarged overlay image of the red, blue and green channels.

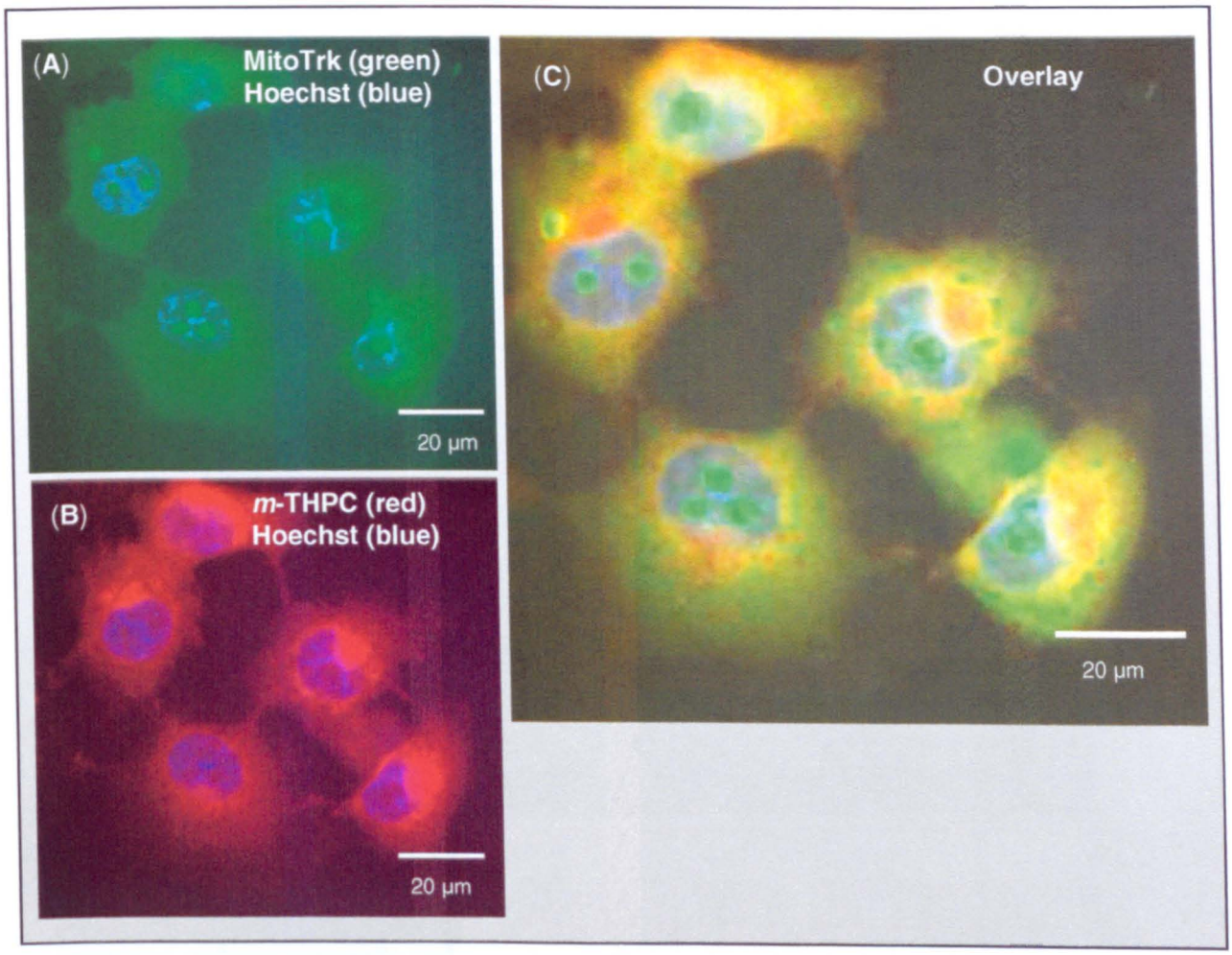

Figure 4.21
***m*-THPC co-localisation with MitoTrk-green in MCF-7 cells.**
MCF-7 cells were incubated with 100 nM MitoTrk-green for 60 min and 4 µg/ml *m*-THPC for 4 h. Micrographs show (**A**) MitoTrk-green and (**B**) *m*-THPC fluorescence in combination with Hoechst 33258 stained nuclei (blue) after fixing. (**C**) Shows an enlarged overlay image of the red, blue and green channels

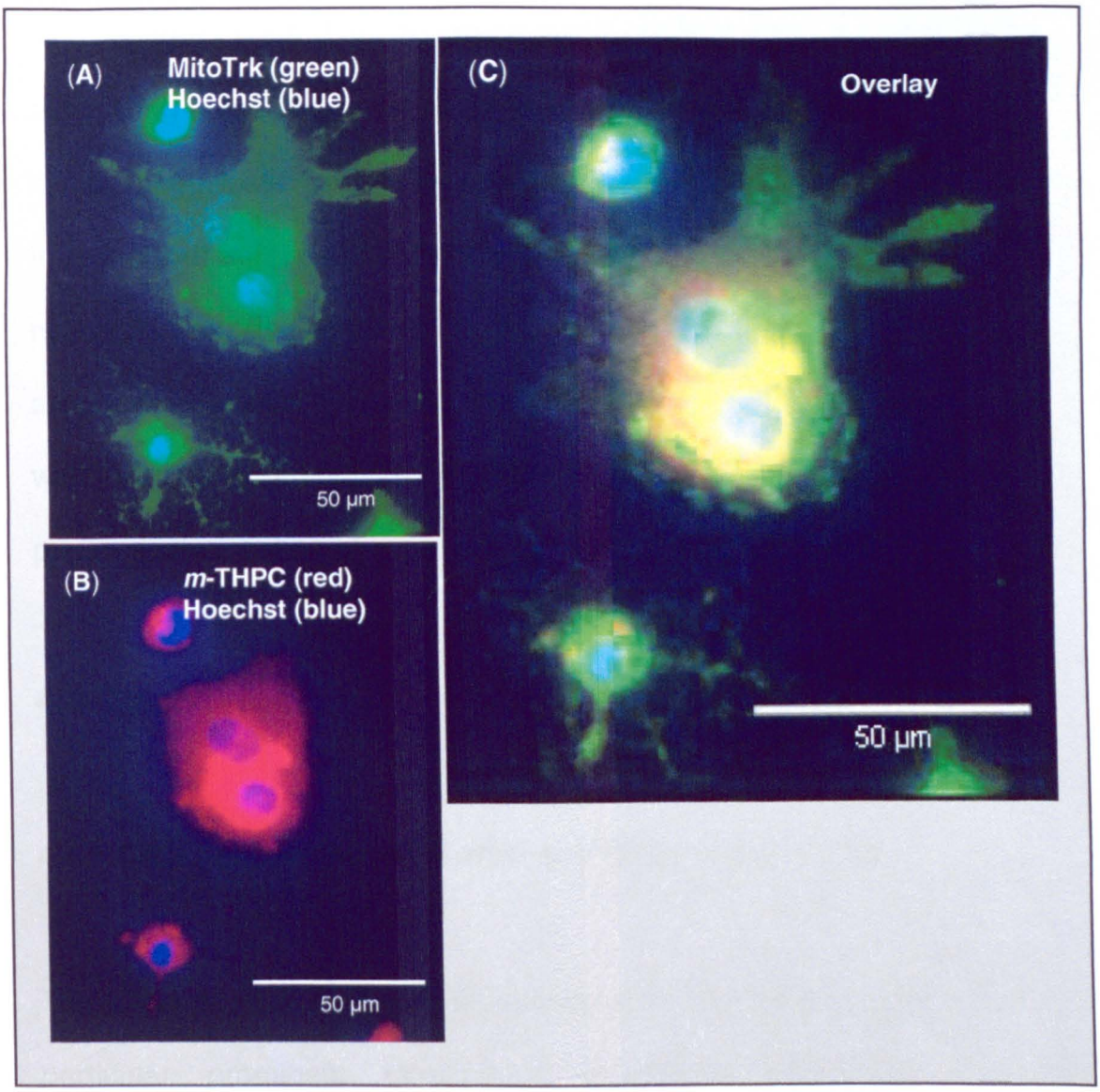

Figure 4.22
***m*-THPC co-localisation with MitoTrk-green in astrocytes.**
Astrocytes were incubated with 300 nM MitoTrk-green for 30 min and 4 µg/ml *m*-THPC for 4 h. Micrographs show (**A**) MitoTrk-green and (**B**) *m*-THPC fluorescence in combination with Hoechst 33258 stained nuclei (blue) after fixing. (**C**) Shows an enlarged overlay image of the red, blue and green channels.

In monolayer cultures of DRG neuronal cell bodies (Figure 4.23) hypericin and MitoTrk-green were diffusely distributed and occupied the same areas of the cell suggesting some degree of co-localisation as was the case for *m*-THPC, although higher magnification would be required in order to establish the true extent of this. In monolayer cultures of satellite cells (Figure 4.24) and MCF-7 cells (Figure 4.25), hypericin was also observed to be generally localised in the cytoplasm in areas around the nucleus and away from the periphery of the cells. Hypericin localised with MitoTrk-green-labelled mitochondria but these organelles were not the predominate location of hypericin within the cells (Figure 4.23, 4.24 and 4.25).

4.4 Discussion

4.4.1 DRG neurone survival after *m*-THPC-mediated PDT

The effect of PDT on a cell is dependent on the cell genotype and phenotype (in particular prominent intracellular antioxidant pathways), the intracellular localisation of the photosensitiser being used, and the specific PDT protocol (i.e. choice of photosensitiser, its concentration, incubation time, and light energy applied) (Almeida. *et al.*, 2004). In addition, interactions between cells can greatly influence their individual responses to PDT treatments (e.g. the interaction between DRG neurones and satellite cells). Uzdensky *et al.* have studied interactions between neurones and satellite cells, and their respective sensitivity to PDT with a range of photosensitisers including *m*-THPC using crayfish nerve models (Lobanov and Uzdensky, 2005). However, little is known about the mechanisms by which mammalian neural cells respond to PDT treatment and the data in Chapter 3 of this thesis are the first demonstration that mammalian DRG

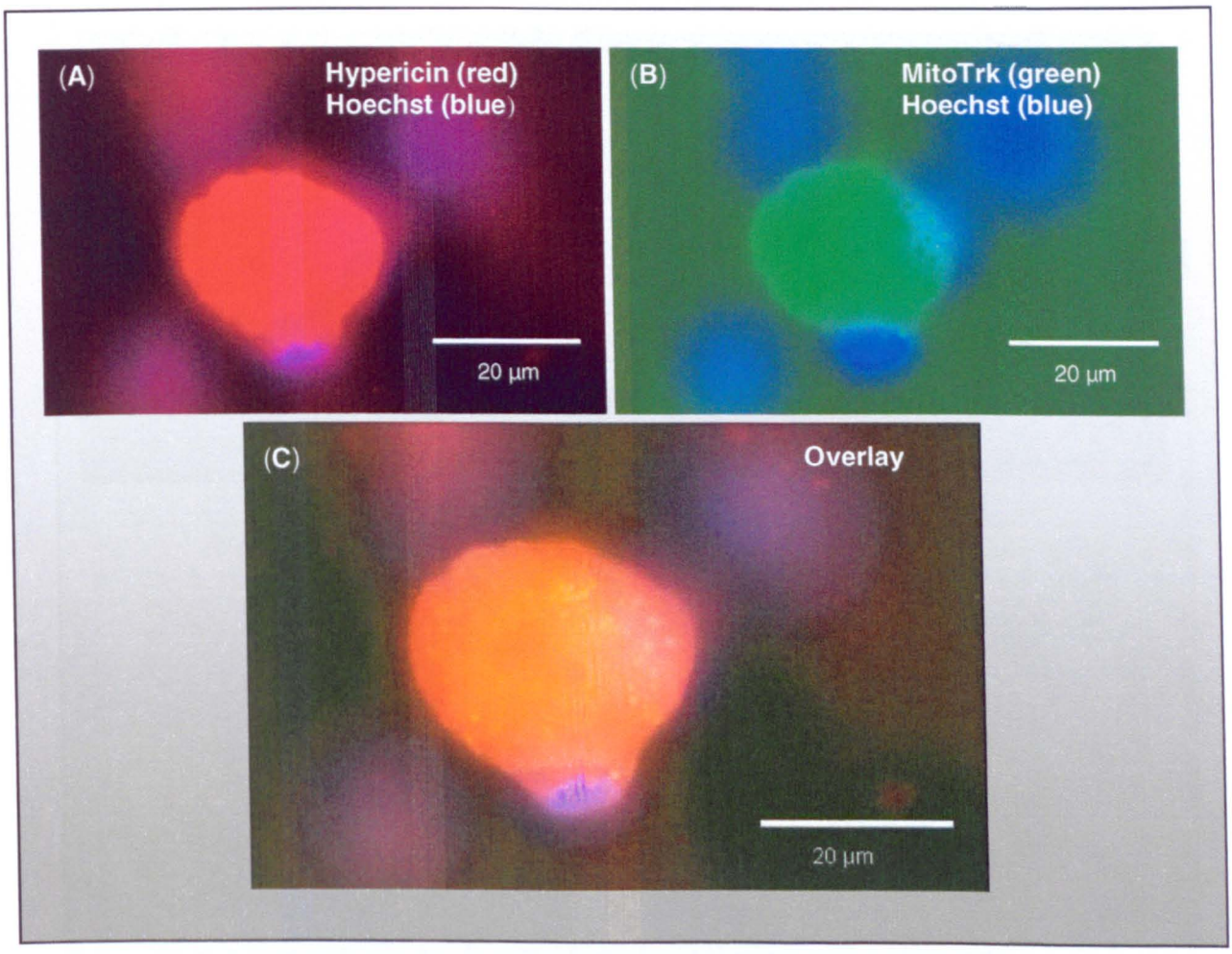

Figure 4.23
Hypericin co-localisation with MitoTrk-green in DRG neurones.
Monolayer DRG cultures were incubated with 1.6 µg/ml hypericin for 7 h and 100 nM MitoTrk-green for 60 min. Micrographs show (**A**) MitoTrk-green and (**B**) hypericin fluorescence in combination with Hoechst 33258 stained nuclei (blue) after fixing. (**C**) Shows an enlarged overlay image of the red, blue and green channels.

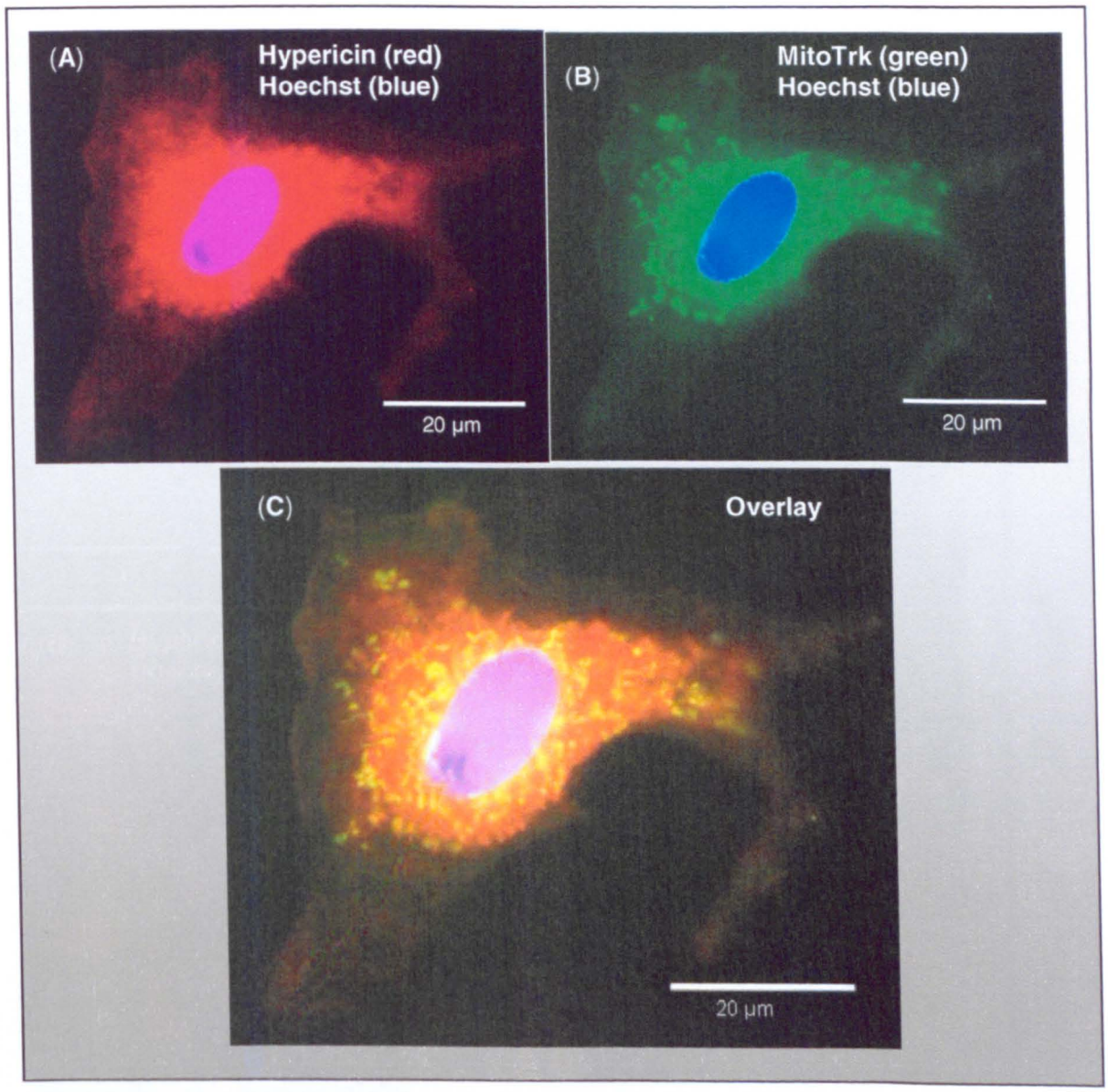

Figure 4.24
Hypericin co-localisation with MitoTrk-green in DRG satellite cells.
Monolayer DRG cultures were incubated with 1.6 µg/ml hypericin for 7 h and 100 nM MitoTrk-green for 60 min. Micrographs show (**A**) MitoTrk-green and (**B**) hypericin fluorescence in combination with Hoechst 33258 stained nuclei (blue) after fixing. (**C**) Shows an enlarged overlay image of the red, blue and green channels. (Note that hypericin is not localised in the nucleus. There is a layer of hypericin on top of the nucleus in this cell.)

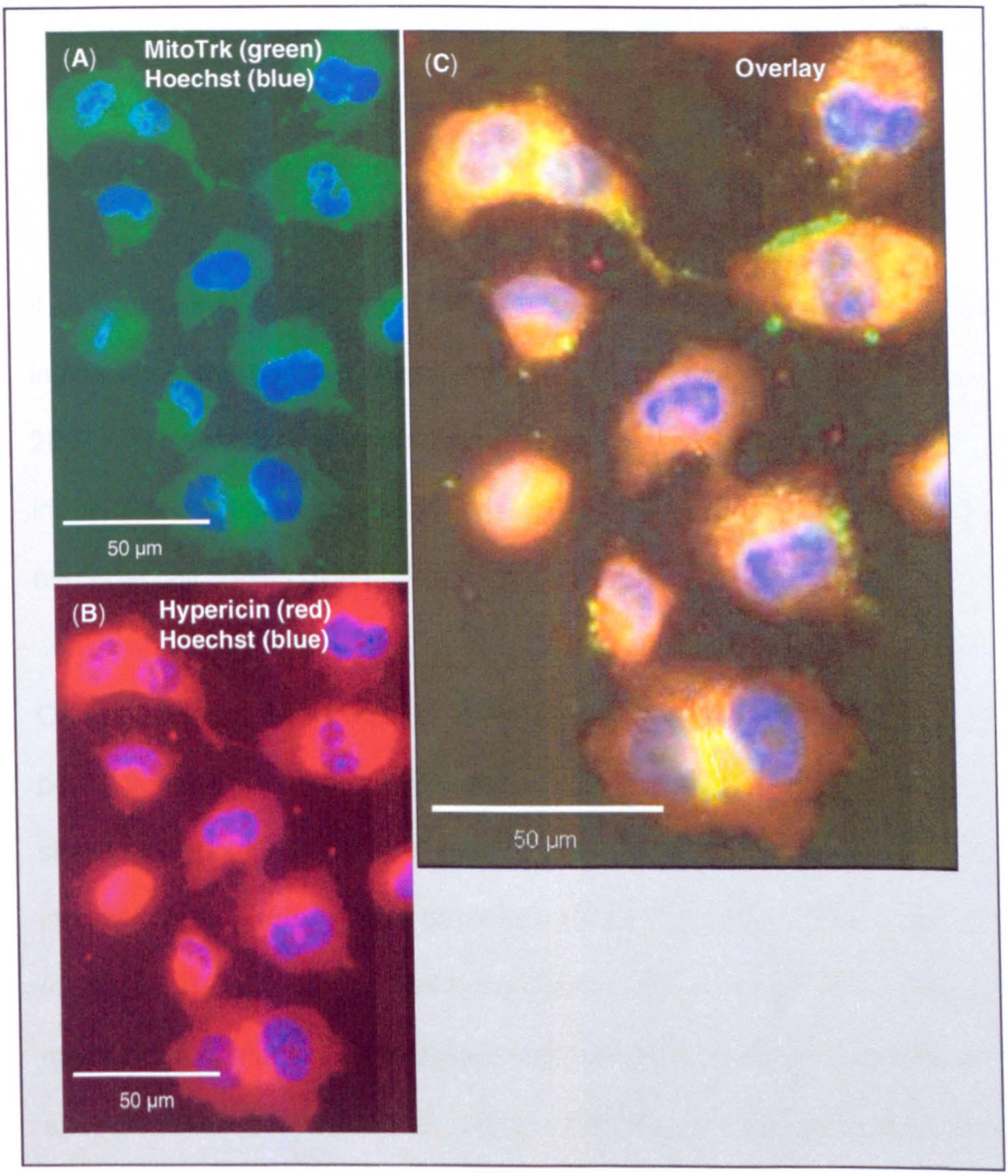

Figure 4.25
Hypericin co-localisation with MitoTrk-green in MCF-7 cells.
MCF-7 cells were incubated with 100 nM MitoTrk-green for 60 min and 1.6 µg/ml hypericin for 7 h. Micrographs show (**A**) MitoTrk-green and (**B**) hypericin fluorescence in combination with Hoechst stained 33258 nuclei (blue) after fixing. (**C**) Shows an enlarged overlay image of the red, blue and green channels.

neurones are relatively insensitive to *m*-THPC-mediated PDT (Wright *et al.*, 2009). The work described in this Chapter confirmed the survival and regenerative capacity of neurones following *m*-THPC-mediated PDT in culture and started to explore the biological mechanisms that might explain the phenomenon.

It is known that in neurones the site of neuronal degeneration is not a reliable indicator of where in the neurone the initial lethal defect occurred (Conforti *et al.*, 2007). For example, when peripheral nerves are damaged by severing or crush injury, it is the axons (neurites) which are initially damaged and this can result in neuronal cell bodies dying (McKay Hart *et al.*, 2002).

One potential problem with an investigation of responses to toxic stress in a cell population such as that undertaken in Chapter 3, where cell death is assessed at a single time point, is that this gives only a 'snapshot' view. This study would be incomplete therefore without some understanding of the time course of cell death (or survival) in the neural cell populations. Assays using one specific time point may underestimate cell death for cells that die by slow non-apoptotic or delayed apoptotic processes (Xe *et al.*, 2001). With this in mind DRG cell survival assays were conducted using a range of latency periods. Furthermore, the ability of neurones to regenerate neurites after apparently surviving PDT was used as a way of confirming neuronal survival.

Over the range of latency periods used (1 to 36 h post-4 μg/ml *m*-THPC-mediated PDT) there were no significant changes in the levels of neuronal and satellite cell death detected by PI exclusion assay. These results supported the observations of a necrotic mode of satellite cell death and of DRG neurone survival after 4 μg/ml *m*-THPC-mediated PDT. At an early time point of 8 h a test with FragEL™ assay

(DAB) was performed to identify any cells exhibiting indicators of apoptosis. DRG neurones were not undergoing apoptosis, because no Frag EL and βIII-tubulin positive cells were detected. Overall, the time course experiments support the suggestion that neurones survived this PDT treatment, and their co-cultured satellite cells died rapidly (by necrosis) following PDT treatment, with no additional delayed cell death up to 36 h. The FragEL™ assay also supported this suggestion with little apoptosis being detected 8 hours post-PDT.

Neurones that had survived *m*-THPC-mediated PDT were assessed for functional viability with respect to their ability to regenerate neurites. Neurite length has been reported to be a useful indicator of the health of neurones (Funk *et al.*, 2007). In this study the level of satellite cell death after *m*-THPC-mediated PDT ranged from 24±6 to 46±5 % across treatment conditions of 3 to 10 μg/ml *m*-THPC-mediated PDT (Chapter 3), and resulted in a neurone-enriched culture post PDT. Glial cells such as satellite cells are required for the continued survival and neurogenesis (neurite growth) of DRG neurones in culture without addition of growth factors (Fallon 1985; Delree *et al.*, 1989). Therefore PDT-treated neurones were cultured with untreated satellite cell-enriched cultures in monolayer in order to provide an optimal environment for viable neurones to regenerate neurites. Under these conditions, neurones treated with 3 and 4 μg/ml *m*-THPC-mediated PDT were shown to retain their ability to re-generate neurites with no significant difference from that of non-PDT treated neurones. This was in contrast to the use of high doses of 10 μg/ml *m*-THPC-mediated PDT, which caused significant reduction in neurone adhesion and neurite regeneration capacity.

This is an important result, which goes beyond assessing the lack of neuronal cell death observed in Chapter 3 and demonstrates that, under the conditions used in

this study, DRG neurones are clearly able to survive *m*-THPC-mediated PDT treatments that are sufficient to kill other cell types, and retain their ability to regenerate neurites to the same extent as untreated neurones.

Having confirmed that DRG neurones survived *m*-THPC-mediated PDT in this study, further experiments were undertaken to understand the mechanism by which this occurred. It was apparent that inhibiting intracellular antioxidant pathways in cells subjected to PDT treatment elicited neuronal cell death, suggesting that these antioxidant pathways were involved in protecting the neurones from PDT-induced oxidative stress. The antioxidant pathways investigated in this study were the glutathione synthase, SOD-1 and SOD-2 pathways and the PDT treatment was the EC_{50} dose for killing MCF-7 cells (i.e. 4 µg/ml *m*-THPC-mediated PDT).

Results suggested that inhibition of either the SOD-1 pathway or the glutathione synthase pathway (specifically γGCS) in neurones was sufficient to render then susceptible to 4 µg/ml *m*-THPC-mediated PDT. This then caused levels of cell death similar to those observed in Chapter 3 for other cell types. However, this was not the case with inhibition of SOD-2 pathway, after which neurones remained resistant to PDT treatment. These results give some insight into the intracellular mechanisms that might be important for protecting neurones during *m*-THPC-mediated PDT. Nevertheless, these results must be interpreted with some caution. While the data from the experiments were robust and appropriate controls were included, further work would need to be undertaken to delineate the precise involvement of these pathways in neuronal protection. For example, alternative inhibitors could be used to target pathways, and inhibitor dose responses should be undertaken; particularly in the case of SOD-2 pathway inhibition (2-$MeOE_2$).

Without confirming that the inhibitor dose used would have been sufficient to block the SOD-2 pathway in these cells, it would be inappropriate to conclude that this pathway was not involved in neuronal protection from PDT.

The glutathione synthase pathway has been previously shown to effectively protect neurones from oxidative stress due to both ethanol (Watts *et al.*, 2005), and oxidised low-density lipoprotein (Wang *et al.*, 2006). Moreover, SOD 1 and 2 pathways have also been previously shown to be involved in human umbilical vein endothelial cell (HUV-EC), human lung carcinoma cell (A549) and MCF-7 cell death responses to Photofrin®-mediated PDT (Saczko *et al.* 2008).

The results in this Chapter are in line with those from other research on neural cells using L-BSO to inhibit the glutathione synthase pathway. Depletion of rat brain cell GSH levels with L-BSO itself was not toxic to CNS neurones, but increased dopaminergic toxicity (McNaught and Jenner, 1999). DRG neurones co-cultured with satellite cells in this study remained viable in culture following the use of L-BSO for 24 h, as well as after incubation with the SOD-1 inhibitor DDC for 1.5 h in all control conditions. This was in contrast with co-cultured satellite cells, which exhibited significant cell death determined by PI uptake in culture under control conditions. Microscopic examination revealed nucleus fragmentation in satellite cells treated with L-BSO and condensed nuclei in satellite cells treated with DDC, indicating apoptotic cell death in many cells. These results suggested that glial cells are more sensitive than DRG neurones to these inhibitors under the conditions used in the culture model. *Since satellite cells are important for neuronal survival, it is important to note that their sensitivity to these inhibitors might influence neuronal behaviour, so any effects attributed to the action of the inhibitors on neurones must be interpreted carefully.*

Mytilineou *et al.* (1999) and de Bernardo *et al.* (2004) suggested that neural cell death due to L-BSO inhibition of the glutathione synthase antioxidant pathway, in the presence of an oxidative stress challenge, is the consequence of events that are mediated by glial cells. Gegg *et al.* (2005) reported that levels of GSH were greater in rat neurones in co-culture with glial cells (astrocytes) than for neurones cultured alone. In addition, de Bernardo *et al.* (2004) reported no toxic effect of L-BSO on rat mesencephalic neurone viability when cultured in isolation in contrast to neurones being more sensitive to L-BSO when cultured with glial cells. It was noted that glial cell GSH depletion did not cause neuronal death, but potentiated the toxicity of oxidative stress from glial cells (astrocytes) (McNaught and Jenner, 1999). This was similar to the results presented in this chapter, in which L-BSO treatment in controls was not toxic to neurones while being highly toxic to glial cells (satellite cells).

Inhibition of the SOD-2 pathway with 2-$MeOE_2$ did not affect the viability of either DRG neurones or co-cultured satellite cells in culture under control conditions, or the level of cell death in response to 4 µg/ml *m*-THPC-mediated PDT. This implied that the SOD-2 cell antioxidant pathway may not be involved in the response of these cells to *m*-THPC-mediated PDT. Alternatively it may imply that the concentration of 1.0 µM 2-$MeOE_2$ incubated for 24 h on these cells was not sufficient to inhibit the SOD-2 antioxidant pathway in these cells.

Previous studies have highlighted a link between the effectiveness of PDT and SOD levels with a major role played by inducible SOD-2, rather than SOD-1, in cancer cell lines in protecting them from PDT (Johnson and Pardini, 1998). There were observed reductions in the cell killing effects of Photofrin®-mediated PDT on a bladder cancer (T24) cell line that was transfected with SOD-2 isoenzyme and in

C-26 and T24 cell lines pre-treated with permeable SOD mimetics. However, this reduction in Photofrin®-mediated PDT killing efficiency was not observed with the transfection of SOD-1 isoenzyme in these cells (Gołąb *et al.*, 2003). Das *et al.* (2000) showed a marked difference between the long-term viability of two human cervical epithelial carcinoma cell lines after low levels of Photofrin II®-mediated PDT. CaSki cells (defective in induction of SOD-2 gene) were more sensitive to PDT treatment than were HeLa cells (where induction of the SOD-2 gene was observed). It would be interesting to extend the present study to explore the expression levels of the components of antioxidant pathways in neurones to see whether there is a link between the relative levels of the various antioxidant molecules and the response to inhibitors shown here.

Combining the γGCS inhibitor and the SOD-1 inhibitor in this study caused approximately 100 % neurone death under control conditions. This prevented combinations of these inhibitors from being used to explore the relationship between the SOD-1 pathway and the glutathione synthase pathway in protecting neurones from PDT. Co-cultured satellite cells also died when exposed to this combination of γGCS inhibitor and the SOD-1 inhibitor. This study demonstrates for the first time the involvement of the glutathione synthase pathway and the SOD-1 pathway in regulating the sensitivity of DRG neurones to *m*-THPC-mediated PDT. It will be important to extend this study in the future to understand the conditions under which neurones might become sensitive to PDT treatment, particularly with a view to predicting how neurones might respond to PDT *in vivo*.

4.4.2 $^1O_2$/ROS detection

Degradation of neurites occurred after exposure of DRG neurones in 2D and 3D co-cultures with satellite cells to *m*-THPC- and hypericin-mediated PDT (Chapter 3 and Wright *et al.*, 2009). Because neurites lacked detectable photosensitiser fluorescence, the generation of $^1O_2$/ROS within these neurite structures was assessed.

In monolayer cultures, small amounts of $^1O_2$/ROS (DCF fluorescence) were detected within neurites after exposure to 4 μg/ml *m*-THPC-mediated PDT. However, after a higher dose of 10 μg/ml *m*-THPC-mediated PDT, no neurites were available for assessment. This means that the question of whether *m*-THPC localises within neurones to a sufficient level to generate damaging $^1O_2$/ROS remains unanswered. Alternative ROS detection assays or more powerful microscopy could be a suitable way of exploring this further in the future.

Very little $^1O_2$/ROS was detected in DRG neuronal cell bodies, until the use of a high *m*-THPC-mediated PDT dose of 10 μg/ml *m*-THPC was administered. At this concentration, only a few DRG neuronal cell bodies showed positive DCF fluorescence, which indicated $^1O_2$/ROS accumulation in the cell. Interpreting these findings in the light of the antioxidant inhibition data reported above suggests that the lack of $^1O_2$/ROS detection in many DRG neurones after exposure to *m*-THPC-mediated PDT might be attributed to the action of intracellular antioxidant pathways within neurones. A higher level of antioxidant protection compared to the other cells under investigation would reduce $^1O_2$/ROS and their oxidation products in neurones, thus reducing DCF levels. It was also observed that DRG neuronal cell bodies, which were positive for $^1O_2$/ROS accumulation (DCF fluorescence),

exhibited reduced *m*-THPC fluorescence in comparison to DRG neuronal cell bodies that did not display DCF fluorescence. The generation of fluorescent DCF molecules within the cell, may play a role in quenching *m*-THPC fluorescence. It would be interesting to investigate the relative levels of *m*-THPC fluorescence and DCF fluorescence in neurones exposed to *m*-THPC-mediated PDT with the addition of the antioxidant pathway inhibitors, since this could give further insight into whether SOD-1 and GSH are involved in reducing the initial $^1O_2$/ROS accumulation.

$^1O_2$/ROS was shown to accumulate in the cytoplasm of astrocytes and MCF-7 cells to a greater extent than in satellite cells and DRG neurones after *m*-THPC-mediated PDT. This large amount of $^1O_2$/ROS detected in astrocyte cultures after exposure to *m*-THPC-mediated PDT, was in line with their high level of sensitivity as demonstrated in Chapter 3.

4.4.3 *m*-THPC and hypericin photosensitiser subcellular localisation

Subcellular localisation of photosensitisers was of interest here as a possible mechanism by which DRG neurones responded differently to other cells to *m*-THPC-mediated PDT. More broadly, little is known about the distribution of *m*-THPC and hypericin in mammalian neurones, satellite cells and astrocytes; therefore any insight into this area would be of interest. The effects of PDT on specific targets may vary with photosensitiser subcellular localisation; therefore allowing organelle-dependent phototoxicity (Dabrowski *et al.*, 2006).

In order to establish the subcellular localisation of photosensitisers, specific organelles need first to be identified. This is commonly done with the use of

organelle markers. Crosstalk is a problem that can occur when dealing with photosensitiser subcellular localisation in conjunction with fluorescent probes for organelle identification. For example, hypericin, when excited with 488 nm light emits fluorescence at both 590 nm and also at 660 nm and this dual emission can cause a spill-over problem when used with green fluorescence probes such as MitoTrk-green or LysoTrk green, possibly resulting in misleading observations (Adigbli *et al.*, 2007). Keeping this in mind, this study first established that the green fluorescent probes were not detected in the red channel, while photosensitiser red fluorescence was not detected in the green channel.

Several publications have reported *m*-THPC as having a diffuse cytoplasmic pattern of distribution within cells. *m*-THPC has been detected previously in many organelles including intracellular membranes of the ER and the Golgi apparatus (Melnikova *et al.*, 1999a; Teiten *et al.*, 2003b; Laville *et al.*, 2003; Marchal *et al.*, 2007), mitochondrial membranes (Melnikova *et al.*, 1999a; Yow *et al.*, 2000; Laville *et al.*, 2003; Sadauskaite *et al.*, 2004), in a diffuse cytoplasmic pattern attributed to lysosomal localisation (Ball *et al.*, 1999; Leung *et al.*, 2002; Laville *et al.*, 2003), peri-nuclear envelopes (Foster *et al.*, 2005; Kiesslich *et al.*, 2007; Lassalle *et al.*, 2008) and as homologously distributed bright fluorescent spots in the plasma membrane (Lassalle *et al.*, 2008). Marchal *et al.* (2005) also proposed that the ER and the Golgi apparatus could be sites from which cell death signals originate during *m*-THPC-mediated PDT and then converge on mitochondria to trigger apoptotic processes in a less efficient manner than photosensitisers which directly target mitochondria. Hypericin has also been reported as being localised in the cell cytosol and to predominantly localise in the nuclear membrane, but like *m*-THPC, it does not localise in the nucleus (Dabrowski *et al.*, 2006).

From the literature it is difficult to find consensus for organelle-specific localisation of *m*-THPC. In this study *m*-THPC localisation in DRG neural cells and MCF-7 cells was observed to be cytoplasmic in nature. However, in some cases a punctate distribution pattern, with intense accumulation in the peri-nuclear regions of satellite cells was observed. This was in comparison to hypericin, which was shown to be more diffusely distributed in the cytoplasm of satellite cells. In this study *m*-THPC and hypericin were found not to be localised within nuclei of neural cells or MCF-7 cells. From visual inspection of micrographs, *m*-THPC was found to be partially co-localised with mitochondria in MCF-7 cells, neuronal cell bodies and satellite cells. Greater co-localisation of *m*-THPC with mitochondria in astrocytes was observed. In comparison, hypericin showed greater mitochondrial co-localisation than *m*-THPC in these cell types. An interesting future study would involve using high resolution fluorescence or confocal microscopy to provide images which could be quantified accurately, in order to establish whether there was any clear difference in the intracellular distribution of *m*-THPC in neurones compared to the other cells types. Also a reduction in the concentration of applied photosensitiser or a reduction in incubation time in localisation studies, could also aid in determining where in cells photosensitisers accumulated. But, results from these studies would have to be interpreted with caution. This is because the photosensitiser concentration or incubation time used would not be the same as during PDT-treatment. In addition, the photosensitiser can aggregate in solution or within cells, potentially influencing its localisation in cells.

In regards to the use of LysoTrk-green for determining photosensitiser localisation in cells, this study's parameters were similar to those of Adigbli *et al.*, 2007. In their study they were able to show hypericin co-localising with lysosomes in MGHU1/R cells (50 nM LysoTrk-DND-26 incubated for 30 minutes). In the same study there

was also some report of re-localisation of both hypericin and LysoTrk-green after illumination.

As previously stated *m*-THPC is known to localise predominantly in the ER and Golgi apparatus, with some reports of mitochondrial and lysosomal localisation. Therefore *m*-THPC would be predicted to be present in mammalian neurites since they contain ER (Goldberg *et al.*, 2003), and many mitochondria (Berghe *et al.*, 2004). However, this could not be demonstrated in this study, although further studies with higher magnification microscopy would be required before concluding that photosensitisers were indeed absent from neurites. A further complication may arise because only the primary localisation of *m*-THPC and hypericin were investigated here, and light-induced re-localisation has been observed with some photosensitisers (Ball *et al.*, 1999). This gives rise to the possibility that the initial localisation site of photosensitisers may not be as important as the secondary site with regard to cell damage and/ or repair (Ball *et al.*, 1999), so further studies would need to investigate photosensitiser localisation at various times after illumination.

4.5 Conclusions

In conclusion, this chapter has confirmed that DRG neurones survived *m*-THPC-mediated PDT and remained capable of regenerating neurites in co-culture with satellite cells. This survival was prevented by inhibitors of the glutathione synthase and the SOD-1 antioxidant pathways. These findings suggest the involvement of these systems, but not the SOD-2 pathway, in neuronal protection during *m*-THPC-mediated PDT.

Investigations into the localisation of $^1O_2$/ROS production within neurones and other cells were undertaken, along with an investigation of the intracellular localisation of *m*-THPC. These studies revealed new information about the distribution of PDT photosensitisers (*m*-THPC and hypericin) and $^1O_2$/ROS in cultured neural cells. While there were no conclusive data that would explain differences in sensitivity to PDT of neurones to other cells tested in this study, an insight was gained into techniques that would permit future studies in order to understand the effects of PDT on cells of the nervous system.

Chapter 5: Assessment of Neurone Sparing After Focal PDT Treatment-Peripheral Nerve Culture System Development

5.1 Introduction

Studies presented in previous Chapters revealed information about how adult DRG neurones may be spared damage during *m*-THPC-mediated PDT. These findings could potentially inform clinicians seeking to treat cancer within or adjacent to the nervous system, but for that to be achieved the phenomenon needs to be understood more thoroughly and its utility explored in animal models. With these aims in mind there are some key aspects of the DRG neurone sparing that could be investigated using more advanced cell culture models than those developed to date.

In particular, the results presented in previous chapters involved exposing the entire DRG culture to PDT treatments. However, in the nervous system, neurites frequently extend long distances from their cell bodies. During PDT exposure of peripheral nerves, often only neurites are illuminated at the focal treatment site, because the neuronal cell bodies are situated quite some distance away. A fundamental question which will influence the future direction of this study, is how neuronal survival and function would be affected by focal application of PDT, to different parts of the neurone (i.e. the neuronal cell body or at various distances away along the length of a neurite). Therefore, in this chapter the results of a series of pilot experiments are presented on the development of model peripheral nerve culture systems in which PDT could be directed towards specific parts of neurones.

5.1.1 Dissected peripheral nerve tissue culture systems

One basic approach to exploring the effects of PDT on the different parts of a peripheral nerve *in vitro* is to explant a fresh nerve from an animal and maintain it in culture (*ex. vivo*), therefore preserving the architecture and arrangement of the tissue. In this way, it would be possible to direct PDT treatment towards the region of the dissected nerve containing neuronal cell bodies (in the DRG) or neurites (in the nerve trunk). *Ex vivo* models can be maintained in culture as free-floating tissues or embedded in substrates such as collagen hydrogels. Dissected sciatic nerves with attached DRGs are one potential nerve model that has been used previously (Svensson *et al.*, 1995; Edström *et al.*, 1996; Tonge *et al.*, 1997). These dissected nerves can be removed from rats pre-injected with *m*-THPC or removed from non-injected rats and subsequently incubated in *m*-THPC solutions.

Dissected DRGs have been used previously to assess neurone-glial cell interactions (Shi *et al.*, 1998), and have been maintained in semi-solid culture medium (with similar properties to hydrogels) which is known to preserve the internal organisation of the tissue so it resembles the *in vivo* situation (Mandys *et al.*, 1998; Gölz *et al.*, 2006). Even though the use of intact nerve tissue may seem the best model for evaluating the effect of *m*-THPC-mediated PDT on the nerve, the use of dissociated cells in tissue engineered models has the advantage of providing a more controlled environment to assess specific nerve cell responses.

5.1.2 Cellular environment for 2D and 3D peripheral nerve culture systems

The required parameters for a peripheral nerve culture system for use in PDT are that it reflects the cellular composition of the endogenous nerve tissue; it is

reproducible and controllable; and it is accessible to treatment with PDT (i.e. photosensitiser and focal light exposures). The nerve trunk contains various cells including sensory and/or motor neurones, Schwann cells and nerve fibroblasts. The extracellular environment of the nerve trunk is a vascularised dense and aligned collagen-rich endoneurium surrounded by a perineurium, which is a barrier to fluid movement, and an outer collagenous epineurium. An overview of the cellular structure of the mammalian nervous system has been provided in Chapter 1.

5.1.2.1 Requirements for peripheral nerve culture systems

A successful culture system would therefore require aligned extended growth of neurites many millimetres from neuronal cell bodies (to facilitate targeted PDT-illumination towards distinct parts of neurones), and a clearly defined neuronal population, supported through interactions with the appropriate glial cells (Schwann cells and/ or satellite cell). A 3D environment rich in collagen would also be beneficial, although such a system would need to be of much lower cell density than an *in vivo* nerve since it would lack the perfusion supplied by the vasculature. The ability to perform cell viability assays and relevant cell type identification using immunohistochemistry (dissected nerves) and immunocytochemistry (2D or 3D culture systems) would also be valuable properties.

Neurones, glial cells and fibroblasts are significant cellular elements of nerve tissue. Inclusion of fibroblasts in nerve culture models is important because fibroblasts have been reported to contribute to glial cell (Schwann cell) alignment in culture (Dubuisson *et al.*, 1999). As presented in Chapter 1, neurones are

dependent on supporting glial cells (e.g. Schwann cells and satellite cells) (Nascimento *et al.*, 2008).

Controlling cellular orientation and proliferation is useful in the modelling of cellular interactions. Schwann cells in the PNS are known to provide both trophic support and guidance for neurite growth; therefore by controlling glial cell orientation in monolayer cultures or in a 3D matrix, neurite elongation can be guided (Schmalenberg and Uhrich, 2005; Thompson and Buettner, 2006). In addition to extracellular signalling molecules from glial cells, extracellular matrix guidance molecules (slit2, and laminin and the related molecule netrin-1) can also induce neurite elongation (Goldberg, 2003). Goldberg (2003) also reported adult DRG neurite growth *in vitro* to be initially highly branched but then to revert to a rapid elongating and minimal branching mode. This change to an elongated mode both *in vivo* and *in vitro* resulted in a 2 fold increase in rate of neurite growth from ~0.5 to1.0 mm per day. This means that a good culture model system should be able to generate sufficient neurite length within a few days in culture in order to facilitate focal PDT application. In general DRG neurones are also known to form no more than 2 or 3 neurites *in vitro*, making it suitable for quantitative research (Stępień *et al.*, 1999) and for the assessment of any change in neurite branching after PDT.

It is important to note that in the peripheral nerve trunk, there are both sensory and motor neurones. In previous chapters of this study and for this chapter on peripheral nerve model development, motor neurones were excluded. This exclusion of motor neurones was because their neurites were severed from their neuronal cell bodies on explantation of DRGs. Therefore the response of motor neurone cell bodies and their neurites to the effects of PDT treatments were not assessed.

5.1.2.2 Existing peripheral nerve culture systems

Nerve models that are presently being used, which could be adapted for use in this focal PDT treatment assay include 2D and 3D nerve culture models. Several different 2D models have been used that facilitated aligned neurite growth, these included but are not limited to scratched glass surfaces (Stępień *et al.*, 1999) or micropatterned grooves (Goldner *et al.*, 2005), where lines were etched into culture surfaces before neurones were cultured and neurites then followed these etchings. The use of micropatterned substrates, where proteins are deposited on culture surfaces before neurones are plated has been shown to result in neurites being able to follow drawn patterns (Schmalenberg and Uhrich, 2005; Turcu *et al.*, 2003; Gustavsson *et al.*, 2007). Cells have been used as neurone culture substrates (e.g. fibroblasts and glial cells), and when neurones are then seeded on top of cell substrates, neurites follow patterns of these cell substrates (Fallon, 1985; Stępień *et al.*, 1999; Thompson and Buettner, 2006). These techniques can also be used in combination to produce improved neurite alignment; for instance the use of a combination of micropatterned grooves and chemical substrates (Zhang *et al.*, 2006). Further to this, the use of bioresorbable glass fibres (Bioglass®) in combination with glial cell substrates (with the ability to align in chains along glass fibres) have been used to promote aligned neurite growth (Bunting *et al.*, 2005).

However, some patterned surfaces would not be suitable for use in PDT as these surfaces would cause refraction of light beams and thereby limit energy application to treatment sites. Alternative techniques to the production of etched surfaces and aligned substrates include the development of stretch-grown neurite models which consist of dissociated DRG neurones seeded at the junction of 2 adjoining plates

which are regularly pulled further apart over time, resulting in neuronal cell bodies localised at the end of the plates with aligned neurites growing across plates (Pfister *et al.*, 2006). A 2D culture system would be the simplest approach for use in these experiments, as long as it can be made so that neuronal cell bodies remain in one place while neurites grow out away from the neuronal cell bodies.

3D culture systems are more complex to develop than 2D culture systems, but they may be more appropriate for some studies. The ability to organise cells in a 3D environment is an important component of tissue engineering (Bellamkonda *et al.*, 1995), which requires the use of scaffolds (Bellamkonda, 2006). Hydrogels have been particularly attractive scaffolds for use in 3D cell culture because they are highly porous with a hydrated structure in which cells can assemble into tissue architectures (O'Connor *et al.*, 2000).

3D tissue engineered peripheral nerve culture systems presently being used include but are not limited to the use of magnetically aligned collagen fibrils in 4 mm diameter rods forming nerve culture systems, which incorporate collagen gel, glial cells and chick embryo DRG tissue such that neurites grow following aligned collagen fibrils (Dubey *et al.*, 1999). Also a 3D cell-seeded tethered collagen culture system exists, which incorporates collagen gels, glial cells, fibroblasts, and DRG tissue and contraction within the tethered collagen gel causes alignment of glial cells and neurite growth (Eastwood *et al.*, 1994; Eastwood *et al.*, 1998; Dubuisson *et al.*, 1999; Phillips *et al.*, 2005). In comparison to *ex vivo* nerve models, these types of tissue engineered culture systems would provide more controlled environments in which to perform focally applied *m*-THPC-mediated PDT experiments.

For this study, Type-I collagen was chosen as a suitable 3D substrate, because it is a natural polymer that is amenable to use in culture systems and is the major ECM component of peripheral nerves. Collagen hydrogels have relatively large pore sizes of ≤ 2 μm, they can support cell attachment, and the gelation process is simple; therefore it is extensively used in cell transplantation and tissue engineering applications (O'Connor *et al.*, 2000). Collagen gels provide a reconstituted network of highly entangled collagen fibrils of 50-500 nm in diameter, which is 99-99.9 % interstitial liquid, dependent on collagen source and reconstitution method (Dubey *et al.*, 1999). Type I collagen is found in the form of fibrils with diameters of about 30 to 300 nm, and is the major structural component of skin, tendon, bone and other connective tissues (Williams *et al.*, 1978).

In this study 3D tethered cell-seeded collagen gels (Eastwood *et al.*, 1994; Eastwood *et al.*, 1998; Phillips *et al.*, 2005) were used in the development of a more advanced peripheral nerve culture system than the thin 3D cell-seeded culture system used in previous chapters. Cells within collagen gels are known to form stable integrin-mediated attachments with collagen fibrils. This is known to trigger cytoskeletal assembly, cell movement and subsequent force generation, which results in the contraction of collagen gels. When collagen gels are tethered at opposite ends of rectangular gels, forces generate a uniaxial strain on the gel along which cells and collagen fibrils become aligned (Eastwood *et al.*, 1994; Eastwood *et al.*, 1998). However, Schwann cells entrapped in collagen gels will revert to their undifferentiated phenotype with features of spherical morphology, delayed spreading, long-axis alignment response and no NGF production (Rosner *et al.*, 2005; East & Phillips 2008).

This study adapted and developed both a 2D glial cell substrate nerve culture system and a 3D cell-seeded tethered aligned collagen system for use in evaluating the effects of targeted *m*-THPC-mediated PDT to DRG neurones.

5.2 Aims and desired properties

The aim of the study presented in this final results chapter was to simulate nerve PDT wounding in *ex vivo* nerve tissue and advanced cell culture models to assess the effects of PDT directed towards distinct parts of neurones. The key properties desired for such a nerve model to be used in focally applied PDT are:

i) To be reproducible and able to be kept under controlled environments.

ii) To contain relevant nerve cells as found in endogenous nerve tissue

iii) To support robust neurite growth, away from the neuronal cell body.

iv) To maintain cell viability throughout the treatment period

v) To enable specific application of focal PDT to different parts of the neurone (cell body and/or different distances along neurites) and subsequent detection of damage.

5.3 Results

5.3.1 Effects of focally applied *m*-THPC-mediated PDT on dissected nerves

In this study *m*-THPC-mediated PDT was applied to dissected nerve tissues, which were then maintained in culture for 2 days before assessing for *m*-THPC uptake and signs of PDT damage. The dissected sciatic nerve tissue complete

with DRGs was similar to that used by Tonge *et al.* (1997). Rats were injected with 0.3 mg/kg *m*-THPC, similar to Coutier *et al.* (2002) who had used this concentration to assess *m*-THPC-mediated PDT on HT29 xenografted nude mice; and Obwegeser *et al.* (1998) who used ^{14}C- labelled-*m*-THPC in C6 rat glioma brain tumour models for uptake and retention studies.

Figure 5.1A shows an illustration of the application of focally applied *m*-THPC-mediated PDT to the nerve trunk of a rat sciatic nerve dissected 24 h after pre-injecting with *m*-THPC (*m*-THPC administered *in vivo*), to a concentration of 0.3 mg/kg or vehicle injection. These nerves were collected as a by-product of another experiment and so the drug dose administered was based on the requirements of the intended study. Crucially, no detectable *m*-THPC red drug fluorescence was detected in nerve tissue under any of the treatment conditions used in this assay (Figure 5.2). There was no obvious tissue degradation in any of the assessed nerve tissue. Also, the 652 nm laser light treatment did not elicit morphological changes in the nerve tissue on its own, nor in combination with intravenous (i.v.) injection of *m*-THPC photosensitiser. These experiments were performed once for treatment parameter 10 J/cm^2 of 652 nm focal laser light only, and 0.3 mg/kg *m*-THPC i.v. injection only, while *m*-THPC-mediated PDT wounded region (~5.0 mm diameter spot), two sciatic nerves from different rats were tested.

An alternative approach to using nerve explants from animals that had been injected with *m*-THPC, was to incubate isolated nerve preparations with *m*-THPC in culture. Figure 5.1B shows focal *m*-THPC-mediated PDT being applied to a nerve explant in a sterile environment using light from a laser directed along an optical fibre light guide. *m*-THPC fluorescence was only detected up to 2.1 mm from the distal cut end of nerve explants, which had been removed from the rat

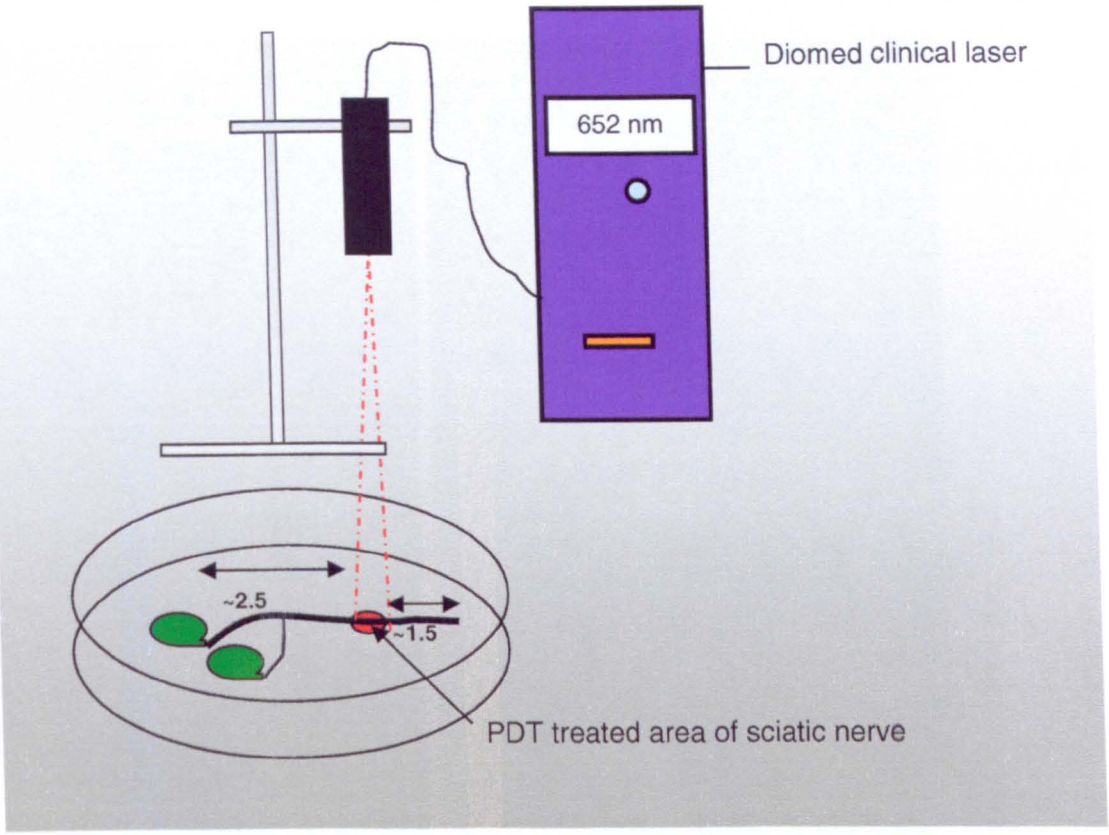

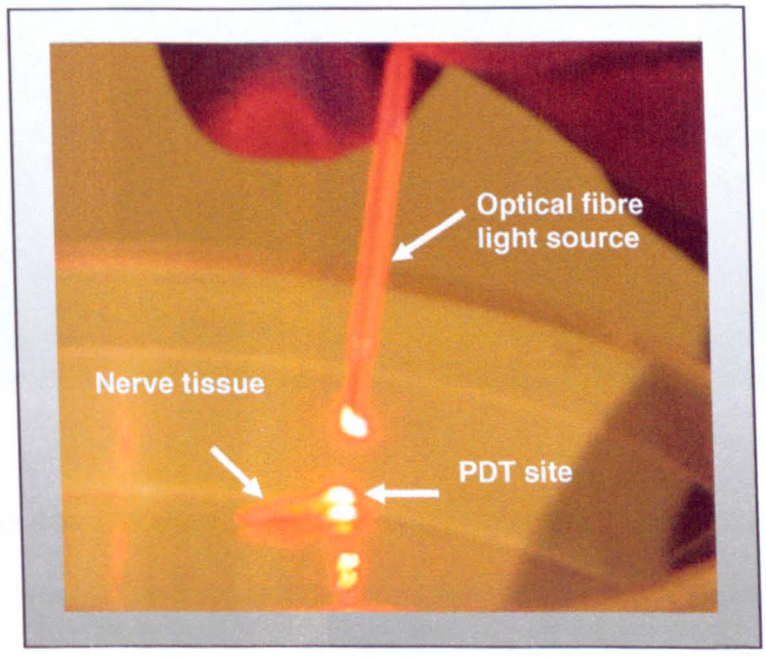

Figure 5.1
Illustration and image of dissected sciatic nerve being exposed to focally applied *m*-THPC-mediated PDT.
Light was delivered using a fibre optic lead under subdued lighting. (**A**) An ~5 mm diameter PDT treatment area (red) was created ~2.5 cm from the DRGs (green) using 652 nm for *in vivo* administered *m*-THPC experiments, and (**B**) 633 nm beam applied to dissected nerve incubated in *m*-THPC for *in vitro* experiments.

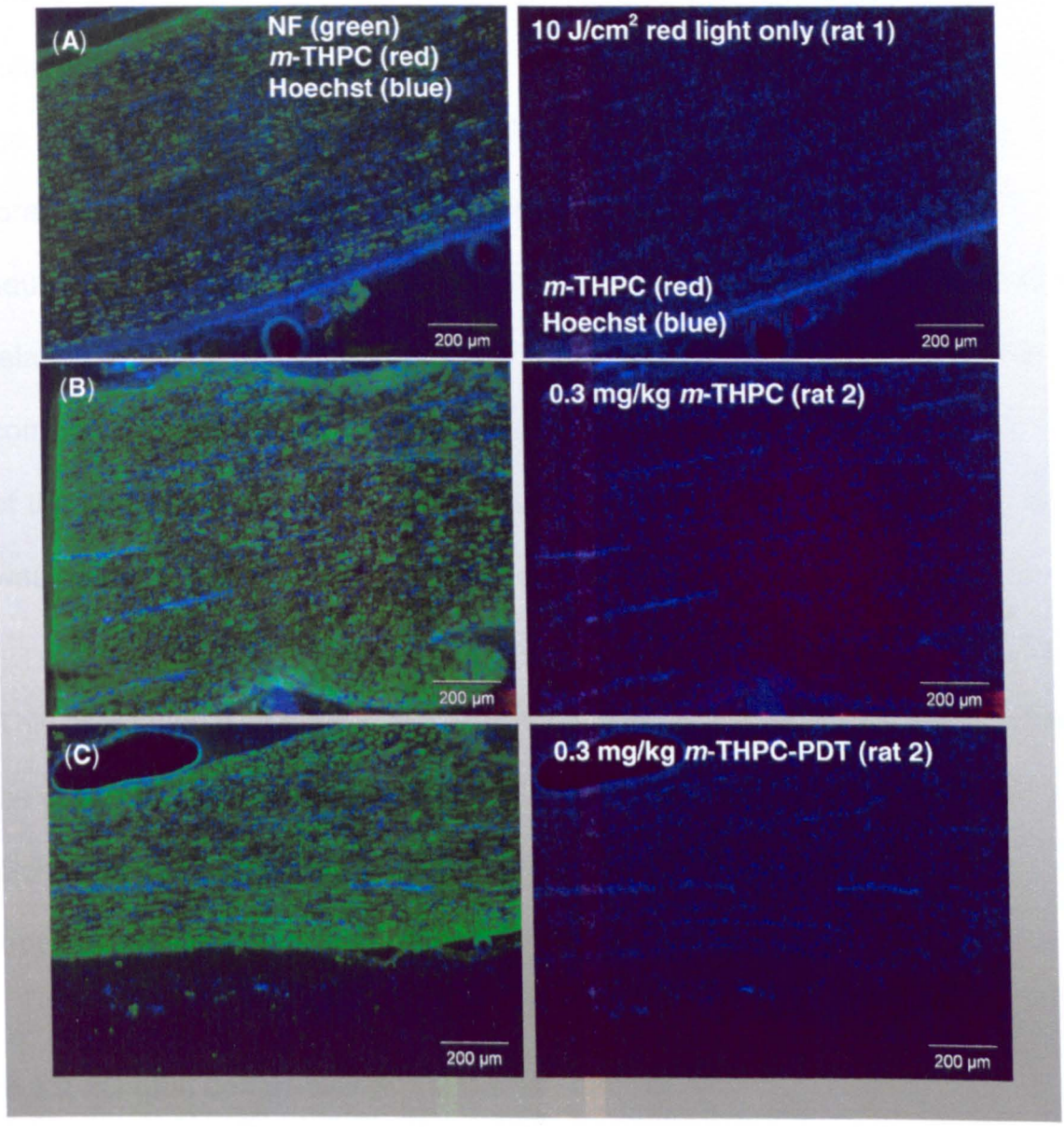

Figure 5.2
Sciatic nerve explants used to assess focal PDT wounding of nerve tissue 24 h after treatment.
Micrographs are of representative fixed cryosections from segments of sciatic nerves ~2.5 cm from the DRG and ~1.5 cm from the distal cut end. (**A**) 10 J/cm^2 of 652 nm focal laser light only, one nerve was tested; (**B**) 0.3 mg/kg *m*-THPC i.v. injection only, one nerve was tested; and (**C**) *m*-THPC-mediated PDT wounded region (~5.0 mm diameter spot made), two nerves were tested. No *m*-THPC fluorescence was detected in nerve tissue under these experimental conditions, and no obvious nerve tissue damage was detected. Neurofilament (NF) immunostained neurites (green), Hoechst 33258 stained nuclei (blue) and fluorescence of *m*-THPC photosensitiser (red).

then incubated for 24 h in 4 µg/ml *m*-THPC (Figure 5.3). This 24 h incubation time was a longer incubation time in comparison to the 4 h used for dissociated cell culture experiments. No *m*-THPC red fluorescence was detected in the DRG or the proximal part of the incubated explants. *m*-THPC fluorescence co-localised (orange) with S-100 positive glial cells (Figure 5.3A), but not with NF positive neurones (Figure 5.3C). Also, no obvious tissue degradation was observed in relation to focal *m*-THPC-mediated PDT treatment. Figures 5.3B and C are composite images of the uptake of *m*-THPC and Hoechst 33258 staining. Because of the lack of consistent *m*-THPC uptake into these nerve explants, this approach was deemed inappropriate for studying focal PDT

This pilot study was conducted to assess whether damage in nerve explants could be quantified by immunolabelling for NF (to reveal neurite loss) or S100 (to reveal Schwann cell loss). This proved to be a promising approach; however it was not applied because the use of nerve explants was discontinued.

5.3.2 2D glial cell substrate nerve culture system

A number of monolayer culture approaches were tested in order to establish a nerve culture system in which neuronal cell bodies are retained at DRG seeding sites and neurites grow away from these neuronal cell bodies. Simply seeding dissociated DRG neurones and satellite cells onto PLL and /or laminin coated or patterned cover glasses, resulted in neuronal cell bodies migrating with satellite cells away from the site of seeding. Neurites were also found to grow mainly around the neuronal cell body itself as illustrated in Figure 5.4A. A solution to this problem is shown in Figure 5.4B which illustrates a glial cell substrate nerve

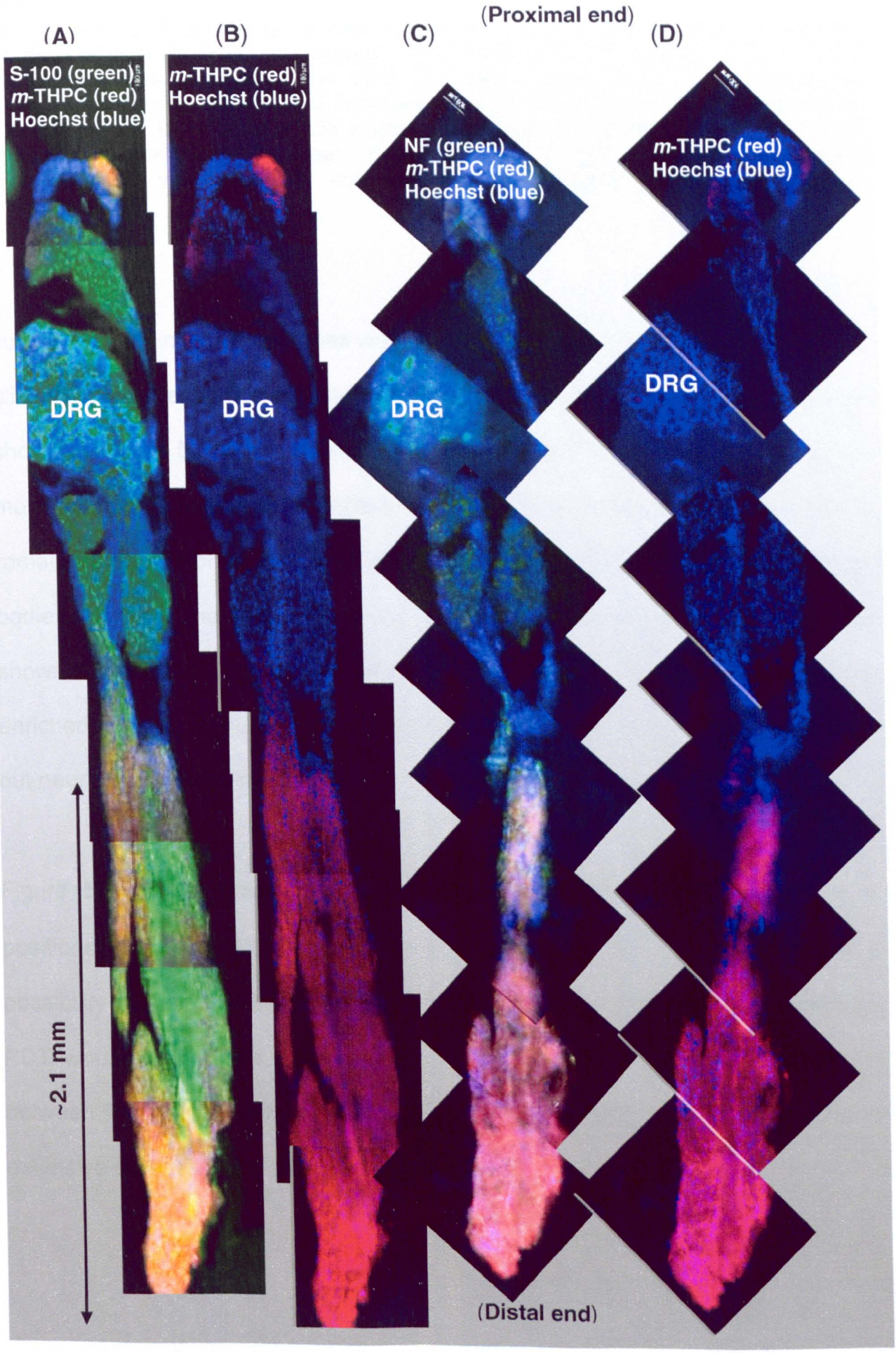
(A)
(B)
(C)
(D)
(Proximal end)
S-100 (green)
m-THPC (red)
Hoechst (blue)
m-THPC (red)
Hoechst (blue)
NF (green)
m-THPC (red)
Hoechst (blue)
m-THPC (red)
Hoechst (blue)
DRG
DRG
DRG
DRG
~2.1 mm
(Distal end)

Figure 5.3

Micrograph montage of *m*-THPC uptake into nerve explant after 24 h incubation in solution.
Micrographs are of representative fixed cryosections from a dissected DRG with attached distal nerve trunk. *m*-THPC was present in the distal parts of the nerve but no *m*-THPC fluorescence was detected in the DRG or proximal parts of the nerve. Composite micrographs showing (**A**) *m*-THPC fluorescence (red) and glial cells labelled with anti-S-100 (green); (**B**, **D**) Hoechst 33258 stained (nuclei); (**C**) neurones labelled with anti-NF (green). Co-localisation (orange) between *m*-THPC fluorescence and S-100 immunostaining was observed, but not between *m*-THPC fluorescence and NF immunostaining.

culture system, in which neurones were seeded on top of a confluent monolayer of glial cells. Neurites in this culture system grew away from neuronal cell bodies as shown in Figure 5.5 which shows dissociated DRG neurones growing on top of monolayers of Schwann cell/fibroblast cultures. Neuronal cell bodies were found to remain at the site of seeding and neurites extended away from the neuronal cell bodies. However, neurites were found to grow in an uneven manner. Figure 5.6 shows dissociated DRG neurones growing on top of monolayer satellite cell-enriched cultures. Here neuronal cell bodies also remained at the seeding sites, but neurites extended in a more even manner.

Figure 5.7 shows attempts at creating focal PDT wounds (between B or C positions of figure 5.6), in these monolayer nerve culture systems. There is a possibility of detecting both 4 µg/ml *m*-THPC- and 1.6 µg/ml hypericin-mediated PDT wounds using the PI exclusion assay. Figure 5.7B shows the difference between PDT treated and non-PDT treated regions. Both PDT treatments showed extensive cell loss at the treatment sites.

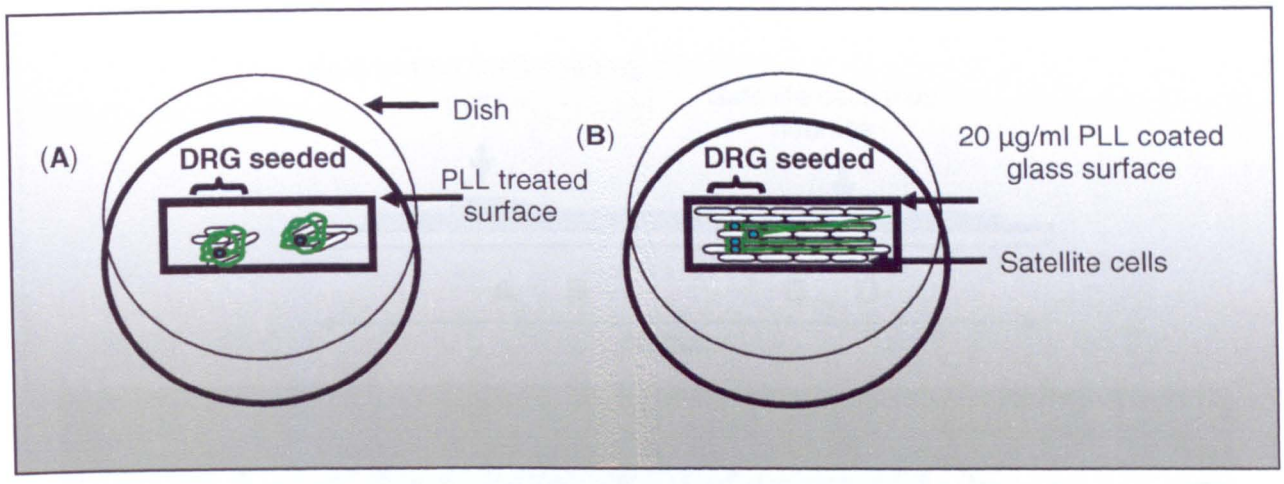

Figure 5.4
Illustration comparing two culture systems.
(**A**) Without glial cell monolayer (substrate) and (**B**) with glial cell substrate.

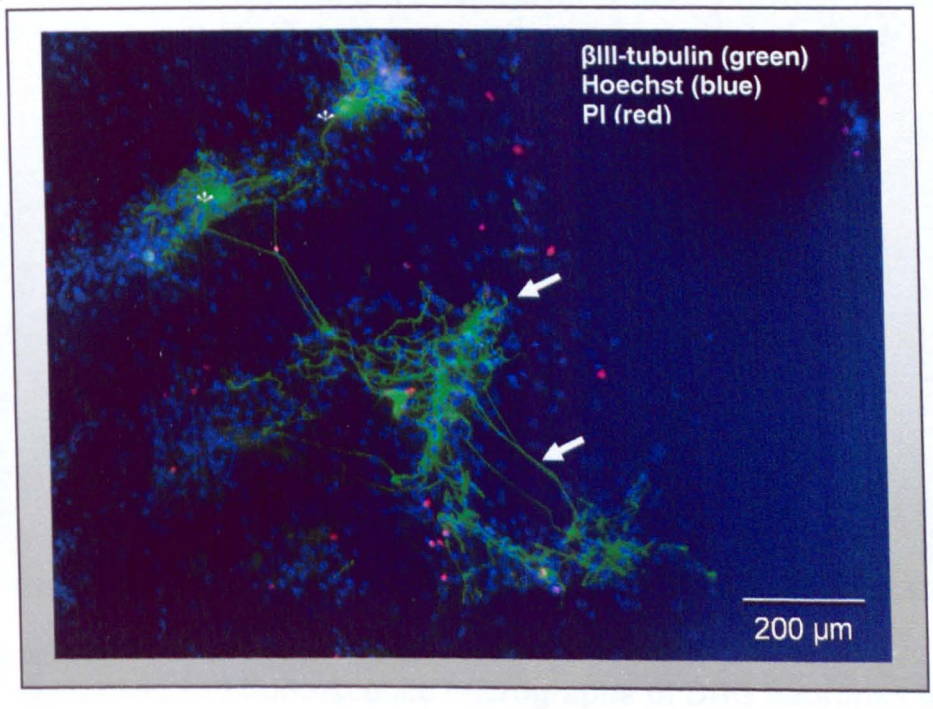

Figure 5.5
Fluorescence micrograph of DRG neurones growing on Schwann cell /fibroblast culture monolayer.
Shows uneven neurite growth on Schwann cell/fibroblast substrate in monolayer cultures after 7 days. Cells were PI stained then fixed and immunostained with βIII-tubulin. βIII-tubulin labelled neurones (green), PI stained dead cell nuclei (red) and Hoechst 33258 stained nuclei (blue). (Arrows indicate neurite growth and (*) indicate neuronal cell bodies)

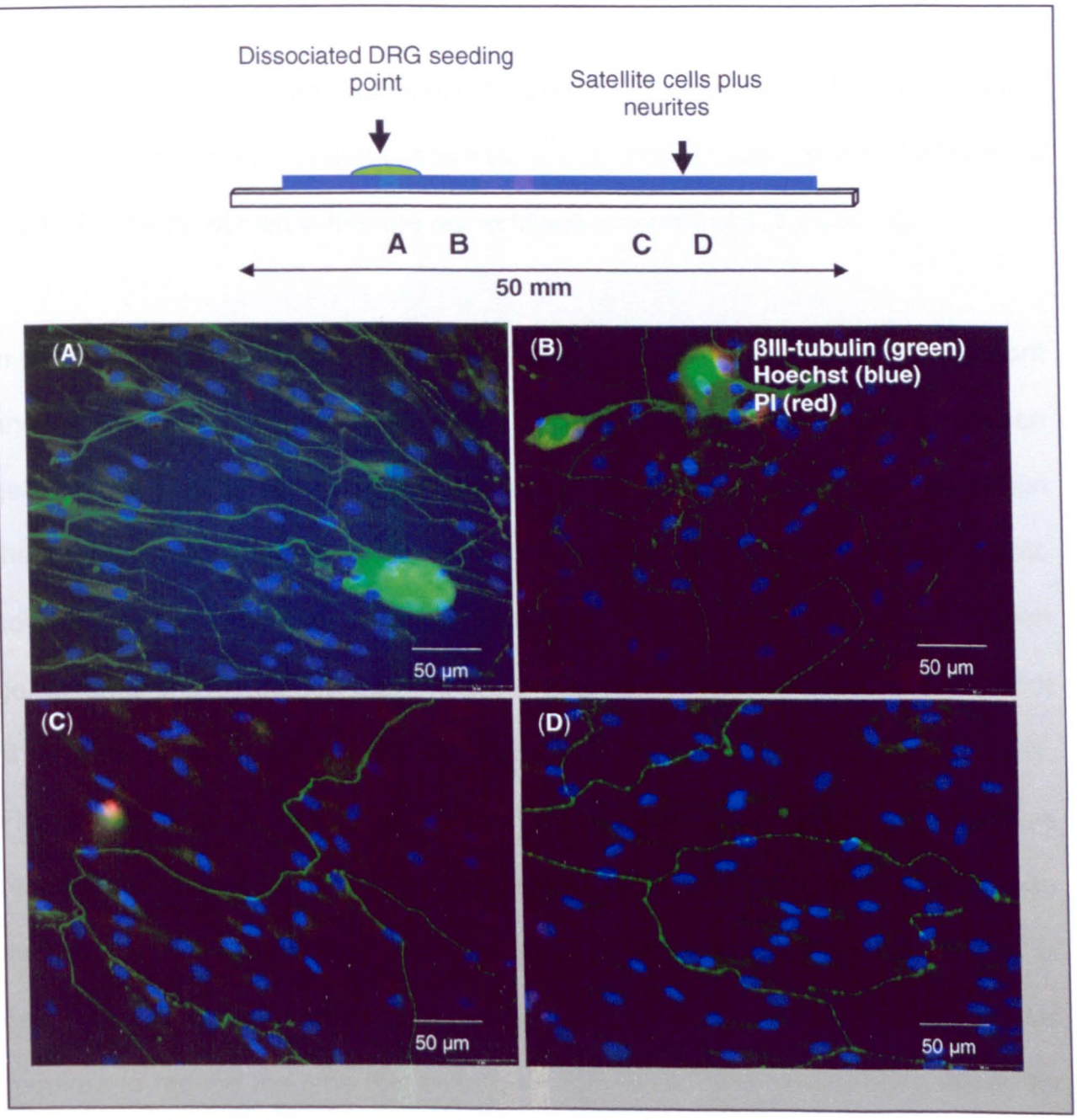

Figure 5.6
An Illustration and fluorescence micrographs of DRG neurones growing on satellite cell culture substrate in monolayer.
Neurites grew evenly across satellite cells in monolayer cultures away from neuronal cell bodies after 7 days in culture. Cells were PI stained then fixed and immunostained with βIII-tubulin. Illustration indicates approximate positioning of micrograph images shown. βIII-tubulin labelled neurones (green), PI stained dead cell nuclei (red) and Hoechst 33258 stained nuclei (blue).

5.3.3 3D collagen tissue engineered peripheral nerve culture system

Initial experiments showed that when DRG explants were cultured in the collagen gels, neurite outgrowth tended not to extend out of the tissue into the surrounding matrix, but rather stayed within the nerve tissue environment (Figure 5.8).

In order to provide guidance cues to encourage neuronal growth out of the explant and into the surrounding collagen matrix, an approach was used in which collagen gels can be seeded with Schwann cells and fibroblasts which contract and align the collagen. Co-cultures of glial cells and nerve fibroblasts were seeded into collagen gels at various densities and assessed for their ability to cause collagen gel contraction. Figure 5.9A shows the ability to distinguish Schwann cells from fibroblasts in monolayer culture samples by their bright S-100 immunoreactivity. Figure 5.9B shows that the use of 300 000 cells/ml of collagen or above was required to cause gel contraction within 24 to 48 h of preparation. This was denoted by smaller gel sizes (cross-sectional areas calculated from the radius of each gel) at corresponding time points. This relatively quick contraction was required to reduce the time this culture system would take before being ready for use.

Using 3D tethered collagen nerve culture systems (Figure 5.10), the extent of collagen gel contraction was assessed in relation to the ratio of Schwann cells to fibroblasts (Table 5.1). These results indicated that gel contraction was independent of percentage fibroblast content since Schwann cell to fibroblast ratio was found to vary greatly across culture preparations, and ranged from 14 % to 89 % Schwann cell (S-100 positive) content. This large variation maybe attributed to cell cultures being preparation from different rat sciatic nerves. Table 5.1 also

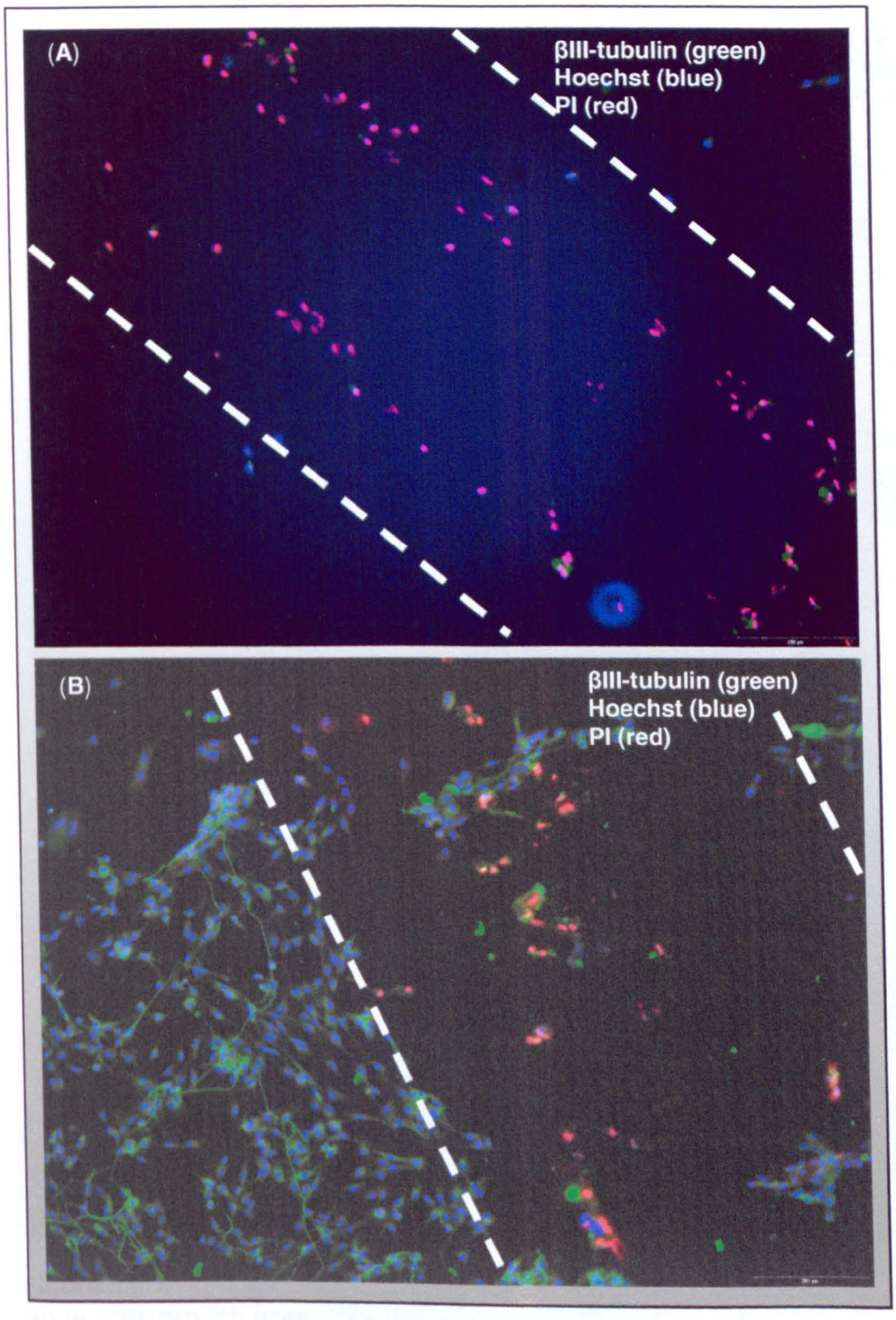

Figure 5.7
PDT wounding in monolayer nerve culture systems.
(**A**) Wound made by focally applied *m*-THPC-mediated PDT and (**B**) wound made by focally applied hypericin-mediated PDT. βIII-tubulin labelled neurones (green), PI stained dead cell (red) and Hoechst 33258 stained nuclei (blue).

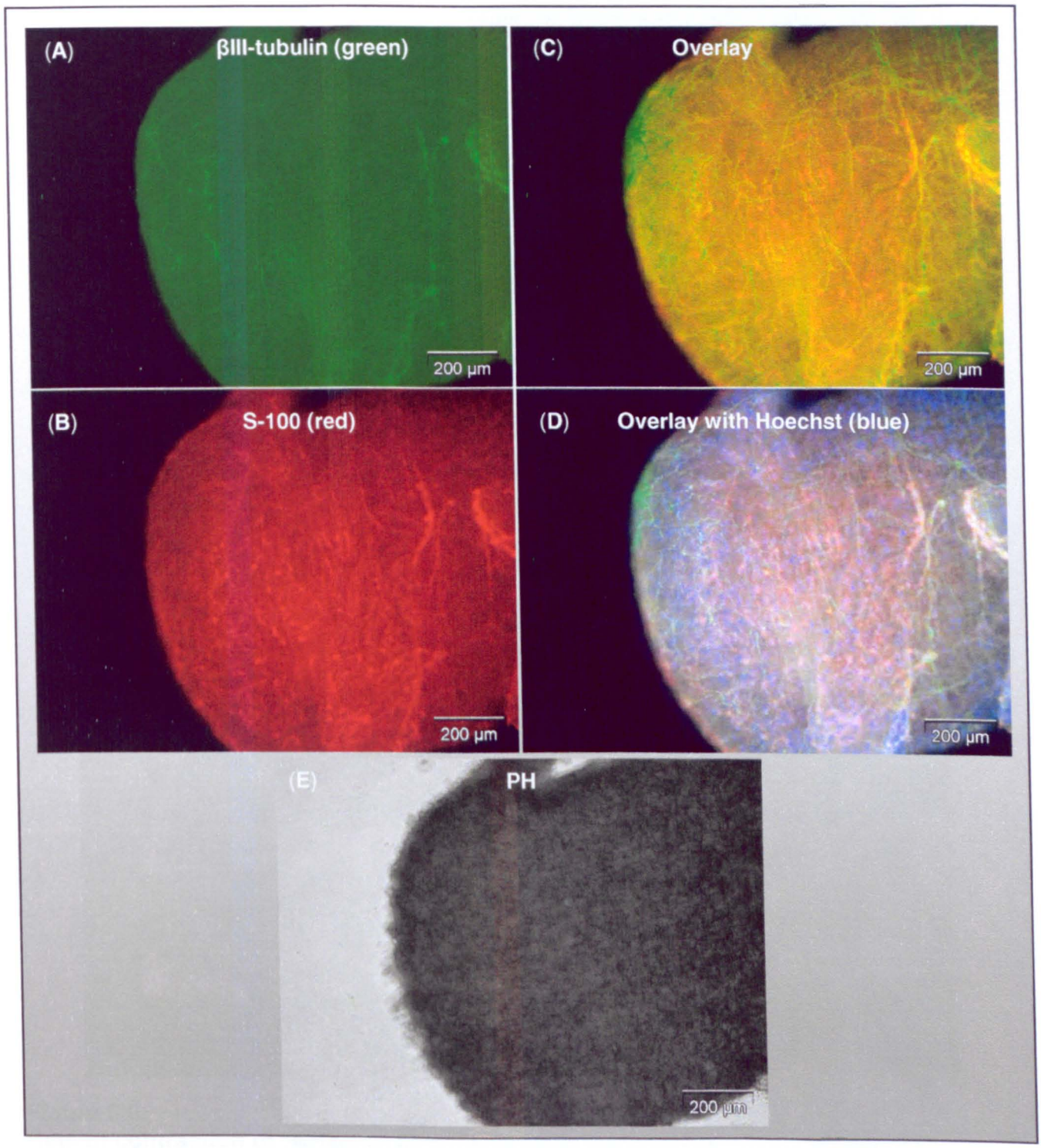

Figure 5.8
No neurite growth from DRG explant into collagen gel matrix.
Micrographs are of whole tissue pieces encased in collagen gel matrix, fixed and immunostained. (**A**) βIII-tubulin immunostained neirites (green), (**B**) S-100 immunostained Schwann cells (red), (**C**) Overlay micrograph of neurones and Schwann cells, with Hoechst 33258 stained nuclei (blue) (**D**). PH micrograph of nerve tissue (**E**). No immunostained structures were detected in the collagen gel matrix outside the nerve tissue.

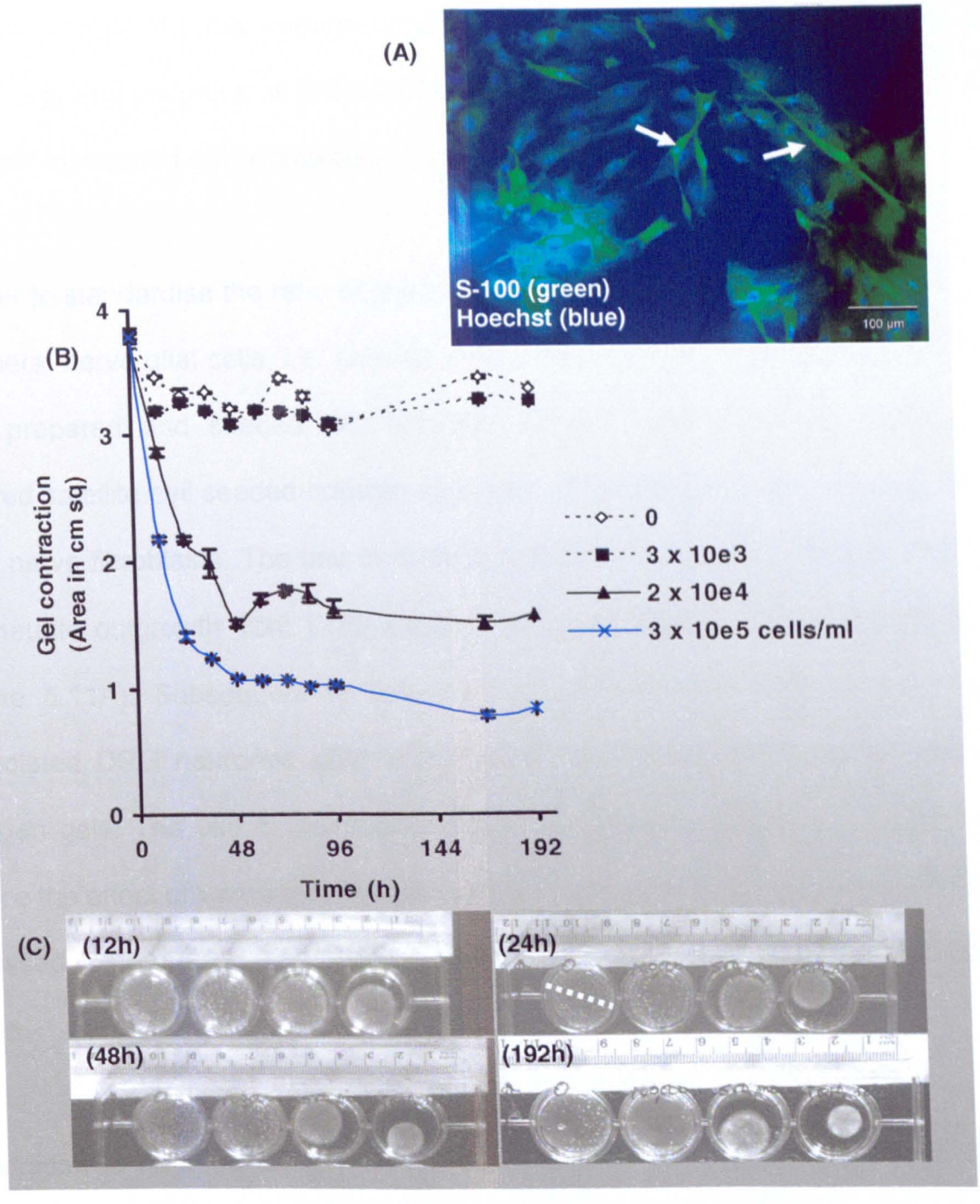

Figure 5.9
Rate of contraction of Schwann cell/ fibroblast seeded untethered collagen gels.
Graph shows the rate of collagen gel contraction as measured from a reduction in area of gels containing zero; 3 x 10^3; 2 x 10^4 and 3 x 10^5 Schwann cells/fibroblasts. (**A**) Shows sciatic nerve culture immunostained with anti-S-100 to distinguish Schwann cells from fibroblasts, and Hoechst nuclei. (**B**) Graph of gel contraction over time at various cell seeding densities and (**C**) Photographs of contracting gels at different time points. Data are presented as mean ± SEM of 3 separate gels per cell seeding density. Images show respective gel contraction over time. (Arrows indicate S-100 positive Schwann cells and broken line indicates diameter measurement taken per gel over time for use in calculating gel contraction rate).

shows that a seeding density of approximately 1 million cells and above per 2.5 ml collagen gel mix (400 000 cells/ml) would result in gel contraction within 24 to 48 h. This supports the previous finding that 300 000 cells/ml and above (Figure 5.9B) will result in required gel contraction.

In order to standardise the ratio of glial cells to fibroblasts, an alternative source of peripheral nerve glial cells, i.e. satellite cells (~100% S-100 positive) from DRGs, were prepared and seeded into tethered collagen gels. However, these 3D tethered satellite cell seeded-collagen gels did not contract without the inclusion of ~5 % nerve fibroblasts. The use of satellite cell-enriched cultures yielded glial cell and neurite outgrowth from DRG explants embedded within the contracted gels (Figure 5.11A). Subsequent to this, Figure 5.11B shows neurite growth from dissociated DRG neurones after implantation into satellite cell-seeded tethered collagen gels. The use of dissociated DRG neurones was preferred as it would reduce the effect of variability between explants, and enable neurone viability to be assessed in future studies, features not provided with the use of whole DRG tissue.

In addition to neurites being extended in this nerve culture system, Figure 5.12 shows that satellite cells were able to myelinate DRG neurites during extended periods in culture.

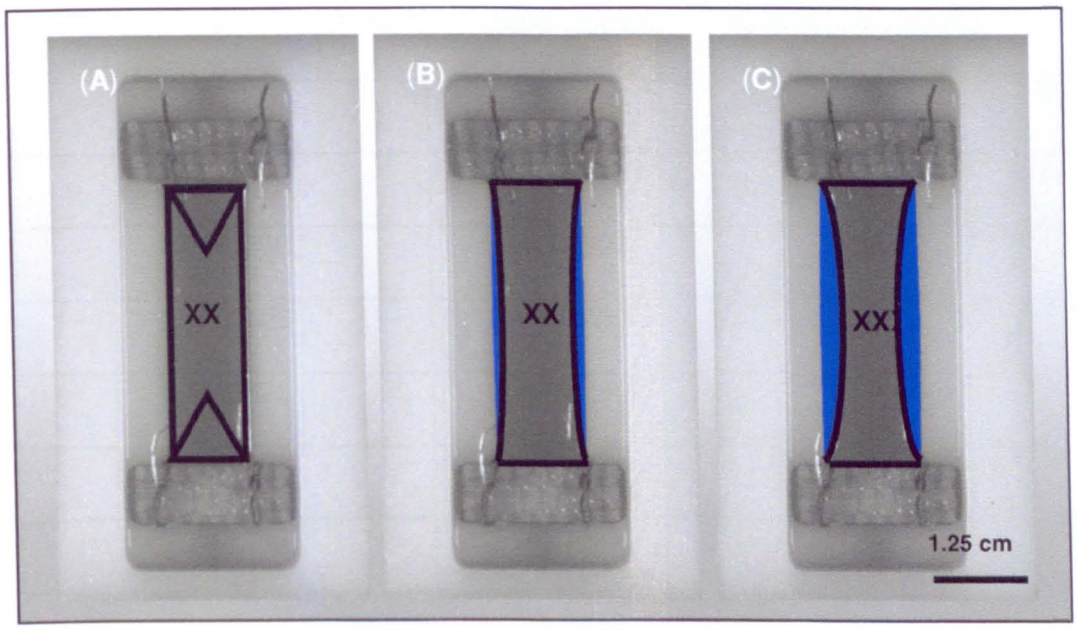

Figure 5.10
Schwann cell/fibroblast-seeded tethered collagen nerve culture system.
Schwann cell/fibroblast seeded collagen gels were allowed to set and contract as shown. (**A**) Tethered gel in mould shows site of DRG implantation and location of triangular stress shielded regions (delta zones). (**B**) Schematic of gel contraction after 12 h and (**C**) after 24 h are illustrated. Tethered rectangular 3D gel contractions are listed in table 5.1 with cell densities greater than 400 000 cells/ml required for gel contraction within 24 h.

Total cell count in 2.5 ml	Cells per ml	% Schwann cells	Effect
296,250	118,500	26	No contraction
448,750	179,500	34	No contraction
1,016,250	406,500	19	Contraction
1,103,125	441,250	14	Contraction
1,185,625	474,250	21	Contraction
1,564,375	625,750	49	Contraction
1,783,750	713,500	89	Contraction

Table 5.1
Collagen gel contraction scored at 24 h using a range of seeding densities and proportions of Schwann cells.
Cell seeding density rather than ratio of Schwann cell to fibroblast content is shown to determine collagen gel contraction in tethered collagen gels. Percentage Schwann cells were obtained for 3 random fields of n=3 cover-glasses form 7 different cultures. Total cell counts are expressed in 2.5 ml based on the volume of collagen gels used per nylon mould, and also in cells per ml of collagen gel mixture.

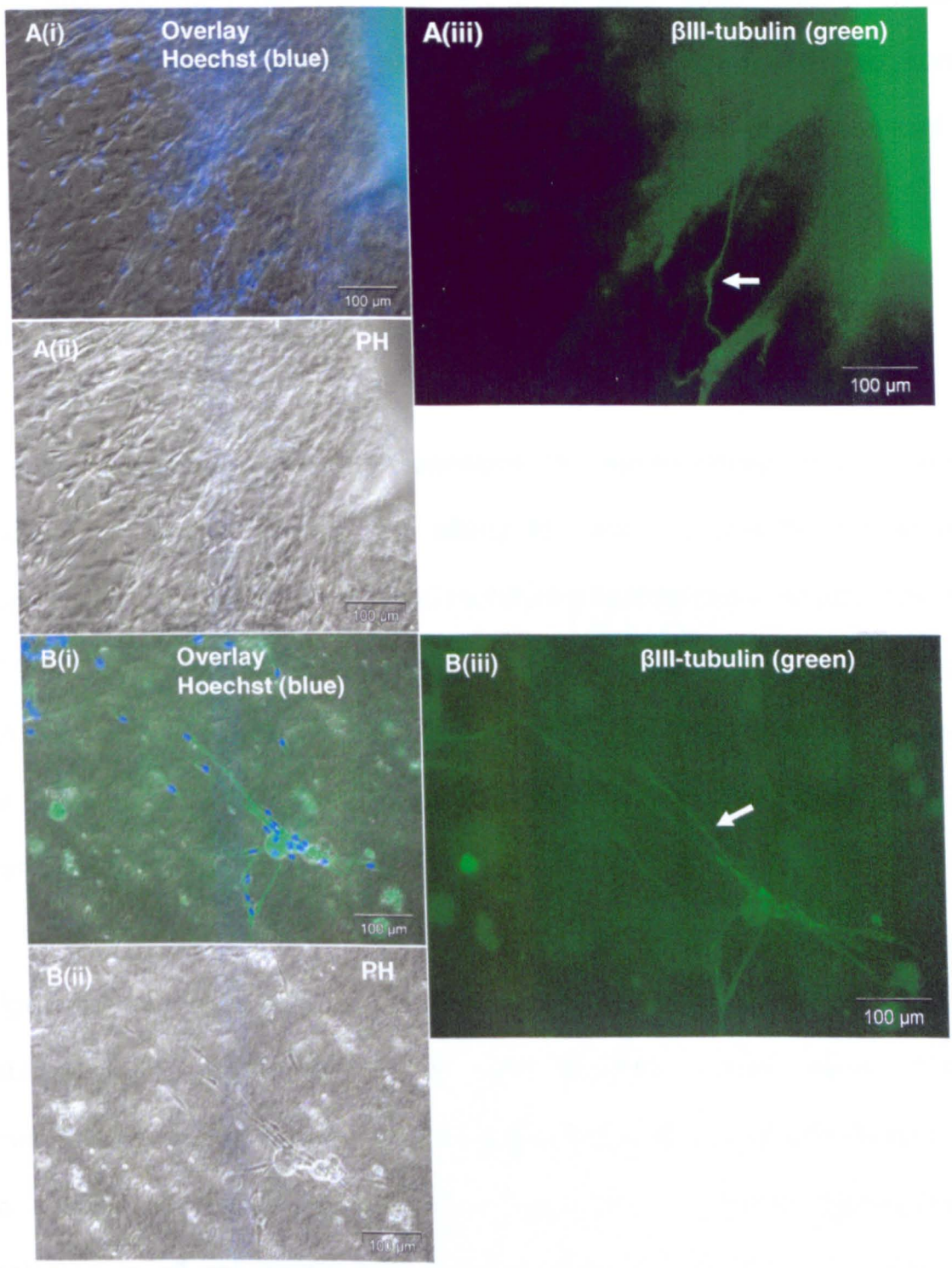

Figure 5.11
3D tethered collagen gels seeded with satellite cell cultures support neurite outgrowth.
Micrographs are of fixed and βIII-tubulin immunostained cells in collagen gels. **A(iii)** shows βIII-tubulin immunostained neurite growth (green) from implanted DRG tissue into gel; and **B(iii)** shows neurite growth from a neuronal cell body into gel. Cells were also stained with Hoechst 33258 nuclei stain (blue). (Arrows indicate neurite growth after ~10 days in culture).

Figure 5.13 shows a pilot study of *m*-THPC-mediated PDT wounding of a satellite cell-seeded collagen gel with the aid of a fibre optic lead. Fluorescence micrographs show a localised wound marked with dead cell (red nuclei PI staining). Non-nuclei red staining is as a result of *m*-THPC being localised in the cell cytoplasm.

5.3.4 Live neurite growth tracking

Having established appropriate conditions for neurite growth in the aligned 3D collagen gel culture system, the ability to track the growth of neurites was investigated. This would be a useful monitoring feature which would allow light for PDT to be targeted to specific segments of neurites as they extended through the gel. A number of fluorescent cell tracker (CellTrk) dyes are commercially available for use in labelling and fluorescently tracking live cells. One such CellTrk tested was CellTrk-red.

Figure 5.14 shows a dissociated DRG culture in monolayer. DRG neurones were labelled with CellTrk-red while the neurones were alive. βIII-tubulin immunostaining and Hoechst 33258 staining were performed after fixation in order to assess co-localisation (orange) of markers. CellTrk-red fluorescence was detected in all cell types, but was not clearly detectable in neurites of DRG neurones.

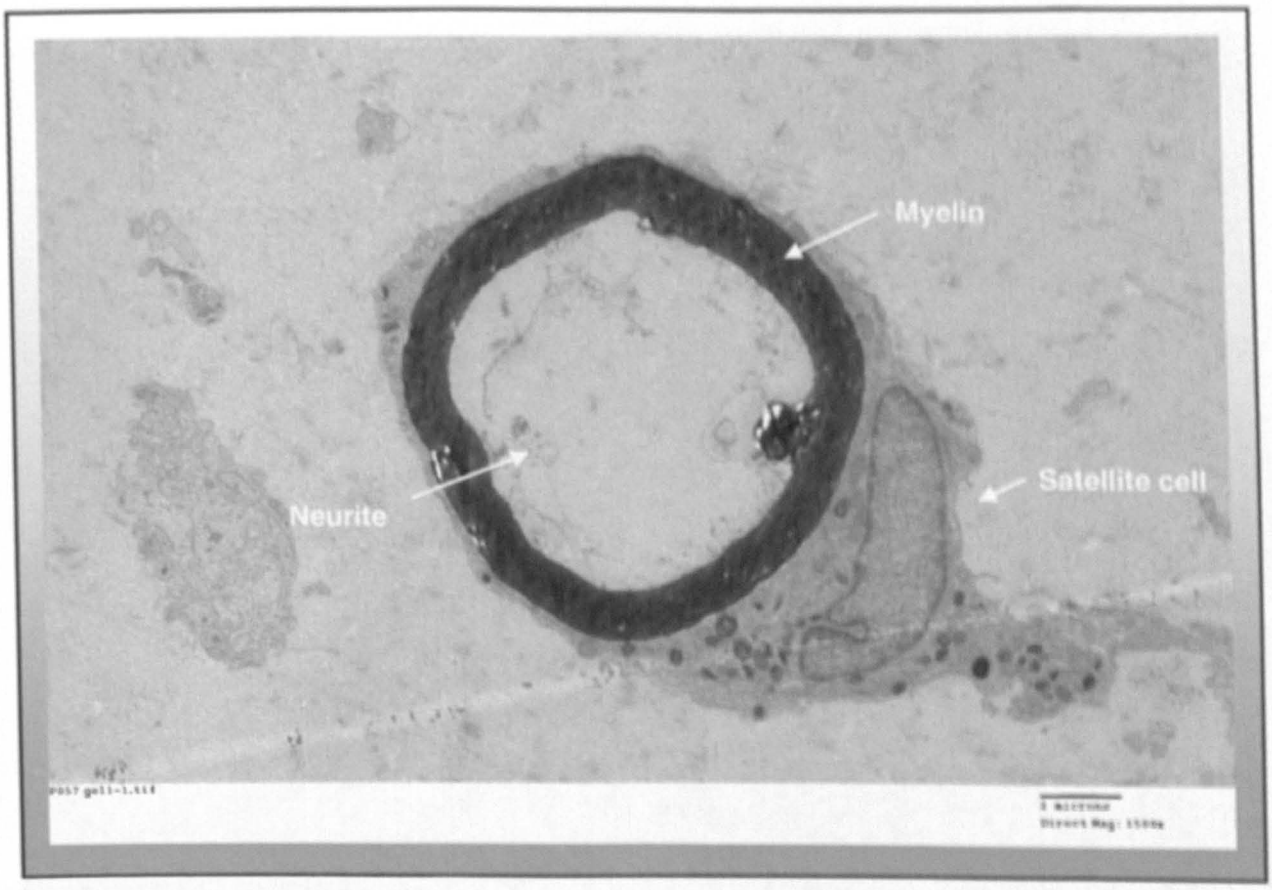

Figure 5.12
A satellite cell myelinating a neurite in a 3D collagen gel culture system.
Tethered aligned collagen gels seeded with satellite cells, 5% fibroblasts, and dissociated DRG neurones were maintained in culture for 12 days then processed for transmission electron microscopy (this image was provided by Dr James Phillips and illustrates an important feature of the culture system, however the electron microscopy was not part of this project so the methodology is not described here).

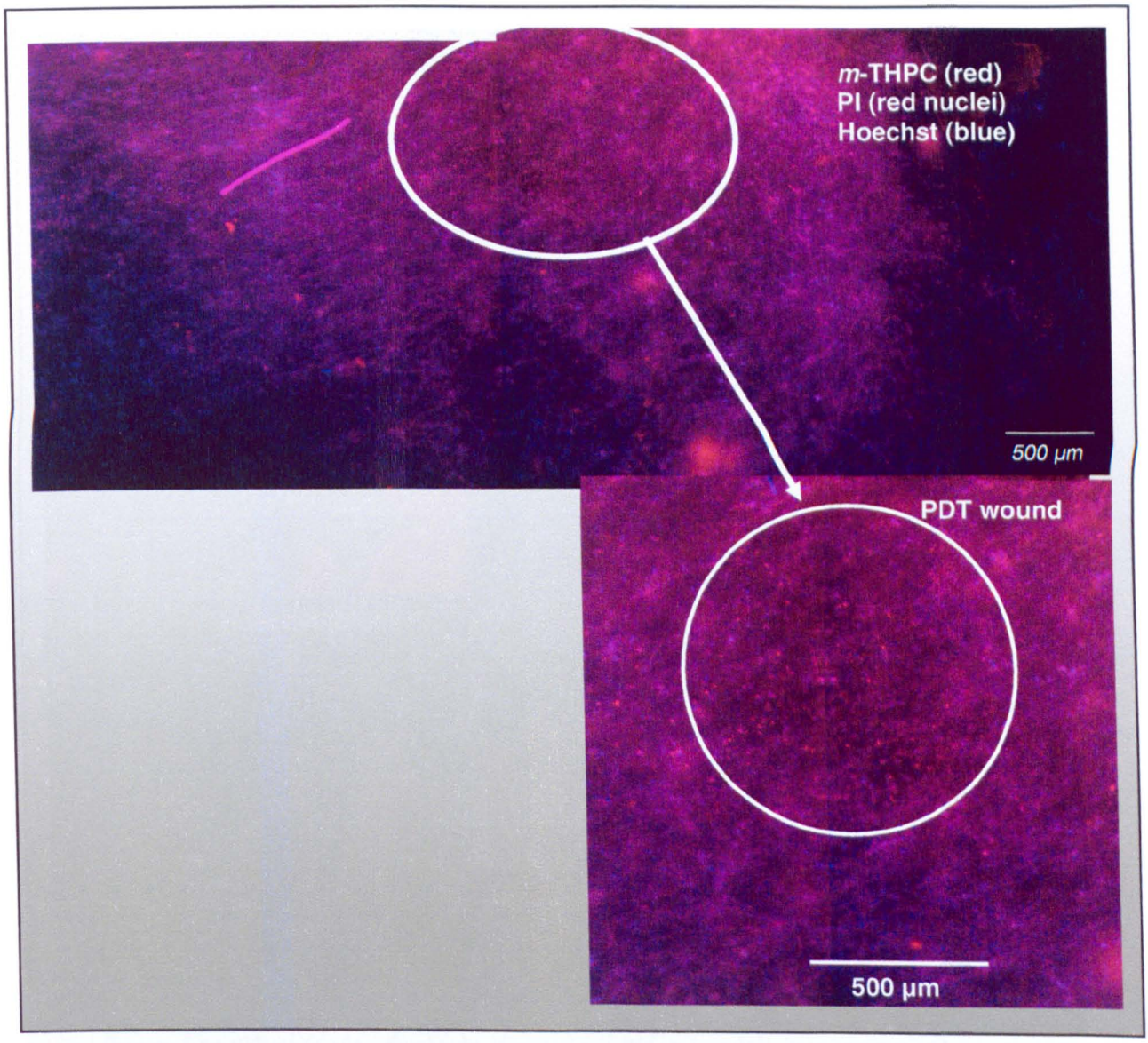

Figure 5.13
***m*-THPC-mediated PDT wounding of a satellite cell-seeded tethered 3D collagen gel.** Fluorescent micrograph shows a section of a satellite cell seeded collagen gel culture stained for dead cells with PI nuclei stain (red), fixed and then Hoechst 33258 nuclei stained (blue), 24 h after exposure to focally applied 4 µg/ml *m*-THPC-mediated PDT using 1 J/cm^2 of 633 nm red laser beam. (Note that non-nucleic red staining is associated with *m*-THPC being localised in the cell cytoplasm)

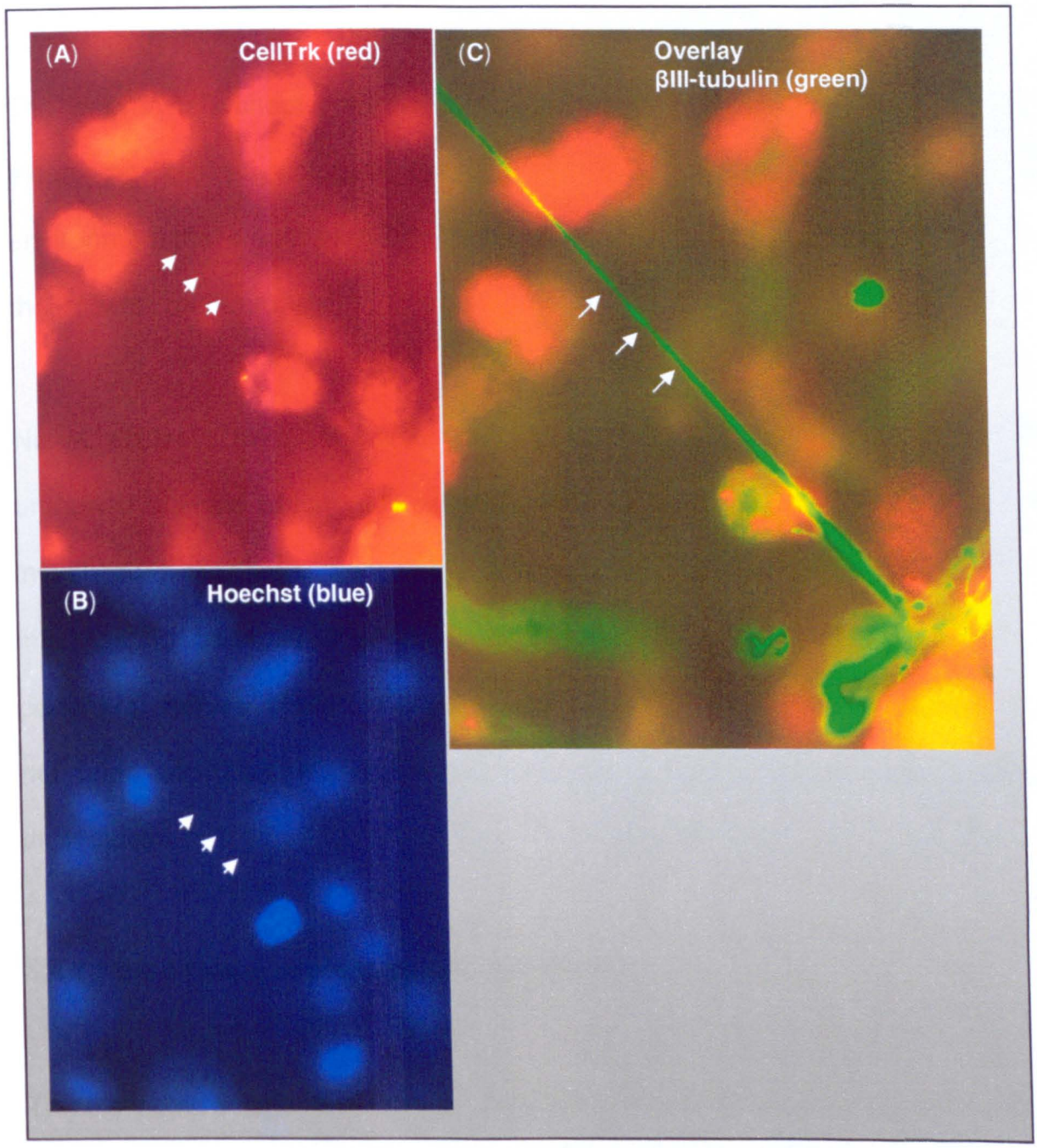

Figure 5.14
CellTrk-red did not label neurites of unfixed neurones sufficiently for tracking.
CellTrk-red labelled glial cells and neuronal cell bodies (red), but was not clearly detected in neurites after fixing and immunostaining with βIII-tubulin for neurones and their associated neurites (green), and Hoechst 33258 nuclei stain (blue). (Arrows indicated position of neurite)

5.4 Discussion

The work in this chapter was aimed at developing a suitable culture system to mimic the key physiological features of peripheral nerves in a controllable environment that would permit focal PDT treatments and subsequent monitoring of their effects on neurones.

Nerve explants from rats after i.v. injection with *m*-THPC, or explants from untreated animals which were subsequently incubated in *m*-THPC solution were investigated. Explants were initially considered to be useful models for this investigation because they possessed the natural tissue architecture of the peripheral nerves along with the appropriate arrangement and proportions of neurones and glial cells which had not been subjected to disruptive enzymatic dissociation.

5.4.1 Nerve tissue explant culture systems

The dissected sciatic nerve tissue complete with DRGs was similar to that used by Tonge *et al.* (1997), and 0.3 mg/kg *m*-THPC tested was similar to Coutier *et al.* (2002) and Obwegeser *et al.* (1998). It is important to note that the *m*-THPC dose administered to rats was lower than the 4 µg/ml dose used for the cell culture studies. This inconsistency was beyond our control, because these nerve tissues were sourced from animals in someone else's experiment. No detectable *m*-THPC fluorescence was observed in cryosections of sciatic nerve from these animals (Figure 5.2), however, tissue biopsies (blood, muscle, skin, lung, colon, kidney and liver) from the same group of rats (24 h post-injection of 0.3 mg/kg *m*-THPC) were

analysed for the presence of *m*-THPC using chemical extraction (Kaščákova *et al.*, 2008). These experiments revealed the presence of *m*-THPC in these tissues (unpublished work by Dr Josephine Woodhams, National Medical Laser Centre, UCL). This method of chemical extraction is a more sensitive approach to assessing low levels of *m*-THPC in tissues and will be used with nerve tissue samples in the future to establish the amount of *m*-THPC localised within nerves which may have been below the limit of detection using fluorescence microscopy in this case (Peng *et al.*, 1995). Commonly in human treatments, a photosensitiser dose of 0.15 mg/Kg *m*-THPC is i.v. injected with a drug-light interval of 4 days (Zimmermann *et al.*, 2001; Lou *et al.*, 2004; Lovat *et al.*, 2005; Moore *et al.*, 2006; Betz *et al.*, 2007). Human studies have shown the presence of *m*-THPC in the brain under these conditions (Zimmermann *et al.*, 2001), however, peripheral nerves have not been assessed for the presence of *m*-THPC. To our knowledge, the present study reports for the first time an investigation into the uptake of *m*-THPC in peripheral nerve tissue after i.v. injection in rats and shows that either higher drug doses or a more sensitive detection method than fluorescence will be required to characterise it properly.

Taking into consideration the low *m*-THPC concentration used, the time post injection before tissue acquisition, and the fast clearance of *m*-THPC; low concentrations of *m*-THPC were not unexpected in these nerve tissues. A low level of *m*-THPC would result in a reduced PDT effect on nerves and this study reports no obvious signs of nerve damage, (e.g. axon pruning and changes in nerve architecture) using NF and S-100 fluorescent staining. Transverse sections of nerve tissue were also assessed here for their possible use in assessing nerve damage, using a quantitative approach developed previously which determines the proportion of Schwann cell 'tubes' which contain axons (Phillips et al., 2005).

This method of nerve damage assessment is based on the assumption that damaged nerves will have a reduced proportion of axons in association with glial tubes, due to neurite degradation. Similar markers like Masson-Trichrome staining used in Kübler *et al.* (2003) could also be used to assess these nerve sections.

However, it is clear that the results of the initial experiments conducted here using explants have indicated that nerve tissue culture systems might not be suitable for use in assessing the effects of focally applied *m*-THPC-mediated PDT on nerve tissue, due to insufficient *m*-THPC levels in nerve tissue under these experimental conditions. A possible shortening in the time post *m*-THPC injection may be required as well as a possible increase in the *m*-THPC concentration administered to the animals in order to elicit a PDT effect. Altering these assay parameters may allow this explant tissue culture system to be used experimentally to determine if nerves are spared the effects of focal PDT application. *More importantly, this nerve tissue culture system could indicate whether m-THPC is taken up at all by nerves in vivo, possibly aiding in determining whether nerve sparing in vivo is a result of lack of m-THPC uptake, without which there can be no direct PDT effect.*

Nerve explants from untreated animals were assessed for uptake of *m*-THPC from solution and focal PDT treatment was administered. Nerve explants were incubated in culture for 24 h in 4 µg/ml *m*-THPC. This however, did not result in an effective uptake of *m*-THPC as determined by detection of drug fluorescence. This is in comparison to Chapter 3 which showed that *m*-THPC was taken up by neuronal cell bodies and glial cells in dissociated DRG cultures after 4 h incubation with 4 µg/ml *m*-THPC to a level that was readily detectable using fluorescence microscopy. In this pilot study the pattern of *m*-THPC fluorescence suggested that

m-THPC may have penetrated the nerve explant via the distal cut end, with little or no *m*-THPC accumulating in the DRG itself.

5.4.2 Nerve cell culture systems

Monolayer cultures of glial cells have been shown to provide a surface on which neurites extend from the cell bodies of cultured neurones (Thompson and Buettner, 2006). In the present study, cultures of Schwann cells or satellite cells served as monolayer substrates to facilitate dissociated DRG neurone survival and growth. Neuronal cell bodies remained relatively stationary and neurites extended away, in particular with the use of satellite cells as the substrate. Without this glial cell substrate layer, neurites were observed to grow in circles around their neuronal cell bodies on top of colonies of migrating satellite cells (from the DRG culture).

This glial cell substrate culture model was a promising system for studying the effect of focal PDT treatment on DRG neurones, however there were some limitations and considerable further optimisation would be necessary before the model could be considered robust. Limitations included the accurate sizing and positioning of the PDT wounding site which was attempted here by masking the base of the culture dishes to create a slit for illumination. The resulting focal PDT wounds were not clearly defined following PI staining, probably due to scattering of light resulting in a more complex pattern of illumination than predicted. In these initial studies neurite loss within the focal PDT wound was observed as in Chapter 3, whereas, outside wounded regions DRG neurones retained their neurites. Therefore it would be possible to evaluate DRG neurone and glial cell responses

to focal PDT wounding using this culture system if a reproducible way of limiting illumination to discrete regions could be optimised.

A range of 3D culture systems for neuroscience research have been developed in recent years (reviewed by Brown and Phillips, 2007; East and Phillips 2008). These model systems overcome some of the limitations of using monolayer cultures, in which nervous system cells often do not resemble their *in vivo* counterparts, but have the advantage of providing a controllable reproducible environment for studying cell behaviour and thus go some way towards bridging the gap between culture systems and animal models (Brown and Phillips, 2007). Much of the progress in this area has been driven by tissue engineering groups seeking substrates for the repair of nerve injuries which can also serve as culture models. For example, Collagen matrices have been previously utilised to engineer 'stretch-grown' axons (Pfister *et al.*, 2006) and magnetically axially aligned collagen fibrils have supported aligned neurite growth (Dubey *et al.*, 1999). In this chapter the collagen (Type-I) hydrogel used in Chapter 3 was used as the basis for the development of a more advanced tissue engineered peripheral nerve culture model that supported aligned neurite growth away from the neuronal cell body. When dissected DRGs (complete with a section of the distal nerve trunk) were embedded within simple untethered collagen gels, the neurites preferentially grew within the nerve tissue rather than extending out into the collagen gel. In order to achieve growth out from the DRGs, it was necessary to provide a more complex external environment with aligned glial cells providing guidance cues and trophic support.

A 3D tethered culture system previously developed in the laboratory of Prof Robert Brown (Eastwood *et al.*, 1994; Eastwood *et al.*, 1998) and adapted for

neuroscience use (Phillips *et al.*, 2005) was chosen for further development and use in this study. This nerve culture system incorporated Schwann cells and sciatic nerve fibroblasts, which together have been shown to encourage axial aligned neurite growth from DRGs into the collagen gel lattice. The axial alignment was achieved by tethering both ends of a rectangular cell-seeded collagen gel, resulting in glial cell alignment parallel to the direction of principal strain. Neurites then extended within this aligned 3D cellular environment.

In order to provide a robust and reproducible model system for focal PDT, this study optimised the key parameters necessary to achieve reliable contraction and alignment. Initially, mixed Schwann cell/fibroblast cultures were used to established that the minimum cell-seeding density required for effective collagen gel contraction was between 300,000 (free-floating circular gels) and 400,000 (tethered gels) cells/ml. These parameters allowed for gel contraction within 1 to 2 days of gel preparation. The ratio of Schwann cells to fibroblasts in these cultures seemed to make little difference in determining whether gels would contract. Despite optimal contraction being achieved in some of these tethered gels, little neurite projection was observed from either DRG explants or dissociated DRG cells implanted into these models before or after gel contraction. This was despite robust neurite growth being observed in previous studies under similar conditions (Phillips *et al.*, 2005, Dubuisson *et al.*, 1999, Pearson *et al.*, 2003), and may have been a result of variations in for example Schwann cell culture technique.

The initial lack of neurite outgrowth was overcome by using Satellite cells from DRGs rather than sciatic nerve Schwann cell cultures for seeding into the collagen gels. Because satellite glial cell cultures contained far fewer contaminating fibroblasts than sciatic nerve Schwann cell cultures, they were enriched with 5 %

neural fibroblasts to facilitate collagen gel contraction. This approach resulted in neurite growth from both DRG explants and dissociated DRG neurones. Fibroblast addition aided collagen gel contraction, but nerve fibroblasts are also known to promote some physiological properties of glial cells (Dubuisson *et al.*, 1999). Fibroblasts may possibly encourage interactions between FGF-2 and S100β in activated satellite cells, which may trigger paracrine actions (neuronal maintenance and plasticity), in these axotomised DRG neurones (Levy Bde *et al.*, 2007).

A similar 3D tethered cell-seeded collagen (Type-I) hydrogel nerve culture system was reported by Dubuisson *et al.* (1999) who initially assessed the contraction rates of free-floating circular collagen gels seeded with neural cells, similar to free-floating gels presented in this study, and determined the need for nerve fibroblasts for gel contraction. Dubuisson *et al.* (1999) also concluded that at least 500,000 satellite cells/ml were needed for contraction of cell-seeded tethered collagen gels with final collagen concentrations of 0.3 and 1.0 mg/ml, and also shows that nerve fibroblasts were required for successful collagen gel contraction. Differences between that culture system and the one used in this study may arise from the fact that a lower concentration of collagen was used in gel preparations in comparison to this study, which used 1.6 mg/ml final concentration. These findings were also supported by Nirmalanandhan *et al.* (2006) with a modified 3D tethered mesenchymal stem cell (MSC)-seeded collagen (Type-I) culture system, which was developed in aid of constructing a successful tendon repair device. The model used by Nirmalanandhan *et al.* (2006), like in Dubuisson *et al* (1999), showed that above a threshold value of cell density (500,000 cells/ml), reducing the concentration of collagen gels influence gel contraction kinetics more than equivalent increases in cell seeding density. Nirmalanandhan *et al.* (2006)

eventually settled with the use of 500,000 cells/ml MSCs and a concentration of 1.3 mg/ml purified bovine collagen (Type-1).

Another potentially important observation in this study was that in addition to the support of neurite outgrowth in an aligned 3D glial cell environment, if cultures were maintained for 12 days then processed and analysed using transmission electron microscopy, extensive myelination of axons was observed (Figure 5.13). This work was peripheral to this PhD project and was conducted in collaboration with Dr James Phillips and Heather Davies; therefore it is not described in detail in this thesis. However, this observation, along with the optimisation of the glial cell environment which was reported here, suggests that this is likely to be a useful model for future work in assessing the effects of PDT on nervous system cells. Because this culture system is capable of supporting aligned neurite outgrowth and then maintenance of axons in a manner that permits glial cells to myelinate them (an important feature that has not been reported in this kind of culture system previously), it can be considered to mimic the *in vivo* situation and thus forms an accessible and exciting culture system for future experimentation.

Focal *m*-THPC-mediated PDT wounding of 3D satellite cell-seeded collagen gel culture systems was attempted, but as with the 2D models there were limitations in terms of the delivery of light to a confined spot on the gel.

For future use of these culture systems, labelling of live neurites in both 2D and 3D cultures would be desirable in order to determine at which time point to use model systems and where to direct the PDT light source in PDT wounding assays. CM-DiI (CellTrk-red) was tested for its ability to labelled live neurites and was found to label both glial cells and neuronal cell bodies, but did not accumulate within

neurites at a level sufficient for effective tracking. Alternative methods which could be adapted for use in tracking live neurites include the labelling and tracking of mitochondrial transport with MitoTracker® Green FM (MitoTrk-green) fluorescence dye as used in the labelling of neurites in live myenteric neurones (Vanden Berghe *et al.*, 2003) and hippocampus neurones (Hayashi *et al.*, 2007). Altermatively, the labelling and tracking of neurofilament and microtubule transport in live neurites with the use of innovative fluorescent probes such as NeuroMag, a neurone-specific transfection reagent (He *et al.*, 2005), or more simply the use of isolated neurones from GFP positive rats could be tried. These live neurone markers would aid in focal PDT application to neurones in culture systems as illustrated in Figure 5.15.

5.5 Conclusions

In conclusion, a range of nerve culture systems have been developed and adapted for investigating the effect of focal PDT treatment on nerves. With a little further refinement it is likely that some of these will provide useful means with which to explore the effect of PDT focally applied to one part of the neurone. In order to mimic the clinical situation in which a peripheral nerve might be exposed to PDT due to its proximity to a cancer treatment site (e.g. the nerves running close to the prostate gland), animal models have been used including rabbits and minipigs (Kübler *et al.*, 2003), and dogs (Chang *et al.*, 1996; Chang *et al.*, 1997; Chang *et al.*, 1999; Dole *et al.*, 2005; Huang *et al.*, 2005). More recently, the effects of PDT on neural tissue in close association with vertebral metastases in murine models has been used to mimic these clinical situations (Burch *et al.*, 2005). While these animal models provide a good assessment of the ultimate effects of PDT on nerve

tissue, it is difficult to extrapolate from these studies what the direct effects of treatments are on neurones and glial cells. Using a culture system like those developed here, will enable future experiments in which the cellular environment can be closely controlled and monitored. These experiments would elucidate the mechanisms by which neurones and glial cells respond to PDT-induced damage. Understanding the fundamental cell biology underlying the response of neural cells to PDT will ultimately aid in the development of new PDT treatments, which could spare neural cells during cancer treatment.

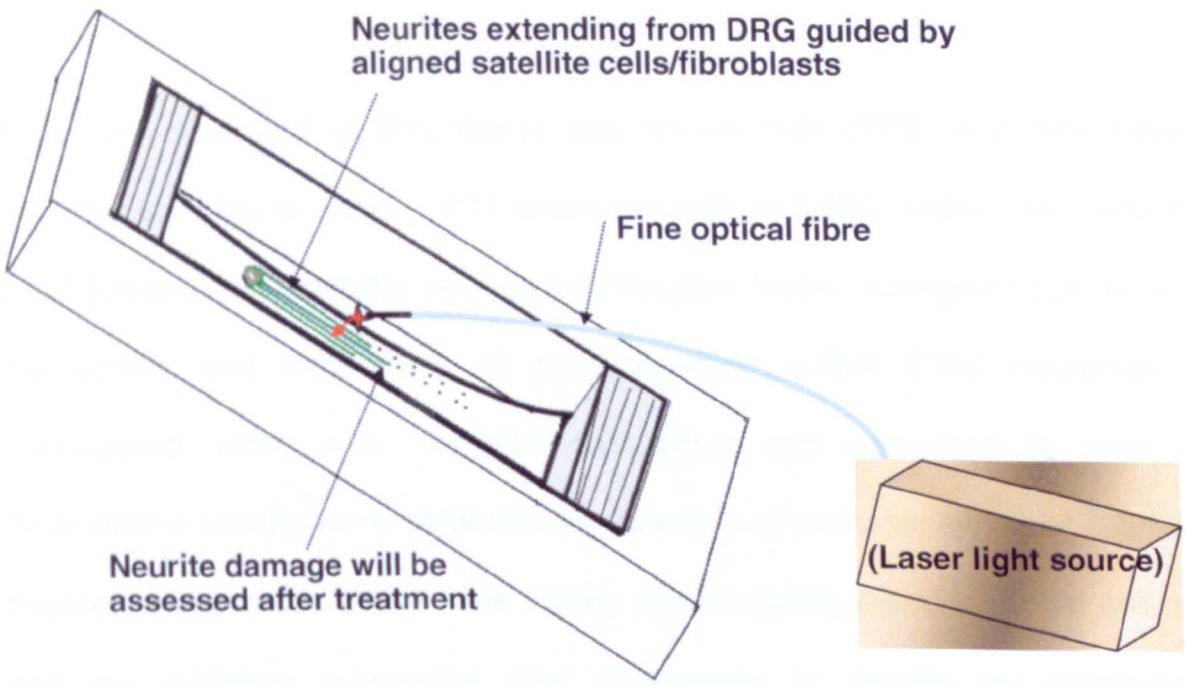

Figure 5.15
Schematic diagram of PDT application to a 3D tethered peripheral nerve culture model.
Illustration shows neurites being targeted with focal PDT. Laser light can be directed at varied distances along the neurite or onto neuronal cell bodies with the aid of a live neurone marker.

Chapter 6: General Discussion, Future Work and Conclusions

6.1 General discussion

Various *in vitro* strategies have been used in this project to explore the effects of PDT on key cells of the nervous system. The focus has been on the drug *m*-THPC, which had previously been shown to spare peripheral nerves in clinical and experimental work (Ris *et al.*, 1996; Moore *et al.*, 2006; Betz *et al.*, 2007; Nyst *et al.*, 2009).

The work described in this thesis has shown that DRG neurones have the remarkable ability to survive PDT treatment with *m*-THPC under conditions which killed tumour cells, satellite cells and astrocytes. Using a range of culture models the uptake and distribution of photosensitiser within DRG neurones were investigated, along with $^1O_2$/ROS production, and compared to other cells. Inconclusive results were obtained for detection of photosensitiser or $^1O_2$/ROS in neurites, but photosensitiser was clearly accumulating within neuronal cell bodies and no evidence suggested that differences in uptake or distribution of photosensitiser could explain the observed neuronal survival. After *m*-THPC-mediated PDT DRG neurones lost their neurites, but retained their ability to regenerate neurites. This confirmed that neurones survived *m*-THPC-mediated PDT in a manner that retained their regenerative functionality. After investigation, DRG neurones were shown to be reliant on intracellular glutathione synthase and SOD-1 antioxidant pathways for neuronal PDT resistance. Furthermore progress was made towards establishing culture systems for exploring the effects of PDT on specific neuronal compartments.

Along the way a number of useful novel model systems were developed. In particular the use of the thin collagen gels (Chapter 3), which allowed neuronal cell viability to be characterised within a mixed cell population and proved to be a robust reliable system (as verified by using a range of cells and a control photosensitiser, hypericin) that will be useful for future studies, (e.g. more work on antioxidant inhibitors, determining the mechanism by which neurites were damaged after PDT, the effect of PDT on neurones in isolation, or what makes *m*-THPC-mediated PDT such an exceptional treatment).

This concluding chapter discusses some possible future directions of this study; its contribution to knowledge in the fields of PDT and neuroscience, identifies some limitations of this approach, and speculates about the relevance of this work to clinical applications.

If DRG neurones survive *m*-THPC-mediated PDT *in vivo* as they do in culture then the treatment of tumours near DRG structures should therefore not result in damage to the neuronal cell bodies contained within DRGs, but this study has indicated that these neurones may lose their neurites. This may not be a serious problem, since this study has also shown that these DRG neurones are able to regenerate their neurites after *m*-THPC-mediated PDT. In addition, satellite cells that are killed at the treatment site may be replaced by new ones, generated through mitosis. This type of PDT may therefore be highly useful in the treatment of tumours situated in close proximity to DRGs, (e.g. vertebral metastasis). The relevance of this study to clinical application involved a possible explanation of the nerve-sparing observed after *m*-THPC-mediated PDT treatment of head and neck, prostate and oesophagus cancers.

Focal application of *m*-THPC-mediated PDT to neuronal cell bodies or neurites still needs to be investigated, in particular the effects of PDT targeted at different distances away from neuronal cell bodies along neurites. The different distance of targeted PDT may result in different effects on DRG neurones. The neurone may re-grow its axon along the same path, there may be branching, or it may result in the death of the neuronal cell body. The culture systems developed in Chapter 5 will provide useful tools for investigating this phenomenon in the future.

From the literature the majority of the molecular and cellular studies in relation to the effect of PDT on nerves have focused on the use and effects of photosens-mediated PDT on the spike response of crayfish nerves, their death response in relation to surrounding glial cells, and the neuronal-glial signalling mechanisms responsible for cell death (Uzdenskii *et al.*, 2008). This study however focused on *m*-THPC-mediated PDT and has highlighted the different cell death responses that exist between different cell types contained in mammalian nerves. This was an indication of the different intracellular survival systems in these cell types, which may be exploited to allow selective PDT damage to one cell type while others survive. Even though there is a marked difference between humans and animals in relation to *m*-THPC distribution in tissue types (Kübler *et al.*, 2003), the use of a rat nerve source here was more appropriate than a crayfish nerve, for predicting human nerve responses to PDT.

In order to establish the mechanism/s by which DRG neurones were protected from the effects of *m*-THPC-mediated PDT, selected intracellular antioxidant pathways were blocked, resulting in neuronal death on exposure to *m*-THPC-mediated PDT. This suggested that DRG neurones used glutathione synthase and SOD-1 antioxidant pathways to counteract the effects of *m*-THPC-mediated PDT

under the conditions used in this study. *However, it is important to investigate the effect of other concentrations of these inhibitors in order to determine their optimal dose in inhibiting antioxidant pathways in DRG neurones.* In particular, higher doses of 2-$MeOE_2$ should be tried before concluding that the SOD-2 antioxidant pathway was not involved in protecting DRG neurones. Furthermore the involvement of other antioxidant pathways in protecting these DRG neurones still needs to be investigated, (e.g. the catalase pathway). Investigating both higher doses of 2-$MeOE_2$ and other commercially available antioxidant pathway inhibitors may well result in 100 % DRG neurone death after exposure to *m*-THPC-mediated PDT.

Advice to other researchers undertaking similar studies as presented in this study would be that it is important to continue this type of research with a multidisciplinary approach. Without this form of investigation the progress made in this area of 'the effects of PDT on nerves', would be considerably less advanced. For example the 3D collagen gel model adapted from the field of tissue engineering was used to resolve a major problem in the field, cell loss after PDT treatment, which would have prevented neuronal sensitivity from being measured. A broad understanding of the field of neuroscience, combined with awareness of recent developments in PDT and tissue engineering research is important for future progress of this research.

6.2 Future work

6.2.1 Effect of *m*-THPC-mediated PDT on other neural cell types

This thin 3D collagen culture system would be useful in further evaluating the response of other neural cell types to *m*-THPC-mediated PDT. If this PDT is to be used for new clinical applications (e.g. to treat vertebral metastasis), it would be important to first assess neural cells response to PDT in areas such as the spinal cord, brain, prostate, bladder and/or oesophagus. In addition the effect of other photosensitisers on neural cells, (e.g. ALA induced PpIX-mediated PDT, known to cause pain during treatment (Wiegell *et al.*, 2003; Algermissen *et al.*, 2003)) would be important in order to determine whether or not these clinically approved photosensitisers may also have nerve sparing properties. Also assessment of photosensitisers with similar properties as *m*-THPC could be of interest, to determine which feature/s of *m*-THPC were responsible for nerve sparing. In investigating nerve sparing properties of clinically approved photosensitisers, specific photosensitisers could be approved for use in PDT in areas rich in nerve structures to reduce nerve damage.

6.2.2 Protective mechanisms of neurones

A possible future direction for the study of neuronal survival following PDT could be to use N-AcetylCysteine (NAC), a precursor to GSH, which has been used on rat CNS co-cultures to increase the protective effect of glial cells on neurones (Watts *et al.*, 2005). Our co-culture system can be used to assess the importance of satellite cells on the survival of neurones after PDT. We can determine the effects of increasing GSH levels above naturally occurring levels in culture using NAC. This could be followed by the assessment of satellite cells for signs of reduced cell death, and neurones for signs of neurite retention after PDT. Therefore, application of NAC in a clinical setting prior to PDT could promote protective effects of satellite cells on neurones at PDT treatment sites.

In addition to further experimentations in inhibiting or promoting antioxidant pathways; it would be of interest in a clinical setting to possibly introduce antioxidants or antioxidant generating agents which may interact with endogenous antioxidant pathways to increase the levels of neurone protection from PDT, (e.g. Bromocriptine with its neuroprotective effects against free radicals (Iwasaki *et al.*, 1997); propyl gallate a synthetic antioxidant widely used in processed food and medicinal preparations (Han *et al.*, 2009); and phenolic α-tocopherol (Vitamin E) which has been shown to cause increase tumour cell death (HT29) while sparing non-tumour cells (MRC-5) (Melnikova *et al.*, 1999c)) . This may be useful in cases were much higher doses of PDT are applied, which on its own may kill neurones or in situations in which a patient's antioxidant protective pathways might be suppressed due to illness or disease. However, systemic antioxidant treatment would have to be tried with caution since it might diminish the effectiveness of PDT on the killing of tumour cells.

Further examination of the inhibition of neuronal resistance to PDT via antioxidant pathways would be useful in understanding how this phenomenon might translate to a clinical setting. Performing *m*-THPC-mediated PDT dose responses after inhibiting glutathione and SOD antioxidant pathways using other commercially available inhibitors could give greater insight into the mechanism for neuronal survival (e.g. the SOD-1 inhibitor, disulfiram (Dimayuga *et al.*, 2007)). Also, investigations into the protective effects of the catalase antioxidant protective pathway would be of interest, by using the catalase inhibitor (e.g. 3-amino-1, 2, 4-triazole (Oyama *et al.*, 1994)). Catalase activity has been shown to increase after PDT in mouse mammary carcinoma (EMT6) cells (Johnson and Pardini, 1998).

Despite the lack of *m*-THPC fluorescence detection in neurites in Chapter 3, and the inconclusive detection of $^1O_2$/ROS after *m*-THPC-mediated PDT in neurites in Chapter 4, mass neurite loss was observed after *m*-THPC-mediated PDT. This was despite the fact that neuronal cell bodies were surviving treatment conditions. In a clinical setting this may result in temporary loss of nerve function, because these neurones retained their ability to re-grow neurites after *m*-THPC-mediated PDT and these new neurites may re-innervate nerve trunks. Also, the possible involvement of DR6 orphan receptors (Nikolaev *et al.*, 2008) in the effect of *m*-THPC-mediated PDT on DRG neurones would be an interesting future investigation. Most PDT treatments are directed at the nerve trunk, which consists of axons. The activation of DR6 receptors has been shown to cause neurite loss; if this receptor could be blocked, maybe a rescuing of the neurites might be possible during PDT treatment. Therefore, this may prevent any temporary loss of nerve function, due to neurite loss after PDT.

Investigating the effect of different caspases in protecting different parts of DRG neurones (neuronal cell bodies or neurites), from *m*-THPC-mediated PDT. DRG neuronal cell bodies have been shown to be protected from oxidative stress by the involvement of caspase 3 and 7, while their neurites are protected by the involvement of caspase 6 (Nikolaev *et al.*, 2008). This would be a useful future direction in determining further mechanisms used by neurones to protect themselves from cell death following exposure to oxidative stress.

6.2.3 Detection systems

To determine *m*-THPC subcellular localisation in neural cells at different incubation times, as well as before and after illumination, would be useful as a means of

determining whether differences in cell type responses are related to *m*-THPC localisation. This could be done by isolating specific organelles from neural cell types preloaded with *m*-THPC, then assessing for *m*-THPC fluorescence. Also, in order to further determine the extent to which *m*-THPC localises with DRG neurites, the use of *m*-THPC-monoclonal antibodies (Vrouenraets *et al.*, 1999) or ^{14}C-labeled *m*-THPC (Obwegeser *et al.*, 1998) could be adopted to enhance detection signal in neurites. In determining the localisation of *m*-THPC at a cellular level, photosensitisers approved for clinical use which display similar localisation could be used to obtain similar nerve sparing results as *m*-THPC-mediated PDT.

In addition to the use of DCF fluorescence, $^1O_2$ production can be more specifically detected by its phosphorescence emission at a wavelength of 1270 nm in solution and in cell culture (Berg, 2007). This method of detection could be used to determine the level of $^1O_2$ generated in specific neural cell types, and in the compartments of the neurone (e.g. neurites versus neuronal cell bodies) after *m*-THPC-mediated PDT. The type of toxic oxygen molecules generated after PDT may also be a factor in influencing cell type specific death response.

6.2.4 Model development

With further investigations into neural cells and nerve tissue, perhaps understanding the reasons behind nerve sparing are not too distant in the future. However, in order for this investigation to progress, there is a need for a nerve culture system in which focal PDT could be applied to specific compartments of neurones. This is because during clinically applied PDT treatments the nerve trunk (containing neurites) is the part of the nerve most frequently exposed to PDT treatments. For translational studies, a useful future direction would be to assess

this treatment in an *in vivo* situation because it would provide a natural environment in which to assess nerve damage after PDT (i.e. with the involvement of the host circulatory and immune system in response to PDT). But, to further elucidate the underlying biology, culture systems are more useful, due to their controllable environment and the ability to monitor changes which may occur.

The ability to label and track live neurites would be invaluable in our 2D and/or 3D culture systems, because it would allow us to determine when to start assays, where to focus the light beam for PDT and would make it possible for us to assess neurite response to PDT-treatments in time. Methods which could be implemented include the use of tritiated amino-acids which can be injected into clusters of neuronal cell bodies and viewed with autoradiography; horseradish peroxidase could be injected among a group of axon terminals (retrograde transport marker); or purified specific antibodies, made using an enzyme involved in a particular transmitter-labelled with fluorescence (Keele *et al.*, 1989).

6.3 Conclusions

DRG neurones survived *m*-THPC-mediated PDT, but with substantial damage to neurites, at levels of treatment which killed both glial cells (satellite cells and astrocytes) and MCF-7 breast cancer tumour cells. DRG neurones were however, able to re-grow neurites to a similar extent as untreated neurones. Furthermore these DRG neurones were found to survive *m*-THPC-mediated PDT by the use of intracellular antioxidant pathways (i.e. glutathione synthase and SOD-1 pathways). This study points to a possible role for more widespread use of *m*-THPC-mediated PDT in the treatment of tumours in close association to nerve structures, such as the treatment of spinal metastases.

REFERENCES

Adigbli, D.K., Wilson, D.G.G., Farooqui, N., Sousi, E., Risley, P., Taylor, I., MacRobert, A.J. and Loizidou, M. (2007). "Photochemical internalisation of chemotherapy potentiates killing of multidrug-resistant breast and bladder cancer cells." British Journal of Cancer **97**: 502-512.

Agostinis, P., Buytaert, E., Breyssens, H. and Hendrickx, N. (2004). "Regulatory pathways in photodynamic therapy induced apoptosis," Photochemical and Photobiological Sciences **3**: 721-729.

Agostinis, P., Vantieghem, A., Merlevede, W. and de Witte, P.A.M. (2002). "Hypericin in cancer treatment: more light on the way." The International Journal of Biochemistry and Cell Biology **34**: 221-241.

Alberts, B., Johnson, A., Lewis, J., Raff, M., Roberts, K. and Walter, P. (2008). "Energy Conversion: Mitochondria and Chloroplasts", Molecular Biology of THE CELL 5th Edition. Garland Science, Taylor and Francis Group, New York (ISBN: 0-8153-4111-3): 813-878.

Algermissen, B., Osterloh, D., Philipp, C.M. and Berlien, H.P. (2003). "Management of ALA-PDT Induced Pain Sensations." Medical Laser Application **18**: 57-64.

Almeida, R.D., Manadas, B.J., Carvalho, A.P. and Duarte, C.B. (2004). "Intracellular signaling mechanisms in photodynamic therapy." Biochimica et Biophysica Acta **1704**:59-86.

Andrade, W., Seabrook, T.J., Johnson, M.G. and Hay, J.B. (1996). "The use of the liphophilic fluoreochrome CM-DiI for tracking the migration of lymphocytes." Journal of Immunological Methods **194**: 181-189.

Antonyuk, S.V., Strange, R.W., Marklund, S.L. and Hasnain, S.S. (2009). "The Structure of Human Extracellular Copper-Zinc Superoxide Dismutase at 1.7 Å Resolution: Insights into Heparin and Collagen Binding." Journal Molecular Biology **388**: 310-326.

Armstrong, S.J., Wiberg, M., Terenghi, G., Kingham, P.J, (2008). "Laminin activates
NF-kappa B in Schwann cells to enhance neurite outgrowth." Neuroscience Letters **439**: 42-46.

Artal-Sanz, M. and Tavernarakis, N. (2005). "Proteolytic mechanism in necrotic cell death and neurodegeneration." FEBS Letters **579**: 3287-3296.

Assefa, Z., Vantieghem, A., Declercq, W., Vandenabeele, P., Vandenheede, J.R., Merlevede, W., de Witte, P. and Agostinis, P. (1999) "The Activation of c-Jun N-terminal Kinase and p38 Mitogen-activated Protein Kinase Signaling Pathways Protects HeLa Cells from Apoptosis Following Photodynamic Therapy with Hypericin." The Journal of Biological Chemistry **274** (13): 8788-8796.

Avshalumov, M.V., Macgregor, D.G., Sehgal, L.M. and Rice, M.E. (2004) "The glial antioxidant network and neuronal ascorbate: protective yet permissive for H_2O_2 signaling." Neuron Glia Biology **1** (4): 365-376.

Ball, D.J., Luo, Y., Kessel, D., Griffiths, J., Brown, S.B. and Vernon D.I. (1998). "The induction of apoptosis by a positively charged methylene blue derivative." Journal of Photochemistry and Photobiology B: Biology **42**: 159-163.

Ball, D.J., Mayhew, S., Wood, S.R., Griffiths, J., Vernon, D.I. and Brown, S.B. (1999). "A Comparative Study of the Cellular Uptake and Photodynamic Efficacy of Three novel Zinc Phthalocyanines of Differing Charge." Photochemistry and Photobiology **69** (3): 390-396.

Bampton, E.T.W. and Taylor, J.S.H. (2005). "Effects of Schwann Cells Secreted Factors on PC12 Cells Neuritogenesis and Survival." Journal of Neurobiology **63**: 29-48.

Banasiak, K.J., Xia Y., Haddad, G.G. (2000). "Mechanisms underlying hypoxia-induced neuronal apoptosis." Progress in Neurobiology **62**: 215-249.

Bancroft, J.D. and Stevens, A. (1990). "Neuropathological techniques." Theory and Practice of Histological Techniques, 3rd Edition; Longman Group UK Limited (ISBN 0-443-03559-8): 343-378.

Baskić, D., Popović, S., Ristić, P. and Arsenijević, N/N. (2006) "Analysis of cytoheximide-incduded apoptosis in human leukocytes: Fluorescence microscopy using annexin V/ propidium iodide versus acridin orange/ethidium bromide." Cell Biology International **30**: 924-932.

Becker, E.B.E. and Bonni A. (2004). "Cellular cycle regulation of neuronal apoptosis in development and disease." Progress in Neurobiology **72**: 1-25.

Bellamkonda, R.V., Ranieri, J.P., Bouche, N. and Aebischer, P. (1995). "Hydrogel-based three-dimensional matrix for neural cells." Biomed Mater Res **29** (5): 663-671.

Bellamkonda, R.V. (2006). "Peripheral nerve regeneration: An opinion on channels, scaffolds and anisotropy." Biomaterials **27**; 3515-3518.

Berg, K. (2007). "Photodynamic Therapy." Photodynamic Therapy at the Cellular Level, Editor Uzdensky A.B; Research Signpost, Kerala, India (ISBN: 978-81-308-0174-2: 1-16)

Betz, C.S., Jäger, H.R., Brookes, J.A.S., Richards, R., Leunig, A. and Hopper, C. (2007). "Interstitial Photodynamic Therapy for a Symptom-Targeted Treatment of Complex Vascular Malformations in the Head and Neck Region." Lasers in Surgery and Medicine **39**: 571-582.

Blank, M., Lavie, G., Mandel, M., Hazan, S., Orenstein, A., Meruelo, D. and Keisari, Y. (2004). "Antimetastatic Activity of the Photodynamic Agent Hypericin in the Dark." International Journal of Cancer **111**: 596-603.

Bourré, L., Rousset, N., Thibaut, S., Eléouet, S., Lajat, Y. and Patrice, T. (2002) "PDT effects of m-THPC and ALA, phototoxicity and apoptosis." Apoptosis **7**: 221-230.

Bragin, D.E., Kolosov, M.S. and Uzdensky, A.B. (2003). " Photodynamic inactivation of isolated crayfish neuron requires protein kinas C, PI 3-kinase and Ca^{2+}." Journal of Photochemistry and Photobiology B: Biology **70**: 99-105.

Brandt, R., Léger, J. and Lee, G. (1995). "Interaction of Tau with the Neural Plasma Membrane Mediated by Tau's Amino-terminal projection Domain." The Journal of Cell Biology **131** (5): 1327-1340.

Brezis, M., Rosen, S., Silva, P. and Epstein, F.H. (1983) "Selective glutathione depletion on function and structure of the isolated perfused rat kidney." Kidney International **24** (2): 178-184.

Brown, R.A., Phillips, J.B. (2007). "Cell Responses To Biomimetic Protein Scaffolds Used In Tissue Repair And Engineering." International Review of Cytology. **262**: 75-150.

Bunting, S., Di Silvio, L. and Hall, S. (2005). "Bioresorbable glass fibres facilitate peripheral nerve regeneration." The Journal of Hand Surgery: Journal of the British Society for Surgery of Hands **30**(3): 242-247.

Burch, S., Bisland, S.K., Bogaards, A., Yee, A.J.M., Whyne, C.M., Finkelstein, J.A. and Wilson, B.C. (2005). "Photodynamic therapy for the treatment of vertebral metastases in a rat model of human breast carcinoma." Journal of Orthopaedic Research **23**: 995-1003.

Buytaert, E., Dewaele, M. and Agostinis, P. (2007). "Molecular effectors of multiple cell death pathways initiated by photodynamic therapy." Biochimica et Biophysica Acta **1776**: 86-107.

Cao, Q., Wei, L., Lu, L., Zhao, C., Zhao, H., and Yang, H. (2007) "Astrocytes protect MN9D neuronal cells against rotenone-induced oxidative stress by a glutathione-dependent mechanism." Acta Physiologica Sinica **59** (3): 253-259.

Castano, A.P., Demidova, T.N., Hamblin, M.R. (2005). "Mechanisms in photodynamic therapy: part two-cellular signalling, cell metabolism and modes of cell death." Photodiagnosis and Photodynamic Therapy **2**: 1-23.

Castro, C., Kuffler, D.P. (2006). "Membrane-bound CSPG mediates growth cone outgrowth and substrate specificity by Schwann cell contact with the DRG neuron cell body and not via growth cone contact." Experimental Neurology **200**:19-25.

Chang, S.C., Buonaccorsi, G., MacRobert, A. and Bown, S.G. (1996). "Interstitial and transurethral photodynamic therapy of the canine prostate using meso-tetra-(m-hydroxyphenyl) chlorine." International Journal of Cancer **67** (4): 555-562.

Chang, S.C., Buonaccorsi, G.A., MacRobert, A.J. and Bown, S.G. (1997). "Interstitial Photodynamic Therapy in the Canine Prostate With Disulfonated Aluminium Phthalocyanine and 5-Aminolevulinic Acid-Induced Protoporphyrin IX." The Prostate **32**: 89-98.

Chang, S.C., Chern, I.F. and Hsu, Y.H. (1999). "Biological responses of dog prostate and adjacent structures after meso-tetra-(m-hydroxyphenyl) chlorine and aluminium disulfonated phthalocyanine based photodynamic therapy." Proceedings of the National Science Council, Republic of China Part B, Life Sciences **23** (4): 158-166.

Chen, Y., McMillan-Ward, E., Kong, J., Israels, S.J. and Gibson, S.B. (2008). "Oxidative stress induces autophagic cell death independent of apoptosis in transformed and cancer cells." Cell Death and Differentiation **15**: 171-182.

Colasanti, A., Kisslinger, A., Liuzzi, R., Quarto, M., Riccio, P., Roberti, G., Tramontano, D. and Villani, F. (2000) "Hypericin photosensitzation of tumor and metastatic cell lines of human prostate." Journal of Photochemistry and Photobiology B: Biology 54: 103-107.

Cole, C.D., Liu, J.K., Sheng, X., Chin, S.S., Schmidt, M.H., Weiss, M.H. and Couldwell, W.T. (2008). "Hypericin-mediated photodynamic therapy of pituitary tumors: preclinical study in a GH4C1 rat tumor model." Journal of Neurooncology **87**: 255-261.

Collins, J.A., Schandl, C.A., Young, K.K., Vesely, J. and Willingham, M.C. (1997). "Major DNA Fragmentation is a late Event in Apoptosis." The Journal of Histochemistry and Cytochemistry **45**(7): 923-934.

Conforti, L., Adalbert, R. and Coleman, M.P. (2007). "Neuronal death: where does the end begin?" TRENDS in Neurosciences **30** (4): 159-166.

Coutier, S., Bezdetnaya, L.N., Foster, T.H., Parache, R.M. and Guillemin, F. (2002). "Effect of irradiation fluence rate on the efficacy of photodynamic therapy and tumor oxygenation in meta-tetra (hydroxyphenyl) chlorin (mTHPC)-sensitized HT29 xenografts in nude mice." Radiation Research. **158** (3): 339-345.

Dabrowski, M.J., Maeda, D., Zebala, J., Doug Lu, W., Mahajan, S., Kavanagh, T.J. and Atkins, W. (2006) "Glutathione *S*-transferase P1-1 expression modulates sensitivity of human kidney 293 cells to photodynamic therapy with hypericin." Archives of Biochemistry and Biophysics **449**: 94-103.

Das, H., Koizumi, T., Sugimoto, T., Yamaguchi, S., Hasegawa, K., Tenjin, Y., Nishimura, R. (2000). "Induction of apoptosis and manganese superoxide dismutase gene by photodynamic therapy in cervical carcinoma cell lines." International Journal of Clinical Oncology **5**: 97-103.

Das, K., Ashby, K.D., Wen, J. and Petrich, J.W. (1999). "Temperature Dependence of the Excited-State Intramolecular Proton Transfer Reaction in Hypericin and Hypocrellin A." The Journal of Physical Chemistry B **103**: 1581-1585.

De Bernardo, S., Canals, S., Casarejos, M.J., Solano, R.M., Menendez, J. and Mena, M.A. (2004). "Role of extracellular signal-regulated protein kinase in neuronal cell death induced by glutathione depletion in neuron/glia mesencephalic cultures." Journal of Neurochemistry **91**: 667-682.

Delree, P., Leprince, P., Schoenen, J. and Moonen, G. (1989) "Purification and Culture of Adult Rat Dorsal Root Ganglia Neurons." Journal of Neuroscience Research **23**:198-206.

Devesa, A., O'Connor, J.E., Graciá, C., Puertes, I.R. and Viña, J.R. (1993). "Glutathione metabolism in primary astrocyte cultures: flow cytometric evidence of heterogeneous distribution of GSH content." Brain Research. **618** (2): 181-189.

Dimayuga, F.O., Wang, C., Clark, J.M., Dimayuga, E.R., Dimayuga, V.M. and Bruce-Keller, A.J. (2007). "SOD1 overexpression alters ROS production and reduces neurotoxic inflammatory signalling in microglial cells." Journal of Neuroimmunology **182**: 89-99.

Dole, K.C., Chen, Q., Hetzel, F.W., Whalen, L.R., Blanc, D. and Huang, Z. (2005). "Effects of Photodynamic Therapy on Peripheral Nerve: *In Situ* Compound-Action Potentials Study in a Canine Model." Photomedicine and Laser Surgery **23** (2): 172-176.

Du, J., Suzuki, H., Nagase, F., Akhand, A.A., Ma, X., Yokoyama, T., Miyata, T. and Nakashima, I. (2001). "Superoxide-Mediated Early Oxidation and Activation of Ask1 are Important for initiating Methylglyoxal-Induced Apoptosis Process." Free Radical Biology and Medicine **31**(4): 469-478.

Dubey, N., Letourneau, P.C. and Tranquillo, R.T. (1999). "Guided Neurite Elongation and Schwann Cell Invasion into Magnetically Aligned Collagen in Simulated Peripheral Nerve Regeneration." Experimental Neurology **158**: 338-350.

Dugan, L.L., and Choi D.W. (1999). "Hypoxic-Ischemic Brain Injury and Oxidative Stress." Basic Neurochemistry-Molecular, Cellular and Medical Aspects 6th, Edition, Editors Siegel, G. J., Agranoff, B.W.; Albers, R. W., Fisher, S. K., Uhler, M. D.; Lippincott Williams and Wilkins, Philadelphia (ISBN-10: 0781717442).

Dutton, G.R., Curry, D.N. and Tear, K. (1981). "An improved method for the bulk isolation of variable perikarya from postnatal cerebellum." Journal of Neuroscience Methods **3**: 421-427.

East, E., Golding, J.P. and Phillips, J.B. (2009). "A Versatile 3D culture model facilitates monitoring of astrocytes undergoing reactive gliosis." Journal of Tissue Engineering and Regenerative Medicine (doi:10.1002/term.209).

East E. and Phillips J.B. (2008). "Tissue Engineered Cell Culture Models For Nervous System Research." Tissue Engineering Research Trends. Editor Greco, G. N.; Nova Science Publishers, Inc, New York (ISBN: 978-1-60456-264-4):141-160.

Eastwood, M., McGrouther D.A. and Brown, R.A. (1994). "A culture force monitor for measurement of contraction forces generated in human dermal fibroblast cultures: evidence for cell-matrix mechanical signalling." Biochimica et Biophysica Acta **1201** (2): 186-192.

Eastwood, M., Mudera, V.C., McGrouther, D.A., and Brown, R.A. (1998). "Effect of Precise Mechanical Loading on Fibroblast Populated Collagen Lattices: Morphological Changes." Cell Motility and the Cytoskeleton **40**:13-21.

Edström, A., Ekström, P.A.R. and Tonge, D. (1996) "Axonal Outgrowth and Neural Apoptosis in Cultured Adult Mouse Dorsal Root Ganglion Preparations: Effects of Neurotrophins, of Inhibition of Neurotrophin Action and of Prior Axotomy." Neuroscience **75**: 1165-1174.

English, D.S., Doyle, R.T., Petrich, J.W. and Haydon, P.G. (1999). "Subcellular Distribution and Excited–State Processes of Hypericin in Neurons." Photochemistry and Photobiology **69** (3): 301-305.

Fabris, C., Valduga, G., Miotto, G., Borsetto, L., Jori, G., Garbisa, S. and Reddi, E. (2001) "Photosensitization with Zinc (II) Phthalocyanine as a Switch in the Decision between Apoptosis and Necrosis." Cancer Research **61**: 7495-7500.

Fallon, J.R. (1985). "Neurite Guidance by Non-neuronal Cells in Culture: Preferential Outgrowth of Peripheral Neurites on Glial as Compared to Nonglial Cell Surfaces." The Journal of Neuroscience **5** (12): 3169-3177.

Fedorenko, G.M and Uzdensky, A.B. (2008). "Dynamics of Ultrastructureal Changes in the Isolated Crayfish mechanoreceptor Neuron Under Photodynamic Impact." Journal of Neuroscience Research **86**: 1409-1416.

Fedorenko, G.M. and Uzdensky, A.B. (2009). "Ultrastructure of neuroglial contacts in crayfish stretch receptor." Cell Tissue Research **337** (3): 477-490.

Fields, R. D. and Stevens-Graham, B. (2002). "New Insights into Neuron-Glia Communication." Science (Science's Compass Review: Neuroscience) **298**: 556-562.

Foster, T.H., Pearson, B.D., Mitra, S. and Bigelow, C.E. (2005). "Fluorescence Anisotropy Imaging Reveals Localization of meso-Tetrahydroxyphenyl Chlorin in the Nuclear Envelope." Photochemistry and Photobiology: 81 (6): 1544-1547.

Francis K., van Beek J., Canova C., Neal J.W. and Gasque P. (2003). "Innate immunity and brain inflammation:the key role of complement." Expert Review in Molecular Medicine **5**: 1-19.

Frank, J., Lornejad-Schäfer, M.R., Schoffl, H., Flaccus, A., Lambert, C. and Biesalski, H.K. (2007). "Inhibition of heme oxygenase-1 increases responsiveness of
melanoma cells to ALA-based photodynamic therapy." International Journal of Oncology **31**: 1539-1545.

Friberg, E.G., Čunderlíková, B., Pettersen, E.O. and Moan, J. (2003). "pH effects on the cellular uptake of four photosensitizing drugs evaluated for use in photodynamic therapy of cancer." Cancer Letters **195**: 73-80.

Funk D., Fricke C., Schlosshauer B. (2007). "Aging Schwann cells in vitro." European Journal of Cell Biology **86**: 207-219.

Gallagher W.M., Allen L.T., O'Shea C., Kenna T., Hall M., Gorman A., Killoran J. and O'Shea D.F. (2005) "A Potential nonporphyrin class of photodynamic therapeutic agent: cellular localisation, cytotoxic potential and influence of hypoxia." British Journal of Cancer **92**: 1702-1710.

Gegg, M.E., Clark, J.B. and Heales, S.J.R. (2005) "Co-culture of neurones with glutathione deficient astrocytes leads to increased neuronal susceptibility to nitric oxide and increased glutamate-cysteine ligase activity." Brain Research **1036**: 1-6.

Ginsburg, I., Yedgar, S. and Varani, J. (1997). "Diethyldithiocarbamate and nitric oxide synergize with oxidants and with membrane-damaging agents to injure mammalian cells." Free Radical Research. **27**(2): 143-164.

Girotti, A.W. (2001). "Photosensitized oxidation of membrane lipids: reaction pathways, cytotoxic effects, and cytoprotective mechanisms." Journal of Photochemistry and Photobiology B: Biology **63**: 103-113.

Goldberg, J.L. (2003). "How does an axon grow?" Genes and Development **17**: 941-958.

Goldner, J.S., Bruder, J.M., Li, G., Gazzola, D. and Hoffman-Kim, D. (2006). "Neurite bridging across micropatterned grooves." Biomaterials **27**: 460-472.

Goldstein, L.S.B. and Yang, Z. (2000). "Microtubule-Based Transport Systems in Neurones: The Role of Kinesins and Dyneins." Annual Review Neuroscience. **23**: 39-71.

Gomer, C.J., Luna, M., Ferrario, A., Rucker, N. (1991). "Increased transcription and translation of heme oxygenase in Chinese hamster fibroblasts following photodynamic stress or Photofrin II incubation." Photochemistry and Photobiology. **53**(2):275-9.

Gonzalez-Zulueta, M., Ensz, L.M., Mukhina, G., Lebovitz, R.M., Zwacka, R.M., Engelhardt, J.F, Oberley, L.W., Dawson, V.L. and Dawson, T.M. (1998). "Manganese Superoxide dismutase protects nNOS Neurons from NMDA and Nitric Oxide-Mediated Neurotoxicity." The Journal of Neuroscience **18** (6): 2040-2055.

Gołąb, J., Nowis, D., Skrzycki, M., Czeczot, H., Barańczyk-Kuźma, A., Wilczyński, G.M., Makowski, M., Mróz, P., Kozar, K., Kamiński, R., Jalili, A., Kopeć, M., Grzela, T. and Jakóbisiak, M. (2003) "Antitumor Effects of Photodynamic Therapy Are Potentiated by 2-Methoxyestradiol. A Superoxide Dismutase Inhibitor." The Journal of Biological Chemistry **278** (1): 407-414.

Gölz, G., Uhlmann, L., Lüdecke, D., Markgraf, N., Nitsch, R. and Hendrix, S. (2006) "The cytokine/neurotrophin axis in peripheral axon outgrowth." European Journal of Neuroscience **24**: 2721-2730.

Griffith, O.W. (1999). "Biologic and Pharmacologic Regulation of Mammalian Glutathione Synthesis." Free Radical Biology and Medicine **27** (9/10): 922-935.

Gupta, S. (2002). "A decision between Life and death during TNF-α-Induced Signaling." Journal of Clinical Immunology **22**(4): 185-194.

Gustavsson, P., Johansson, F., Kanje, M., Wallman, L., Linsmeier, C.E. (2007). "Neurite guidance on protein micropatterns generated by a piezoelectric microdispenser." Biomaterials **28**:1141-1151.

Hahn, K., Robinson, B., Anderson, C., Li, W., Pardo, C.A., Morgello, S., Simpson, D. and Nath, A. (2008). "Differential Effects of HIV infected macrophages on the dorsal root ganglia neurons and axons." Experimental Neurology **210**:30-40.

Hamilton, D., Wu, J.H. and Batist, G. (2007). "Structure-Based Identification of Novel Human γ-Glutamylcysteine Synthetase Inhibitors." Molecular Pharmacology **71** (4): 1140-1147.

Han, Y.H., Moon, H.J., You, B.R., Kim, S.Z., Kim, S.H. and Park, W.H. (2009). "The effects of buthionine sulfoximine, diethyldithiocarbamate or 3-amino-1,2,4-triazole on propyl gallate-treated HeLa cells in relation to cell growth, reactive oxygen species and glutathione." International Journal of Molecular Medicine **24**(2):261-268.

Hayashi, S., Yamazaki, T. and Okamoto, K. (2007). "Nonapoptotic cell death caused by the inhibition of RNA polymerase disrupts organelle distribution." Journal of the Neurological Sciences **256**: 10-20.

He, Y., Francis, F., Myers, K.A., Yu, W., Black, M.M. and Baas, P.W. (2005). "Role of cytoplasmic dynein in the axonal transport of microtubules and neurofilaments." The Journal of Cell Biology **168** (5): 697-703.

Heinzelmann-Schwarz, V., Fedier, A., Hornung, R., Walt, H., Haller, U. and Fink, D. (2003). "Role of p53 and ATM in Photodynamic Therapy-Induced Apoptosis." Lasers in Surgery and Medicine **33**: 182-189.

Hempel, S.L., Buettner, G.R., O'Malley, Y.Q., Wessels, D.A. and Flaherty, D.M. (1999) "Dihydrofluorecein Diacetate is Superior For Detecting Intracellular Oxidants: Comparison With 2', 7'-Dichlorodihydrofluorescein Diacetate, 5(and 6)-Carboxy-2',7'-Dichlorodihydrofluorescein Diacetate, and Dihydrorhodamine 123." Free Radical Biology and Medicine **27** (1/2): 146-159.

Hirokawa, N. and Takemura, R (2005). "Molecular Motors and Mechanisms of Directional Transport in Neurons." Nature Reviews Neuroscience **6**: 201-214.

Hornung, R., Walt H., Crompton, N.E.A., Keefe, K.A., Jentsch, B., Perewusnyk, G., Haller, U., and Köchli, O.R. (1998). "*m*-THPC-Mediated Photodynamic Therapy (PDT) Does Not Induce Resistance to Chemotherapy, Radiotherapy or PDT on Human Breast Cancer Cells *In Vitro*." Photochemistry and Photobiology **68**(4): 569-574.

Huang, Z., Chen, Q., Luck, D., Beckers, J., Wilson, B.C., Trncic, N., LaRue, S.M., Blanc, D. and Hetzel, F.W. (2005). "Studies of a Vascular-Acting Photosensitizer, Pd-Bacteriopheophorbide (Tookad), in Normal Canine Prostate and Spontaneous Canine Prostate Cancer." Lasers in Surgery and Medicine **36**: 390-397.

Huguet, E.L., McMahon, J.A., McMahon, A.P., Bicknell, R. and Harris, A.L. (1994). "Differential Expression of Human *Wnt* Genes 2, 3, 4, and 7B in Human Breast Cell Lines and Normal and Disease States of Human Breast Tissue." Cancer Research **54**: 2615-2621.

Inbal, B., Bialik, S., Sabanay, I., Shani, G. and Kimchi, A. (2002). "DAP kinase and DRP-1 mediate membrane blebbing and the formation of autophagic vesicles during programmed cell death." The Journal of Cell Biology **157** (3): 457-468.

Iwasaki, Y., Ikeda, K., Shiojima, T., Tagaya, N., Kobayashi, T. and Kinoshita, M. (1997). "Bromocriptine prevents neuron damage following inhibition of superoxide dismutase in cultured ventral spinal cord neurones." Neurological Research. **19** (4): 389-392.

Jessen, K.R. (2004) "Cells in focus-Glial cells." The International Journal of Biochemistry and Cell Biology **36**: 1861-1867.

Ji, Z., Yang, G., Vasovic, V., Cunderlikova, B., Suo, Z., Nesland, J.M. and Peng, Q. (2006) "Subcellular localization pattern of protoporphyrin IX is an important determinant for its photodynamic efficiency of human carcinoma and normal cell lines." Journal of Photochemistry and Photobiology B: Biology **84**: 213-220.

Johnson, S.A. and Pardini, R.S, (1998) "Antioxidant enzyme response to hypericin in EMT6 mouse mammary carcinoma cells." Free Radical Biology and Medicine **24**(5):817-26.

Kamuhabwa, A., Agostinis, P., Ahmed, B., Landuyt, W., van Cleynenbreugel, B., van Poppel, H. and de Witte, P. (2004). "Hypericin as a potential phototherapeutic agent in superficial transitional cell carcinoma of the bladder." Photochemical and Photobiological Sciences. **3**: 772-780.

Kandel ,E.R. (1991). "Nerve Cells and Behaviour." Principles of Neural Science 3rd Edition, Editors Kandel, E.R., Schwartz, J.H. and Jessell, T.M.; Appleton and Lange, Connecticut (ISBN: 0-8385-8068-8): 18-32.

Kaščákova, S., Kruijt, B., de Bruijn, H.S., van der Ploeg-van den Heuvel, A., Robinson, D.J., Sterenborg, H.J.C.M. and Amelink, A. (2008). "Ex vivo quantification of mTHPC concentration in tissue: influence of chemical extraction on the optical properties." Journal of Photochemistry and Photobiology B: Biology **91**: 99-107.

Ke, M.S., Xue, L., Feyes, D.K., Azizuddin, K., Baron, E.D., McCormick, T.S., Mukhtar, H., Panneerselvam, A., Schluchter, M.D., Cooper, K.D., Oleinick, N.L. and Stevens, S.R. (2008) "Apoptosis Mechanisms Related to the Increased Sensitivity of Jurkat T-cells vs A431 Epidermoid Cells to Photodynamic Therapy with the Phthalocyanine Pc 4." Photochemistry and Photobiology **84** (2): 407-414.

Keele, C.A., Neil, E. and Joels, N. (1989). Samson Wright's Applied Physiology 13th Edition: Muscle, and the nervous system." Oxford Press, New York: 290.

Keller, J.N., Kindy, M.S., Holtsberg, F.W., St. Clair, D.K., Yen, H., Germeyer, A., Steiner, S.M., Bruce-Keller, A.J., Hutchins, J.B., and Mattson, M.P. (1998). "Mitochondrial Manganese Superoxide Dismutase Prevents Neural Apoptosis and Reduces Ischemic Brain Injury: Suppression of Peroxynitrite Production, Lipid Peroxidation, and Mitochondrial Dysfunction." The Journal of Neuroscience **18** (2): 687-697.

Kiesslich, T., Berlanda, J., Plaetzer, K., Krammer, B. and Berr, F. (2007). "Comparative characterization of the efficiency and cellular pharmacokinetics of Foscan®- and Foslip®- based photodynamic treatment in human biliary tract cancer cell lines." Photochemical and Photobiological Sciences **6**; 619-627.

Kiesslich, T., Plaetzer, K., Oberdanner, C. B., Berlanda, J., Obermair, F.J. and Krammer, B. (2005) "Differential effects of glucose *deprivation* on the cellular sensitivity towards photodynamic treatment-based production of reactive oxygen species and apoptosis-induction." FEBS Letters **579**: 185-190.

Kim, J.B., Stein, R., O'Hare, M.J. (2004) Three-dimensional in vitro tissue culture models of breast cancer-a review." Breast Cancer Research and Treatment. **85**: 281-291.

Klein, S.D., Walt, H. and Richter, C. (1997). " Photosensitization of Isolated Rat Liver Mitochondria by Tetra(*m*-hydroxyphenyl)chlorine." Archives of Biochemistry and Biophysics **348** (2): 313-319.

Koechli, O.R., Schaer, G.N., Schenk, V., Haller, U., Walt, H. (1995). "Assessment of effect of photosensitizers on cytotoxicity of photodynamic therapy in human breast cancer cell cultures." Archives of Gynecology and Obstetrics. **256**: 167-176.

Kolosov, M. and Uzdensky, A.B. (2006). "Crayfish mechanoreceptor neuron prevents photoinduced apoptosis of satellite glial cells." Brain Research Bulletin **69**: 495-500.

Krasnovsky Jr, A.A. (2007) "Singlet oxygen and primary mechanisms of photodynamic therapy and photodynamic diseases" Photodynamic Therapy at the Cellular Level, Editor Uzdensky, A.B.; Research Signpost, Kerala, India (ISBN: 978-81-308-0174-2): 17-62.

Kubin, A., Wierrani, F., Burner, U., Alth, G. and Grünberger, W. (2005). "Hypericin-The Facts About a Controversial Agent." Current Pharmaceutical Design **11**: 233-253.

Kunz, L. and MacRobert, A.J. (2002) "Intracellular Photobleaching of 5, 10, 15, 20-Tetrakis *(m*-hydroxyphenyl) chlorine (Foscan®) Exhibits a Complex Dependence on Oxygen Levels and Fluence Rate." Photochemistry and Photobiology **75** (1): 28-35.

Kübler, A.C., Stenzel, W., Rühling, M., Meul, B. and Fischer, J.H. (2003). "Experimental Evaluation of Possible Side Effects of Intra-operative Photodynamic Therapy on Rabbit Blood Vessels and Nerves." Lasers in Surgery and Medicine **33**: 247-255.

Lane, N. (2002). "OXYGEN-The Molecule that made the World." Oxford University Press, Oxford, UK (ISBN 0-19-850803-4): 121.

Lassalle, H.P., Wagner, M., Bezdetnaya, L., Guillemin, F. and Schneckenburger, H. (2008). "Fluorescence imaging of Foscan® and Foslip in the plasma membrane and in whole cells." Journal of Photochemistry and Photobiology B: Biology **92**: 47-53.

Laville, I., Figueiredo, T., Loock, B., Pigaglio, S., Maillard, Ph., Grierson, D.S., Carrez, D., Croisy, A. and Blais, J. (2003). "Synthesis, Cellular Internalization and Photodynamic Activity of Glucoconjugated Derivatives of Tri and Tetra(*meta*-hydroxyphenyl)chlorines." Bioorganic and Medical Chemistry **11**:1643-1652.

Layton, B.E. and Sastry, A.M. (2004). "A Mechanical Model for Collagen Fibril Load Sharing in Peripheral Nerve of Diabetic and Nondiabetic Rats." Journal of Biological Engineering **126**: 803-814.

LeBel, C.P., Ali, S.F., McKee, M. and Bondy, S.C. (1990). "Organometal-induced increases in oxygen reactive species: The potential of 2', 7'-

dichlorofluorescin diacetate as index of neurotoxic damage." Toxicology and Applied Pharmacology **104** (1): 17-24.

Leung, W.N., Sun, X., Mak, N.K. and Yow, C.M.N. (2002) "Photodynamic Effect of m-THPC on Human Colon Adenocarcinoma Cells: Photocytotoxicity, Subcellular Localization and Apoptosis." Photochemistry and Photobiology **75** (4): 406-411.

Levy Bde, F., Cunha Jdo, C. and Chadi, G. (2007). "Cellular analysis of S100Beta and fibroblast growth factor-2 in the dorsal root ganglia and sciatic nerve of rodents, focus on paracrine actions of activated satellite cells after axotomy." International Journal of Neuroscience **117**(10): 1481-1503.

Lewis-Wambi, J.S., Kin, H.R., Wambi, C., Patel, R., Pyle, J.R., Klein-Szanto, A.J. and Jordan, V.C. (2008). "Buthionine sulfoximine sensitizes antihormone-resistant human breast cancer cells to estrogen-induced apoptosis." Breast Cancer Research **10**: R104.

Li, H., Wigley, C. and Hall, S.M. (1998) "*Chronically* Denervated Rat Schwann Cells Respond to GCF In Vitro." GLIA **24**: 290-303.

Li, J., Altschuler, M.D., Hahn, S.M. and Zhu, T.C. (2008) "Optimization of light sources parameters in the photodynamic therapy of heterogeneous prostate." Physics in Medicine and Biology **53**: 4107-4121.

Lichtman, J.W. and Conchello, J. (2005). "Fluorescence Microscopy." Nature Methods **2**: 910-919.

Lilge, L., Portnoy, M. and Wilson, B.C. (2000). "Apoptosis induced in vivo by photodynamic therapy in normal brain and intracranial tumour tissue." British Journal of Cancer **83** (8): 1110-1117.

Lin, X. and Nelson, W.G. (2003) "Methyl-CpG-binding Domain Protein-2 Mediates Transcriptional Repression Associated with Hypermethylated *GSTP1* CpG Islands in MCF-7 Breast Cancer Cells." Cancer Research **63**: 498-504.

Lobanov, A.V. and Uzdensky, A.B. (2005). "PDT-Induced Death of Sensory Neurons and Glial Cells in the Isolated Crayfish Stretch Receptor After Proteolytic Treatment." Journal of Neuroscience Research **82**: 866-874.

Lou, P.J., Jäger, H.R., Jones, L., Theodossy, T., Bown, S.G. and Hopper, C. (2004). "Interstitial photodynamic therapy as salvage treatment for recurrent head and neck cancer." British Journal of Cancer **91**: 441-446.

Lovat, L.B., Jamieson, N.F,, Novelli, M.R., Mosse, C.A., Selvasekar, C., Mackenzie, G.D., Thorpe, S.M., Bown, S.G. (2005). "Photodynamic therapy with m-tetrahydroxyphenyl chlorin for high-grade dysplasia and early cancer in Barrett's columnar lined esophagus." Gastrointestinal Endoscopy **62**(4):617-23

Ma, L., Moan, J. and Berg, K. (1994) "Evaluation of A New Photosensitiser, Meso-tetra-hydroxyphenyl-chorin, For Use in Photodynamic Therapy: A Comparison of Its Photobiological Properties With Those of Two Other Photosensitizers." International Journal of Cancer **57** (6): 883-888.

MacDonald, I.J. and Dougherty, T.J. (2001). "Basic principles of photodynamic therapy." Journal of Porphyrins and Phthalocyanines 5: 105-129.

McHugh, J.M. and McHugh, W.B. (2004). "Diabetic and peripheral sensory neurons *What we don't know and how it can hurt us.*" AACN Clinical Issues **15** (1):136-149.

McKay Hart, A., Brannstrom, T., Wiberg, M. and Terenghi, G. (2002). "Primary sensory neurons and satellite cells after peripheral axotomy in the adult rat: timecourse of cell death and elimination." Experimental Brain Research **142** (3): 308-318.

McNaught, K. St. P. and Jenner, P. (1999) "Altered Glial Function Causes Neural Death and Increases Neural Susceptibility to 1-Methyl-4-phenylpyridinium- and 6-Hydroxydopamine-induced Toxicity in Astrocytic/Ventral Mesencephalic Co-Cultures." Journal of Neurochemistry **73**: 2469-2476.

Maffi, S.K., Rathinam, M.L., Cherian, P.P., Pate, W., Hamby-Mason, R., Schenker, S. and Henderson, G.I. (2008) "Glutathione content as a potential mediator of the vulnerability of cultured fetal cortical neurons to ethanol-induced apoptosis." Journal of Neuroscience Research **86**(5): 1064-1076.

Mandys, V., Jirsová, K., Jirsa, M. and Vrana, J. (1998). "Neurotoxicity of tetraphenylporphinesulfonate ($TPPS_4$) and a hematoporphyrin derivative (photosan) in organotypic cultures of chick embryonic dorsal root ganglia." Journal of Photochemistry and Photobiology B: Biology **47**: 197-201.

Mannino, S., Molinari, A., Sabatino, G., Ciafrè, S.A., Colone, M., Maira, G., Anile, C., Arancia, G. and Mangiola, A. (2008). "Intratumoral vs systemic administration of meta-tetrahydroxyphenylchorin for photodynamic therapy of malignant gliomas: assessment of uptake and spatial distribution in C6 rat glioma model." International Immunopathol Pharmacol **21** (1): 227-231.

Marchal, S., Bezdetnaya, L. and Guillemin, F. (2004) "Modality of Cell Death Induced by Foscan®-Based Photodynamic Treatment in Human Colon Adenocarcinoma Cell Line HT29." Biochemistry (Moscow) **69** (1): 45-49.

Marchal, S., Fadloun, A., Maugain, E., D'Hallewin, M., Guillemin, F. and Bezdetnaya, L. (2005) "Necrotic and apoptotic features of cell death in response to Foscan® photosensitization of HT29 monolayer and multicell spheroids." Biochemical Pharmacology **69**: 1167-1176.

Marchal, S., François, A., Dumas, D., Guillemin, F. and Bezdetnaya, L. (2007) "Relationship between subcellular localisation of Foscan® and caspase activation in photosensitised MCF-7 cells." British Journal of Cancer **96**: 944-951.

Marks, D.B., Marks, A.D. and Smith C.M. (1996a). "Basic Medical Biochemistry-A Clinical Approach." Williams and Wilkins, Baltimore USA, ISBN 0-683-05595-X, **Chapter 10**: 129-145.

Marks, D.B., Marks, A.D. and Smith, C.M. (1996b). "Basic Medical Biochemistry-A Clinical Approach." Williams and Wilkins, Baltimore USA, ISBN 0-683-05595-X, **Chapter 21**: 327-340.

Martin, M.N., Saladores, P.H., Lambert, E., Hudson, A.O. and Leustek, T. (2007). "Localization of Membranes of the γ-Glutamyl Transpeptidase Family Identifies Sites of Glutathione and Glutathione S-Conjugate Hydrolysis[1[W] [OA]]." Plant Physiology **144**: 1715-1732.

Martini, R. (2005) "Schwann cells and myelin" Neuroglia 2nd Edition, Editors Kettenmann, H. and Ransom, B.R.; Oxford University Press, Oxford (ISBN10: 0195152220): 48-59.

Mason, M.D. (1999). "Cellular aspects of photodynamic therapy for cancer." Reviews in Contemporary Pharmacotherapy **10** (1): 25-37.

Mauzeroll, J., Bard, A.J., Owhadian, O. and Monks, T.J. (2004). "Menadione metabolism to thiodione in hepatoblastoma by scanning electrochemical microscopy." PNAS **101** (51): 17582-17587.

Meister, A. (1994). " Glutathione, Ascorbate, and Cellular Protection." Cancer Res (Suppl) **54**: 1969s-1975s.

Meister, A. (1995) "Mitochondrial changes associated with glutathione deficiency." Biochimica et Biophysica Acta (BBA) **1271** (1): 35-42.

Melnikova, V.O., Bezdetnaya, L.N., Bour, C., Festor, E., Gramain, M.P., Merlin, J.L., Potapenko, A.Y. and Guillemin, F. (1999a). "Subcellular localization of meta-tetra (hydroxyphenyl) chlorine in human tumor cells subjected to photodynamic treatment." J. Photchem Photobiol B **49**(2-3): 96-103.

Melnikova, V.O., Bezdetnaya, L.N., Potapenko, A.Y. and Guillemin, F. (1999b). "Photodynamic properties of meta-tetra(hydroxyphenyl)chlorine in human tumor cells." Radiat Res **152**(4): 428-435.

Melnikova, V., Bezdetnaya, L., Belitchenko, I., Potapenko, A., Merlin, J. and Guillemin, F. (1999c). "Meta-tetra(hydroxyphenyl)chlorine-sensitizeed photodynamic damage of cultured tumor and normal cells in the presence of high concentrations of α-tocopherol." Cancer Letters **139**: 89-85.

Miccoli, L., Beurdeley-Thomas, A., De Pinieux, G., Sureau, F., Oudard, S., Dutrillaux, B. and Poupon, M.F. (1998). "Light-induced Photoactivation of Hypericin Affects the Energy Metabolism of Human Glioma cells by Inhibiting Hexokinase Bound to Mitochondria." Cancer Research **58**: 5777-5786.

Michael-Titus, A., Revest, P. and Shortland, P. (2008). "Elements of Cellular and Molecular Neuroscience." The Nervous System: Basic Science and Clinical Conditions; Churchill Livingstone, Elsevier Ltd, Philadelphia, USA: 33-49.

Mikeš, J., Kleban, J., Sačková, V., Horváth, V., Jamborová, E., Vaculová, A., Kozubík, A., Hofmanová, J. and Fedoročko, P. (2007) "Necrosis predominates in the cell death of human colon adenocarcinoma HT-29 cells treated under variable conditions of photodynamic therapy with Hypericin." Photochemical and Photobiological Sciences **6**: 758-766.

Miller, R.L., Sun, G.Y. and Sun, A.Y. (2007) "Cytotoxicity of paraquat in microglial cells: involvement of PKCδ- and ERK1/2-dependent NADPH oxidase." Brain Research **1167**: 129-139.

Mirsky, R. and Jessen, K.R. (1996). "Schwann cell development, differentiation and myelination." Current Opinion in Neurobiology **6**: 89-96.

Miskovsky, P., Sureau, F., Chinsky, L., Turpin, P.Y. (1995). "Subcellular distribution of hypericin in human cancer cells." Photochemistry and Photobiology. **62**(3):546-549.

Mizushima, N., Ohsumi, Y. and Yoshimori, T. (2002). "Autophagosome Formation in mammalian Cells." Cell Structure and Function **27**: 421-429.

Moan, J., Ma, L.W. and Bjørklund, E. (1999). "The effect of glucose and temperature on the in vivo efficiency of photochemotherapy with *meso*-tetra-hydroxyphenyl-chlorin." Journal of Photochemistry and Photobiology B: Biology **50**; 94-98.

Molinari, A., Bombelli, C., Mannino, S., Stringaro, A., Toccacieli, L., Calcabrini, A., Colone, M., Mangiola, A., Maira, G., Luciani, P., Mancini, G. and Arancia, G. (2007) "m-THPC-mediated photodynamic therapy of malignant gliomas: Assessment of a new transfection strategy." International Journal of Cancer **121**: 1149-1155.

Moore, C.M., Nathan, T.R., Lees, W.R., Mosse, C.A., Freeman, A., Emberton, M., Bown, S.G. (2006). "Photodynamic Therapy Using Meso Tetra Hydroxy Phenyl Chlorin (mTHPC) in Early Prostate Cancer." Lasers in Surgery and Medicine **38** (5): 356-363.

Morlet, L., Vonarx, V., Foultier, M., Gouyette, A., Stewart, C., Lenz, P. and Patrice, T. (1997). "In vitro and in vivo spectrofluorometry of a water-soluble *meta*-(tetrahydroxyphenyl) chlorin (*m*-THPC) derivative." Journal of Photochemistry and Photobiology B: Biology **39**: 249-257.

Mytilineou, C., Kokotos Leonardi, E.T., Kramer, B.C., Jamindar, T. and Warren Olanow, C. (1999). "Glial Cells Mesiate Toxicity in Glutathione-Depleted Mesencephalic Cultures." Journal of Neurochemistry **73** (1): 112-119.

Müller, S., Walt, H., Dobler-Girdziunaite, D., Fiedler, D. and Haller, U. (1998) "Enhanced photodynamic effects using fractionated laser light." Journal of Photochemistry B: Biology **42**: 67-70.

Nascimento, R.S., Santiago, M.F., Marques, S.A., Allodi, S. and Martinez, A.M.B. (2008) "Diversity among satellite glial cells in dorsal root ganglia of the rat." Brazilian Journal of Medical and Biological Research **41**: 1011-1017.

Ndubaku, U. and de Bellard, M.E. (2008) "Glial cells: Old cells with new twists." Acta Histochemica **110** (3):182-195.

Nevřelová, P., Kolářová, H., Bajgar, R., Maceček, J., Tomečka, M., Tománková, K. and Strnad, M. (2005). "Measurement of Reactive Oxygen Species After Photodynamic Therapy *In Vitro*." Scripta Medica (BRNO) **78** (5): 281-290.

Nicholls, D.G. and Budd, S.L. (2000). "Mitochondria and Neuronal Survival." Physiological Reviews **80**: 315-360.

Nicole, A., Santiard-Baron, D. and Ceballos-Picot, I. (1998). "Direct evidence for glutathione as mediator of apoptosis in neuronal cells." Biomedicine and Pharmacotherapy: **52**: 349-355.

Nikolaev, A., McLaughlin, T., O'Leary, D.D.M. and Tessier-Lavigne, M. (2009). "APP binds DR6 to trigger axon pruning and neuron death via distinct caspases." Nature **457**: 981-989 (doi: 10.1038/nature07767).

Nirmalanandhan, V.S., Levy, M.S., Huth, A.J. and Butler, D.L. (2006). "Effects of cell Seeding Density and Collagen Concentration on Contraction Kinetics of Mesenchymal Stem Cell-Seeded Collagen Constructs." Tissue Engineering **12** (7): 1865-1872.

Noodt, B.B., Berg, K., Stokke, T., Peng, Q. and Nesland, J.M. (1999). "Different apoptotic pathways are induced from various intracellular sites by tetraphenylporphyrins and light." British Journal of Cancer **79**(1): 72-81.

Nyst, H.J., Bing, Tan, I., Stewart, F.A. and Balm, A. J.M. (2009). "Is photodynamic therapy a good alternative to surgery and radiotherapy in the treatment of head and neck cancer?" Photodiagnosis and Photodynamic Therapy **6**: 3-11.

Oberdanner, C.B., Plaetzer, K., Kiesslich, T. and Krammer, B. (2005) "Photodynamic Treatment with Fractionated Light Decreases Production of Reactive Oxygen Species and Cytotoxicity *In Vitro* via Regeneration of Glutathione." Photochemistry and Photobiology **81**: 609-613.

Obwegeser, A., Jakober, R. and Kostron, H. (1998). "Uptake and kinetics of ^{14}C-labelled meta-tetrahydroxyphenylchlorin and 5-aminolaevulinic acid in the C6 rat glioma model." British Journal of Cancer **78**(6): 733-738.

Ochsner, M. (1997). "Photophysical and photobiological processes in the photodynamic therapy of tumours." Journal of Photchemistry and Photobiology B: Biology **39**: 1-18

O'Connor, S.M., Stenger, D.A., Shaffer, K.M., Maric, D., Barker, J.L. and Ma, W. (2000). "Primary neural precursor cell expansion, differentiation and

cytosolic Ca^{2+} response in three-dimensional collagen gel." Journal of Neuroscience Methods **102**: 187-195.

Oleinick, N.L., Morris, R.L. and Belichenko, I. (2002). The role of apoptosis in response to photodynamic therapy: what, where, why, and how." Photochemical and Photobiological Sciences **1**: 1-21 (doi: 10.1039/b108586g)

Paba, V., Quarto, M., Varriale, L., Crescenzi, E. and Palumbo, G. (2001) "Photo-activation of Hypericin with low doses of light promotes apparent photo-resistance in human histiocytic lymphoma U937 cells." Journal of Photochemistry and Photobiology B: Biology: **60**: 87-96.

Pajonk, F., Scholber, J. and Fiebich, B. (2005). "Hypericin-an inhibitor of proteasome function." Cancer Chemotherapy and Pharmacology: **55**: 439-446.

Pearson, R.G., Molino, Y., Williams, P.M., Tendler, S.J., Davies, M.C., Roberts, C.J., Shakesheff, K.M. (2003). "Spatial confinement of neurite regrowth from dorsal root ganglia within nonporous microconduits." Tissue Engineering. **9**(2): 201-208.

Peng, Q., Moan, J., Ma, L. and Nesland, J.M. (1995). "Uptake, Localisation, and Photodynamic Effect of *meso*-Tetra(hydroxyphenyl)porphine and Its Corresponding Chlorin in Normal and Tumor Tissues of Mice Bearing Mammary Carcinoma." Cancer Research **55**: 2620-2626.

Peng, T.I., Chang, C.J., Guo, M.J, Wang, Y.H., Yu, J.S., Wu, H.Y. and Jou, M.J. (2005) "Mitochondrion-Targeted Photosensitiser Enhances the Photodynamic Effect-Induced Mitochondrial Dysfunction and Apoptosis." Annals New York Academy of Sciences **1042**: 419-428.

Perry, J.J.P., Hearn, A.S., Cabelli, D.E., Nick, H.S., Tainer, J.A. and Silverman, D.N. (2009). "Contribution of Human Manganese Superoxide Dismutase Tyrosine 34 to Structure and Catalysis." Biochemistry **48**: 3417-3424.

Pfister, B.J., Iwata, A., Taylor, A.G., Wolf, J.A., Meaney, D.F. and Smith, D.H. (2006) "Development of transplantable nerve tissue constructs comprised of stretch-grown axons." Journal of Neuroscience Methods **153**: 95-103.

Phillips, J.B., Bunting, S.C., Hall, S.M., Brown, R.A. (2005). "Neural Tissue Engineering: A Self-Organizing Collagen Guidance Conduit." Tissue Engineering **11** (9/10): 1611-1617.

Phillips, J. and Harle, J. (2008). "Understanding The Structure of Tissues." Trauma, Repair and Recovery. Editor Phillips J.; Oxford, Oxford University Press and The Open University Press, Milton Keynes (ISBN 978-0-1992-3734-0): 27-52.

Plaetzer, K., Kiesslich, T., Verwanger, T. and Krammer, B. (2003). "The Modes of Cell Death Induced by PDT: An Overview." Medical Laser Application **18**: 7-19.

Plant, J.A. (2007a) "Prostate Cancer, Understand, Prevent and Overcome Prostate Cancer." London: Virgin Book Limited, ISBN 978 0 7535 1298 2: 13-14.

Plant, J.A. (2007b) "Prostate Cancer, Understand, Prevent and Overcome Prostate Cancer." Virgin Book Limited, London (ISBN 978 0 7535 1298 2): 64-67.

Porter, R.A., Brown, R.A., Eastwood, M., Occleston, N.L. and Khaw, P.T. (1998) "Ultrastructural changes during contraction of collagen lattice by ocular fibroblasts." Wound Repair and Regeneration **6** (2):157-166

Raginov, I.S., Chelyshev, Y.A. and Shagidullin, T.F. (2004). "Interaction of Sensory Neurons and Satellite Cells during Stimulation of Nerve Regeneration." Neuroscience and Behavioral Physiology **34** (1): 79-81.

Raimondi, A., Mangolini, A., Rizzardini, M., Tartari, S., Massari, S., Bendotti, C., Francolini, M., Borgese, N., Cantoni, L. and Pietrini, G. (2006). "Cell culture models to investigate the selective vulnerability of motoneuronal mitochondria of familial ALS-linked G93ASOD1." European Journal of Neuroscience **24**: 387-399.

Rancan, F., Wiehe, A., Nöbel, M., Senge, M.O., Omari, S.A., Böhm, F., John, M. and Röder, B. (2005) "Influence of substitutions on asymmetric dihydroxychlorines with regard to intracellular uptake, subcellular localisation and photosensitization of Jurkat cells." Journal of Photochemistry and Photobiology B: Biology **78**: 17-28.

Ris, H.B., Altermatt, H.J., Nachbur, B., Stewart, C.M., Wanf, Q., Lim, C.K., Bonnett, R. and Althaus, U. (1996). "Intraoperative Photodynamic Therapy with m-Tetrahydroxyphenylchlorin for Chest Malignancies." Laser in Surgery and Medicine **18**: 39-45.

Ris, H.B., Giger, A., Hof, V.I., Mettler, D., Stewart, J.C.M., Althaus, U. and Altermatt, H.J. (1997). "Experimental assessment of photodynamic therapy with chlorines for malignant mesothelioma." European Journal of Cardiothoracic Surgery **12**: 542-548.

Ritz, R., Müller, M., Weller, M., Dietz, K., Kuci, S., Roser, F. and Tatagiba, M. (2005). "Hypericin: a promising fluorescence marker for differentiating between glioblastoma and neurons in vitro." International Journal of Oncology **27** (6): 1543-1549.

Ritz, R., Wein, H., Dietz, K., Schenk, M., Roser, F., Tatagiba, M. and Strauss, W.S.L. (2007) "Photodynamic therapy of malignant glioma with hypericin: Comprehensive *in vitro* study in human glioblastoma cell lines." International Journal of Oncology **30**: 659-667.

Robinson, M.D. and Bryant, P.R. (2006). "Peripheral Nerve Injuries, Chapter 9." Rehabilitation of the Injured Combatant, **2**: 428.

Rosner, B.I., Hang, T. and Tranquillo, R.T. (2005). "Schwann cell behaviour in three-dimensional collagen gels: Evidence for differential mechano-transduction and the influence of TGF-beta 1 in morphological polarization and differentiation." Experimental Neurology **195**; 81-91.

Rota, C., Chignell, C.F. and Mason, R.P. (1999). "Evidence For Free Radical Formation During The Oxidation of 2'-7'-Dichlorofluorescin To The Fluorescent Dye 2'-7'-dichlorofluorescein By Horseradish Peroxidase: Possible Implications For Oxidative Stress Measurements." Free Radical Biology and Medicine **27** (7/8): 873-881.

Rothstein, J.D., Bristol, L.A., Hosler, B., Brown Jr., R. H and Kuncl, R. W. (1994) "Chronic inhibition of superoxide dismutase produces apoptotic death of spinal neurons." Proceedings of the National Academy of Sciences USA **91**: 4155-4159.

Rousset, N., Kerninon, E., Eléouet, S., Le Néel, T. Auget, J., Vonarx, V., Carré, J., Lajat, Y. and Patrice, T. (2000) "Use of alkaline Comet assay to assess DNA repair after *m*-THPC-PDT." Journal of Photochemistry B: Biology **56**: 118-131.

Roychowdhury, S., Luthe, A., Keilhoff, G., Wolf, G. and Horn, T. F. W. (2002) "Oxidative Stress in Glial Cultures: Detection by DAF-2 Fluorescence Used as a Tool to Measure Peroxynitrite Rather Than Nitric Oxide." Glia" **38**: 103-114.

Saczko, J., Chwiłkowska, A., Kulbacka, J., Berdowska, I., Zieliński, B., Drąg-Zalesińska, M., Wysocka, T., Ługowski, M. and Banaś, T. (2008). "Photooxidative Action in Cancer and Normal Cells induced by the Use of Photofrin® in Photodynamic Therapy." Folia Biologica (Praha) **54**: 24:29.

Sadauskaite, A., Mickuviene, I., Kadziauskas, J. and Kirveliene, V. (2004). "Cellular response to mitochondria-targeted photodynamic treatment." ELSO Meetings: Mitochondria, chloroplasts and) Poster **275**.

Sasnouski, S., Kachatkou, D., Zorin, V., Guillemin, F. and Bezdetnaya, L. (2006) "Redistribution of Foscan® from plasma proteins to model membranes." Photochemical and Photobiological Sciences **5**: 770-777.

Sasnouski, S., Pic, E., Dumas, D., Zorin, V., D'Hallewin, M-A., Guillemin, F., and Bezdetnaya, L. (2007) "Influence of Incubation Times and Sensitizer Localization on Meta-tetra (hydroxyphenyl)chorin (mTHPC)-induced Photoinactivation of Cells." Radiation Research **168** (2): 209-217.

Sattler, R., Charlton, M.P., Hafner, M. and Tymianski, M. (1997) "Determination of the Time Course and Extent of Neurotoxicity at Defined Temperatures in Cultured Neurons Using a Modified Multiwell Plate Fluorescence Scanner." Journal of Cerebral Blood Flow and Metabolism **17**: 455-463.

Saw, C.L.L., Olivo, M., Chin, W. W. L., Soo, K.C. and Heng, P.W.S. (2005). "Transport of Hypericin across Chick Chorioallantotic Membrane and

Photodynamic Therapy Vasculature Assessment." Biological and Pharmaceutical Bulletin **28** (6): 1054-1060.

Sayan, H., Ozacmak, V.H., Ozen, O.A., Coskun, O. Arsian, S.O., Sezen, S.C. and Aktas, R.G. (2004). "Beneficial effects of melatonin on reperfusion injury in rat sciatic nerve." Journal of Pineal Research **37**: 143-148.

Sáez, J.C., Kessler, J.A., Bennett, V.L. and Spray, D.C. (1987). "Superoxide dismutase protects cultured neurons against death by starvation." Proceedings of the National Academy of Sciences of the United States of America **84**: 3056-3059.

Scherz-Shouval, R. and Elazar, Z. (2007). "ROS, mitochondria and the regulation of autophagy." TRENDS in Cell Biology **17** (9): 422-427.

Schmalenberg, K.E. and Uhrich, K.E. (2005). "Micropatterned polymer substrates control alignment of proliferating Schwann cells to direct neuronal regeneration." Biomaterials **26**: 1423-1430.

Shi, T. J. S., Holmberg, K., Xu, Z. D., Steinbusch, H., de Vente, J. and Hökfelt, T. (1998). "Effect of peripheral nerve injury on cGMP and nitric oxide synthase levels in rat dorsal root ganglia: time course and coexistence." Pain **78**: 171-180.

Shinder, V. and Devor, M. (1994). "Structural basis of neuron-to-neuron cross-excitation in dorsal root ganglia." Journal of Neurocytology **23** (9): 515-531.

Simstein, R., Burow, M., Parker, A., Weldon, C. and Beckman, B. (2003). "Apoptosis, Chemoresistance, and Breast Cancer: Insights From the MCF-7 Cell Model System." Experimental Biology and Medicine **228**: 995-1003.

Standring, S. Crossman, A.R., Turlough FitzGerald, M.J. and Collins P. (2005). "Neuroanatomy." Gray's Anatomy: The Anatomical Basis of Clinical Practice 39th Edition; Churchill Livingstone, Elsevier Ltd, London (ISBN-10: 0443071683): 225-438.

Stasio, B.D., Frochot, C., Dumas, D., Even, P., Zwier, J., Müller, A., Didelon, J., Guillemin, F., Viriot, M. and Barberi-Heyob, M. (2005) "The 2-aminoglucosamide motif improves cellular uptake and photodynamic activity of tetraphenylporphyrin." European Journal of Medical Chemistry **40**: 1111-1122.

Stępień, E., *Stanisz*, J. and Korohoda, W. (1999). "Contact Guidance of Chick Embryo Neurons on Single *Scratches* in Glass and on Underlying aligned Human Skin Fibroblasts." Cell Biology International **23** (2): 105-116.

Sundquist, T., Moravec, R., Niles, A., O'Brien, M. and Riss, T. (2006) "Timing Your Apoptosis Assays." Cell Notes **16**: 18-21.

Svensson, B., Ekström, P.A.R. and Edström, A. (1995) "Increased levels of mitogen activated protein kinase (MAP-K) detected in the injured adult mouse sciatic nerve." Neuroscience Letters **200**: 33-36.

Syroid, D.E., Maycox, P.R., Burrola P.G., Liu, N., Wen, D. Lee, K., Lemke, G. and Kilpatrick, T.J. (1996). "Cell death in the Schwann cell lineage and its regulation by neuregulin." Proceedings of the National Academy of Sciences of the United States of America **93**: 9229-9234.

Tanioka, H., Mizushima, T., Shirahige, A., Matsushita, K., Ochi, K., Ichimura, M., Matsumura, N., Shinji, T., Tanimoto, M. and Koide, N. (2005). "Xanthine oxidase-derived free radicals directly activate rat pancreatic stellate cells." Journal of Gastroenterology and Hepatology **21**: 537-544.

Taylor, C.T. and Moncada, S. (2009). "Nitric Oxide, Cytochrome C Oxidase, and the Cellular Response to Hypoxia." Arteriosclerosis Thrombosis and Vascular Biology (doi: 10.1161/ATVBAHA.108.181628).

Teiten, M.-H., Bezdetnaya, L., Morlière, P., Santus, R. and Guillemin, F. (2003) "Endoplasmic reticulum and Golgi apparatus are the preferential sites of Foscan® localisation in cultured tumour cells." British Journal of Cancer **88**:146-152.

Theodossiou, T., Spiro, M.D., Jacobson, J., Hothersall, J.S. and MacRobert A.J. (2004). "Evidence for Intracellular Aggregation of Hypericin and the Impact on its Photocytotoxicity in PAM 212 Murine Keratinocytes." Photochemistry and Photobiology **80**: 438-443.

Thompson, D.M. and Buettner, H.M. (2006) "Neurite Outgrowth Is Directed by Schwann Cell Alignment in the Absence of Other Guidance Cues." Annals of Biomedical Engineering **34** (1): 161-168.

Toates, F. (2004). "Introduction to Brains, Minds and Consciousness." Cells to Consciousness." Milton Keynes, The Open University Press: 1-42.

Tonge, D., Edström, A. and Ekström, P. (1997). "Use of Explanted Cultures of Peripheral Nerves of Adult Vertebrates to Study Axonal Regeneration *In Vitro*." Progress in Neurobiology **54**: 459-480.

Topp, K.S. and Boyd, B.S. (2006). "Structure and Biomechanics of Peripheral Nerves: Nerve Responses to Physical Stresses and Implications for Physical Therapist Practice." Physical Therapy **86** (1): 92-109.

Tortora, G.J. and Derrickson, B. (2006a). "Nervous Tissue and Homeostasis." Principles of Anatomy and Physiology, 11th Edition; John Wiley and Sons, Inc. (ISBN 10: 0471689343): 403-437.

Tortora, G.J. and Derrickson, B. (2006b). "Sensory Motor and Integrative Systems." Principles of Anatomy and Physiology, 11th Edition; John Wiley and Sons, Inc. (ISBN 10: 0471689343): 548.

Triesscheijn, M., Ruevekamp, M., Aalders, M., Baas, P. and Stewart, F.A. (2004) "Comparative Sensitivity of Microvascular Endothelial Cells, Fibroblasts and Tumor Cells after *In Vitro* Photodynamic Therapy with *meso*-Tetra-Hydroxyphenyl-Chlorin." Photochemistry and Photobiology **80**: 236-241.

Tucker, B.A., Rahimtula, M. and Mearow, K.M. (2005) "A procedure for selecting and culturing subpopulations of neurons from rat dorsal root ganglia using magnetic beads." Brain Research Protocols **16**: 50-57.

Turcu, F., Tratsk-Nitz, K., Thanos, S., Schuhuhmann, W. and Heiduschka, P. (2003). "Ink-jet printing for micropattern generation of laminin for neuronal adhesion." Journal of Neuroscience Methods **131**: 141-148.

Uzdenskii, A.B., Kolosov, M.S., and Lobanov, A.V. (2008). "Neuron and Gliocyte Death Induced by Photodynamic Treatment: Signal Processes and Neuron-Glial Interactions." Neuroscience and Behavioral Physiology **38** (7): 727-735.

Uzdensky, A.B., Bragin, D.E., Kolosov, M.S., Dergacheva, O. and Fedorenko, G. (2002). "Photodynamic Inactivation of Isolated Crayfish Mechanoreceptor Neuron: Different Death Modes Under Different Photosensitizer Concentration." Photochemistry and Photobiology **76** (4): 431-437.

Uzdensky, A.B., Bragin, D.E., Kolosov, M.S., Kubin, A., Loew, H.G. and Moan, J. (2003). "Photodynamic effect of hypericin and a water-soluble derivative on isolated crayfish neuron and surrounding glial cells." Journal of Photochemistry and Photobiology B: Biology **72**: 27-33.

Uzdensky, A.B., Dergacheva, O.Y., Zhavoronkova, A.A., Reshetnikov, A.V. and Ponomarev, G.V. (2004). "Photodynamic effect of novel chlorin e_6 derivatives on a single nerve cell." Life Sciences **74**: 2185-2197.

Uzdensky, A.B., Kolosov, M., Bragin, D., Dergacheva, O., Vanzha, O. and Oparina, L. (2005). "Involvement of Adenylate Cyclase and Tyrosine Kinase Signaling Pathways in Response of Crayfish Stretch Receptor Neuron and Satellite Glia Cell to Photodynamic Treatment." Glia **49**: 339-348.

Uzdensky, A.B. Lobanov, A., Bibov, M. and Petin, Y. (2007). "Involvement of Ca^{2+}- and Cyclic Adenosine Monophosphate-Mediated Signaling Pathways in Photodynamic Injury of Isolated Crayfish Neuron and Satellite Glial Cells." Journal of Neuroscience Research **85**: 806-870.

Valencia, A. and Morán, J. (2004). "Reactive Oxygen Species Induce Different Cell Death Mechanisms in Cultured Neurones." Free Radical Biology and Medicine **36** (9): 1112-1125.

Vanden Berghe, P., Hennig, G.W. and Smith, T.K. (2004). "Characteristics of intermittent mitochondrial transport in guinea pig enteric nerve fibers." American Journal of Physiol Gastrointest Liver Physiol **286**: G671-G682.

Vandenbogaerde, A.L., Cuveele, J.F., Proot, P., Himpens, B.E., Merlevede, W.J. and de Witte, P.A. (1997). "Differential cytotoxic effects induced after photosensitization by Hypericin." Journal of Photobiology B: Biology **38**: 136-142.

Van De Putte, M., Roskams, T., Bormans, G., Verbruggen, A. and De Witte, P.A.M. (2006). "The impact of aggregation on the biodistribution of hypericin." International Journal of Oncology **28**: 655-660.

Varija, D., Kumar, K.P., Reddy, K.P. and Reddy, K.P. (2009). "Prolonged constriction of sciatic nerve affecting oxidative stressors & antioxidant enzymes in rat." Indian Journal Medical Research **129** (5): 587-592.

Vásquez, O.L., Almeida, Á. and Bolaños, J.P. (2001). "Depletion of glutathione up-regulates mitochondrial complex I expression in glial cells." Journal of Neurochemistry **76**: 1593-1596.

Vrouenraets, M.B., Visser, G.W.M., Stewart, F.A., Stigter, M., Oppelaar, H., Postmus, P.E., Snow, G.B. and Van Dongen, G.A.M.S. (1999). "Development of *meta*-Tetrahydroxyphenylchlorin-Monoclonal Antibody Conjugates for Photoimmunotherapy." Cancer Research **59**: 1505-1513.

Wang, H.P., Qian, S.Y., Schafer, F.Q., Domann, F.E., Oberley, L.W. and Buettner, G.R. (2001) "Phospholipid Hydroperoxide Glutathione Peroxidase Protects Against Singlet Oxygen-Induced Cell Damage of Photodynamic Therapy." Free Radical Biology and Medicine **30** (8): 825-835.

Wang, Y., Qiao, M., Mieyal, J.J., Asmis, L.M. and Asmis, R. (2006) "Molecular mechanism of glutathione-mediated protection from oxidized low-density lipoprotein-induced cell injury in human macrophages: Role of glutathione reductase and glutaredoxin." Free Radical Biology and Medicine **41**: 775-785.

Watts, L.T., Rathinam, M.L., Schenker, S. and Henderson, G.I. (2005) "Astrocytes Protect Neurones From Ethanol-Induced Oxidative Stress and Apoptotic Death." Journal of Neuroscience Research **80**: 655-666.

Wiegell, S.R., Stender, I.M., Na, R. and Wulf, H.C. (2003). "Pain Associated With Photodynamic Therapy Using 5-Aminolevulinic Acid or 5-Aminolevulinic Acid Methylester on Tape-Stripped Normal Skin." Archives of Dermatology **139**: 1173-1177.

Williams, B.R., Gelman, R.A., Poppke, D.C. and Piez, K.A. (1978). "Collagen Fibril Formation." The Journal of Biological Chemistry **253** (18): 6578-6585.

Willingham M.C. (1999). "Cytochemical Methods for the Detection of Apoptosis." The Journal of Histochemistry and Cytochemistry **47**(9): 1101-1109.

Wilson, B.C. (2003). "Potential Applications of Photodynamic Therapy in Regenerative Medicine." The Journal of Craniofacial Surgery **14** (3): 278-283.

Winsz-Szczotka, K., Komosińska-vassev, K. and Olczyk, K. (2006). "The metabolism of glycosaminoglycans in the course of Graves' disease." Postępy higieny i medycyny doświadczalnej (online) **60**: 184-191.

Witold, J. and Grzegorz, B. (2000). "2, 7-Dichlorofluorescin oxidation and reactive oxygen species: What does it measure?" Cell Biology international **24** (10): 757-760.

Wright, K.E., Liniker, E., Loizidou, M., Moore, C., MacRobert, A.J. and Phillips, J.B. (2009) "Peripheral neural cell sensitivity to mTHPC-mediated photodynamic therapy in a 3D in vitro model." British Journal of Cancer **101**: 658-665.

Xie, X.; Hudson, J.B. and Guns E.S. (2001). "Tumor-specific and Photodependent Cytotoxicity of Hypericin in the Human LNCaP Prostate Tumor Model." Photochemistry and Photobiology **74** (2): 221-225.

Yow, C.M.N., Chen, J.Y., Mak, N.K., Cheung, N.H. and Leung A.W.N. (2000). "Cellular uptake, subcellular localization and photodamaging effect of Temoporfin (mTHPC) in nasopharyngeal carcinoma cells: comparison with hematoporphyrin derivative." Cancer Letters **157**: 123-131.

Zelko, I.N., Mariani, T.J. and Folz, R.J. (2002). "Superoxide Dismutase Multigene Famaily: A Comparison Of The CuZn-SOD, Mn-SOD (SOD2), And EC-SOD (SOD3) Gene Structure Evolution, And Expression." Free Radical Biology and Medicine **33** (3): 337-349.

Zhao L. (2001). "Singlet Oxygen." Free Radical and Radiation Biology Graduate Program, Department of Radiology, B-180 ML. The University of Iowa, Iowa City: 1-10.

Zimmermann, A., Ritsch-Marte, M. and Kostron, H. (2001). "mTHPC-mediated Photodynamic Diagnosis of Malignant Brain Tumors." Photochemistry and Photobiology **74** (4): 611-616.

Zong, W.X. and Thompson, C.B. (2006). "Necrotic death as a cell fate." Genes and Development **20**: 1-15.

APPENDIX-I

TdT-FragEL™ kit Instruction

100 µl 3 % (v/v) H_2O_2 was incubated for 5 min at room temperature to inactivate endogenous peroxidises. Samples were rinsed with PBS before being incubated with 100 µl 1xTdT Equilibrium Buffer for 10 to 30 min. TdT Equilibrium Buffer was removed and immediately 60 µl TdT Labelling Reaction Mixture (57 µl TdT Labelling Reaction Mixture and 3 µl TdT Enzyme) were added per sample. Samples were covered with parafilm and incubated for 1.5 h at 37° C in a humidified incubator. Parafilm was removed and samples rinsed in PBS. 100 µl Stop Solution was used to cover gels for 5 min before rinsing with PBS. 100 µl Blocking Buffer was added and incubated for 10 min; removed, then immediately 100 µl of 1x Conjugate was added and incubated a 30 min in a humidified chamber. Samples were rinsed in PBS then incubated with 100 µl DAB solution (one tablet of DAB and one tablet of H_2O_2/Urea in 1 ml of tap water) for 10-15 min before finally being rinsed with dH_2O. Cultures were viewed under bright-field for DAB (apoptotic cells) and fluorescence for neurone identification using an Olympus BX61 fluorescence microscope.